Conformational variability of MHC class I molecules

Inaugural-Dissertation
to obtain the academic degree
Doctor rerum naturalium (Dr. rer. nat.)

submitted to
the Department of Biology, Chemistry and Pharmacy
of
Freie Universität Berlin

by
Pravin Kumar
from Siwan, India

2009

असतो मा सद् गमय।

तमसो मा ज्योतिर्गमय।

मृत्योर्मा अमृतं गमय।

- बृहदारण्यक उपनिषद् (१.३.२८.)

Führe mich von der Unwahrheit zur Wahrheit.
Führe mich von der Dunkelheit ins Licht.
Führe mich vom Tod zum ewigen Leben.

From falsehood, lead me to truth.
From darkness, lead me to light.
From death, lead me to immortality.

- Brihadaranyaka Upanishad (1.3.28.)

This thesis is based on research conducted from 2004 to 2009 at the Institut für Immungenetik, Charité - Universitätsmedizin Berlin under the supervision of Prof. Dr. rer. nat. Andreas Ziegler, Dr. rer. nat. Barbara Uchanska-Ziegler and Prof. Dr.-ing. Wolfram Saenger (Institut für Kristallographie, FU Berlin).

First Reviewer:	Prof. Dr. Andreas Ziegler
Second Reviewer:	Prof. Dr. Udo Heinemann
Date of Submission:	November 13, 2009
Date of Defence:	February 3, 2010

DECLARATION

I hereby declare that the work presented in this thesis has been conducted independently and without any inappropriate support, and that all sources of content, experimental or intellectual, are suitably referenced and acknowledged.

I further declare that this thesis has not been submitted before, either in the same or a different form, to this or any other university for a degree.

Pravin Kumar Berlin, 12 November 2009

ACKNOWLEDGEMENT

First and foremost, I would like to gratefully acknowledge the supervision of Prof. Andreas Ziegler who has been an extraordinary supervisor and mentor. I have immensely benefitted from his knowledge, enthusiasm, planning, resourcefulness, meticulousness and humor. I can never thank him enough for his time, confidence and generosity, and for reading this dissertation on a very short notice. I cannot aptly express my gratitude in words to Dr. Barbara Uchanska-Ziegler whose mentoring lies at the core of every success that was achieved during the course of this study. She has had a profound effect on my intellectual and personal development over the period of my thesis. I express my deepest gratitude to Prof. Wolfram Saenger who brought me into the fascinating world of crystallography. His exemplary commitment and dedication to research has been an inspiration for me, and his guidance and support has been pivotal in my doctoral research. I extend my special thanks to Prof. Udo Heinemann who honored a last minute request to chair the thesis evaluation committee.

I wish to thank a number of other people who have been involved in my work over the last five years: Dr. A. Vahedi-Faridi, Dr. R. Misselwitz and Dr. A. Ziegler for their outstanding cooperation, support, collaboration and friendship; Prof. J.A. López de Castro for his constant mentorship, and for his passion and enthusiasm for HLA biology that has been a major stimulation for me; Ms. A. Zank, Ms. C. Schnick, Ms. C. Backhaus and Ms. C. Alings for their invaluable help, and for their participation in my experiments; my colleagues Pablo, Thomas and Chee Seng for creating a stimulating and jovial research environment in the lab, and for their friendship; Dr. A. Volz, Dr. Y. Roske, Dr. C. Petter, Dr. U. Müller, Dr. H. Huser, Dr. J. Ziegler and Dr. C. Rückert for their guidance and assistance in different stages of this work; Elena and Juan José for their enthusiastic collaboration, hospitality and friendship; and all other members and collaborators of the research groups of Prof. Ziegler and Prof. Saenger who have helped me on numerous occasions. I specially appreciate Pablo's crucial assistance in preparing the Zusammenfassung of this work. I gratefully acknowledge the financial support of the Volkswagen Foundation, the Senate of Berlin and the Deutsche Forschungsgemeinschaft.

I thank my friends, especially Mushu and Mario, for their emotional support and care that proved particularly vital during my initial days in Berlin, and my parents and siblings for their continued support and love.

SUMMARY

Major histocompatibility complex (MHC; human leukocyte antigen (HLA) complex in humans) class I molecules are responsible for pathogen detection and transplant rejection, and play a key role in immune surveillance by presenting antigens derived from endogenous proteins to effector cells such as cytotoxic T cells (CTL). The successful recognition of MHC molecules and the presented antigens by receptors located on effector cells such as T cell receptors (TCR) or killer cell immunoglobulin-like receptors (KIR), elicits appropriate immune responses by these cells. Despite extensive cellular, biochemical and structural studies of the interaction of peptide-MHC complexes (pMHC) with effector cells, the molecular basis for these interactions is still insufficiently understood. The major focus of this doctoral work was to study the conformational variability of MHC class I molecules due to polymorphism, differences in the residues of the bound peptides, post-translational modification of the bound peptides and ligand binding, and to relate the variability with the relevant biological functions of the MHC class I molecules.

In the first part of the work, a comparative analysis of peptide presentation by two human disease-associated MHC subtypes, HLA-B14 and HLA-B27, was performed with the aim of understanding the role of MHC polymorphism in peptide presentation by distantly related MHC alleles. The crystal structures of the common self-ligand pCatA (IRAAPPPLF, derived from cathepsin A) in complex with B*1402, B*2705 and B*2709 show the peptide bound in nearly identical conformations by the three HLA-B subtypes, whereas the crystal structures of the viral-ligand pLMP2 (RRRWRRLTV, derived from Epstein-Barr virus latent membrane protein 2) in complex with B*1402, B*2705 and B*2709 reveal that the viral peptide is bound in drastically different conformations by all three HLA-B subtypes. The similarities in conformations of pCatA in the three HLA-B subtypes suggest that TCR of alloreactive CTL may find similar docking points on the three pCatA complexes, whereas due to the differential binding of pLMP2 to the three subtypes, TCR will likely be unable to find similar docking points on the three pLMP2 complexes. These results provide a structural basis for T cell alloreactivity due to similarities in binding modes of common peptide ligands by different MHC molecules.

In the second part of this work, the structures of the HLA-B*2705 molecule presenting a self-peptide pB27 (RRKSSGGKGGSY) derived from the cytoplasmic tail of the B*2705 molecule itself and a sequence-related *Chlamydia trachomatis*-derived peptide pCP (RRFKEGGRGGK) were determined to investigate the similarities in the conformations of the self and the bacterial peptides. Despite significant sequence similarity, these two peptides are presented by B*2705 in different conformations. Both peptides are bound relatively flexibly, but the pB27 peptide is presented in three distinct conformations whereas pCP is presented in a single, conventional conformation. Furthermore, there are indications of the existence of dynamics in the conformations of pB27, which may allow an intermediate conformation to overlap with the pCP conformation so as to permit “dynamic mimicry”. The conformational variability in presentation of the two sequence-related peptides by B*2705 may be relevant in the context of Chlamydia-induced Reactive Arthritis (ReA), which is an autoimmune condition believed to be caused due to CTL cross-reactivity between self- and bacterial peptides. In a related study, the effects of citrullination, a post-translation protein modification common in inflamed tissues, on the presentation of a self-peptide by the differentially disease-associated HLA subtypes B*2705 and B*2709 was studied.

In the third part of the work, a comparison of structural alterations in pMHC induced by the binding of recombinant antibodies with TCR-like specificity and natural ligand molecules such as TCR and KIR was first performed, which reveals subtle, systematic differences in unliganded and liganded pMHC structures that can be attributed to ligand-binding.

Furthermore, a method to embed pre-rendered 3D models of macromolecular structures into electronic files of portable document format (PDF) was devised which facilitates inclusion of 3D models in electronic publications, showing subtle structural details of macromolecules such as the dual conformation of the pVIPR peptide in the B*2705:pVIPR structure. This permits readers to gain a 3D understanding of the subject matter of an article without using any additional molecular visualization softwares.

The molecular analyses revealed, in addition to further insights, that certain water molecules conserved in different HLA class I molecules mediate crucial interactions between peptide and HLA heavy chain residues, and possibly render the structure the necessary flexibility to accommodate peptides with diverse sequences. The structural evidence for conformational dynamics of the B*2705-bound pB27 peptide provides the first example of dynamics in binding of a peptide to an MHC class I molecule and points to a potential connection between conformational flexibility and antigenic mimicry. The results outlined in this work provide a basis for studies on conformational variation of MHC class I molecules and their functional implications.

ZUSAMMENFASSUNG

Klasse I Moleküle des Haupthistokompatibilitätskomplexes (major histocompatibility complex (MHC); Humaner Leukozyten Antigen (HLA) Komplex beim Menschen) sind für die Erkennung von Krankheitserregern und die Abstoßung von Transplantaten von ausschlaggebender Bedeutung, und spielen bei der immunologischen Überwachung eine wichtige Rolle durch die Präsentation von Antigenen körpereigener Proteine gegenüber Effektor-Zellen wie zytotoxischen T-Zellen (CTL). Die erfolgreiche Erkennung von MHC-Molekülen mitsamt den von ihnen präsentierten Antigenen durch Membranrezeptoren von Effektorzellen wie T-Zellrezeptoren (TCR) oder Killerzell-Ig-ähnlichen Rezeptoren (KIR), lösen Immunreaktionen in diesen Zellen aus. Trotz umfangreicher zellulärer, biochemischer und struktureller Untersuchungen der Interaktionen von Peptid-MHC-Komplexen (pMHC) mit Effektorzellen, ist unser Verständnis über die molekulare Grundlage dieser Wechselwirkungen noch immer lückenhaft. Der Schwerpunkt dieser Doktorarbeit war es, die konformationelle Variabilität der MHC-Klasse-I-Moleküle durch ihren Polymorphismus, durch Unterschiede bei den Aminosäuren der gebundenen Peptide, durch post-translationale Änderungen der gebundenen Peptide und durch die Ligandenbindung zu untersuchen, und diese Variabilität mit relevanten biologischen Funktionen der MHC-Klasse-I-Moleküle in Verbindung zu bringen.

Im ersten Teil der Arbeit wurde eine vergleichende Analyse der Peptid-Präsentation zweier menschlicher Krankheits-assoziierter MHC-Subtypen (HLA-B14 und HLA-B27) durchgeführt. Diese Analyse hatte zum Ziel, die Rolle des MHC Polymorphismus bei der Präsentation von entfernt verwandten MHC Allelen zu verstehen. Die Kristallstrukturen des Selbstliganden pCatA (IRAAPPPLF, von Cathepsin A abgeleitet) im Komplex mit B*1402, B*2705 und B*2709 zeigen, dass das Peptid von den drei HLA-B-Subtypen in nahezu identischen Konformationen gebunden wird, während die Kristallstrukturen des viralen Liganden pLMP2 (RRRWRRLTV, von Epstein-Barr-Virus, *latent membrane protein 2,* abgeleitet) im Komplex mit B*1402, B*2705 und B*2709 belegen, dass das virale Peptid in drastisch unterschiedlichen Konformationen von den drei HLA-B-Subtypen gebunden wird. Die Ähnlichkeiten der pCatA Konformationen der

drei HLA-B-Subtypen deuten darauf hin, dass der TCR alloreaktiver CTL ähnliche Docking-Punkte bei den drei pCatA Komplexen nützt. Dies ist nicht der Fall für die drei pLMP2 Komplexe, die aufgrund der unterschiedlichen Bindung von pLMP2 an die drei Subtypen einem TCR wahrscheinlich keine ähnlichen Docking-Punkte bieten können. Diese Ergebnisse liefern eine strukturelle Grundlage für die T-Zelle-Alloreaktivität im HLA-B14/HLA-B27 System.

Im zweiten Teil dieser Arbeit wurden die Strukturen des HLA-B*2705 Moleküls mit dem Selbstpeptid pB27 (RRKSSGGKGGSY) aus dem zytoplasmatischen Schwanz des B*2705 Moleküls selbst und dem von *Chlamydia trachomatis* abgeleiteten Peptid pCP (RRFKEGGRGGK), bestimmt. Ziel hier war, mögliche Ähnlichkeiten in den Konformationen des körpereigenen und des bakteriellen Peptids zu untersuchen. Trotz bemerkenswerten Sequenzähnlichkeiten werden beide Peptide durch B*2705 in verschiedenen Konformationen präsentiert. Beide Peptide werden relativ flexibel gebunden, wobei das pB27 Peptid in drei verschiedenen Konformationen, pCP jedoch nur in einer einzigen, konventionellen Konformation präsentiert werden. Darüber hinaus gibt es Anhaltspunkte für die Existenz einer Konformationsdynamik bei pB27, die pCP-überlappende Konformationen erlauben könnte und damit „dynamische Mimikry“ ermöglichen würde. Die konformationelle Variabilität bei der Präsentation der beiden Sequenz-verwandten Peptide durch B*2705 könnte im Rahmen der Chlamydia-induzierten Reaktiven Arthritis relevant sein. Dabei handelt es sich um eine Autoimmunerkrankung, von welcher angenommen wird, dass sie auf CTL Kreuzreaktivität zwischen einem selbst- und dem bakteriellen Peptid beruht. In einer weiteren Studie wurden die Auswirkungen der Citrullinierung, einer in entzündeten Geweben häufigen post-translationalen Proteinmodifikation, auf die Präsentation eines Selbstpeptids durch die unterschiedlich krankheitsassoziierten HLA-Subtypen B*2705 und B*2709 untersucht.

Im dritten Teil der Arbeit wurde ein Vergleich der strukturellen Veränderungen bei einem pMHC durchgeführt, die durch die Bindung eines rekombinanten Antikörpers mit TCR-ähnlicher Spezifität und natürlichen Ligandenmolekülen (TCR und KIR) induziert werden. Diese Untersuchung zeigte subtile, jedoch systematische Unterschiede

zwischen *„unliganded"* und *„liganded"* pMHC Strukturen auf, die auf die Ligandbindung zurückzuführen sind.

Darüber hinaus wurde ein Verfahren zum Einbetten von 3D-Modellen von makromolekularen Strukturen in elektronische Dateien im Portable Document Format (PDF) entwickelt. Dieses Verfahren ermöglicht die Aufnahme von 3D-Modellen in elektronische Publikationen, die subtile strukturelle Details von Makromolekülen, wie z. B. die duale Konformation des Peptids pVIPR in der B*2705:pVIPR Struktur, zeigen können. Das erlaubt dem Leser ein 3D-Verständnis der im Artikel beschriebenen Strukturen zu gewinnen, ohne dass zusätzliche Software für molekulare Visualisierung notwendig ist.

Neben anderen Ergebnissen ergab die Analyse der untersuchten HLA Klasse I Strukturen, dass bestimmte Wassermoleküle, die in verschiedenen HLA-Klasse-I-Molekülen gebunden vorliegen, grundlegende Bedeutung für die Interaktion zwischen Peptid und Aminosäuren der schweren HLA Kette haben, und vielleicht der Struktur die notwendige Flexibilität ermöglichen, um Peptide mit unterschiedlichen Sequenzen aufzunehmen.

Die im Teil 2 beschriebene strukturelle Evidenz für eine konformationelle Dynamik des von B*2705-gebundenen pB27-Peptids stellt das erste Beispiel der Dynamik eines Peptids das, welches in MHC-Klasse-I gebundener Form vorliegt. Die gefundene Dynamik deutet auf eine mögliche Verbindung zwischen konformationeller Flexibilität und antigener Mimikry hin. Die in dieser Arbeit dargestellten Ergebnisse legen eine Grundlage für Studien über Konformationsänderungen von MHC Klasse I Molekülen, sowie über ihre funktionelle Bedeutung.

LIST OF PUBLICATIONS

1. Kumar P*, Vahedi-Faridi A*, Merino E, López de Castro JA, Volz A, Ziegler A, Saenger W, Uchanska-Ziegler B. Expression, purification and preliminary X-ray crystallographic analysis of the human major histocompatibility antigen HLA-B*1402 in complex with a viral peptide and with a self-peptide. Acta Crystallogr. Sect. F Struct. Biol. Cryst. Commun. (**2007**) 63, 631– 634

2. Kumar P*, Ziegler A*, Ziegler J, Uchanska-Ziegler B, Ziegler A. Grasping molecular structures through publication-integrated 3D models. Trends Biochem. Sci. (**2008**) 33, 408–412

3. Beltrami A*, Rossmann M*, Fiorillo MT, Paladini F, Sorrentino R, Saenger W, **Kumar P**, Ziegler A, Uchanska-Ziegler B. Citrullination-dependent differential presentation of a self-peptide by HLA-B27 subtypes. J. Biol. Chem. (**2008**) 283, 27189–27199

4. Kumar P*, Vahedi-Faridi A*, Saenger W, Ziegler A, Uchanska-Ziegler B. Conformational changes within the HLA-A1:MAGE-A1 complex induced by binding of a recombinant antibody fragment with TCR-like specificity. Prot. Sci. (**2009**) 18, 37– 49

5. Kumar P, Vahedi-Faridi A, Saenger W, Merino E, López de Castro JA, Uchanska-Ziegler B, Ziegler A. Structural Basis for T Cell Alloreactivity among Three HLA-B14 and HLA-B27 Antigens. J. Biol. Chem. (**2009**) 284, 29784 –29797

This is a cumulative dissertation primarily based on the above publications. In addition, the unpublished results of an ongoing analysis aimed at investigating the “Exceptional conformational plasticity of a dodecameric self-peptide bound by the HLA-B*2705 antigen” have also been included in chapter 3.

---

*Equal contribution

LIST OF ABBREVIATIONS

ABC (Transporter)	ATP-binding Cassette (Transporter)
APC	Antigen Presenting Cells
AS	Ankylosing Spondylitis
B*2705	HLA-B*2705
CD	Cluster of Differentiation
CD (Spectroscopy)	Circular Dichroism (spectroscopy)
CDR	Complementarity Determining Region
CTL	CD8+ T cells or cytotoxic T cells
CW	Conserved Water
DSC	Differential Scanning Calorimetry
ER	Endoplasmic Reticulum
FcRn	Neonatal Fc Receptor
FRET	Förster Resonance Energy Transfer
HC	Heavy Chain
HLA	Human Leukocyte Antigen
Ig	Immunoglobin
KIR	Killer Immunoglobin-like Receptor
MAGE-A1	Peptide with Sequence EADPTGHSY, Residues 161-169 of the Melanoma Antigen-encoding Gene - A1 molecule
MD (Simulations)	Molecular Dynamics (Simulations)
MHC	Major Histocompatibility Complex
NK (Cells)	Natural Killer (Cells)
NMR	Nuclear Magnetic Resonance
pB27	Peptide with Sequence RRKSSGGKGGSY, Residues 309–320 of the Cytoplasmic Tail of the HLA-B27 Molecule
pCatA	Peptide with Sequence IRAAPPPLF, Residues 2-10 of the Signal Sequence of Cathepsin A
pCP	Peptide with Sequence RRFKEGGRGGK, Residues 211-222 of the DNA Primase of *Chlamydia trachomatis*
PDF	Portable Document Format
pLMP2	Peptide with Sequence RRRWRRLTV, Residues 236-244 of Latent Membrane Protein 2 of Eppstein-Barr Virus
pMHC	Peptide:MHC Complexes
PTM	Post-translational Modification
pVIPR	Peptide with Sequence RRKWRRWHL, Residues 400-408 of Vasoactive Intestinal Peptide Type I Receptor
ReA	Reactive Arthritis
SpA	Spondyloarthropathy
sTCR	Soluble T cell Receptor
TAP	Transporter Associated with Antigen Processing
TCR	αβ-T cell Receptor
TNF	Tumor Necrosis Factors
β_2m	β_2-microglobulin

TABLE OF CONTENTS

1. Introduction

1.1 The Major Histocompatibility Complex

The major histocompatibility complex (MHC; human leukocyte antigen (HLA) complex in humans) is a family of genes which plays a decisive role in the immune system of vertebrates (Fig.1.1). It is involved in the recognition of foreign substances, autoimmunity, organ and graft transplant rejection and reproduction (Klein 1986, Ziegler et al. 2005).

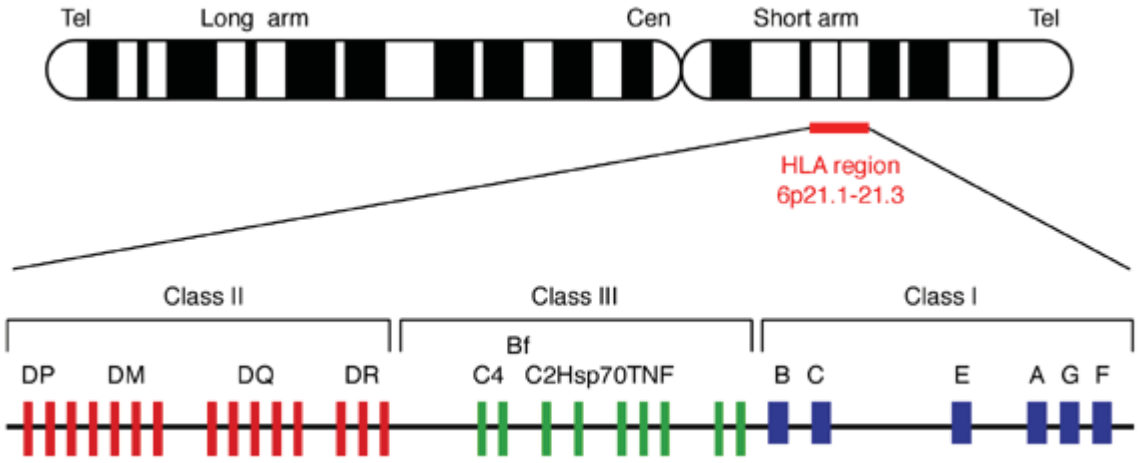

FIGURE 1.1.Gene map of the HLA locus on chromosome 6. The HLA region spans about 4 megabases of DNA on the short arm of chromosome 6 from 6p21.1 to p21.3. The class II (red), class III (green) and class I (blue) genes are located from the centromeric (Cen) to the telomeric (Tel) end as indicated. The class I locus contains the classical genes, A, B and C, and the non-classical genes E, F and G. (Adapted from Mehra and Kaur 2003)

Research on MHC molecules was initially aimed at understanding their role in graft rejection following tissue or organ transplants, but it later became clear that the primary function of MHC antigens is to provide protection against pathogens (Horton et al. 2004). The process of detection and control of pathogens involves sophisticated pathways in which MHC molecules present endogenous and exogenous antigens to T cells (Fig. 1. 2). The class I molecules (HLA-A, -B, -C, -E, -F and -G antigens) are found on most nucleated cells, are involved in pathogen detection and organ/graft rejection, and present peptides derived mostly from endogenous proteins (e.g. self-proteins, proteins produced within the cell after a viral infection etc.) to effector cells such as CD8+ T cells (“cytotoxic” T cells, CTL) (Klein 1986). The class II molecules (HLA-DR, -

DQ and -DP antigens) are found only on professional antigen presenting cells (APC) such as dendritic cells, macrophages and B-cells, and present peptides that are primarily derived from exogenous proteins (e.g. bacterial proteins engulfed by endocytosis or phagocytosis by APC) to CD4+ T cells (“helper” T cells), which may trigger appropriate immune responses such as recruitment of phagocytes, or antibody production following B cell activation (Klein 1986, Murphy et al. 2008). Both class I and class II molecules show an exceptional degree of polymorphism which enables them to present different types of peptides, helping the immune system to respond to many different types of intracellular and external agents and infections (Madden 1995). The class III molecules are a diverse group of proteins, often occurring in soluble form that participate in cell lysis and mediate inflammatory responses (Beck and Trowsdale 2000). This group includes complement proteins, inflammatory cytokines, tumor necrosis factor (TNF), and heat shock proteins. There is much less polymorphism in class III molecules in comparison to class I and II molecules, or the many framework genes of the MHC class I and II regions (Horton et al. 2004).

1.2 Antigen presentation by MHC class I molecules

Antigen presentation by MHC class I molecules plays crucial roles in innate and adaptive immune systems as a central event in self-nonself differentiation. In particular, two key components of immune surveillance, T cells and natural killer (NK) cells, regulate their involvement in cytotoxic processes based on antigen presentation by these MHC molecules. The purpose of immune surveillance is to recognize and destroy abnormal cells, e.g. those infected with pathogens or that have turned malignant. T cells and NK cells possess specific ability to recognize nonself and self peptides, respectively, presented by MHC molecules and this ability is used to identify abnormal cells before their lysis (Lanier 2005, Smith-Garvin et al. 2009). As some infections and malignancies involve concomitant down-regulation of MHC expression on the cells, the specificity of NK cells for self-peptides enables their participation in both innate and adaptive immune systems while T cells are primarily involved in the adaptive immune system (Panda et al. 2009).

During antigen presentation, degradation products of proteins are loaded onto MHC class I molecules and the resulting peptide:MHC complexes (pMHC) are transported to the cell surface where they are presented to receptors located on effector cells such as αβ-T cell receptor (TCR) of T cells or killer immunoglobulin (Ig)-like receptor (KIR) of NK cells (Jensen 1999). The MHC-bound peptides are recognized by these receptors in a peptide- and MHC-restricted fashion and trigger appropriate immune responses by effector cells. The pathways of peptide loading on MHC and pMHC transport to the cell surface are described in Figure 2.

MHC class I molecules present peptides derived mainly from endogenous proteins (York and Rock 1996) to effector cells during immune surveillance (Fig. 1. 2, DeFranco et al. 2007). Although peptides derived from exogenous proteins are also known to be sometimes processed and presented by MHC class I molecules (Groothuis and Neefjes 2005, Shen and Rock 2006), their primary role is presenting peptides derived from endogenous proteins and the following description of the mechanism of antigen presentation by MHC class I molecules will primarily focus on endogenous proteins.

Processing of endogenous unwanted proteins and defective ribosome products begins after a covalent conjugation with ubiquitin that targets the proteins for selective degradation by the proteasome, a multi-subunit cylindrical protease assembly in the cytosol, to produce short peptides that can be transported into the endoplasmic reticulum (ER) for complexation with MHC (Hershko and Ciechanover 1998). Pathogen infections upregulate γ-interferon levels in the cell, which in turn induce production of “immunoproteasome” β-subunits such as LMP2, LMP7 and MECL-1 that replace specific, closely related constitutive β-subunits in the proteasome assembly to tune its specificity to produce peptides with optimal size and composition for binding to MHC class I molecules (Pamer and Cresswell 1998, Voges et al. 1999). The mechanism of peptide generation is only partly understood, and it has been noted that ubiquitin-conjugation is not always essential for generation of peptides suitable for presentation by MHC class I molecules (Pamer and Cresswell 1998). The peptides produced by the proteasome are transported from the cytosol into the ER by the TAP (transporter associated with antigen processing) transporter, an ABC (ATP-binding cassette)

transporter present in the ER membrane in the form of a heterodimer of the two subunits TAP1 and TAP2 (Solheim 1999). Evidence suggests that some of the imported peptides are further processed for optimal binding to MHC class I molecules by proteases present in the ER such as ERAP1 and ERAP2. The chaperone tapasin aids in loading of peptides into the binding grooves of MHC class I molecules (Raghavan et al. 2009). However, there is still a limited understanding of peptide processing within the ER. Processing of exogenous antigens taken up by APC by the general mechanisms of endocytosis and phagocytosis for presentation by MHC class I molecules is not understood in any detail, but it is believed that cellular substrates of proteasomes and preprocessed peptide antigens are involved (Norbury et al. 2004, Shen and Rock 2004, Blachère et al. 2005, Raghavan et al. 2009). Some exogenous soluble proteins are also known to be directly trafficked to the ER during cross-presentation (Ackerman et al. 2005).

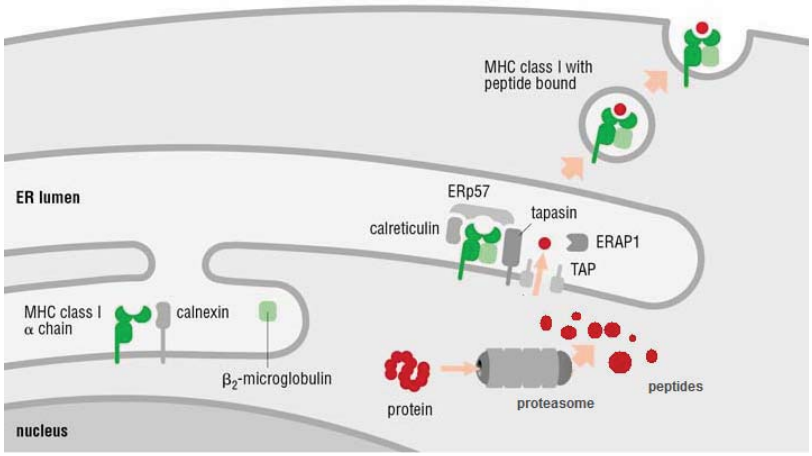

FIGURE 1.2. Overview of peptide presentation by MHC class I molecules. The newly synthesized MHC class I HC undergoes a series of chaperonemediated interactions in the lumen of the ER to form a part of the multicomponent MHC class I peptide loading complex which generally includes calreticulin, ERp57, TAP1, TAP2 and tapasin in addition to HC and β_2m. Meanwhile in the cytosol, endogenous proteins are degraded by the proteasome into peptides, some of which are imported into the lumen of the ER by TAP transporters and loaded in the peptide binding groove of HC by the peptide loading complex to form a pMHC complex. The pMHC complexes are then shuttled via the secretory pathway to the cell surface, where they are scanned by the receptors located on effector cells. (Figure adapted from DeFranco et al. 2007, includes some modifications)

The assembly of MHC class I molecules involves a series of interactions in the lumen of ER, which may vary between different MHC subtypes (Pamer and Cresswell 1998). The newly synthesized and partially folded HC interacts with the chaperone calnexin, followed by association of β_2m with HC and simultaneous disassociation of calnexin

(Cresswell et al. 2005). The HC-β_2m complex further interacts with calreticulin, TAP, tapasin and ERp57 to form the MHC class I peptide loading complex, which facilitates loading of the peptides transported into the ER lumen by the TAP transporter into the peptide binding groove of the “empty” MHC molecule (Cresswell et al. 2005, Dong et al. 2009, Raghavan et al. 2009). When a peptide binds to an “empty” MHC molecule with sufficiently high affinity, a stable pMHC complex is formed which dissociates from the peptide loading complex, exits the ER, and is transported to the cell surface via transport vesicles and the Golgi apparatus where it is surveyed by receptors located on effector cells (Cresswell et al. 2005).

Much effort has been devoted to studying the molecular determinants of pMHC recognition by the receptors of effector cells, but the details of the involved interactions are only partly understood (Rudolph et al. 2006, Chen et al. 2009). The recognition of pMHC and associated signaling events occur in a localized environment on T cells and require the coordinated activities of several TCR-associated molecules, including the coreceptors CD3 (cluster of differentiation 3) and CD8 (or CD4 in case of MHC class II molecules), and other costimulatory receptors (Rudolph et al. 2006). The multimolecular complex of pMHC, TCR, CD8 and CD3 (Fig. 1. 3, Chen et al. 2009) is believed to hold the key to understanding the biochemical principles governing TCR recognition of pMHC and the structural determinants governing self-nonself discrimination by TCR. The interactions between pMHC and TCR, pMHC and CD8 and TCR and CD3 have been analyzed in several biochemical studies, but the molecular determinants of pMHC recognition by T cells have not yet been identified (Rudolph et al. 2006, Chen et al. 2009). The interactions of pMHC with its two direct binding partners, TCR and CD8, have been mapped through structural and biophysical analyses, which revealed remarkable variability in these interactions, especially in the case of pMHC-TCR interactions (Cole and Gao 2004, Pecht and Gakamsky 2005, Rudolph et al. 2006, Chen et al. 2009). The structural details of the interactions of pMHC with TCR and CD8 will be discussed in the next section.

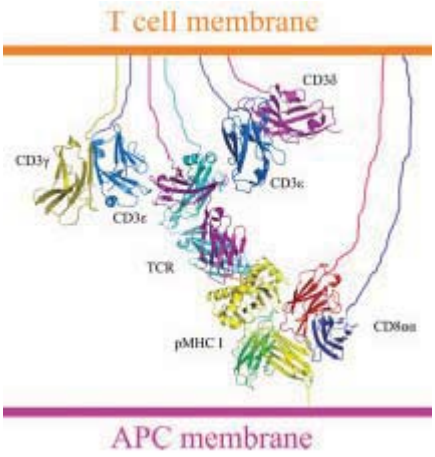

FIGURE 1.3. Schematic representation of the multi-molecular interaction between pMHC, TCR, CD8 and CD3 molecules during antigen presentation to T cells by MHC class I molecules. The interactions are based on superposition of separate models of HLA-A2:CD8, TCR:HLA-A2 and CD3. (Adapted from Chen et al. 2009)

As in case of cytotoxic T cells, the cytotoxic activity of NK cells is crucial for the destruction of certain virally infected and malignant cells (Orange and Ballas 2006). In addition to their valuable role in the innate immune response, they also participate in the development of specific adaptive immune responses through production of chemokines and cytokines, such as interferon γ or TNFα, and by activating dendritic cells (Krzewski and Strominger 2008). A variety of inhibibory or activating receptors can mediate the cytolytic activity of NK cells by binding specific ligands, which for some receptors are classical or non-classical MHC class I molecules, on target cells (Cerwenka and Lanier 2001, Farag et al. 2002). The recognition by the activation receptors of ligands expressed on the surface of target cells triggers a cytotoxic response leading to cytolytic granule release resulting in the lysis of the target cell, whereas interaction of inhibitory receptors with ligands negatively regulates NK cell activity (Krzewski and Strominger 2008).

KIR are a family of receptors located on the surface of NK cells that mostly bind MHC class I or class I-like molecules as ligand and can be inhibitory or activating. This property is based, respectively, on whether KIR contain a long cytoplasmic tail with the immune tyrosine-based inhibitory motifs, or a short cytoplasmic tail lacking the inhibitory motifs (Vilches and Parham 2002). Recognition of pMHC by KIR is MHC subtype specific, and to a lesser extent also peptide selective and specific (Vilches and Parham 2002, Lanier 2005). The NK cell signaling mechanisms utilizing KIR-MHC interactions

remain to be deciphered, however the binding of two KIR molecules, KIR2DL2 and KIR2DL1, with their cognate MHC class I molecules, HLA-Cw3 and HLA-Cw4 respectively, have been studied by X-ray crystallography (Boyington et al. 2000, Fan et al. 2001) and will be discussed in the next section.

1.3 Architecture of MHC class I complex

MHC class I complexes are composed of three polypeptide chains – the HC of about 360 residues that spans the membrane bilayer, the light chain β_2m of 99 residues and a peptide of 8-12 residues length which is usually imported into the ER from the cytosol by the TAP transporters (Madden 1995, Peaper and Cresswell 2008). The extracellular domain of HC of about 275 residues is non-covalently attached with β_2m and the peptide (Fig. 1. 4). The HC is divided into three structural domains, called α1, α2 and α3 domains, consisting of about 90 residues each (Fig. 1. 4). The α3 and β_2m domains are closer to the membrane and show sequence and structural similarity to constant domains of Ig molecules, while the α1 and α2 domains face away from the membrane and have no similarity with Ig-molecules (Madden 1995). The α1 and α2 domains are extremely polymorphic and are responsible for the crucial ability of MHC molecules to bind a large variety of peptides.

Both the α1 and α2 domains consist of four anti-parallel β strands and an α-helix (Fig. 1. 4B). In case of the α2-domain, the α-helix has a 'kink' at positions 150-152 near the N-terminus of the helix. The α1 and α2 domains form a binding groove containing six 'binding pockets', termed A-F, that are responsible for accommodating residues of the bound peptides (Section 4.2.1, Fig. 1E, Kumar et al. 2009b).

MHC class II complexes also have a very similar structure, as do CD1 molecules, neonatal Fc receptor FcRn, human hemochromatosis protein HFE and some viral homologs (Wilson and Bjorkman 1998). Thus, the MHC-fold can also be employed by the host immune system to perform functions other than peptide presentation to effector cells, while it may have developed

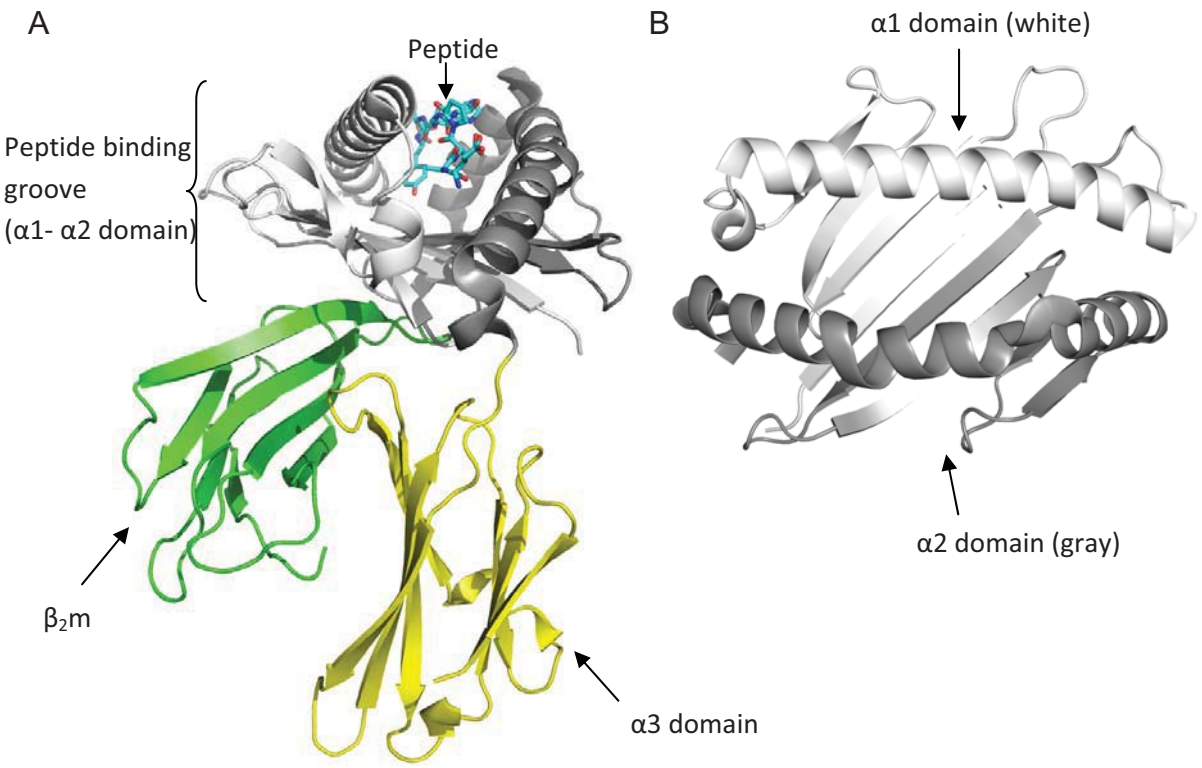

FIGURE 1.4. Schematic representation of a pMHC complex (A) and a close-up of its peptide binding groove (B). The α1 (white), α2 (gray), and α3 (yellow) domains as well as β_2m (green) are shown in cartoon representation, and the peptide (cyan) is shown in stick representation. The molecule is HLA-A1:MAGE-A1 (Kumar et al. 2009b).

in pathogens in response to innate immune defence of the host especially by NK cells (Wilson and Bjorkman 1998, Arase et al. 2002, Adams et al. 2007).

1.4 Docking of CD8, TCR and KIR on pMHC

As discussed previously, the recognition by T cells of antigens presented on APC surface involves docking of CD8 and TCR on pMHC. While a single structure of this tri-molecular complex has not yet been determined, the details of the interactions of pMHC with CD8 and TCR have been separately characterized by structural studies (Gao et al. 1997, Rudolph et al. 2006, Chen et al. 2009).

The CD8 coreceptor is expressed either in homodimeric (CD8αα) or in heterodimeric (CD8αβ) form on the T cell surface and both dimers can serve as a coreceptor for T cell activation and differentiation by binding to pMHC in an MHC-dependent, but peptide-

independent manner, although their cellular distributions are distinct and their ligand binding partners are unique (Chang et al. 2005). Structural and biochemical analyses of the complexes of pMHC with CD8αα and CD8αβ have shown that the binding of CD8 to pMHC mainly involves the α3 domain, β_2m and, to a lesser extent, the α2 domain (Chen et al. 2009, Wang et al. 2009).

The docking of αβTCR on pMHC is critical for initiation and propagation of a cellular immune response, as well as the generation and maintenance of the body's T-cell repertoire (Armstrong et al. 2008). While the structural and biochemical principles governing the binding of TCR on pMHC and the signaling mechanism are not yet fully understood, many common features have emerged from the studies undertaken so far (Garcia and Adams 2005, Rudolph et al. 2006, Armstrong et al. 2008, Collins and Riddle 2008). TCRs bind pMHC in a diagonal to near-orthogonal (relative to the peptide binding groove) docking mode through their highly variable CDR (complementarity determining region) loops located in the variable domains of the α and β chains. The majority of the conserved contacts between the TCR and the α1-α2 helices of pMHC are formed by CDR 1 and 2, while the peptide residues are primarily contacted by CDR3 loops, which also have the largest genetic variability and show induced-fit of largest magnitude among the three CDR loops upon pMHC binding (Rudolph et al. 2006, Armstrong et al. 2008). The residues in the middle regions of the α1- and α2-helices of pMHC are the most common targets for TCR docking, with residues 65 and 155 most frequently contacted by TCR (Fig. 1. 5) (Rudolph et at. 2006).

There are only two reports available of successful structural studies of the interactions between KIR and their ligand pMHC molecules (Boyington et al. 2000, Fan et al. 2001). The structures of KIR2DL1:HLA-Cw4 and KIR2DL2:HLA-Cw3 reveal important features of KIR (having two Ig-like domains in their extracellular region) docking on their cognate pMHC molecules (Jones 2001).

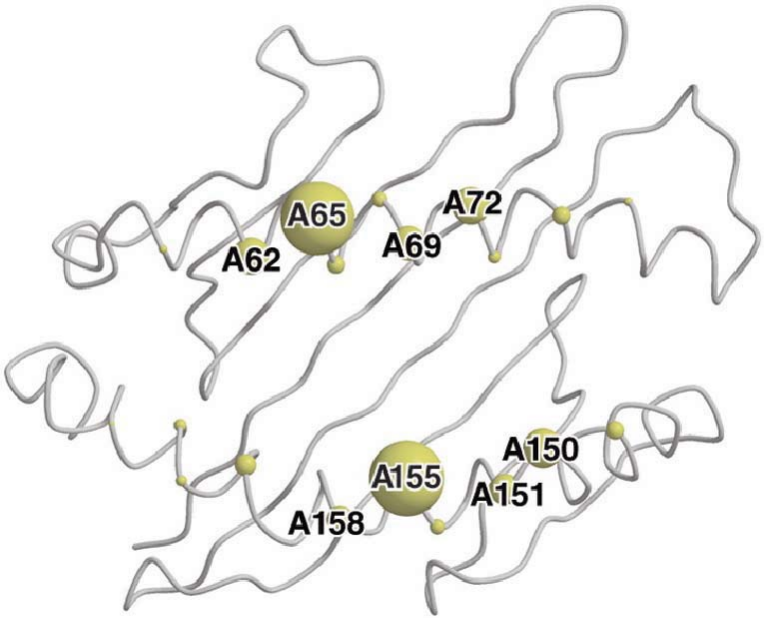

FIGURE 1.5. MHC class I residues most commonly contacted by αβ TCR. The spheres are drawn so that their diameters are in proportion to their numbers of contacts to TCR (so that the large spheres represent residues with the most contacts). (Adapted from Rudolph et al. 2006)

The KIR2DL1 and KIR2DL2 molecules (collectively 'KIR2D molecules') have two tandem Ig-like domains, designated D1 and D2, that are connected by a linker of three to five amino acids. The angle between the D1 and D2 domains is different in each of the known KIR2D structures (ranging from 55° to 84°), indicating the potential for significant variability of the interdomain angle, despite a relatively conserved set of hydrophobic residues in the hinge region and a large buried surface area of approximately 1000 $Å^2$ between D1 and D2 (Natarajan et al. 2002, Vilches and Parham 2002). The binding of KIR2D molecules to their pMHC ligands involves interactions between the six loops near the interdomain hinge region and the α1 and α2 helices and the C-terminal portions of the bound peptides of pMHC (Fig. 1. 6) (Boyington et al. 2000, Fan et al. 2001).

The 'footprints' of both KIR2D on pMHC are similar, as are the buried solvent accessible surface areas (around 1500 $Å^2$) and the shape complementarity Sc values (around 0.7) for the two complexes, but residue-to-residue interactions differ (Fan et al. 2001, Natarajan et al. 2002). The polymorphic residue 80 of the α1 helix of pMHC determines the allelic specificity of the interaction of the KIR2D molecules with HLA-C subtypes (Fan et al. 2001, Natarajan et al. 2002). The docking of KIR2D molecules near the C-terminal portion of peptides is dependent on the peptide residues in that region, and the

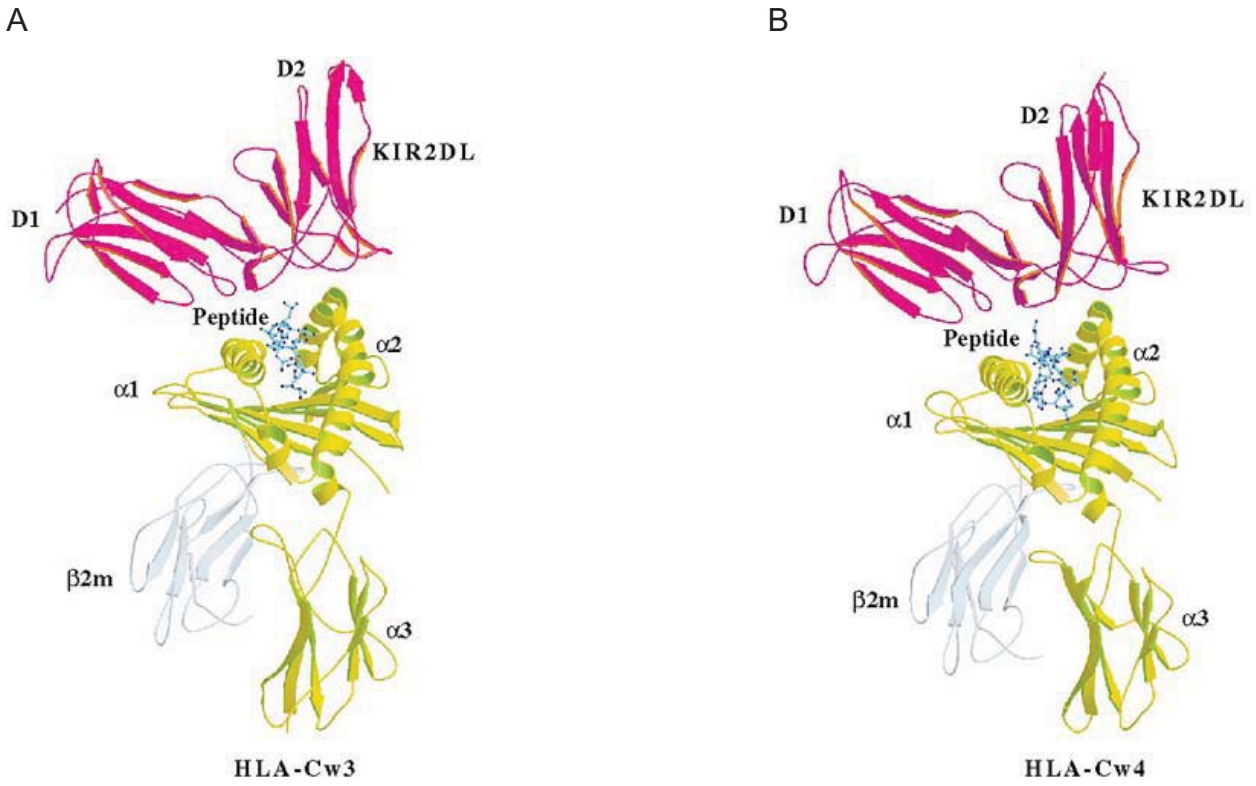

FIGURE 1.6. Crystal structures of (A) KIR2DL2:HLA-Cw3 and (B) KIR2DL1:HLA-Cw4 complexes. Both KIR2D molecules dock in similar binding modes near the C-terminal ends of the peptide binding grooves of their cognate pMHC molecules. (Adapted from Natarajan et al. 2002)

residue at peptide position Ω–1 (p8 in nonamers) is specially crucial for the docking. In the KIR2DL1:HLA-Cw4 structure there are no direct hydrogen bonds formed between the KIR2D and pLys8 of the peptide, but the KIR2D surface around pLys8 is overall negatively charged, and thus substitution of pLys8 with a negatively charged residue abrogates KIR-pMHC binding due to electrostatic repulsion (Fan et al. 2001, Vilches and Parham 2002). In the KIR2DL2:HLA-Cw3 structure, the main chain amide nitrogen of pAla8 forms a hydrogen bond with Gln71 of KIR2DL2, which explains why substitution of pAla8 with much larger amino acids such as lysine or tyrosine abolishes binding to the KIR2D and why smaller amino acids are preferred for KIR2D-binding at this position (Boyington et al. 2000, Natarajan et al. 2002, Vilches and Parham 2002).

1.5 Recombinant antibodies with TCR-like specificity

pMHC-directed agents that target the antigen-MHC complex in an antigen- and MHC-specific manner can be used for direct visualization and quantifcation of pMHC as well as targeted delivery of toxins and drugs (Denkberg and Reiter 2006, Ziegler et al. 2007).

A suitable agent for these applications would be a soluble TCR (sTCR) with specificity for the pMHC complex. However, due to the low affinity of TCR-pMHC recognition, detection of targets in normal assay conditions would be possible only if the affinity of sTCR could be increased at least 100-fold by employing in vitro affinity maturation procedures that are cumbersome and often unsuccessful (Denkberg and Reiter 2006, Ziegler et al. 2007). The second alternative is recombinantly produced antibodies that bind pMHC in an antigen- and MHC-specific manner, resulting in TCR-like specificity. The higher affinity and relative stability of these antibodies make them ideal for the above applications and they are being vigorously researched (Denkberg and Reiter 2006).

The complex of HLA-A1 with a melanoma-associated antigen (MAGE)-A1-derived peptide (HLA-A1:MAGE-A1) is a tumor marker which has been used to define target cells in anti-tumor immuno- and gene- therapy (Maeurer et al. 1996, de Vrij et al. 2008). The Fab fragment of an affinity-matured variant of an antibody, called Fab-hyb3, directed against the HLA-A1:MAGE-A1 complex (Chames et al. 2000) was crystallized in complex with HLA-A1:MAGE-A1 to study the structural determinants of peptide specificity of MHC- and peptide-restricted antibodies (Hülsmeyer et al. 2005). More recently, the interactions between the Fab-fragment of another such ‘TCR-like’ antibody and its cognate pMHC has been studied by X-ray crystallography (Mareeva et al. 2008). Both these studies reveal that the Fab fragments bind with pMHC in TCR-like diagonal binding modes and have similar CDR usage as TCR for docking on pMHC (Hülsmeyer et al. 2005, Rudolph et al. 2006, Mareeva et al. 2008). The striking similarities in binding behavior of antibody Fab fragments and TCR with pMHC suggest that the antibodies may have potential uses as TCR surrogates for biochemical and clinical applications.

1.6 Antigen presentation and autoimmunity

MHC molecules present peptides derived from self as well as nonself sources, while it is desired that an immune response against APC is mounted by T cells only in cases where the presence of a foreign entity is signaled through the presentation of a nonself peptide. This crucial self-nonself discrimination ability is acquired by T cells during development in the thymus through a two-step process.

T cells with αβTCR originate in the bone marrow in the form of hematopoetic progenitor cells and develop in the thymus into double-positive thymocytes, i.e. $CD4^+$ $CD8^+$ T cells, before undergoing thymic selection. The first step, 'positive selection', occurs in the cortex of thymus, where double positive thymocytes that bind with MHC molecules with moderate affinity survive, while those that bind with high affinity or do not bind at all are subject to apoptosis (Starr et al. 2003, Ziegler et al. 2009b). The details of this selection step are not known in exact details and the traditional belief that this selection step involves presentation of self-peptides by MHC molecules (Janeway 2001, Starr et al. 2003) has been questioned in the light of recent discoveries (Ziegler et al. 2009b). The T cells surviving positive selection are transported into the medulla of the thymus to undergo the second selection step, 'negative selection'. The purpose of negative selection is to test the T cells for reactivity against self peptides presented by MHC molecules and only those cells that do not react with an affinity higher than a certain threshold survive this selection (Liu 2006). The T cells emerging from this step are generally capable of self-nonself discrimination and have developed specificity for either class I or class II MHC molecules by losing either $CD4^+$ or $CD8^+$ coreceptors.

It has been recently pointed out that also non-self peptides might reach the thymus via bloodstream or as part of cells that present them (Bosco et al. 2009), however their participation in thymic selection remains to be studied. It is widely believed that the entire thymic selection process is self-referential, i.e. the selection steps involve almost exclusively self peptides. Thus the possibility of survival of some self-directed T cells that may react with the host's own cells in peripheral tissues does exist. Such self-reactive T cells are kept in check by several immune cells that have suppressive or

immunomodulatory properties. Regulatory T cells are a prominent example of such cells that have a dedicated role of suppressing self-reactive immune response (Josefowicz and Rudensky 2009, Riley et al. 2009). Despite these sophisticated regulatory frameworks, a fraction of the total CTL population is known to be cross-reactive between self and nonself antigens (Holler and Kranz 2004, Frankild et al. 2008). The basis for CTL crossreactivity is not yet known, but it is proposed that molecular or antigenic mimicry between self and nonself constitutive peptide ligands of an MHC molecule may result in the crossreactivity of some of the CTL directed against the nonself peptide with the self peptide, thereby leading to autoimmunity, tissue injury and inflammation (Benjamin and Parham, 1990, Gaston 2006, López de Castro 2007).

Autoimmune diseases are characterized by an immune response against cells and tissues belonging to oneself. Many autoimmune diseases are chronic, degenerative and may even be life-threatening. They affect a small, but sizeable fraction of the population. Known autoimmune diseases include diabetes mellitus type I, coeliac disease, multiple sclerosis, and a spondyloarthropathy (SpA) such as reactive arthritis (ReA), while ankylosing spondylitis (AS) is suspected to be an autoimmune disease (Caillat-Zucman 2009). Many inflammatory diseases have been found to be associated with different HLA subtypes, of which the association of spondyloarthropathies, in particular AS, with HLA-B27 is the strongest (Brewerton et al. 1973a, 1973b, Schlosstein et al. 1973, López de Castro 2007).

The molecular mechanisms underlying the association between HLA alleles and inflammatory diseases are not yet understood. Several hypotheses have attempted to explain the association of HLA-B27 with spondyloarthropathies including the two most popular theories of “the HLA-B27 misfolding hypothesis” and “the arthritogenic peptide hypothesis” (Benjamin and Parham 1990, Bowness 2002, Gaston 2006, Colbert et al. 2009). The misfolding hypothesis suggests that the higher propensity of HLA-B27 to misfold after synthesis could cause ER overload with misfolded proteins resulting in the generation of unfolded protein response (Turner et al. 2005). The arthritogenic peptide hypothesis, on the other hand, attempts to explain the disease causing mechanism of HLA-B27 through its main biological role of peptide presentation to T cells. It proposes

that CD8+ T cells developed in response to a microbial infection (and thus directed against pathogen-derived peptides) may also cross-react with self-peptides that share structural and/or electrostatic features with the pathogen-derived peptide against which the T cell is directed (Benjamin and Parham 1990). In other words, molecular mimicry, i.e. similarity in overall shape as well as charge distribution for an interaction surface (Lang et al. 2002), of pathogen-derived peptides and self-peptides may lead to a T cell response against self-peptides, thereby perpetuating an autoimmune reaction.

This theory is supported by observations such as the presence of the same antigen recognition motif in CDR3 of TCR derived from different HLA-B27-positive SpA patients (May et al. 2002), suggesting that these different patients could have developed these T cells in response to the same pathogen-derived antigen. In a previous structural and cellular study (Hülsmeyer et al. 2004, Fiorillo et al. 2005), a self and nonself pair of HLA-B27-ligands were found to have striking structural and electrostatic similarities with each other when bound to a disease associated molecule, HLA-B*2705 (B*2705 in short). The HLA-B27 subtypes B*2705 and B*2709 show differential association with SpA: B*2705 is strongly associated with SpA while B*2709, which differs from B*2705 at the single amino acid position 116 by an Asp to His exchange, is not or only weakly associated with SpA, specifically AS and ReA (D'Amato et al. 1995, Siala et al. 2009). While the search for arthritogenic peptides involved in AS and ReA is still ongoing, two self-nonself peptide pairs have been identified that seem to be promising candidates for molecular mimicry in the context of AS and ReA association of B*2705. The self-peptide pVIPR (RRKWRRWHL, derived from vasoactive intestinal peptide type I receptor, residues 400-408) and the sequence-related viral peptide pLMP2 (RRRWRRLTV, derived from latent membrane protein 2 of Eppstein-Barr Virus, residues 236-244) appear to be potential candidates for molecular mimicry in the context of the role of B*2705 in AS pathogenesis (Brooks et al. 1993, Fiorillo et al. 2000). The molecular mimicry of a second self-nonself peptide pair (pB27 peptide [RRKSSGGKGGSY], derived from the cytoplasmic tail of the HLA-B27 molecule itself, residues 309–320, and pCP peptide [RRFKEGGRGGK], from DNA primase of *Chlamydia trachomatis*, residues

211-222) is proposed to be involved in the pathogenesis of ReA (Ramos et al. 2002, Cragnolini and López de Castro 2008).

The crystal structure of B*2705 in complex with pVIPR showed that the pVIPR peptide is bound by B*2705 in two conformations (Fig. 1. 7) - termed p4α and p6α, based on the position of the only residue in the nonameric peptide that exhibit φ/ψ torsion angles in the α-helical region of the Ramachandran plot (Hülsmeyer et al. 2004). The p6α conformation is facilitated by salt-bridges between pArg5 and Asp116, the only polymorphic residue between B*2705 and B*2709. The viral peptide pLMP2 is bound by B*2705 in a single p6α conformation and shares striking similarity with pVIPR only, when it assumes the p6α conformation (Fig. 1. 7) (Fiorillo et al. 2005). The crystal structures of B*2709 in complex with these two peptides reveal that both peptides are bound in single, drastically different p4α conformations (Fig. 1. 8) (D'Amato et al. 1995, Hülsmeyer et al. 2004, Fiorillo et al. 2005). In combination with functional studies, these

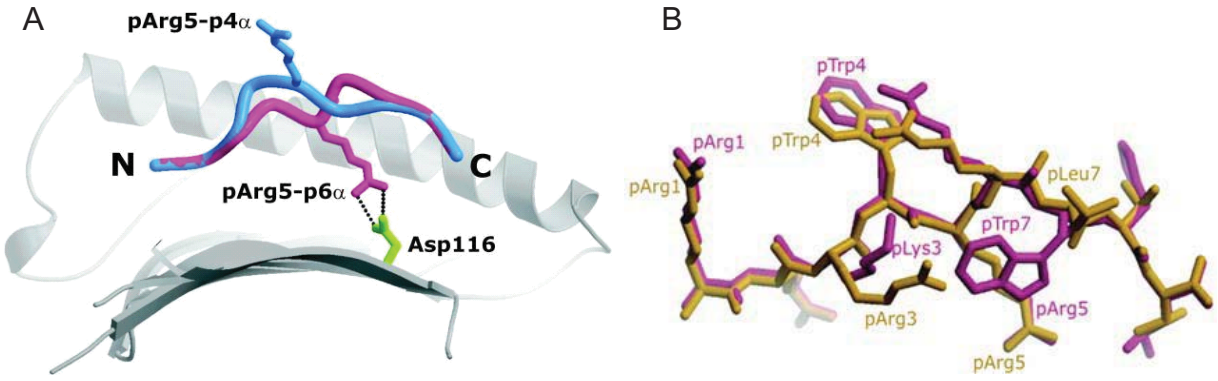

FIGURE 1.7. (A) The dual conformation of the pVIPR peptide in the B*2705:pVIPR structure. Only the p6α conformation exploits the presence of the polymorphic residue 116. (B) Overlay of the p6α conformation of pVIPR in the B*2705:pVIPR structure on the conformation of the pLMP2 peptide in the B*2705:pLMP2 structure. (Adapted from Wucherpfennig 2004 and Fiorillo et al. 2005)

structural results suggest that molecular mimicry of pLMP2 and pVIPR is more likely in the case of B*2705-positive individuals than in case of B*2709-positive individuals, which correlates with the disease association of these two HLA-B27 subtypes (Hülsmeyer et al. 2004, Fiorillo et al. 2005).

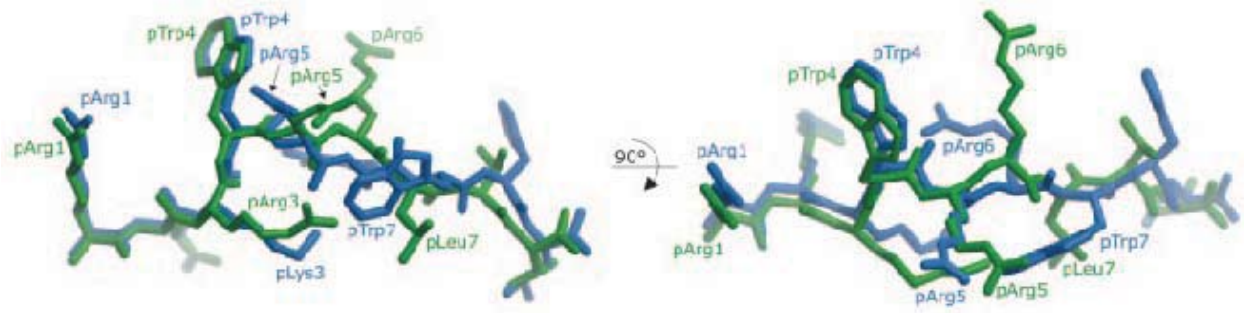

FIGURE 1.8. Overlay of the conformations of pVIPR (green) and pLMP2 (blue) as presented by the B*2709 molecule. The peptides are shown from the side of the α2-helix (left) or from the "top" of the complex (right). Although both peptides assume the p4α conformation, molecular mimicry is largely absent. (Adapted from Fiorillo et al. 2005)

Cellular studies (Fiorillo et al. 2000) have shown that HLA-B27-autoreactive CTL lines are more commonly found in B*2705-positive patients with AS than in B*2705-positive healthy individuals, while such autoreactive CTL are only rarely found in B*2709 positive individuals (Fiorillo et al. 2000). In another study, four pLMP2/pVIPR cross-reactive CTL lines (two CTL lines obtained from a B*2705-positive AS patient, and two CTL lines obtained from a B*2709-positive individual) were tested for their reactivity toward pLMP2 and pVIPR at low concentrations (Fiorillo et al. 2005). The CTL derived from the B*2709-positive individual had similar preferences for both pLMP2 and pVIPR peptides, but the pVIPR-stimulated CTL derived from the B*2705-positive AS patient showed a nearly 100-fold higher preference for pLMP2. These results indicate that the CTL lines derived from the B*2705-positive AS patient have a higher propensity to cross-react (Fiorillo et al. 2005).

1.7 Peptide presentation and T cell alloreactivity

The structural and cellular studies of presentation of pVIPR and pLMP2 peptides by B*2705 provide a basis for T cell crossreactivity between the two B*2705-bound peptides and add to the existing circumstantial evidence for the involvement of T cell cross-reactivity and peptides in inflammatory diseases (Hülsmeyer et al. 2004, Fiorillo et al. 2005). A related phenomenon called T cell alloreactivity, in which T cells directed against an MHC molecule crossreact with an MHC molecule of another individual of the same species, has been implicated in rejection of graft and organ transplants (Afzali et

al. 2007). While the exact molecular mechanism of alloreactivity is not understood (Koch et al. 2008), in case of B*1403 and B*2705 the total alloreactive CTL population (2.9%) and the peptide repertoire shared between two HLA-B subtypes (2.7-5.0%) correlate well, suggesting a link between peptide presentation and alloreactivity between these two subtypes (Merino et al. 2005). The shared peptide repertoire and total alloreactive CTL population for the B*1402 and B*2705 subtypes are also believed to be in the same percentage range and correlate well with each other (Merino et al. 2005).

1.8 Conformational variability - an intrinsic property of pMHC

The different biological functions of MHC class I molecules, as for every other protein, are closely linked to their conformational variability. The polymorphism of peptide binding groove residues of MHC molecules permits them to present a diverse range of antigens to effector cells in mostly unique conformations, permitting efficient self-nonself discrimination. With the identification of key residues involved in the process of TCR-pMHC binding as well as the characterization of other biophysical aspects of the binding, a clearer understanding of the complicated process of TCR recognition of pMHC has now started to develop (Rudolph et al. 2006, Armstrong et al. 2008). However, the differential T cell recognition of B*2705 and B*2709 complexes (Fiorillo et al. 2004) adds additional complexity to the understanding of T cell recognition of pMHC, as the two near-identical molecules that differ from each other only at residue 116 (which is buried deep inside the peptide binding groove and is not a TCR binding motif, see Fig. 1. 7) reveal remarkable differences in peptide presentation and T cell recognition. While it has now become possible to predict efficient binding of peptides for a large number of MHC molecules based on the identification of anchor residues (Sieker et al. 2009), it still remains largely impossible to predict the precise conformation of bound peptides in pMHC complexes without determination of X-ray structures. The functional implications of the dual-conformation of the pVIPR peptide in the B*2705:pVIPR complex and its partial overlap with the conformation of the pLMP2 peptide in the B*2705:pLMP2 complex are far-reaching (Hülsmeyer et al. 2004, Fiorillo et al. 2005), since a thorough structural understanding of peptide presentation by MHC

molecules forms the basis of our understanding of the initiation of immune responses. Besides MHC polymorphism, there are other sources of conformational variability in MHC molecules, including binding of ligands such as TCR, KIR and antibodies with TCR-like specificity (Boyington and Sun 2002, Rudolph et al. 2006, Ziegler et al. 2007), and post-translational modification (PTM) of peptide epitopes (Engelhard et al. 2006, Purcell et al. 2008, Petersen et al. 2009).

On a related note, it was noticed that subtle, but biologically highly relevant structural details such as the dual conformation of the pVIPR peptide in the B*2705:pVIPR structure can not be visualized by the Jmol java viewer, which is the default 3D viewer on the protein data bank (PDB) website and is used widely to provide nonspecialist users with interactive access to 3D structural data. This signals a larger problem regarding the obstacles in communicating 3D structural data effectively to nonspecialists through the largely inadequate existing channels.

1.4 Scope and objectives of this study

This doctoral work was aimed at determining the effects of three major sources of conformational variability in pMHC complexes - (a) subtype-specific substitutions in the HC residues belonging to the peptide binding groove, (b) sequence differences among different peptides and PTM of peptides, and (c) binding of ligands (TCR, KIR and antibodies with TCR-like specificity) to pMHC. A fourth component of the work will be (d) to make an effort to find a method for communication of 3D structural information such that there is less need for compromise on important factors like accuracy, ease of use, pre-rendering, interactivity and availability while communicating the information.

(a) The studies addressing structural effects on peptide presentation of subtype-specific substitutions in the HC residues of peptide binding groove will focus on peptide presentation by the B*1402, B*2705 and B*2709 subtypes. B*1402 differs from B*2705 and B*2709 subtypes at 18 positions located in the peptide binding groove, including positions 171 and 116 which have been shown to have dramatic effects on the anchoring of the peptide N-terminus and the pArg5 residue, respectively, in other pMHC

complexes (Maenaka et al. 2002, Hülsmeyer et al. 2004). These 18 substitutions result in differences in 'anchor residues' of B*1402 and the two HLA-B27 subtypes, such that pArg5 is an anchor residue only for HLA-B14, but pArg2 is a common anchor residue for both HLA-B14 and HLA-B27 despite differences within their B-pockets (DiBrino et al. 1994, Merino et al. 2005). To study how pArg2 is capable of efficiently binding the three HLA-B molecules despite substitutions in the B-pocket, the presentation of the only pArg2-containing common nonameric natural ligand of the three HLA-B subtypes, pCatA (IRAAPPPLF, derived from cathepsin A (Merino et al. 2005)) will be investigated by X-ray crystallography.

The Trp97Asn and Phe116Asp substitutions between HLA-B14 and –B27 have the potential to abrogate the hydrogen bond between pArg5 and residue 116 (Hülsmeyer et al. 2004), so that the anchoring of pArg5 in the groove of B*1402 molecule, if present, must adopt a novel conformation as it is an anchor residue for this subtype (Merino et al. 2005). To investigate this, the presentation of a pArg5 containing peptide, pLMP2, which has anchor residues for HLA-B14 as well as for the two HLA-B27 subtypes will also be investigated by X-ray crystallography. The results of the analyses with the pCatA and pLMP2 peptides were expected to shed light on the structural basis for T cell alloreactivity between these.

(b) The study investigating the effects of sequence differences among different peptides on peptide presentation will focus on X-ray and thermodynamic analyses of the presentation of the pB27 and pCP peptides, which share six common residues and differ at five residues including pΩ, by the B*2705 molecule. The similarities between the peptides at the two N-terminal residues and the presence of the GGxGG motif with very similar 'x' residues (K or R) in the middle section imply that the two peptides are highly likely to be presented in similar conformations (Ramos et al. 2002, Cragnolini and López de Castro 2008). On the other hand, the differences at positions p3, p4, p5 and pΩ, and in the lengths of the peptides suggest that any differences in their conformations will provide valuable information regarding the exact roles of these differences. The potential involvement of molecular mimicry between these two peptides in the pathogenesis of *Chlamydia*-induced ReA presents a rare opportunity to correlate

the similarities or differences in presentation of sequence-related peptides by a disease-associated MHC molecule with the molecular pathogenesis of the disease.

I also participated in a crystallographic and cellular study mainly conducted by my colleagues Ms. A. Beltrami and Mr. M. Rossmann as well as the group of Prof. Sorrentino (Rome, Italy) analyzing the effects of citrullination of pArg5 of pVIPR on presentation by the B*2705 and B*2709 molecules. The results were expected to shed light on the effects of PTM of a crucial peptide residue on peptide presentation by the B*2705 and B*2709 subtypes.

(c) The study investigating the changes induced in pMHC by the binding of TCR, KIR and antibodies with TCR-like specificity will involve the determination of the crystal structure of the HLA-A1:MAGE-A1 complex followed by a comparison of this structure with the structure of the same pMHC complex bound to Fab-Hyb3 (Hülsmeyer et al. 2005). The comparison will be extended to other existing structures of class I pMHC complexes whose structures are available in free form as well as in complex with a TCR or KIR ligand. This study will provide an insight into the structural changes associated with ligand binding to pMHC and permit us to conduct a comparative analysis of the binding to pMHC of natural ligands TCR and KIR and a recombinant antibody ligand with TCR-like specificity.

(d) Access to 3D imagery can greatly enhance the readers' ability to grasp complicated information that can not be suitably represented in 2D figures. The only options currently available to inquisitive readers facing such a situation who are unable to use molecular visualization programs like Rasmol or Pymol is to visit the PDB website and view the 3D imagery accompanying the structure using Jmol viewer browser plugin which does not display subtle conformational changes such as the dual conformation of the pVIPR peptide in the groove of the B*2705 molecule. Together with Dr. A. Ziegler, a colleague with experience in 3D imagery of zoological specimens (Ziegler et al. 2008), I was involved in developing a method to disseminate 3D structural information in electronic versions (portable document format, PDF) of publications. This pertained especially to those structures exhibiting subtle and crucial conformational variability.

The aim was to provide a user-friendly, intuitive, accessible and widely available channel.

2. Effects of substitutions in heavy chain on pMHC conformations

2.1 Summary

Many structural studies have been performed on pMHC molecules and these studies have enormously improved our understanding of the role of MHC molecules within the immune system. However, the effect of MHC polymorphism on the conformation of bound peptides is not yet sufficiently understood. The objective of the studies described in the articles included in this chapter was to determine exact structural effects of polymorphism in certain crucial positions in the pMHC molecules on the conformations of the bound peptides and in other parts of the molecules. To achieve this, in the first part of the work the crystal structures of B*1402, B*2705 and B*2709 in complex with a self-ligand, pCatA, and of B*1402 in complex with a nonself-ligand, pLMP2 were determined and the structures were compared among themselves and with the previously reported structures of B*2705 and B*2709 molecules in complex with pLMP2 (Fiorillo et al. 2005). This permitted a detailed comparison of the effects of polymorphism between B*1402 and B*2705/B*2709 (18 positions) and between B*2705 and B*2709 (1 position) on presentation of pCatA and pLMP2 peptides to be carried out, and allowed also a correlation with the results from T cell alloreactivity studies between these HLA-B subtypes. Collectively, these results provided a better understanding of the effects of the mutations in residues belonging to the HC on antigen presentation by MHC class I molecules.

2.2 Publications

2.2.1. Kumar P*, Vahedi-Faridi A*, Merino E, López de Castro JA, Volz A, Ziegler A, Saenger W, Uchanska-Ziegler B. (*Equal contribution) Expression, purification and preliminary X-ray crystallographic analysis of the human major histocompatibility antigen HLA-B*1402 in complex with a viral peptide and with a self-peptide Acta Crystallogr. Sect. F Struct. Biol. Cryst. Commun. (**2007**) 63, 631– 634

2.2.2. Kumar P, Vahedi-Faridi A, Saenger W, Merino E, López de Castro JA, Uchanska-Ziegler B, Ziegler A. Structural Basis for T Cell Alloreactivity among Three HLA-B14 and HLA-B27 Antigens. J. Biol. Chem. (**2009**) 284, 29784 –29797

Acta Crystallographica Section F
Structural Biology and Crystallization Communications
ISSN 1744-3091

Expression, purification and preliminary X-ray crystallographic analysis of the human major histocompatibility antigen HLA-B*1402 in complex with a viral peptide and with a self-peptide

Pravin Kumar,[a]‡ Ardeschir Vahedi-Faridi,[b]‡ Elena Merino,[c] José A. López de Castro,[c] Armin Volz,[a] Andreas Ziegler,[a] Wolfram Saenger[b]* and Barbara Uchanska-Ziegler[a]*

[a]Institut für Immungenetik, Charité – Universitätsmedizin Berlin, Humboldt-Universität zu Berlin, Thielallee 73, 14195 Berlin, Germany, [b]Institut für Chemie und Biochemie/Kristallographie, Freie Universität Berlin, Takustrasse 6, 14195 Berlin, Germany, and [c]Centro de Biología Molecular Severo Ochoa, Consejo Superior de Investigaciones Cientificas, Universidad Autónoma de Madrid, Facultad de Ciencias, Universidad Autónoma, 28049 Madrid, Spain

‡ These authors contributed equally to this work.

Correspondence e-mail: saenger@chemie.fu-berlin.de, barbara.uchanska-ziegler@charite.de

Received 18 May 2007
Accepted 13 June 2007

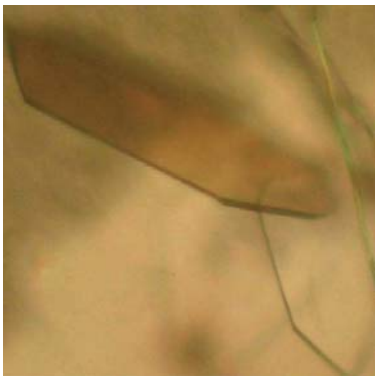

The product of the human major histocompatibility (HLA) class I allele *HLA-B*1402* only differs from that of allele *HLA-B*1403* at amino-acid position 156 of the heavy chain (Leu in HLA-B*1402 and Arg in HLA-B*1403). However, both subtypes are known to be differentially associated with the inflammatory rheumatic disease ankylosing spondylitis (AS) in black populations in Cameroon and Togo. HLA-B*1402 is not associated with AS, in contrast to HLA-B*1403, which is associated with this disease in the Togolese population. The products of these alleles can present peptides with Arg at position 2, a feature shared by a small group of other HLA-B antigens, including HLA-B*2705, the prototypical AS-associated subtype. Complexes of HLA-B*1402 with a viral peptide (RRRWRRLTV, termed pLMP2) and a self-peptide (IRAAPPPLF, termed pCatA) were prepared and were crystallized using polyethylene glycol as precipitant. The complexes crystallized in space groups $P2_1$ (pLMP2) and $P2_12_12_1$ (pCatA) and diffracted synchrotron radiation to 2.55 and 1.86 Å resolution, respectively. Unambiguous solutions for both data sets were obtained by molecular replacement using a peptide-complexed HLA-B*2705 molecule (PDB code 1jge) as a search model.

1. Introduction

Major histocompatibility complex (MHC) class I molecules consist of a highly polymorphic MHC-encoded heavy chain (HC; $M_r \simeq 32\,000$) that is noncovalently associated with an invariant protein [β_2-microglobulin (β_2m), $M_r \simeq 12\,000$]. The HC forms a groove that is able to bind peptides, usually with a length of 8–13 amino acids, in an allele-dependent fashion (Madden, 1995). These peptides are typically derived from fragmented intracellular proteins that may also include viral antigens in the case of a virus-infected cell. The involvement of the MHC in disorders that are characterized by cellular or antibody responses against self-antigens (autoimmune diseases) is insufficiently understood. This is exemplified by the human MHC class I allele *HLA-B27* and ankylosing spondylitis (AS; Brewerton *et al.*, 1973; Schlosstein *et al.*, 1973), which exhibits the strongest known association of a disease with an HLA class I allele (Horton *et al.*, 2004). Recently, *HLA-B*1403*, an allele present only in African populations of Cameroon and Togo, was reported to be associated with AS in the Togolese population (López-Larrea *et al.*, 2002), where both this disease and *HLA-B27* are rare. The closely related allele *HLA-B*1402* has a widespread distribution that also includes Caucasians, but has never been found to be associated with AS. The products of these subtypes differ only at residue 156 (Leu in HLA-B*1402, Arg in HLA-B*1403). HLA-B*2705 differs from the two HLA-B14 HCs at 18 amino-acid positions located within the first two domains (α1 and α2) of the extracellular region of the molecules.

A considerable research effort has been devoted towards unravelling the molecular basis of this disease association, but no in-depth understanding of AS pathogenesis has yet been obtained (Khan & Ball, 2002; Ramos & López de Castro, 2002; López de Castro, 2007). As there are suggestions that the recognition of HLA class I complexes by cytotoxic T lymphocytes (CTL) or natural killer cells might play a role in the pathogenesis (Benjamin & Parham,

1990; Ramos & López de Castro, 2002; López de Castro, 2007), peptide presentation by these molecules has provided a research focus in the last decade. AS patients with the *HLA-B*2705* subtype have been found to possess elevated levels of CTL directed against the self-peptide pVIPR (RRKWRRWHL, derived from vasoactive intestinal peptide type 1 receptor, residues 400–408), about one sixth of which cross-react with HLA-B*2705-positive cells presenting the viral pLMP2 peptide (RRRWRRLTV, derived from latent membrane protein 2 of Epstein–Barr virus, residues 236–244) (Fiorillo *et al.*, 2000, 2005). Individuals with another subtype, *HLA-B*2709*, the product of which differs from that of *HLA-B*2705* at only one position (Asp116 in HLA-B*2705, His116 in HLA-B*2709), do not possess CTL that cross-react with the self-peptide pVIPR (Fiorillo *et al.*, 2000), suggesting the existence of an *HLA-B27* subtype-dependent correlation with AS pathogenesis.

A major feature of HLA-B27 ligands is the presence of arginine at position 2 (pArg2; Jardetzky *et al.*, 1991; Madden *et al.*, 1992; Urban *et al.*, 1994; López de Castro *et al.*, 2004), which binds tightly into the so-called B pocket of the molecule's peptide-binding groove. Since this pocket is made up of residues that are polymorphic among HLA class I molecules, few allotypes other than HLA-B27, such as HLA-B14, bind peptides with pArg2 (Merino *et al.*, 2005). Two peptides were found to be shared by HLA-B*1402, HLA-B*1403, HLA-B*2705 and HLA-B*2709 (Merino *et al.*, 2005 and unpublished work). One of these is a self-peptide (pCatA, IRAAPPPLF) derived from the signal sequence (residues 2–10) of cathepsin A.

In contrast to the high degree of overlap among the constitutive peptide repertoires of HLA-B27 subtypes (Ramos *et al.*, 2002), HLA-B*1402 and HLA-B*1403 differ considerably regarding the peptides that are bound within the binding groove of the molecules (Merino *et al.*, 2005). However, the HLA-B27-bound and HLA-B14-bound peptide repertoires show even less overlap (about 3–5%; Merino *et al.*, 2005), although both pairs of subtypes share some important peptide-binding properties, such as the preference for pArg2, with HLA-B27 exhibiting a much higher restriction for this motif. It may therefore be envisaged that a thorough structural study of the HLA-B14 antigens and their comparison with the extensive structural findings in the HLA-B*2705/HLA-B*2709 system (Hülsmeyer *et al.*, 2002, 2004, 2005; Hillig *et al.*, 2004; Fiorillo *et al.*, 2005; Rückert *et al.*, 2006) would enhance our understanding of the differential AS association of these four HLA-B subtypes and would help to shed light on the generality of the arthritogenic peptide theory (López de Castro, 2007).

2. Materials and methods

2.1. Protein preparation

The nonapeptides pLMP2 (RRRWRRLTV) and pCatA (IRAAPPPLF) were chemically synthesized and purified by reverse-phase HPLC (EZBiolab, Westfield, USA). The HLA-B*1402 HC (Merino *et al.*, 2005) was cloned into the pHN vector. Both HC and β_2m were untagged. They were expressed separately and formed inclusion bodies in *Escherichia coli* that were solubilized with 50%(*w*/*v*) urea. The HLA-B14–peptide complexes were prepared by reconstituting the HC (12 mg), β_2m (10 mg) and the respective peptide (4 mg) according to a previously described procedure (Garboczi *et al.*, 1992). Briefly, the reconstitution mixture (400 ml, containing 400 m*M* arginine–HCl, 2 m*M* EDTA, 5 m*M* reduced glutathione, 0.5 m*M* oxidized glutathione and 100 m*M* Tris–HCl pH 7.5) was incubated at 277 K for 8–12 weeks, concentrated using Amicon Ultra-15 concentrators and purified by size-exclusion chromatography with Sephadex 75 (Pharmacia). Fractions containing the respective ternary complex were pooled and their composition (HC, β_2m) was surveyed by SDS–PAGE. The protein complexes were then concentrated to 15 mg ml^{-1} using Amicon Ultra-15 in a buffer system containing 20 m*M* Tris–HCl pH 7.5, 150 m*M* NaCl, 0.01%(*w*/*v*) sodium azide and used for crystallization trials.

2.2. Crystallization and data collection

For the HLA-B*1402–pLMP2 complex, a high-throughput robotic crystallization station (Protein Structure Factory, Berlin, Germany; Heinemann *et al.*, 2000) was used to screen several standard crystallization screen kits from Hampton Research (Aliso Viejo, USA). Sitting-drop vapour-diffusion crystallization trays with 100 µl reservoir solution and 500 nl drops consisting of equal volumes of reservoir and protein solutions were set up and the trays were kept at 291 K for crystal formation. Crystals of HLA-B*1402–pLMP2 that diffracted to 2.74 Å resolution grew in 3 d over a well containing 20%(*w*/*v*) polyethylene glycol (PEG) 10 000 and 0.1 *M* HEPES buffer pH 7.5. Crystallization trials for the HLA-B*1402–pCatA complex were performed in a hanging-drop vapour-diffusion setup at 291 K (1 ml reservoir solution, 2 µl drops consisting of equal volumes of reservoir and protein solutions), but otherwise under conditions identical to those used for crystallizing HLA-B*1402–pLMP2. Crystals diffracting to 2.35 Å were obtained in 5 d in a well containing 24%(*w*/*v*) PEG 10 000, 0.1 *M* HEPES buffer pH 7.5.

Since the initially grown crystals were too small for X-ray analysis, the crystallization conditions for HLA-B*1402–pLMP2 and HLA-B*1402–pCatA were optimized by varying the molecular weight of the PEG and the concentrations of the various constituents in the hanging-drop trays. Drops were streak-seeded with crushed crystals of the same complex from previous experiments using cat whiskers. Thin plate-like hexagonal crystals of HLA-B*1402–pLMP2 with maximum dimensions of about 150 × 100 × 5 µm grew in 20–22%(*w*/*v*) PEG 20 000, 0.1 *M* HEPES buffer pH 7.5 and 24%(*w*/*v*) PEG 8000, 0.1 *M* HEPES buffer pH 7.5, while needle-shaped crystals of HLA-B*1402–pCatA with maximum dimensions of about 300 × 10 × 5 µm grew under similar conditions in 24–27%(*w*/*v*) PEG 20 000 with 0.1 *M* HEPES pH 7.5. Crystals of both complexes were finally transferred to cryoprotectant solution containing the respective reservoir solution and glycerol. The optimum concentrations of glycerol were found to be 20%(*w*/*v*) for HLA-B*1402–pLMP2 crystals and 15%(*w*/*v*) for HLA-B*1402–pCatA crystals.

X-ray diffraction data sets were collected for both complexes at 100 K on beamline 14.2 at the BESSY II synchrotron facility in Berlin, Germany using a wavelength of 0.91841 Å. The beamline is equipped with a fast-scanning CCD detector from MAR Research (Norderstedt, Germany). The crystals were exposed for 6.75–10 s during data collection. The HLA-B*1402–pLMP2 crystal was flash-annealed (Harp *et al.*, 1998) by shielding the cryostream for about 5 s. The crystals of the HLA-B*1402–pLMP2 and HLA-B*1402–pCatA complexes belonged to space groups $P2_1$ and $P2_12_12_1$ and diffracted to 2.55 and 1.85 Å resolution, respectively. The collected data sets were integrated and scaled using the *HKL*-2000 suite (Otwinowski & Minor, 1997). There are two complexes and one complex per crystal asymmetric unit in the HLA-B*1402–pLMP2 and HLA-B*1402–pCatA crystals, respectively. Their Matthews coefficients and solvent contents (Matthews, 1968) were calculated to be 2.5 Å^3 Da^{-1} and 50.2%, and 2.6 Å^3 Da^{-1} and 52.2%, respectively, based on an approximate M_r of ∼45 000 for each of the complexes. Crystallographic data and X-ray data-collection statistics are summarized in Table 1.

Table 1
Data-collection statistics of HLA-B*1402–pLMP2 and HLA-B*1402–pCatA.

Values in parentheses are for the highest resolution shell.

	HLA-B*1402–pLMP2	HLA-B*1402–pCatA
Space group	$P2_1$	$P2_12_12_1$
Unit-cell parameters (Å)	a = 53.4, b = 79.9, c = 105.4, α = 90, β = 99.5, γ = 90	a = 50.8, b = 82.1, c = 110.7, α = 90, β = 90, γ = 90
Solvent content (%)	50.2	52.2
Matthews coefficient† (Å^3 Da^{-1})	2.5	2.6
Resolution (Å)	30.0–2.55 (2.64–2.55)	50.0–1.86 (1.93–1.86)
Unique reflections	26733 (2177)	38359 (3023)
Completeness (%)	93.0 (76.8)	96.8 (78.0)
$\langle I\rangle/\langle\sigma(I)\rangle$	7.9 (1.4)	22.5 (3.5)
R_{sym}‡	0.137 (0.457)	0.049 (0.239)
R_{merge}§	0.138 (0.449)	0.073 (0.247)
$R_{r.i.m.}$§	0.165 (0.585)	0.082 (0.294)
$R_{p.i.m.}$§	0.089 (0.371)	0.036 (0.155)
Redundancy	3.0 (1.8)	4.6 (2.7)

† According to Matthews (1968). ‡ $R_{sym} = \sum_h \sum_i |I_{h,i} - \langle I\rangle| / \sum_h \sum_i I_{h,i}$. § According to Weiss (2001).

The *CCP*4 suite (Collaborative Computational Project, Number 4, 1994) program *Phaser* (Storoni *et al.*, 2004) was used for phase determination of the HLA-B*1402–pLMP2 crystal data employing the atomic coordinates of a high-resolution structure of HLA-B*2705–m9 as a search model (PDB code 1jge; Hülsmeyer *et al.*, 2002), as *MOLREP* (Vagin & Teplyakov, 1997) failed to find a satisfactory solution. HC and β_2m coordinates were used as separate ensembles in *Phaser* and the best final solution obtained by this program was based on top log-likelihood gain (LLG) values of 1609 for HC and 3441 for β_2m. The final Z score was over 13 for each of the two HCs and each of the two β_2m molecules in the asymmetric unit. The molecular-replacement solution for the HLA-B*1402–pCatA crystal data was obtained by *MOLREP* using the same high-resolution structure of HLA-B*2705–m9 as a search model (PDB code 1jge; Hülsmeyer *et al.*, 2002) with the omission of water molecules and peptide.

Models of both HLA-B*1402 complexes pack sensibly in the unit cells and show no clashes. Examination of electron-density maps calculated from the initial phases permitted us to identify the presence of the respective nonapeptides as well as the HC residues unique to HLA-B*1402 in both structures. Modelling of the respective peptides in electron density and rigid-body refinement yielded models with R and R_{free} of 0.262 and 0.342, respectively, and an $F_o - F_c$ correlation coefficient of 0.882 for HLA-B*1402–pLMP2, and R and R_{free} values of 0.256 and 0.285, respectively, and an $F_o - F_c$ correlation coefficient of 0.901 for HLA-B*1402–pCatA.

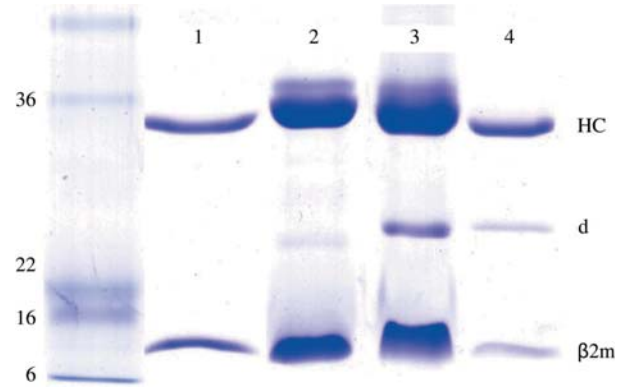

Figure 1
SDS–PAGE analysis of refolded HLA-B*1402–pLMP2 (lanes 2 and 3, about 75 µg each) and HLA-B*1402–pCatA (lanes 1 and 4, about 20 µg each) complexes. Purified complexes were electrophoretically analyzed under reducing (lanes 1 and 2) and nonreducing conditions (lanes 3 and 4) using Coomassie Brilliant Blue stain. Approximate molecular weights of marker proteins are indicated in kDa on the left. HLA-B*1402 heavy-chain (HC) and β_2-microglobulin (β_2m) bands are indicated. A faint β_2m dimer (d) band is visible under nonreducing conditions (lanes 3 and 4) and even under reducing conditions when very high amounts of HLA–peptide complex are loaded onto a gel (lane 2). This has so far not been observed to hinder crystallization of the complex.

3. Results and discussion

Highly pure HLA-B*1402–pLMP2 and HLA-B*1402–pCatA complexes (Fig. 1) were crystallized using PEG as precipitant. Crystal formation was optimized by varying the PEG molecular weight and concentration as well as by streak-seeding using crystals of the same complex from previous experiments, which resulted in well ordered crystals (Fig. 2). X-ray diffraction analysis (Fig. 3) revealed that the crystals of the two complexes were non-isomorphous and belonged to space groups $P2_1$ and $P2_12_12_1$, respectively, which are also typical for

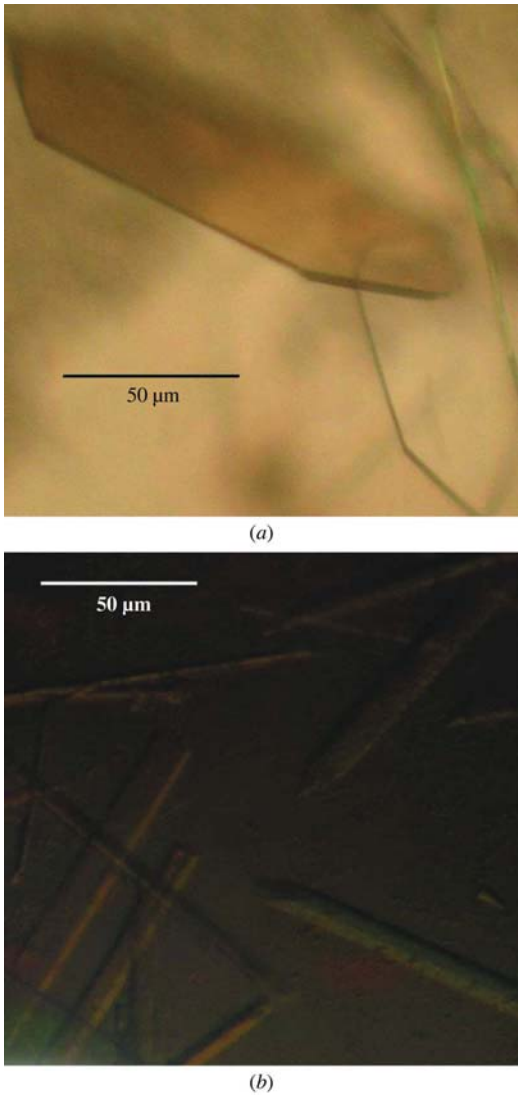

Figure 2
Crystals of (*a*) HLA-B*1402–pLMP2 and (*b*) HLA-B*1402–pCatA complexes exhibit remarkably different morphology and size.

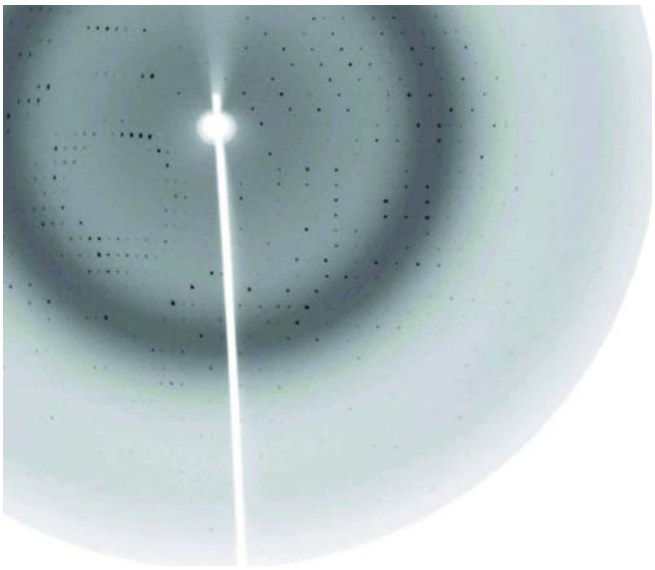

Figure 3
Diffraction pattern of an HLA-B*1402–pCatA crystal collected at BESSY II synchrotron facility in Berlin.

HLA-B27–peptide complexes (see, for example, Hülsmeyer *et al.*, 2002, 2004, 2005). Previously described crystals of HLA-B27 subtypes with the pLMP2 peptide belong to either space group $P2_1$ (HLA-B*2705 and HLA-B*2709; Fiorillo *et al.*, 2005) or $P2_12_12_1$ (HLA-B*2703, HLA-B*2704 and HLA-B*2706; Loll, Zawacka, Biesiadka, Petter *et al.*, 2005; Loll, Zawacka, Biesiadka, Rückert *et al.*, 2005; Zawacka *et al.*, 2005). However, two complexes per asymmetric unit as found for HLA-B*1402–pLMP2 have not been observed in any crystal of HLA-B27–pLMP2. Information with regard to the conformation of the bound peptide cannot be inferred from these similarities or differences, since crystals of HLA-B*2705–pLMP2 and HLA-B*2709–pLMP2, which are near-isomorphous and share the same space group ($P2_1$), nevertheless display the pLMP2 peptide in completely different binding modes (Fiorillo *et al.*, 2005). Modelling of solvent molecules in unassigned electron density is in progress for both structures and complete structural details will be reported separately.

The structure of the HLA-B*1402 complexes will permit comparison with other previously determined structures of HLA-B27 molecules in complex with these peptides, enabling a direct assessment of the binding mode of the same peptide (pLMP2) in complex with significantly distinct HLA class I molecules. A detailed structural study of peptide presentation by these complexes will improve our understanding of HLA-B subtype-dependent T-cell recognition and might also shed light on the causes underlying the association of certain *HLA-B27* and *HLA-B14* alleles with spondyloarthropathies.

Financial support for this work was provided by Deutsche Forschungsgemeinschaft (SFB 449/B6 and Z3), the European Union (EFRE 2000-2006 2ü/2), Fonds der Chemischen Industrie, Sonnenfeld Stiftung, Berlin, Senate of Berlin (NaFöG fellowship, PK), grant SAF2005-03188 from the Spanish Ministry of Education and Science (EM and JALC) and an institutional grant of the Fundación Ramon Areces to the Centro de Biología Molecular Severo Ochoa. We thank Christina Schnick for excellent technical assistance and are grateful for allocation of beam time and support at BESSY II (Berlin).

References

Benjamin, R. & Parham, P. (1990). *Immunol. Today*, **11**, 137–142.
Brewerton, D. A., Hart, F. D., Nicholls, A., Caffrey, M., James, D. C. & Sturrock, R. D. (1973). *Lancet*, **1**, 904–907.
Collaborative Computational Project, Number 4 (1994). *Acta Cryst.* D**50**, 760–763.
Fiorillo, M. T., Maragno, M., Butler, R., Dupuis, M. L. & Sorrentino, R. (2000). *J. Clin. Invest.* **106**, 47–53.
Fiorillo, M. T., Rückert, C., Hülsmeyer, M., Sorrentino, R., Saenger, W., Ziegler, A. & Uchanska-Ziegler, B. (2005). *J. Biol. Chem.* **280**, 2962–2971.
Garboczi, D. N., Hung, D. T. & Wiley, D. C. (1992). *Proc. Natl Acad. Sci. USA*, **89**, 3429–3433.
Harp, J. M., Timm, D. E. & Bunick, G. (1998). *Acta Cryst.* D**54**, 622–628.
Heinemann, U., Frevert, J., Hofmann, K., Illing, G., Maurer, C., Oschkinat, H. & Saenger, W. (2000). *Prog. Biophys. Mol. Biol.* **73**, 347–362.
Hillig, R. C., Hulsmeyer, M., Saenger, W., Welfle, K., Misselwitz, R., Welfle, H., Kozerski, C., Volz, A., Uchanska-Ziegler, B. & Ziegler, A. (2004). *J. Biol. Chem.* **279**, 652–663.
Horton, R., Wilming, L., Rand, V., Lovering, R. C., Bruford, E. A., Khodiyar, V. K., Lush, M. J., Povey, S., Talbot, C. C. Jr, Wright, M. W., Wain, H. M., Trowsdale, J., Ziegler, A. & Beck, S. (2004). *Nature Rev. Genet.* **5**, 889–899.
Hülsmeyer, M., Fiorillo, M. T., Bettosini, F., Sorrentino, R., Saenger, W., Ziegler, A. & Uchanska-Ziegler, B. (2004). *J. Exp. Med.* **199**, 271–281.
Hülsmeyer, M., Hillig, R. C., Volz, A., Rühl, M., Schröder, W., Saenger, W., Ziegler, A. & Uchanska-Ziegler, B. (2002). *J. Biol. Chem.* **277**, 47844–47853.
Hülsmeyer, M., Welfle, K., Pöhlmann, T., Misselwitz, R., Alexiev, U., Welfle, H., Saenger, W., Uchanska-Ziegler, B. & Ziegler, A. (2005). *J. Mol. Biol.* **346**, 1367–1379.
Jardetzky, T. S., Lane, W. S., Robinson, R. A., Madden, D. R. & Wiley, D. C. (1991). *Nature (London)*, **353**, 326–329.
Khan, M. A. & Ball, E. J. (2002). *Best Pract. Res. Clin. Rheumatol.* **16**, 675–690.
Loll, B., Zawacka, A., Biesiadka, J., Petter, C., Rückert, C., Saenger, W., Uchanska-Ziegler, B. & Ziegler, A. (2005). *Acta Cryst.* F**61**, 939–941.
Loll, B., Zawacka, A., Biesiadka, J., Rückert, C., Volz, A., Saenger, W., Uchanska-Ziegler, B. & Ziegler, A. (2005). *Acta Cryst.* F**61**, 372–374.
López de Castro, J. A. (2007). *Immunol. Lett.* **108**, 27–33.
López de Castro, J. A., Alvarez, I., Marcilla, M., Paradela, A., Ramos, M., Sesma, L. & Vazquez, M. (2004). *Tissue Antigens*, **63**, 424–445.
López-Larrea, C., Mijiyawa, M., Gonzalez, S., Fernandez-Morera, J. L., Blanco-Gelaz, M. A., Martinez-Borra, J. & López-Vazquez, A. (2002). *Arthritis Rheum.* **46**, 2968–2971.
Madden, D. R. (1995). *Annu. Rev. Immunol.* **13**, 587–622.
Madden, D. R., Gorga, J. C., Strominger, J. L. & Wiley, D. C. (1992). *Cell*, **70**, 1035–1048.
Matthews, B. W. (1968). *J. Mol. Biol.* **33**, 491–497.
Merino, E., Montserrat, V., Paradela, A. & López de Castro, J. A. (2005). *J. Biol. Chem.* **280**, 35868–35880.
Otwinowski, Z. & Minor, W. (1997). *Methods Enzymol.* **276**, 307–326.
Ramos, M. & López de Castro, J. A. (2002). *Tissue Antigens*, **60**, 191–205.
Ramos, M., Paradela, A., Vazquez, M., Marina, A., Vazquez, J. & López de Castro, J. A. (2002). *J. Biol. Chem.* **277**, 28749–28756.
Rückert, C., Loll, B., Fiorillo, M. T., Moretti, R., Biesiadka, J., Saenger, W., Ziegler, A., Sorrentino, R. & Uchanska-Ziegler, B. (2006). *J. Biol. Chem.* **281**, 2306–2316.
Schlosstein, L., Terasaki, P. I., Bluestone, R. & Pearson, C. M. (1973). *N. Engl. J. Med.* **288**, 704–706.
Storoni, L. C., McCoy, A. J. & Read, R. J. (2004). *Acta Cryst.* D**60**, 432–438.
Urban, R. G., Chicz, R. M., Lane, W. S., Strominger, J. L., Rehm, A., Kenter, M. J., UytdeHaag, F. G., Ploegh, H., Uchanska-Ziegler, B. & Ziegler, A. (1994). *Proc. Natl Acad. Sci. USA*, **91**, 1534–1538.
Vagin, A. & Teplyakov, A. (1997). *J. Appl. Cryst.* **30**, 1022–1025.
Weiss, M. S. (2001). *J. Appl. Cryst.* **34**, 130–135.
Zawacka, A., Loll, B., Biesiadka, J., Saenger, W., Uchanska-Ziegler, B. & Ziegler, A. (2005). *Acta Cryst.* F**61**, 1097–1099.

THE JOURNAL OF BIOLOGICAL CHEMISTRY VOL. 284, NO. 43, pp. 29784–29797, October 23, 2009

Structural Basis for T Cell Alloreactivity among Three HLA-B14 and HLA-B27 Antigens*

Received for publication, June 26, 2009, and in revised form, July 9, 2009 Published, JBC Papers in Press, July 18, 2009, DOI 10.1074/jbc.M109.038497

Pravin Kumar[‡], Ardeschir Vahedi-Faridi[§], Wolfram Saenger[§], Elena Merino[¶], José A. López de Castro[¶], Barbara Uchanska-Ziegler[‡], and Andreas Ziegler[‡1]

From the [‡]Institut für Immungenetik, Charité-Universitätsmedizin Berlin, Campus Benjamin Franklin, Freie Universität Berlin, Thielallee 73, 14195 Berlin, Germany, the [§]Institut für Chemie und Biochemie/Kristallographie, Freie Universität Berlin, Takustrasse 6, 14195 Berlin, Germany, and the [¶]Centro de Biología Molecular Severo Ochoa, Consejo Superior de Investigaciones Cientificas and Universidad Autónoma de Madrid, Nicolás Cabrera, N.1, Universidad Autónoma, 28049 Madrid, Spain

The existence of cytotoxic T cells (CTL) cross-reacting with the human major histocompatibility antigens HLA-B14 and HLA-B27 suggests that their alloreactivity could be due to presentation of shared peptides in similar binding modes by these molecules. We therefore determined the crystal structures of the subtypes HLA-B*1402, HLA-B*2705, and HLA-B*2709 in complex with a proven self-ligand, pCatA (peptide with the sequence IRAAPPPLF derived from cathepsin A (residues 2–10)), and of HLA-B*1402 in complex with a viral peptide, pLMP2 (RRRWRRLTV, derived from latent membrane protein 2 (residues 236–244) of Epstein-Barr virus). Despite the exchange of 18 residues within the binding grooves of HLA-B*1402 and HLA-B*2705 or HLA-B*2709, the pCatA peptide is presented in nearly identical conformations. However, pLMP2 is displayed by HLA-B*1402 in a conformation distinct from those previously found in the two HLA-B27 subtypes. In addition, the complexes of HLA-B*1402 with the two peptides reveal a non-standard, tetragonal mode of the peptide N terminus anchoring in the binding groove because of the exchange of the common Tyr-171 by His-171 of the HLA-B*1402 heavy chain. This exchange appears also responsible for reduced stability of HLA-B14-peptide complexes *in vivo* and slow assembly *in vitro*. The studies with the pCatA peptide uncover that CTL cross-reactive between HLA-B14 and HLA-B27 might primarily recognize the common structural features of the bound peptide, thus neglecting amino acid replacements within the rim of the binding grooves. In contrast, structural alterations between the three complexes with the pLMP2 peptide indicate how heavy chain polymorphisms can influence peptide display and prevent CTL cross-reactivity between HLA-B14 and HLA-B27 antigens.

T cells possessing the ability to recognize major histocompatibility complex (MHC)[2] molecules from another individual of the same species, also termed alloreactive T cells, may constitute up to 10% of the T cell pool of an individual, and their precursor frequency can be 100–1,000-fold higher than that of self-restricted T cells directed against a foreign peptide (1, 2). The ability of alloreactive T cells to cross-react with nonself-MHC molecules is a major obstacle preventing successful organ transplantations (3–5). Two mechanisms, direct or indirect allorecognition, can be responsible for the rejection of a transplant by alloreactive T cells (6). In the first case, donor cells expressing MHC molecules are directly recognized by host T cells (7), whereas indirect allorecognition involves the presentation of peptides derived from donor proteins by MHC molecules of the host, followed by the detection of the complexes by the host T cells (8). However, although alloreactive T cells are very common and of great clinical importance, neither the primary basis for their existence nor the reasons underlying their cross-reactivity are sufficiently understood to draw general conclusions (9–11). Only very few studies have addressed the structural basis for the recognition of distinct MHC antigens by cross-reactive T cells (12–18). One of the most important questions regards the individual contribution of the bound peptide and binding groove residues of the heavy chain (HC) of MHC class I antigens to the interaction with T cell receptors (TCR).

Here we analyze an HLA-B14 subtype, HLA-B*1402 (named B*1402), as well as two HLA-B27 subtypes, HLA-B*2705 and HLA-B*2709 (named B*2705 and B*2709), to shed light on the structural basis of peptide presentation and T cell alloreactivity among these HLA-B molecules. The amino acid sequences of B*1402 and B*2705 HC differ from each other at 18 positions, all of which are part of the peptide-binding groove (Fig. 1). These amino acid exchanges result in different repertoires of bound peptides; B*1402 and B*2705 share only about 4% of their peptides (19), whereas this value rises to 88% for the B*2705 and B*2709 subtypes (20), which are distinguished only by a single residue at the floor of the binding groove (B*2705, Asp-116; B*2709, His-116). The structural similarities between the two HLA-B27 subtypes (21–27) permit extensive cross-reactivity (up to 90%) of cytotoxic T cells (CTL) (28), whereas CTL alloreactivity between B*1402 and B*2705 is drastically reduced (to about 3%) (19), in line with the very limited overlap of their peptide repertoires.

* This work was supported by VolkswagenStiftung Grant I/79 983 (to A. Z.) and a stipend (to P. K.), Deutsche Forschungsgemeinschaft Grants SFB 449, TP B6, and Z3 (to W. S., B. U.-Z., and A. Z.), the Senate of Berlin NaFöG Fellowship (to P. K.), and Spanish Plan Nacional de I+D Grant SAF2008/00461 (to J. A. L. d. C.).

The atomic coordinates and structure factors (codes 3BXN, 3BVN, 3BP4, and 3BP7) have been deposited in the Protein Data Bank, Research Collaboratory for Structural Bioinformatics, Rutgers University, New Brunswick, NJ (http://www.rcsb.org/).

[1] To whom correspondence should be addressed. Tel.: 49-30-450-564731; Fax: 49-30-450-564920; E-mail: andreas.ziegler@charite.de.

[2] The abbreviations used are: MHC, major histocompatibility complex; AS, ankylosing spondylitis; CTL, cytotoxic T lymphocytes; HC, heavy chain; HLA, human leukocyte antigen; p1, p2,…, peptide position 1, 2,…; r.m.s.d., root mean square deviation; TCR, T cell receptor; β_2m, β_2-microglobulin.

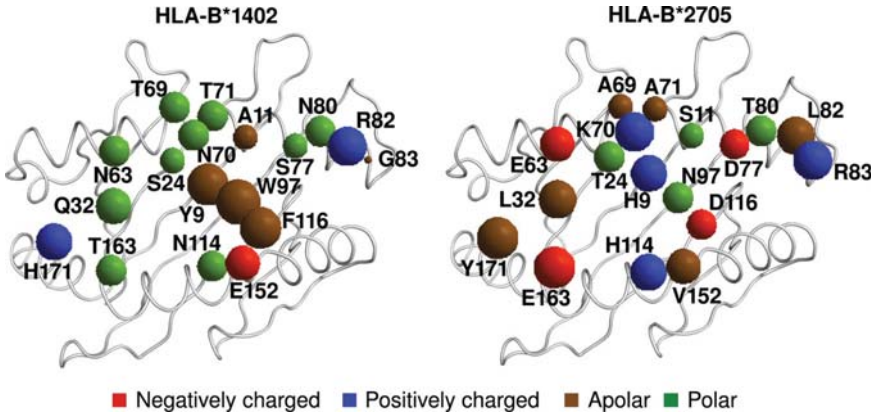

FIGURE 1. **Amino acid sequence differences among B*1402 and B*2705 HC.** The 18 residues distinguishing the two subtypes are all located in or in the immediate vicinity of the peptide-binding groove. B*2705 differs from B*2709 only by a D116H exchange (not shown). The residues are indicated by *spheres* with volumes roughly proportional to the volumes of the respective amino acid side chain in solution (77). The *spheres* are colored according to the biochemical properties of the respective amino acids, as indicated at the *bottom* of the image.

The HLA-B14 and HLA-B27 subtypes are distinguished from most other HLA class I molecules in their requirement for an arginine at anchor position 2 of the bound peptide (p2) (20, 29, 30). This preference is nearly absolute in B*2705 and B*2709 (31), whereas B*1402 tolerates also glutamine, glutamate, and proline as p2 anchors (19, 29). Statistically significant differences between B*1402 and B*2705 are also found at several other peptide positions (19). Previous structural and cellular studies of the HLA-B27 subtypes have suggested that molecular mimicry between the viral peptide pLMP2 (RRRWRRLTV, derived from Epstein-Barr virus latent membrane protein 2, residues 236–244) and the self-peptide pVIPR (RRKWRRWHL, derived from vasoactive intestinal peptide type 1 receptor, residues 400–408), when bound to B*2705, serves as an example of how a cellular immune response could be triggered that might contribute to the onset of ankylosing spondylitis (AS) through an autoimmune mechanism (22, 24). CTL that recognize the B*2705 and the B*2709 subtypes in complex with the self-peptide pVIPR (22) exemplify alloreactivity in this system, although the D116H micropolymorphism is deeply buried and not directly accessible to a TCR.

Alloreactive T cells are known to recognize a very diverse array of alloantigen-bound peptides (32, 33), so that virtually each T cell clone can be assumed to be specific for a distinct peptide. For this reason, the substantial correlation found in previous studies between peptide and the alloreactive T cell epitope sharing among HLA-B27 (reviewed in Ref. 34) or HLA-B14 subtypes (only 28.4% partial or full cross-reactivity, similar to peptide overlapping between the subtypes B*1402 and B*1403, see Ref. 19) supports a prominent role of peptides in determining alloreactive T cell cross-reaction, and it suggests that many shared ligands adopt antigenically similar conformations when bound to distinct HLA-B molecules. On the other hand, the results reported by Merino *et al.* (19) also demonstrate that the few CTL that cross-react with B*1402 and B*2705 did not exhibit cross-reactivity with B*1403, which is distinguished from B*1402 only by a single amino acid exchange in the α2-helix. Furthermore, they show that alloreactive CTL from various donors directed against B*2705 did not lyse cells expressing either B*1402 or B*1403, although the number of CTL tested might not have been high enough to detect a presumably low degree of cross-reactivity. Without structural data from HLA-B14 subtypes, however, these results are difficult to interpret.

The pCatA peptide (IRAAPPPLF, derived from the signal sequence of cathepsin A, residues 2–10) is among the very few known common ligands of B*1402, B*2705 (19), and B*2709[3] and can thus serve to study how a very different (B*1402) and two very similar subtypes (B*2705 and B*2709) handle a common ligand. On the other hand, the pLMP2 peptide is a proven natural ligand only of B*2705, whose possible presentation *in vivo* by B*2709 and HLA-B14 is not yet known, although this peptide can be complexed *in vitro* with B*2709 (24) and also with B*1402 (35). From previous crystallographic studies, it was known that pLMP2 is presented by the two HLA-B27 antigens in very different conformations (24). We expected that the pronounced sequence differences between B*1402 and the HLA-B27 alloantigens (Fig. 1) might even enhance the conformational dissimilarities that are observed when two very closely related subtypes such as B*2705 and B*2709 are compared. Discrepancies in peptide display could reasonably be expected to prevent CTL cross-reaction, so that pLMP2 might be considered as a representative of the vast majority of HLA-B14- and HLA-B27-presented ligands that must be responsible for the low degree of CTL cross-reactivity between these alloantigens. Despite these presumed differences between pCatA and pLMP2, both peptides may be seen as examples of ligands that could principally allow direct allorecognition.

Here we report the crystal structures of B*1402·pCatA, B*2705·pCatA, B*2709·pCatA, and B*1402·pLMP2, and we compare them with each other and with the previously reported structures of B*2705·pLMP2 and B*2709·pLMP2 (24).

MATERIALS AND METHODS

Protein Expression and Purification—The HC of B*1402 (19), B*2705, and B*2709 (21), as well as β_2-microglobulin (β_2m) were expressed separately in *Escherichia coli* as inclusion bodies, purified and dissolved in 50% (w/v) urea solution. The chemically synthesized nona-peptides pCatA (IRAAPPPLF) and pLMP2 (RRRWRRLTV) were purchased from EZBiolab, Westfield, IN. The HLA-B-peptide complexes were prepared by reconstituting a given HC, β_2m, and the respective peptide according to protocols described previously (21, 35, 36). Briefly, the reconstitution mixture of HC, β_2m, and a peptide (3 mg of HC, 2.5 mg of β_2m, and 1 mg of peptide in a 100-ml solution containing 400 mM arginine-HCl, 2 mM EDTA, 5 mM

[3] E. Merino and J. A. López de Castro, unpublished observations.

reduced glutathione, 0.5 mM oxidized glutathione, and 100 mM Tris-HCl, pH 7.5) was incubated at 277 K for 8–12 weeks (B*1402) or 7–15 days (HLA-B27 subtypes), concentrated using Amicon Ultra-15 concentrators, and purified by size-exclusion chromatography using Sephadex 75 columns (GE Healthcare). The purified protein complexes were electrophoretically checked for purity, concentrated to ~15 mg/ml, and used for crystallization trials.

Crystallization, X-ray Data Collection, and Structure Determination—The crystallization of the B*1402·pCatA and the B*1402·pLMP2 complexes have already been described in detail (35). Crystals of the B*2705·pCatA and the B*2709·pCatA complexes were obtained in a hanging-drop vapor diffusion setup using a reservoir solution containing 20–24% polyethylene glycol 8000, 100 mM Tris-HCl, pH 7.5 or 8.0, and a drop containing 1.1 μl of protein solution and 1.1 μl of reservoir solution. The crystals of all four complexes were soaked for 20–30 s in cryoprotectant solutions containing the respective reservoir solution and glycerol. Optimal concentrations of glycerol were found to be 20% (w/v) for B*1402·pLMP2, 15% (w/v) for B*1402·pCatA, 17% (w/v) for B*2705·pCatA, and 15% (w/v) for B*2709·pCatA crystals.

X-ray diffraction data sets of all four complexes were collected at 100 K on Protein Structure Factory beamline 14.2 at the BESSY II synchrotron facility in Berlin, Germany, using a wavelength of 0.91841 Å. Crystals of the B*1402·pLMP2 complex diffracted to 2.55 Å resolution, whereas the crystals of the other three complexes diffracted to about 1.8 Å resolution. The collected data sets were integrated and scaled using the HKL2000 suite (37). The B*1402·pLMP2 crystal has two complexes per crystal asymmetric unit, whereas the other three crystals contain only one complex per asymmetric unit. Data collection and refinement statistics are listed in Table 1. The data collection statistics for the two HLA-B14 complexes have already been provided by Kumar *et al.* (35) and are only shown here for comparison with the HLA-B27 structures.

The CCP4 (38) suite programs MolRep (39) and PHASER (40) were used for the localization of the HLA-B molecules in crystal unit cells by molecular replacement. The atomic coordinates of HC and β_2m obtained from the structures of B*2705·m9 (Protein Data Bank accession code 1JGE) (21) and B*2709·pLMP2 (Protein Data Bank accession code 1UXW) (24) were employed as a search model for the localization of HC and β_2m of the B*2709-pCatA and the B*1402·pLMP2 complexes, respectively, in their unit cells. The atomic coordinates of HC and β_2m obtained from the refined models of B*2709·pCatA and B*1402·pLMP2 were then used as search models for the localization of HC and β_2m of the B*2705·pCatA and the B*1402·pCatA complexes, respectively, in their unit cells by molecular replacement. The obtained models were subjected to iterative cycles of restrained maximum likelihood refinement, including isotropic temperature factor adjustment using CNS (41) for the B*1402·pLMP2 structure and REFMAC (42) for the other three structures, followed by manual rebuilding using COOT (43). Water molecules were positioned using CNS for the B*1402·pLMP2 structure and Arp/Warp (44) for the other three structures. All contacts were calculated with the CONTACT program of the CCP4 suite. All superpositions and root mean square deviation (r.m.s.d.) calculations were performed with LSQKAB (45). Calculations of the electrostatic surface potentials were performed by employing the PDB2PQR web server (46) and the Adaptive Poisson-Boltzmann Solver program (47). Unless otherwise mentioned, the Cα atoms of HC peptide-binding groove residues (1–180 of a HC) were overlaid during comparisons.

The two-dimensional figures showing structural details were prepared using PyMOL (48). The fully interactive three-dimensional Fig. 3 (*A* and *B*) is embedded into conventional two-dimensional images and was created using the Adobe Acrobat 3D Toolkit and Adobe Acrobat software. We have recently described the procedure to generate such images (49, 50), starting from raw Protein Data Bank files (3BXN, 3BVN, 3BP4, 1UXS, 3BP7, and 1UXW).

RESULTS

Reconstitution of the HLA-B14 and HLA-B27 Complexes in Vitro—Reconstitution of the HLA-B14 complexes required a much longer time than in the case of the HLA-B27 complexes. Whereas complexes of B*2705 and B*2709 could be purified from the reconstitution mixture, although in low yield, already after 7 days of incubation, the B*1402 complexes required a minimum of 3 weeks of incubation for complex formation. The yield of reconstitution of the B*1402·pCatA complex was about 30 times lower than that of the B*2709·pCatA molecule. In general, the yields following reconstitution of B*1402 complexes were >10 times lower than the yields obtained after refolding the HLA-B27 complexes. Attempts to optimize the yield of the B*1402 complexes by varying the relative amounts of HC, β_2m, and peptide, by changing the concentrations of oxidized and reduced glutathione or by adding glycerol (51), failed.

General Features of the Structures—The complexes of the B*1402, B*2705, and B*2709 subtypes with the pCatA peptide crystallized isomorphously in the orthorhombic space group $P2_12_12_1$ with one molecule per asymmetric unit, whereas the complex of B*1402 with pLMP2 crystallized in the monoclinic $P2_1$ space group with two molecules in the asymmetric unit. All four complexes exhibit the typical MHC class I architecture (52). The structures were refined to R_{cryst} and R_{free} values of 16.9/21.9% (B*1402·pCatA), 17.1/22.1% (B*2705·pCatA), and 16.7/20.4% (B*2709·pCatA), all at about 1.8 Å resolution, and the B*1402·pLMP2 complex structure was refined to R_{free} and R_{cryst} values of 24.0 and 26.8% at 2.55 Å resolution (Table 1). The complexes of B*2705 and B*2709 with pLMP2 crystallized in the monoclinic space group $P2_1$ as well, albeit under different crystallization conditions, and their crystals contained one molecule per asymmetric unit (24). The high quality electron density maps enabled us to model the molecules unambiguously (Fig. 2, *A–C, G,* and *H*).

The peptide-binding grooves of B*1402 and B*2705 differ from each other at 18 positions (Fig. 1). These amino acid exchanges influence at least three features as follows: the general shape of the binding grooves, the interactions of several pocket-forming residues with atoms of the peptide, and the potential of residues of the α1- and α2-helices to interact with cell surface-expressed receptor molecules on effector cells. However, the overall structures of the HC and β_2m of all

TABLE 1
Data collection and refinement statistics

Data collection	B*1402:pLMP2	B*1402:pCatA	B*2705:pCatA	B*2709:pCatA
Space group	$P2_1$	$P2_12_12_1$	$P2_12_12_1$	$P2_12_12_1$
Unit cell *a; b; c* [Å; Å; Å] *α; β; γ* [°; °; °]	53.38; 79.95; 105.44 90.00; 99.51; 90.00	50.79; 82.14; 110.73 90.00; 90.00; 90.00	51.16; 82.40; 109.85 90.00; 90.00; 90.00	51.19; 83.00; 110.78 90.00; 90.00; 90.00
No. of molecules per asymmetric unit	2	1	1	1
Resolution [Å] [A]	50.0 – 2.55 (2.64 – 2.55)	50.0 – 1.86 (1.93 – 1.86)	50.0 – 1.85 (1.92 – 1.85)	50.0 – 1.80 (1.85 – 1.80)
Unique reflections [A]	26,731 (2,177)	38,358 (3,022)	38,830 (3,323)	41,600 (3,694)
Completeness [%] [A]	93.1 (76.8)	96.8 (78.0)	95.8 (83.7)	93.3 (84.3)
$\langle I\rangle/\langle\sigma(I)\rangle$ [A]	7.9 (1.4)	22.5 (3.5)	12.4 (3.0)	19.4 (3.0)
R_{sym} [A,B]	0.137(0.457)	0.049 (0.239)	0.080 (0.311)	0.057 (0.331)
Refinement				
R_{cryst} [A,C]	0.240 (0.354)	0.169 (0.193)	0.173 (0.222)	0.167 (0.217)
R_{free} [A,D]	0.268 (0.339)	0.219 (0.248)	0.223 (0.292)	0.204 (0.260)
Total no. of non-hydrogen atoms	6615	3744	3680	3696
Heavy chain, no. of atoms/average B factor [Å^2]	2254/26.5	2269/16.9	2258/22.0	2265/15.0
β_2m, no. of atoms/average B factor [Å^2]	1658/27.3	829/21.0	837/25.9	842/18.1
Peptide, no. of atoms/average B factor [Å^2]	184/24.3	70/16.2	70/19.7	70/13.3
Water, no. of molecules/average B factor [Å^2]	251/24.8	552/33.5	503/34.9	513/27.3
Glycerol, no. of atoms/average B factor [Å^2]	-	24/39.9	12/31.1	6/21.0
rmsd [E] from ideal geometry, bond length [Å] bond angles [°]	 0.010 1.63	 0.013 1.44	 0.022 1.82	 0.017 1.63
PDB entry code	3BVN	3BXN	3BP4	3BP7

[A] Values in parentheses refer to the highest resolution shell.
[B] $R_{sym} = \Sigma_h\Sigma_i|I_{h,i} - \langle I_h\rangle|/\Sigma_h\Sigma_i I_{h,i}$.
[C] $R_{cryst} = \Sigma_h|F_o - F_c|/\Sigma F_o$ (working set, no σ cutoff applied).
[D] R_{free} is the same as R_{cryst} but calculated on 5% of the data excluded from refinement.
[E] r.m.s.d. is from target geometries.

complexes described here are very similar, with r.m.s.d. values for Cα overlay (HC/β_2m) of 0.8/0.2 Å (B*1402·pCatA on B*1402·pLMP2), 0.3/0.2 Å (B*1402·pCatA on B*2705·pCatA or B*2709·pCatA), 0.7/0.3 Å (B*1402·pLMP2 on B*2705·pLMP2), and 0.6/0.3 Å (B*1402·pLMP2 on B*2709·pLMP2).

The pCatA peptide is displayed by the three HLA-B molecules in almost identical conventional orientations termed p4α (*i.e.* the main chain φ and ψ torsion angles are in α-helical conformation at p4, and all other φ/ψ torsion angles as in β-strands) (Fig. 2, *A–C*). In all cases, the primary anchor residue pArg2 and the secondary anchor residue pPhe9 are bound in nearly indistinguishable fashion in the B and F pockets, despite the presence of polymorphic HC residues that could influence peptide accommodation (Fig. 1). The interactions of other pCatA amino acids with residues of the binding groove are similar in the three complexes as well (Table 2). A comparison of the *B*-factor values shows that all atoms of pCatA exhibit low thermal vibration (Fig. 2, *D–F*).

On the other hand, the pLMP2 peptide is presented by B*1402 in the noncanonical "p6α"-binding mode (*i.e.* the main chain φ and ψ torsion angles are in α-helical conformation at p6, and all other φ/ψ torsion angles as in β-strands), with the residue pArg5 anchored deep in the binding groove, where it forms salt bridges with Asp-74 and a very short intra-peptide H-bond with pLeu7^O (Table 3 and Fig. 2, *G* and *H*) (24). These interactions are instrumental in holding the side chain of pArg5 firmly within the groove as indicated by low *B*-factor values (Fig. 2*I*). In contrast, high *B*-factor values are found for several pLMP2 residues, most notably pTrp4 but also in case of the arginine residues at p1, p2, and p3, when contrasted *e.g.* with pVal9 (Fig. 2*I*). Although the different resolutions preclude a direct comparison of B*1402 and of HLA-B27 with the pLMP2 peptide, the primary anchor residue pArg2 clearly exhibits a very low degree of flexibility when bound to B*2705 and B*2709 (Fig. 2, *J* and *K*), and this residue is also more fixed in the B*1402·pCatA complex (Fig. 2*D*).

An overlay of the bound peptides (Fig. 3, *A* and *B*) reveals that the distances between the Cα atoms of the N- and C-terminal residues in the two B*1402 complexes are smaller than in case of the HLA-B27-peptide complexes as follows: B*1402 in comparison with either B*2705 or B*2709, 0.3 Å for complexes with bound pCatA, 1.2 Å for B*1402/B*2705·pLMP2, and 0.7 Å for B*1402/B*2709-pLMP2.

To clarify differences in the conformations of the peptides in the three HLA-B complexes, we compared interactive three-dimensional models (49, 50) of pCatA and pLMP2 in B*1402 and in the two HLA-B27 subtypes (Fig. 3, *A* and *B*). Access to the three-dimensional feature is obtained by clicking on any part of the conventional two-dimensional figures in the PDF. A better understanding of many structural features is thus provided, and it is particularly helpful to be able to compare the peptide conformations by zooming in and by rotating the structures. The freely available Adobe Reader (version 9) is required as well as any Windows-based computer with a modern graphic card (128+ MB memory) and sufficient RAM (1024+ MB). The "Help" option within the program provides an introduction into the possibilities that are offered. A further useful feature of the three-dimensional images is the possibility to hide certain structural elements such as β_2m, HC, or any of the peptide conformations. A "tour" of the molecule resembling a pre-rendered video file of the structures is available through the pre-set views as well. At any stage, however, full interaction with the structures remains possible.

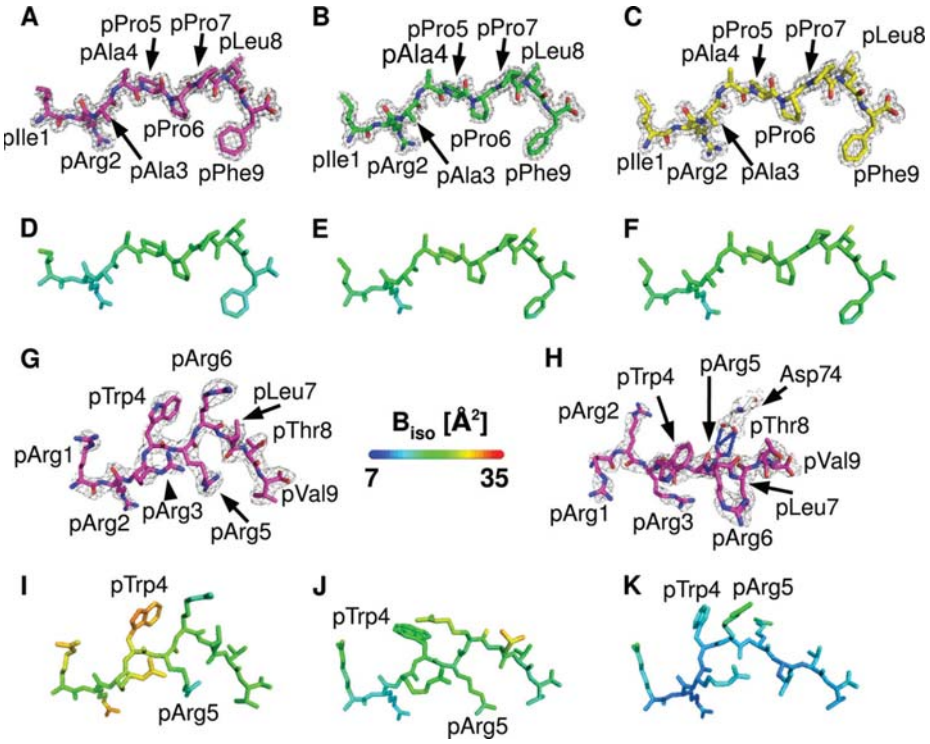

FIGURE 2. **General properties of the pCatA and pLMP2 peptides bound to three HLA-B subtypes.** *A–C,* final $2F_o - F_c$ electron density of pCatA conformations in B*1402 (*A*), B*2705 (*B*), and B*2709 (*C*), contoured at 1.5σ level. *D–F,* pCatA bound by B*1402 (*D*), B*2705 (*E*), and B*2709 (*F*) color-coded by isotropic *B*-factor. *G* and *H,* final $2F_o - F_c$ electron density of pLMP2 in B*1402 shown from the α2-helix (*G*) or the top of the binding groove (*H*), contoured at 1.5σ level. Electron density is depicted only for one molecule in the asymmetric unit. *I–K,* pLMP2 bound by B*1402 (*I*), B*2705 (*J*), and B*2709 (*K*) color-coded by isotropic *B*-factor. In all figures, unless mentioned otherwise, peptides bound to B*1402 are shown in *violet*, and peptides bound to B*2705 are shown in *green,* and peptides bound to B*2709 in are shown in *yellow*.

In the case of Fig. 3*A*, an overlay of the three pCatA structures allows us to view the peptide conformations from the side of the α2-helix (view 1), then from the top (view 2), and finally in the context of the whole HLA-B complex (views 3–6). The pCatA conformations are extremely similar when superimposed, because noticeable differences are only found for the N- and C-terminal residues. In contrast, the noncanonical p6α conformation of pLMP2 in B*1402 bears resemblance only to the noncanonical binding mode observed for pLMP2 in complex with B*2705 (Fig. 3*B* and views 1–10). The peptide backbone has very similar conformations in the two structures, and with the exception of pTrp4 and pArg6, all peptide residue side chains have comparable orientations. However, the precise location of similarly oriented side chains can differ considerably, *e.g.* in case of pArg1, pArg5, and pVal9 (Table 3). The three-dimensional images show these features very clearly, and they reveal also the distinct coordination of pArg5, either with Asp-74 in B*1402 (view 6) or with Asp-116 in B*2705 (view 7). As expected from the previously described differences between the B*2705 and B*2709 subtypes in complex with pLMP2 (24), the orientations of this peptide bound to B*1402 and B*2709, where the latter occupies the conventional "p4α" binding mode, have very little in common, in contrast to B*1402 and B*2705 (Fig. 3*B*, views 9 and 10). With the exception of pArg2, the side chains of all other peptide residues occupy distinct and in most cases totally different locations, whereas a comparison of the pLMP2-binding modes in B*2705 and B*2709 shows that despite the distinct peptide orientations at least pArg1, pArg2, pThr8, and pVal9 are bound in a nearly identical manner (Fig. 3*B* and Table 3) (24).

Consequences of Differential A Pocket Architectures—The N termini of peptides are anchored through a pentagonal network of hydrogen bonds in nearly all known MHC class I structures (52), including the four HLA-B27 structures compared here. This network additionally encompasses Tyr-7, Tyr-59, Tyr-171, and a water molecule termed "*W*" in Fig. 4 and Table 4. This water molecule is also contacted by residue 63 (Asn in B*1402 and Glu in B*2705 and B*2709), as shown by the B*2705·pCatA complex (Fig. 4*A*). In exceptional cases, here exemplified by B*3501 in complex with the octameric peptide nef (Fig. 4*B*) (53) and A*0201 presenting a peptide without its N-terminal amino acid (Fig. 4*C*) (54), a water molecule (W′) takes the place of $p1^N$, thus retaining the pentagonal network, although the peptide N terminus is no longer part of it. However, in the B*1402·pCatA complex, $p1^N$ is connected to a tetragonal network of hydrogen bonds formed by Tyr-7, Tyr-59, and two water molecules (W and W′) (Fig. 4*D* and Table 4). The two water molecules serve as hydrogen bonding partners of $p1^N$ and His-171^{NE}, as well as Glu-45 and Asn-63, respectively. The N terminus of pLMP2 in the B*1402 complex is anchored in both molecules of the asymmetric unit in precisely the same way, with all the elements of the tetragonal network identically positioned, including the water molecule (W′) at the position where it is located in B*1402·pCatA. However, the electron density map of B*1402·pLMP2 permits the placement of W′ only in one complex within the asymmetric unit. Since the tetragonal network engages also Asn-63 and Glu-45, two HC residues that possess identical conformations, and because the electron density map contoured at 0.8σ level shows some electron density at the position where W′ is located in the B*1402·pCatA complex, it is likely that the tetragonal network is present also in the other molecule of B*1402·pLMP2 within the asymmetric unit.

The B*5101 subtype is one of the few HLA-B molecules that possess His-171. There are two structures available for this subtype, both in complex with immunodominant peptides as follows: KM1 (LPPVVAKEI) and KM2 (TAFTIPSI) of human immunodeficiency virus, type 1 (55). The N terminus of the KM1 peptide is displayed in the 2.2 Å resolution structure of the B*5101-KM1 complex in the same nonconven-

TABLE 2

Comparison of pCatA binding to the B*1402, B*2705, and B*2709 molecules

Only direct hydrogen bonds (HB, ≤3.5Å), salt bridges (SB, ≤3.5Å), and van der Waals interactions (vdW, ≤4.0Å) between peptide residues and HLA residues are listed. In case of peptide residues, van der Waals interactions between backbone atoms and between atoms of neighboring residues are not shown. Water-mediated interaction are not shown as well.

	B*1402:pCatA				B*2705:pCatA				B*2709:pCatA			
Peptide residue	**Atom**	**Contact residue**	**Distance [Å]**	**Type**	**Atom**	**Contact residue**	**Distance [Å]**	**Type**	**Atom**	**Contact residue**	**Distance [Å]**	**Type**
pIle1	*Solvent-exposed*				*Solvent-exposed*				*Solvent-exposed*			
	pIle1^{O}	Tyr159^{OH}	2.6	HB	pIle1^{O}	Tyr159^{OH}	2.6	HB	pIle1^{O}	Tyr159^{OH} Tyr7^{OH}	2.6 3.5	HB HB
					pIle1^{N}	Tyr7^{OH} Tyr171^{OH}	2.8 2.7	HB HB	pIle1^{N}	Tyr7^{OH} Tyr171^{OH}	2.9 2.7	HB HB
	pIle1	Tyr59, Trp167	3.4-3.8	vdW	pIle1	Tyr7, Trp167	3.5-3.9	vdW	pIle1	Tyr7, Tyr59, Trp167	3.4-3.9	vdW
pArg2	*Buried*				*Buried*				*Buried*			
	pArg2^{N}	Asn63^{OD1}	3.0	HB	pArg2^{N}	Glu63^{OE2}	3.1	HB	pArg2^{N}	Glu63^{OE2}	3.0	HB
	pArg2^{NE}	Glu45^{OE1} Glu45^{OE2} Cys67^{SG}	2.7 3.4 3.3	HB HB HB	pArg2^{NE}	Glu45^{OE1} Glu63^{OE1}	2.8 3.3	HB HB	pArg2^{NE}	Glu45^{OE1} Glu63^{OE1}	2.9 3.2	HB HB
	pArg2^{NH1}	Tyr9^{OH} Ser24^{OG}	2.9 2.8	HB HB	pArg2^{NH1}	Thr24^{OG1}	2.9	HB	pArg2^{NH1}	Thr24^{OG1}	2.9	HB
	pArg2^{NH2}	Ser24^{OG} Glu45^{OE2} Glu45^{OE1}	3.4 2.9 3.5	HB SB SB	pArg2^{NH2}	Thr24^{OG1} Glu45^{OE1}	3.2 2.8	HB SB	pArg2^{NH2}	Thr24^{OG1} Glu45^{OE1}	3.0 2.9	HB HB
					pArg2^{O}	Arg62^{NH1}	3.0	HB	pArg2^{O}	Arg62^{NH1} Arg62^{NH2}	3.0 3.3	HB HB
	pArg2	Tyr7, Ser24, Glu45, Ile66, Cys67, Tyr159	3.4-3.9	vdW	pArg2	Tyr7, Thr24, Arg62, Glu63, Ile66, Cys67, Tyr159	3.5-3.9	vdW	pArg2	Tyr7, Thr24, Glu63, Ile66, Cys67, Tyr159	3.5-3.9	vdW
pAla3	*Buried*				*Buried*				*Buried*			
	pAla3^{N}	Tyr159^{OH} Tyr99^{OH}	3.5 2.9	HB HB	pAla3^{N}	Tyr99^{OH}	2.9	HB	pAla3^{N}	Tyr99^{OH}	2.9	HB
					pAla3	Tyr99, Tyr159	3.6-3.9	vdW	pAla3	Tyr99, Tyr159	3.7-3.9	vdW
pAla4	*Solvent-exposed*				*Solvent-exposed*				*Solvent-exposed*			
									pAla4	Gln155	3.6	vdW
pPro5	*Buried*				*Buried*				*Buried*			
	pPro5	Thr69, Asn70	3.8-4.0	vdW	pPro5	Ala69	3.9	vdW	pPro5	Gln155	3.6	vdW
pPro6	*Buried*				*Buried*				*Buried*			
	pPro6	Trp97, Phe116	3.8-3.9	vdW					pPro6	Trp147, Val152	3.7-3.9	vdW
pPro7	*Solvent-exposed*				*Solvent-exposed*				*Solvent-exposed*			
					pPro7^{O}	Trp147^{NE1}	3.3	HB	pPro7^{O}	Trp147^{NE1}	3.2	HB
	pPro7	Trp147, Glu152	3.5-3.9	vdW	pPro7	Val152	3.4	vdW	pPro7	Val152	3.8	vdW
pLeu8	*Solvent-exposed*				*Solvent-exposed*				*Solvent-exposed*			
	pLeu8^{O}	Trp147^{NE1}	3.2	HB	pLeu8^{O}	Trp147^{NE1}	3.2	HB	pLeu8^{O}	Trp147^{NE1}	3.2	HB
	pLeu8	Thr73, Glu76	3.6-3.9	vdW	pLeu8	Thr73, Glu76	3.7-3.9	vdW	pLeu8	Glu76	3.9	vdW
pPhe9	*Buried*				*Buried*				*Buried*			
	pPhe9^{N}	Ser77^{OG}	3.0	HB	pPhe9^{N}	Asp77^{OD1}	2.9	HB				
	pPhe9^{O}	Asn80^{ND2} Tyr84^{OH} Lys146^{NZ}	2.9 3.1 2.7	HB HB SB	pPhe9^{O}	Tyr84^{OH} Lys146^{NZ}	3.4 2.8	HB SB	pPhe9^{O}	Tyr84^{OH} Lys146^{NZ}	3.5 2.8	HB SB
	pPhe9^{OXT}	Thr143^{OG1} Tyr84^{OH}	2.9 2.6	HB HB	pPhe9^{OXT}	Thr143^{OG1} Tyr84^{OH}	2.7 2.7	HB HB	pPhe9^{OXT}	Thr143^{OG1} Tyr84^{OH}	2.7 2.7	HB HB
	pPhe9	Ser77, Leu81, Leu95, Phe116, Tyr123, Thr143, Lys146, Trp147	3.4-3.9	vdW	pPhe9	Asp77, Leu81, Leu95, Asp116, Tyr123, Thr143, Lys146, Trp147	3.6-3.9	vdW	pPhe9	Asp77, Leu81, Tyr84, Leu95, His116, Tyr123, Thr143, Lys146, Trp147	3.4-4.0	vdW

tional mode of N-terminal anchoring that has been observed for the B*1402 subtype (Fig. 4, *D* and *E*). The binding mode of the N terminus of the KM2 peptide to B*5101 is somewhat different from that resulting in the tetragonal network (data not shown), very likely because of the lower resolution (3.0 Å) of this structure, which may not have permitted unam-

TABLE 3

Comparison of pLMP2 binding to B*1402, B*2705, and B*2709

Only direct hydrogen bonds (HB, ≤3.5Å), salt bridges (SB, ≤3.5Å), van der Waals interactions (vdW, ≤4.0Å), and amino aromatic interactions (AA) between peptide residues and HLA residues are listed. In case of peptide residues, van der Waals interactions between backbone atoms and between atoms of neighboring residues are not shown. Water-mediated interactions are not shown as well.

	B*1402:pLMP2				B*2705:pLMP2				B*2709:pLMP2			
Peptide residue	**Atom**	**Contact residue**	**Distance [Å]**	**Type**	**Atom**	**Contact residue**	**Distance [Å]**	**Type**	**Atom**	**Contact residue**	**Distance [Å]**	**Type**
pArg1	*Solvent-exposed*				*Solvent-exposed*				*Solvent-exposed*			
					pArg1^{N}	Tyr7^{OH} Tyr171^{OH}	3.0 2.6	HB HB	pArg1^{N}	Tyr7^{OH} Tyr171^{OH}	3.1 2.7	HB HB
	pArg1^{O}	Tyr159^{OH}	2.6	HB	pArg1^{O}	Tyr159^{OH}	2.7	HB	pArg1^{O}	Tyr159^{OH}	2.7	HB
					pArg1^{NE}	Glu163^{OE1}	2.9	HB	pArg1^{NE}	Glu163^{OE1}	2.8	HB
	pArg1^{NH1}	Thr163^{OG1}	3.5*	HB	pArg1^{NH2}	Glu163^{OE1} Glu163^{OE2}	3.2 2.9	SB SB	pArg1^{NH2}	Glu163^{OE1}	3.3	SB
	pArg1	Tyr7, Arg62, Thr163, Trp167	3.4-3.8	vdW	pArg1	Tyr7, Tyr59, Arg62, Glu163, Trp167	3.4-3.9	vdW		Tyr7, Tyr59, Arg62, Tyr159, Glu163, Trp167, Tyr171	3.4-3.9	vdW
pArg2	*Buried*				*Buried*				*Buried*			
	pArg2^{N}	Asn63^{OD1}	3.1	HB	pArg2^{N}	Glu63^{OE2}	3.0	HB	pArg2^{N}	Glu63^{OE2}	3.0	HB
	pArg2^{NE}	Glu45^{OE1} Glu45^{OE2} Cys67^{SG}	2.7 3.3 3.2	HB HB HB	pArg2^{NE}	Glu45^{OE1} Glu63^{OE2}	2.8 3.2	HB HB	pArg2^{NE}	Glu45^{OE1} Glu63^{OE2}	2.8 3.2	HB HB
	pArg2^{NH1}	Tyr9^{OH} Ser24^{OG} Cys67^{SG}	3.0 3.0 3.4*	HB HB HB	pArg2^{NH1}	Thr24^{OG1}	3.0	HB	pArg2^{NH1}	Thr24^{OG1}	2.9	HB
	pArg2^{NH2}	Ser24^{OG} Glu45^{OE2}	3.5 2.8	HB SB	pArg2^{NH2}	Thr24^{OG1} Glu45^{OE1}	3.0 2.9	HB SB	pArg2^{NH2}	Thr24^{OG1} Glu45^{OE1}	3.0 2.9	HB SB
					pArg2^{O}	Arg62^{NH1}	3.1		pArg2^{O}	Arg62^{NH1}	3.0	HB
	pArg2	Tyr7, Ser24, Glu45, Cys67	3.4-3.9	vdW	pArg2	Tyr7, Thr24, Glu63, Ile66, Cys67, Tyr159	3.6-3.9	vdW	pArg2	Tyr7, Thr24, Glu63, Ile66, Cys67, Tyr159	3.5-3.9	vdW
pArg3	*Partly solvent-exposed*				*Partly solvent-exposed*				*Partly solvent-exposed*			
	pArg3^{N}	Tyr99^{OH}	2.9	HB	pArg3^{N}	Tyr99^{OH}	3.1	HB	pArg3^{N}	Tyr99^{OH}	3.0	HB
	pArg3^{NH2}	Glu152^{OE1} Glu152^{OE2}	3.5* 2.7	SB SB					pArg3^{NH1}	Gln155^{OE1}	3.1	HB
	pArg3	pArg5, Tyr99, Glu152, Tyr159	3.4-3.9	vdW	pArg3	pArg5, Tyr99, Leu156, Tyr159	3.5-3.9	vdW	pArg3	pArg5, Ile66, Leu156, Tyr159	3.5-3.9	vdW
pTrp4	*Solvent-exposed*				*Solvent-exposed*				*Solvent-exposed*			
	pTrp4	pArg6, Ile66, Thr69	3.4-3.9	vdW	pTrp4	pArg6	3.2-3.9	vdW	pTrp4	Arg62, Gln65, Ile66	3.4-3.9	vdW
						pArg6	3.2-3.6	AA				
pArg5	*Buried*				*Buried*				*Solvent-exposed*			
	pArg5^{NH1}	Asp74^{OD2} pLeu7^{O}	2.9 2.7	SB HB	pArg5^{NH1}	Asn97^{ND2} Asp116^{OD1} Asp116^{OD2}	3.4 3.4 3.0	HB SB SB				
	pArg5^{NH2}	Asn70^{OD1} Asp74^{OD1} Asp74^{OD2}	3.5* 2.7 3.1	HB SB SB	pArg5^{NH2}	Asp116^{OD1} Asp116^{OD2}	3.1 3.0	SB SB				
	pArg5	pArg3, pLeu7, Asn70, Thr73, Trp97, Phe116	3.2-3.9	vdW	pArg5	pArg3, Asn97, His114	3.5-3.8	vdW	pArg5	pArg3, Gln155	3.5-3.6	vdW
pArg6	*Solvent-exposed*				*Solvent-exposed*				*Solvent-exposed*			
	pArg6	pTrp4	3.4-3.9	vdW	pArg6	pTrp4, Arg62, Gln65, Ile66, Ala69	3.2-3.9	vdW	pArg6^{NH1}	Gln72^{NE2}	3.1	HB
						pTrp4	3.2-3.6	AA	pArg6^{NH2}	Gln72^{NE2}	3.1	HB
										Ala69, Thr73	3.5-3.9	vdW

TABLE 3—*continued*

pLeu7	*Solvent-exposed*				*Solvent-exposed*				*Solvent-exposed*			
	pLeu7	Arg5, Thr73, Trp147, Ala150, Glu152	3.2-3.9	vdW	pLeu7	Lys146, Val152, Trp147	3.7-3.8	vdW	pLeu7	Thr73, Asp77, His114, Trp147, Val152	3.5-4.0	vdW
pThr8	*Solvent-exposed*				*Solvent-exposed*				*Solvent-exposed*			
	pThr8^{O}	Trp147^{NE1}	2.8	HB	pThr8^{O}	Lys146^{NZ} Trp147^{NE1}	3.2 3.0	HB HB	pThr8^{O}	Lys146^{NZ} Trp147^{NE1}	3.0 2.8	HB HB
					pThr8^{OG1}	Lys146^{NZ}	3.2	HB	pThr8^{OG1}	Lys146^{NZ}	2.7	HB
	pThr8	Asn80	3.5	vdW	pThr8	Glu76	3.7	HB	pThr8	Thr73	3.7-3.9	HB
pVal9	*Buried*				*Buried*				*Buried*			
	pVal9^{N}	Ser77^{OG}	3.1	HB	pVal9^{N}	Asp77^{OD1}	2.8	HB	pVal9^{N}	Asp77^{OD1}	2.8	HB
	pVal9^{O}	Asn80^{ND2} Tyr84^{OH} Lys146^{NZ}	2.8 3.2 3.4*	HB HB SB	pVal9^{O}	Lys146^{NZ}	3.0	SB	pVal9^{O}	Lys146^{NZ}	3.0	SB
	pVal9^{OXT}	Thr143^{OG1} Tyr84^{OH}	2.9 2.5	HB HB	pVal9^{OXT}	Thr143^{OG1} Tyr84^{OH}	2.7 2.8	HB HB	pVal9^{OXT}	Thr143^{OG1} Tyr84^{OH} Lys146^{NZ}	2.7 2.8 3.4	HB HB SB
	pVal9	Leu81, Leu95, Tyr123, Thr143, Lys146	3.6-4.0	vdW	pVal9	Asp77, Tyr84, Thr143, Trp147	3.5-3.9	vdW	pVal9	Asp77, Thr80, Tyr84, Thr143, Trp147	3.7-3.9	vdW

* This bond exists in only one of the two molecules in the asymmetric unit.

biguous positioning of all atoms participating in anchoring of the KM2 N terminus.

As a consequence of the nonconventional location, the N termini of both B*1402-bound peptides in the crystal asymmetric unit are anchored rather shallowly and are shifted "upward" by 1.6–1.7 Å in comparison with the HLA-B27-bound peptides (Fig. 3, *A* and *B*). Furthermore, the location of the methyl group of the pIle1 side chain of the pCatA peptide differs between the B*1402 and B*2705 complexes, and also the apex of the pArg1 side chain of the pLMP2 peptide is separated by 3.37 Å between these HLA-B molecules (Fig. 3, *A* and *B*). Residue 163 (Thr in B*1402 and Glu in B*2705 and B*2709) contributes to fixing the side chain of pArg1 through direct contacts in all three structures. Thus, although stabilization of the pArg1 side chain, a predominant residue among HLA-B27 ligands, is dependent on Glu-163, substitution of this residue by Thr still allows hydrogen bonding with pArg1. Furthermore, whereas Arg-62 and Trp-167 also have important roles in anchoring an N-terminal arginine in HLA-B27 molecules (56), hydrophobic interactions with these two residues are largely abrogated in the B*1402·pLMP2 structure (Fig. 5, *D–F*).

Pockets for Primary and Secondary Peptide Anchors—The B pocket of the peptide-binding groove, which accommodates the primary anchor of the peptide (p2) in both the B*1402 and the HLA-B27 subtypes, exhibits four substitutions in B*1402, relative to B*2705 or B*2709 as follows: Y9H, S24T, N63E, and N70K. These exchanges, however, do not result in a reorientation of the pArg2 side chain in the two complexes with B*1402. Despite a number of distinct contacts, this amino acid is accommodated in nearly identical conformations in all six structures compared here (Tables 2 and 3). In neither of the two B*2705 complexes does Lys-70 form water-mediated hydrogen bonds with pArg2 or pAla/Arg3, whereas Asn-70 forms water-mediated hydrogen bonds with both of these peptide residues in the B*1402·pCatA structure. The apparent absence of these water-mediated contacts in the B*1402·pLMP2 complex could be due to the lower resolution of this structure.

A surface representation of the three HLA-B molecules (Fig. 5) demonstrates that in the HLA-B27-peptide complexes, a bridge-like structure arches over the N-terminal half of a peptide, connecting Arg-62 and Glu-163 via a water molecule (Fig. 5, *B, C, E,* and *F*), as described previously in detail for the structure of B*2709 complexed to the s10R peptide that contains, like pLMP2, an arginine at p1 (56). With a glycine at this position, as in case of the m9 peptide (21), the side chain of Arg-62 assumes a distinct orientation that results in loss of the "bridge." Similarly, the E163T exchange between HLA-B27 and B*1402 alters the orientation of the Arg-62 side chain, leading to an abrogation of the Arg-62 to Glu-163 contact between the two α-helices (Fig. 5, *A* and *D*).

Second only to the B pocket, the F pocket also fulfills an important role in both B*1402 and HLA-B27 (19, 29, 30). It exhibits differences at positions S77D, N80T, and F116D between B*1402 and B*2705 (Fig. 1). Apart from a difference in charge, the exchange of residue 116 leads also to a higher occupation of the F pocket by more atoms in B*1402, to which the bulky Trp-97 (instead of Asn in B*2705) is also likely to contribute. Although no difference between the coordinations of pPhe9 in B*1402 and the HLA-B27 structures can be observed (Table 2), apart from the replacement of a direct pPhe9^{O} → Asn-80^{ND2} contact in B*1402 by a water-mediated interaction between the pPhe9^{O} and Thr-80^{OG1} in B*2705 and B*2709 (not shown in Table 2), the aromatic ring of pPhe9 in the pCatA peptide is oriented at an angle of ~60° in the B*1402 complex in comparison with the two HLA-B27 complexes (Fig. 6*A*). This peculiar orientation facilitates an optimal face-to-edge stacking

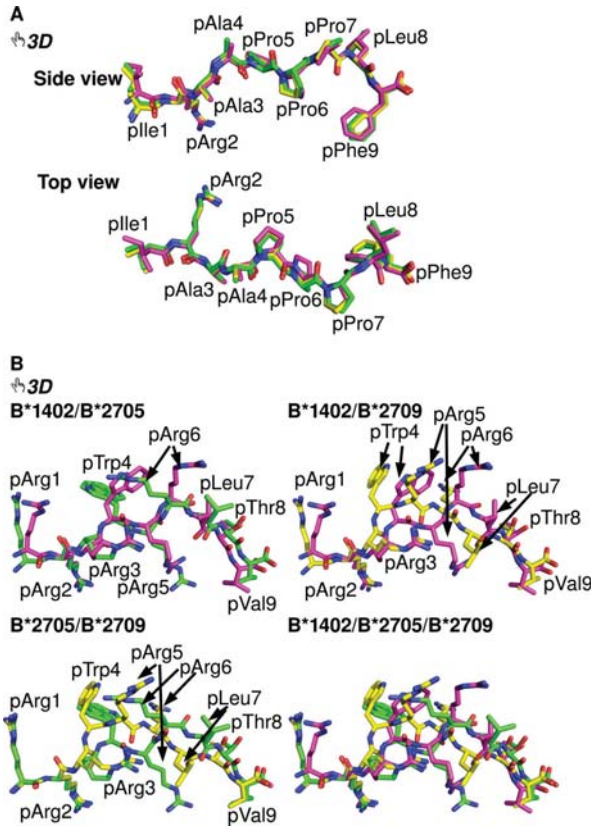

FIGURE 3. **Interactive three-dimensional comparison of the pCatA and pLMP2 peptides bound to three HLA-B molecules.** An overlay of the conformations of pCatA in B*1402 (*violet*), B*2705 (*green*), and B*2709 (*yellow*) is provided in *A* and for pLMP2 in *B*. By clicking on each of the two-dimensional images in the PDF version of the article, the three-dimensional functions for a given peptide become available (they can be terminated by right-clicking on the three-dimensional display and choosing the "Disable three-dimensional" function). In each case, the model tree icon allows the view of individual components (with their designations shown on the *left*) of the three-dimensional model, and offers a preselected "tour" of the model. During the tour (with 6 and 10 images for B*1402 or B*2705, respectively), each of the models can be manipulated individually using the mouse (the tools to rotate, pan, or zoom an image can be selected through the toolbar or the contextual menu). A better understanding of many structural characteristics of the models can be obtained by "playing" with the structures. For example, the different contacts made by pArg5 in the binding grooves of B*1402 and B*2705, respectively, are easily compared with each other, as Asp-74 and the polymorphic residue 116 (Phe in B*1402, Asp in B*2705, and His in B*2709) are shown, along with residue 97 (views 6–10). Colors of the peptides as in Fig. 2.

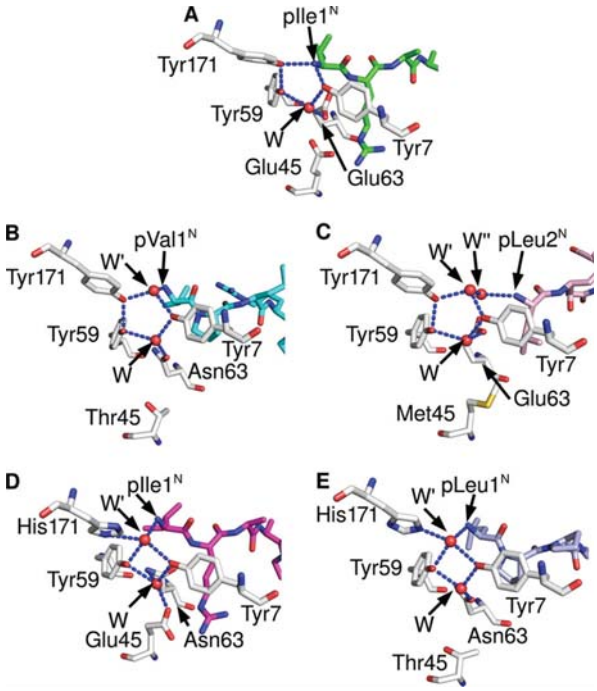

FIGURE 4. **HLA-B subtype-dependent anchoring of peptide N termini.** The crucial role of the Y171H exchange for the anchoring of peptide N termini is revealed by comparing the A pockets of B*2705·pCatA (*A*), B*3501 bound to the octameric nef peptide (*B*), A*0201 complexed with an N-terminally truncated peptide (*C*), B*1402·pCatA (*D*), and B*5101·KM1 (*E*). Whereas the first three structures (all with Tyr-171) show a pentagonal hydrogen bonding network, the subtypes B*1402 and B*5101 anchor the peptide N terminus only indirectly, via a water molecule (*W'*) which is also contacted by His-171^{NE}, resulting in the formation of a tetragonal network of H-bonds. HC residues are colored *gray*, and peptide residues are in different colors.

(C-H-π bonding) between the aromatic rings of pPhe9 and Phe-116. Comparable interactions are frequently found in protein structures (57) and allow a better sharing of π electrons. The C-terminal residue of the pCatA peptide is also stabilized by C-H-π bonding to the nonpolymorphic residue Tyr-123 in all three structures.

Anchoring of the Middle of the Peptides—In contrast, striking HLA-B subtype-dependent changes are observed when residues in the middle of the peptides are considered, in particular pTrp4, pArg5, and pArg6 in the case of pLMP2. However, conformational differences are also found between the three structures with pCatA as follows: the presence of Phe-116 (B*1402), but not Asp-116 (B*2705) or His-116 (B*2709), permits van der Waals contacts with pPro6, leading to a shift (0.3 Å) of this residue into the binding groove (Fig. 6*A*). This location of pPro6 is also stabilized through van der Waals interactions with Trp-97 (B*1402), which cannot form with the much smaller Asn-97 that is found in the two HLA-B27 molecules (Fig. 6*A*). These differences do not, however, lead to a very pronounced displacement of the pCatA peptide between B*1402 and B*2705/B*2709 (Fig. 3*A*).

Prolines in native proteins are always observed in either completely *cis* or *trans* form, because the relative ease of flipping between these forms is overwhelmed by favorable interactions with proximal groups (58). All three prolines of the pCatA peptide are in *trans* conformation in the three structures. We built *trans*-Pro-*cis*-Pro variant models of the pCatA peptide, disregarding electron density maps and keeping the Cα1–Cα9 distance and the orientation of the residues p1–p3 and p9 the same as in the B*1402·pCatA structure. All models with one to three *cis*-Pro were found to contain at least two and a maximum of five residues lying in disallowed regions of the Ramachandran plot, suggesting that the all-*trans* model that is observed in the three structures is sterically the most favored.

In contrast to pCatA, drastic conformational changes are obvious with regard to the pLMP2 peptide (Fig. 3*B*). As mentioned previously, these are primarily due to the different orientations of pArg5 in the three structures, and although this residue is solvent-exposed in B*2709 (Fig. 2*K*), it contacts Asp-74 (B*1402) or Asp-116 (B*2705) within the binding groove through salt bridges (interactive Fig. 3*B* and Fig. 6, *B* and

TABLE 4

Compilation of atoms comprising the pentagonal or tetragonal network of hydrogen bonds within the A pocket of various HLA class I molecules

Atom	HLA class I subtypes and complexed peptides				
	Pentagonal network			Tetragonal network	
	B*2705:pCatA	B*3501:nef	A*0201:Tax8	B*1402:pCatA	B*5101:KM1
$Tyr7^{OH}$	+[§]	+	+	+	+
Water (W)[#]	+	+	+	+	+
$Tyr59^{OH}$	+	+	+	+	+
$Tyr171^{OH}$	+	+	+	absent	absent
$His171^{NE}$	absent	absent	absent	+	+
$p1^{N*}$	+	-[&]	-	-	-
Water (W')[#]	absent	+	+	+	+

[§] The atom is part of the network.
[#] For designations of the water atoms, please refer to Fig. 5.
[*] N terminus of the peptide is shown.
[&] The atom is not part of the network.

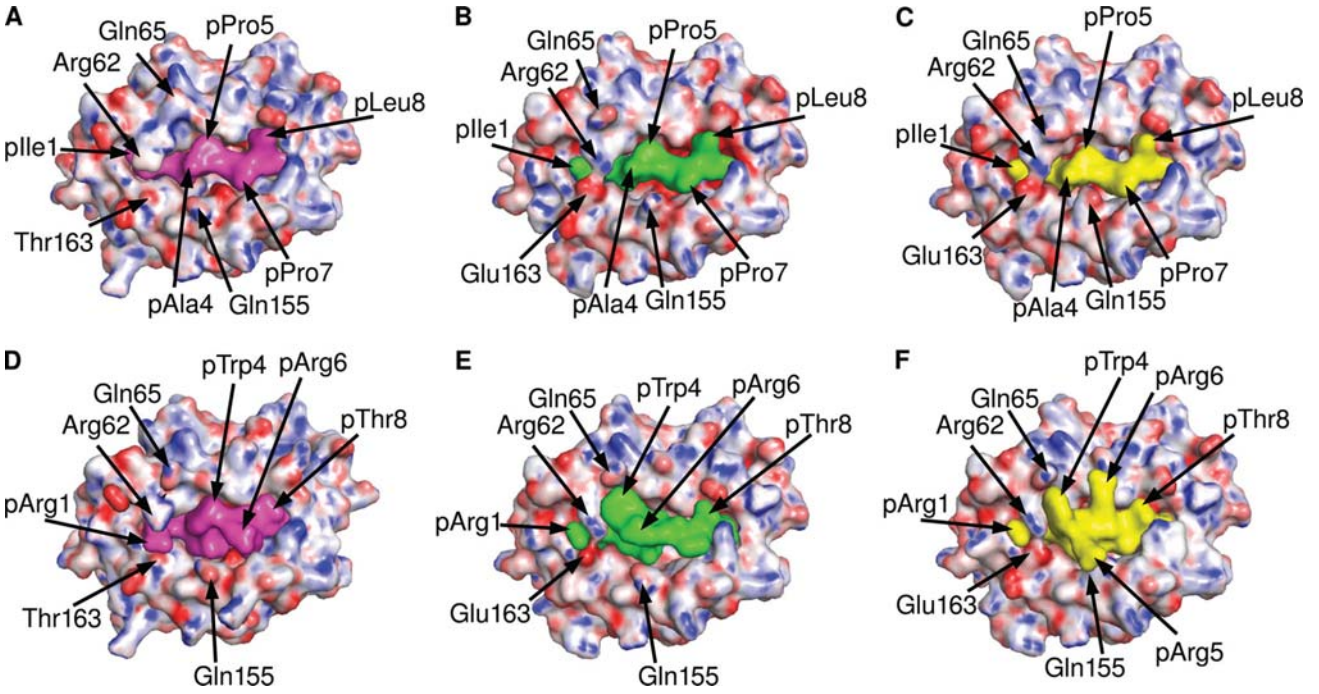

FIGURE 5. **Molecular surfaces of the pCatA and pLMP2 peptides bound to three HLA-B subtypes.** Shown are molecular surface representations of B*1402 (*A* and *D*), B*2705 (*B* and *E*), and B*2709 (*C* and *F*) complexed with the pCatA peptide (*A–C*) or the pLMP2 peptide (*D–F*), respectively, as viewed by an approaching TCR. Colors of the peptides are as in Fig. 2. In each image, electrostatic surfaces are shown only for the respective HC, with *red* indicating a negative and *blue* a positive charge. *Gray* areas are uncharged. A number of crucial peptide or HC residues (see text) are indicated.

C). Whereas these distinct anchoring modes of pArg5 are responsible for the differences found in the pLMP2-binding modes, it is more difficult to explain the considerable changes between B*1402 and B*2705 that characterize the conformations of other peptide side chains (Fig. 3*B*). Apart from alterations that are a consequence of A pocket polymorphisms (Fig. 4), the short salt bridge between pArg3 and Glu-152 (Table 3) could influence the insertion of pLMP2 into the B*1402-binding groove. In both HLA-B27 subtypes, pArg3 forms an intrapeptide hydrogen bond with $pTrp4^{O}$ instead. pArg6 and pTrp4 contact each other by van der Waals bonds both in B*1402 and B*2705, despite the distinct orientations of the side chains of both residues (Fig. 2, *I* and *J*).

DISCUSSION

The present crystallographic study was primarily undertaken to provide a better understanding for the observation that alloreactive CTL can be generated against cells expressing B*1402 that cross-react with HLA-B27 molecules, despite the considerable exchanges that characterize the peptide-binding grooves of the two antigens (Fig. 1) (19). Most of these differences affect the α1-helix and the floor of the binding groove with eight and

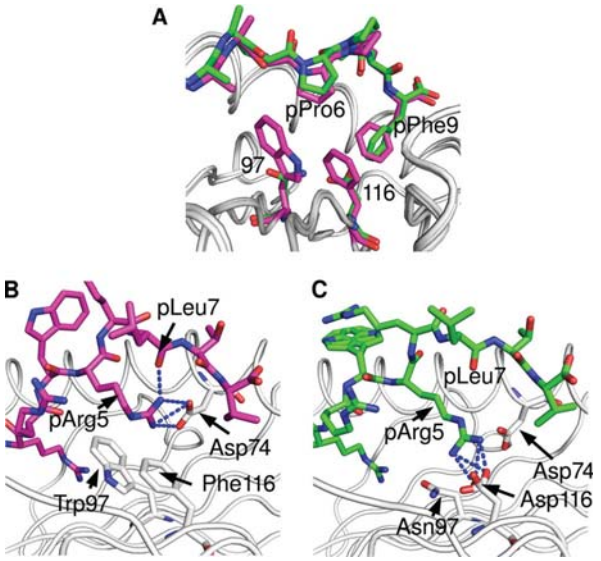

FIGURE 6. **Differential anchoring of the middle of the pCatA and pLMP2 peptides.** The bulky residues at HC positions 97 (Trp) and 116 (Phe) in the B*1402 subtype lead to differential contacts when compared with B*2705 (Asn-97 and Asp-116). The structures with pCatA (*violet*) (*A*) and pLMP2 (*B*) (*green, A* and *C*) are shown. Whereas pPro6 of pCatA is shifted only slightly into the groove in case of B*1402, the smaller side chains of residues 97 and 116 do not contact pPro6. The pArg5 residue of the pLMP2 peptide forms a bidentate salt bridge with Asp-74 and a hydrogen bond with pLeu7 in B*1402, whereas salt bridges with Asp-116 characterize the noncanonical pLMP2 conformation in case of B*2705.

seven exchanges, respectively, whereas there are only three α2-helical exchanges. We analyzed a proven shared ligand of B*1402 and HLA-B27 antigens, the self-peptide pCatA, as well as a nonself-ligand, the viral peptide pLMP2. The overall structures of the B*1402 and HLA-B27 complexes with both peptides are related, but a detailed comparison of the two peptides reveals that they are bound either very similarly (pCatA) or in distinct conformations (pLMP2) (Tables 2 and 3; Figs. 2 and 3).

The anchoring of the N termini of bound peptides through a pentagonal hydrogen bond network within the A pocket (Fig. 4; Table 4) is known to be one of the most concordant features of peptide presentation by MHC molecules (52). Furthermore, the structure of B*3501 in complex with an octameric peptide reveals that the pentagonal network can also exist in a slightly modified form in which the N terminus of the peptide is shifted upwards, preventing its direct participation but permitting the establishment of a connection to the pentagonal network through a water molecule (53), instead of forming one of the five corners of the pentagonal network. The latter represents the "normal" situation and can be found in HLA-B35 molecules presenting nonameric peptides (15, 16, 59), in all other published structures of "classical" MHC class I molecules, or in the structures of the HLA-B27 subtypes with the pCatA peptide described here. A comparison of the binding of the nonameric Tax peptide (Tax9) and an N-terminally truncated octamer (Tax8) to HLA-A2 shows that the removal of p1, a residue essential for formation of the pentagonal network, significantly reduces the affinity of the interaction between the ligand and the A pocket (54), but it does not eliminate the pentagonal network that is present in the Tax9 as well as the Tax8 peptide structures, with positions of the p1 atoms crucial for connecting the peptide with the ring formed by water molecules in the Tax8 structure.

However, a drastically different coordination of the peptide N terminus is triggered by the presence of His-171, as in B*1402. It results in the formation of a tetragonal network of hydrogen bonds. The water molecule (*W′* in Fig. 4), which "replaces" the hydroxyl group of Tyr-171, is also contacted by the peptide N terminus. In contrast, the involvement of the other three members of both the tetragonal and the pentagonal networks (Tyr-7, the water molecule W, and Tyr-59) remains unchanged. The causative role of His-171 in implementing the formation of a tetragonal network is supported by the only other high resolution structure in which the MHC molecule exhibits this exchange at residue 171, B*5101 in complex with the KM1 peptide (55). A comparison of the diverse contacts formed by the pentagonal and tetragonal networks in the different structures (Fig. 4; Table 4) reveals that it is in fact the exchange at residue 171, and not that of the polymorphic A pocket residue Asp/Asn-63 (Fig. 1), that is responsible for the formation of the unusual network in B*1402 and B*5101; Asn-63 occurs also, for example, in B*3501 and B*3508, both of which bind the N terminus of nonoctameric peptides via a pentagonal network (15, 16, 59). A further and very divergent solution for the N-terminal anchoring of a ligand is realized in case of the mouse H-2M3 antigen. It binds only peptides with an *N*-formylated methionine at the N terminus. A number of crucial A pocket polymorphisms are responsible for a unique architecture that permits this molecule to adjust to the specialized binding requirements of ligands derived from the N terminus of proteins produced by bacteria and mitochondria (60).

The presence of the tetragonal network only in the B*1402 and the B*5101 antigens strongly suggests that their exceptional reconstitution behavior *in vitro* is a consequence of this structural alteration; complexes of both HLA-B molecules need 2–3 months to reconstitute (35, 55), whereas HLA-B27 molecules require 2–3 weeks (21), and the majority of other MHC class I molecules only a few days (36). HLA-B14-peptide complexes also exhibit a high maturation rate and a reduced stability *in vivo* when compared with B*2705, as well as a substantial rate of dissociation in post-endoplasmic reticulum compartments. These distinguishing features are possibly due to a less optimized peptide repertoire (61). A reduced stability of HLA-B14 antigens might additionally be ascribed to the absence of the water-mediated contact between Arg-62 and Glu-163 that characterizes all HLA-B27-peptide complexes except those with pGly1 (see Refs. 21–26, 62 and this study). This bridge-like structural feature contributes to keeping the peptide in place; it cannot form in B*1402 because of the presence of Thr-163 (Fig. 5). Nevertheless, the *B*1402* subtype is widely distributed in various human populations, suggesting that the seemingly disadvantageous structural and biochemical features that are due to its unorthodox A pocket are no impediment for being a "successful" HLA class I antigen. However, the biological advantage conferred by expressing HLA-B14 molecules or of possessing *HLA-B14*-carrying haplotypes (63), if any, remains currently unclear.

Possibly the most conspicuous biochemical feature that the HLA-B14 and the HLA-B27 antigens have in common is the

preference (HLA-B14) (19, 29) or nearly absolute requirement (HLA-B27) (20, 31) for pArg2 of a bound peptide, despite the many amino acid exchanges that characterize the binding grooves of these HLA-B molecules (Fig. 1). The capacity to bind peptides with pArg2 is a feature of a relatively small number of MHC class I molecules, many of which seem to predispose to a development of spondyloarthropathies. Besides the well known and very strong association of HLA-B27 with AS (30, 64–66), B*3901 is associated with spondyloarthropathies in Japanese individuals (67, 68). This class I molecule as well as the very closely related B*3909 subtype present peptides with pArg2 (69, 70), and B*3901 binds also HLA-B27 ligands *in vitro* (68). Similarly, although carriers of the *B*1402* allele are not at risk to develop AS, the very closely related *B*1403* allele (distinguished only by an L156R exchange) is strikingly associated with AS in sub-Saharan populations from Togo (71) and Zambia (72), where AS is very infrequently encountered. B*1403 shares the preference for pArg2 of a bound peptide with B*1402 (19). Our finding that the pArg2 residues of the pCatA and pLMP2 peptides are similarly accommodated by the HLA-B14 and HLA-B27 B pockets (Figs. 2 and 3) provides a strong argument in favor of a role for this pocket in AS pathogenesis (30).

Further support for this contention can be gained from studies in gorillas with spondyloarthropathies. Gogo-B*0101 is an allele of an MHC class I molecule that binds peptides containing pArg2 (73) and is very frequently observed in affected animals. Residues belonging to the B pocket of this molecule exhibit a number of alterations in comparison with the AS-associated HLA-B27 alleles, most notably an exchange of Glu-45 (HLA-B27) to Met-45. Although this drastic mutation, when introduced into HLA-B27 molecules, abrogates the capacity of the mutant to bind peptides with pArg2 (74), it does not affect the B pocket preference for pArg2 in Gogo-B*0101 due to compensatory changes, mainly H9D (73). Thus, a variety of B pockets are able to bind pArg2 either with a highly conserved binding mode, as illustrated in this study for B*1402, B*2705, and B*2709, or in a different way, as in the Gogo-B*0101 antigen. However, neither the structure of the B pocket *per se* nor the capacity to present peptides with Arg-2 is sufficient to predispose to AS, as is obvious from the lack of association of B*2709 and B*1402 with this disease.

Anchoring of pArg5 to the floor of the peptide-binding groove is believed to be the defining feature for the accommodation of a peptide in a noncanonical binding mode by HLA-B27 molecules (22, 24, 26). In all the cases known so far, residue 116 forms a salt bridge (pArg5) or a hydrogen bond (citrulline at p5) with the side chain of the residue in the middle of a peptide, thus providing an additional anchor for the peptide and permitting it to adopt the noncanonical conformation. The B*1402·pLMP2 complex, however, exploits a further, and to our knowledge novel, mode of pArg5 anchoring to the groove; due to the exchange of Asp-116 by Phe-116, pArg5 forms a salt bridge with Asp-74. This binding mode appears also to be the result of steric hindrance because of the bulky residues on the floor of the peptide-binding groove (Figs. 1, 3, and 6), and it explains the observation that the B*1402 and in particular the B*1403 antigens show a marked preference for peptides with pArg5 (19). Because this preference is much higher than in case of B*2705, it is likely that the contact between pArg5 and Asp-74 in HLA-B14 molecules, despite the seemingly disadvantageous geometry of the curved pArg5 side chain, has a higher stabilizing effect on bound peptides than the interaction between pArg5 and Asp-116 in B*2705 (Figs. 3 and 6).

Despite recent advances in the field of MHC molecules and their recognition by TCR (9, 10, 18, 75), there was no specific insight regarding the structural basis for similarities and differences in peptide presentation by the B*1402, B*2705, and B*2709 antigens. Our study now provides a better understanding of T cell alloreactivity among the HLA-B14 and the HLA-B27 antigens. The results with the pCatA peptide demonstrate that a proven self-ligand can be presented by the three alloantigens in nearly identical conformations (Fig. 5). A T cell receptor with a focus on the peptide (76) might thus be able to recognize all complexes, despite the dissimilarities between the three HC. The fact that a number of amino acids that are known to be crucial for the docking of many TCR (18) are unchanged between HLA-B14 and HLA-B27 (*i.e.* residues at positions 65 and 155 of an HC) permits us to predict that alloreactive T cells might exploit these similarities and "prefer" to neglect the many differences among potential contact residues.

On the other hand, the three distinct structures with the pLMP2 peptide (Fig. 5) show also how alloreactivity between these antigens can be prevented; in addition to the allelic differences, the display of the peptide is so divergent in the three structures that T cell cross-reactivity will almost certainly not occur.

It might be argued that the similar conformations adopted by pCatA bound to B*1402 and the HLA-B27 subtypes exemplify an exceptional situation favored by the presence of three consecutive proline residues in the peptide sequence, a feature that might limit the conformational flexibility of a bound ligand. However, the remarkable correlation between peptide overlap and alloreactive T cell epitope sharing found not only between B*1402 and B*2705 (19) but also very frequently among HLA-B27 subtypes (reviewed in Ref. 34) argues against this view. This correlation suggests that many shared ligands adopt antigenically similar conformations when bound to distinct MHC class I allotypes. Thus, the similar binding mode observed for pCatA in multiple contexts might not be unusual.

Acknowledgments—We thank Yvette Roske and Claudia Alings for help with the crystallization trials and the beamline staff at BESSY II, Berlin, Germany, for valuable assistance.

REFERENCES

1. Lindahl, K. F., and Wilson, D. B. (1977) *J. Exp. Med.* **145,** 508–522
2. Suchin, E. J., Langmuir, P. B., Palmer, E., Sayegh, M. H., Wells, A. D., and Turka, L. A. (2001) *J. Immunol.* **166,** 973–981
3. Afzali, B., Lechler, R. I., and Hernandez-Fuentes, M. P. (2007) *Tissue Antigens* **69,** 545–556
4. Kamoun, M., Holmes, J. H., Israni, A. K., Kearns, J. D., Teal, V., Yang, W. P., Rosas, S. E., Joffe, M. M., Li, H., and Feldman, H. I. (2008) *Proc. Natl. Acad. Sci. U.S.A.* **105,** 18883–18888
5. Morris, G. P., and Allen, P. M. (2009) *J. Immunol.* **182,** 6639–6643
6. Gould, D. S., and Auchincloss, H., Jr. (1999) *Immunol. Today* **20,** 77–82
7. Bevan, M. J. (1984) *Immunol. Today* **5,** 128–130
8. Matzinger, P., and Bevan, M. J. (1977) *Cell Immunol.* **29,** 1–5

9. Felix, N. J., and Allen, P. M. (2007) *Nat. Rev. Immunol.* **7,** 942–953
10. Archbold, J. K., Macdonald, W. A., Burrows, S. R., Rossjohn, J., and McCluskey, J. (2008) *Trends Immunol.* **29,** 220–226
11. Kazansky, D. B. (2008) *J. Immunotoxicol.* **5,** 369–384
12. Paradela, A., García-Peydró, M., Vázquez, J., Rognan, D., and López de Castro, J. A. (1998) *J. Immunol.* **161,** 5481–5490
13. Reiser, J. B., Darnault, C., Guimezanes, A., Grégoire, C., Mosser, T., Schmitt-Verhulst, A. M., Fontecilla-Camps, J. C., Malissen, B., Housset, D., and Mazza, G. (2000) *Nat. Immunol.* **1,** 291–297
14. Luz, J. G., Huang, M., Garcia, K. C., Rudolph, M. G., Apostolopoulos, V., Teyton, L., and Wilson, I. A. (2002) *J. Exp. Med.* **195,** 1175–1186
15. Tynan, F. E., Elhassen, D., Purcell, A. W., Burrows, J. M., Borg, N. A., Miles, J. J., Williamson, N. A., Green, K. J., Tellam, J., Kjer-Nielsen, L., McCluskey, J., Rossjohn, J., and Burrows, S. R. (2005) *J. Exp. Med.* **202,** 1249–1260
16. Hourigan, C. S., Harkiolaki, M., Peterson, N. A., Bell, J. I., Jones, E. Y., and O'Callaghan, C. A. (2006) *Eur. J. Immunol.* **36,** 3288–3293
17. Colf, L. A., Bankovich, A. J., Hanick, N. A., Bowerman, N. A., Jones, L. L., Kranz, D. M., and Garcia, K. C. (2007) *Cell* **129,** 135–146
18. Rudolph, M. G., Stanfield, R. L., and Wilson, I. A. (2006) *Annu. Rev. Immunol.* **24,** 419–466
19. Merino, E., Montserrat, V., Paradela, A., and López de Castro, J. A. (2005) *J. Biol. Chem.* **280,** 35868–35880
20. Ramos, M., Paradela, A., Vazquez, M., Marina, A., Vazquez, J., and Lopez de Castro, J. A. (2002) *J. Biol. Chem.* **277,** 28749–28756
21. Hülsmeyer, M., Hillig, R. C., Volz, A., Rühl, M., Schröder, W., Saenger, W., Ziegler, A., and Uchanska-Ziegler, B. (2002) *J. Biol. Chem.* **277,** 47844–47853
22. Hülsmeyer, M., Fiorillo, M. T., Bettosini, F., Sorrentino, R., Saenger, W., Ziegler, A., and Uchanska-Ziegler, B. (2004) *J. Exp. Med.* **199,** 271–281
23. Hülsmeyer, M., Welfle, K., Pöhlmann, T., Misselwitz, R., Alexiev, U., Welfle, H., Saenger, W., Uchanska-Ziegler, B., and Ziegler, A. (2005) *J. Mol. Biol.* **346,** 1367–1379
24. Fiorillo, M. T., Rückert, C., Hülsmeyer, M., Sorrentino, R., Saenger, W., Ziegler, A., and Uchanska-Ziegler, B. (2005) *J. Biol. Chem.* **280,** 2962–2971
25. Rückert, C., Fiorillo, M. T., Loll, B., Moretti, R., Biesiadka, J., Saenger, W., Ziegler, A., Sorrentino, R., and Uchanska-Ziegler, B. (2006) *J. Biol. Chem.* **281,** 2306–2316
26. Beltrami, A., Rossmann, M., Fiorillo, M. T., Paladini, F., Sorrentino, R., Saenger, W., Kumar, P., Ziegler, A., and Uchanska-Ziegler, B. (2008) *J. Biol. Chem.* **283,** 27189–27199
27. Ziegler, A., Loll, B., Misselwitz, R., and Uchanska-Ziegler, B. (2009) in *Molecular Mechanisms of Spondyloarthropathies* (López-Larrea, C., and Díaz-Peña, R., eds) Vol. 649, pp. 177–195, Landes Bioscience, Austin, TX
28. García-Peydró, M., Martí, M., and López de Castro, J. A. (1999) *J. Immunol.* **163,** 2299–2305
29. DiBrino, M., Parker, K. C., Margulies, D. H., Shiloach, J., Turner, R. V., Biddison, W. E., and Coligan, J. E. (1994) *J. Biol. Chem.* **269,** 32426–32434
30. Ramos, M., and López de Castro, J. A. (2002) *Tissue Antigens* **60,** 191–205
31. Lopez de Castro, J. A., Alvarez, I., Marcilla, M., Paradela, A., Ramos, M., Sesma, L., and Vázquez, M. (2004) *Tissue Antigens* **63,** 424–445
32. Heath, W. R., Kane, K. P., Mescher, M. F., and Sherman, L. A. (1991) *Proc. Natl. Acad. Sci. U.S.A.* **88,** 5101–5105
33. Wang, W., Man, S., Gulden, P. H., Hunt, D. F., and Engelhard, V. H. (1998) *J. Immunol.* **160,** 1091–1097
34. López de Castro, J. A. (2009) in *Molecular Mechanisms of Spondyloarthropathies* (López-Larrea, C., and Díaz-Peña, R., eds) Vol. 649, pp. 196–209
35. Kumar, P., Vahedi-Faridi, A., Merino, E., López de Castro, J. A., Volz, A., Ziegler, A., Saenger, W., and Uchanska-Ziegler, B. (2007) *Acta Crystallogr. Sect. F Struct. Biol. Cryst. Commun.* **63,** 631–634
36. Garboczi, D. N., Hung, D. T., and Wiley, D. C. (1992) *Proc. Natl. Acad. Sci. U.S.A.* **89,** 3429–3433
37. Otwinowski, Z., and Minor, W. (1997) *Methods Enzymol.* **276,** 307–326
38. Collaborative Computational Project, Number 4 (1994) *Acta Crystallogr. D Biol. Crystallogr.* **50,** 760–763
39. Vagin, A., and Teplyakov, A. (1997) *J. Appl. Crystallogr.* **30,** 1022–1025
40. Storoni, L. C., McCoy, A. J., and Read, R. J. (2004) *Acta Crystallogr. D Biol. Crystallogr.* **60,** 432–438
41. Brünger, A. T., Adams, P. D., Clore, G. M., DeLano, W. L., Gros, P., Grosse-Kunstleve, R. W., Jiang, J. S., Kuszewski, J., Nilges, M., Pannu, N. S., Read, R. J., Rice, L. M., Simonson, T., and Warren, G. L. (1998) *Acta Crystallogr. D Biol. Crystallogr.* **54,** 905–921
42. Murshudov, G. N., Vagin, A. A., and Dodson, E. J. (1997) *Acta Crystallogr. D Biol. Crystallogr.* **53,** 240–255
43. Emsley, P., and Cowtan, K. (2004) *Acta Crystallogr. D Biol. Crystallogr.* **60,** 2126–2132
44. Morris, R. J., Perrakis, A., and Lamzin, V. S. (2003) *Methods Enzymol.* **374,** 229–244
45. Kabsch, W. (1976) *Acta Crystallogr. A* **32,** 922–923
46. Dolinsky, T. J., Czodrowski, P., Li, H., Nielsen, J. E., Jensen, J. H., Klebe, G., and Baker, N. A. (2007) *Nucleic Acids Res.* **35,** W522–525
47. Baker, N. A., Sept, D., Joseph, S., Holst, M. J., and McCammon, J. A. (2001) *Proc. Natl. Acad. Sci. U.S.A.* **98,** 10037–10041
48. DeLano, W. L. (2002) *The PyMOL Molecular Graphics System,* DeLano Scientific, Palo Alto, CA
49. Kumar, P., Ziegler, A., Ziegler, J., Uchanska-Ziegler, B., and Ziegler, A. (2008) *Trends Biochem. Sci.* **33,** 408–412
50. Kumar, P., Vahedi-Faridi, A., Saenger, W., Ziegler, A., and Uchanska-Ziegler, B. (2009) *Protein Sci.* **18,** 37–49
51. Loll, B., Zawacka, A., Biesiadka, J., Petter, C., Rückert, C., Saenger, W., Uchanska-Ziegler, B., and Ziegler, A. (2005) *Acta Crystallogr. Sect. F Struct. Biol. Cryst. Commun.* **61,** 939–941
52. Madden, D. R. (1995) *Annu. Rev. Immunol.* **13,** 587–622
53. Smith, K. J., Reid, S. W., Stuart, D. I., McMichael, A. J., Jones, E. Y., and Bell, J. I. (1996) *Immunity* **4,** 203–213
54. Khan, A. R., Baker, B. M., Ghosh, P., Biddison, W. E., and Wiley, D. C. (2000) *J. Immunol.* **164,** 6398–6405
55. Maenaka, K., Maenaka, T., Tomiyama, H., Takiguchi, M., Stuart, D. I., and Jones, E. Y. (2000) *J. Immunol.* **165,** 3260–3267
56. Hillig, R. C., Hülsmeyer, M., Saenger, W., Welfle, K., Misselwitz, R., Welfle, H., Kozerski, C., Volz, A., Uchanska-Ziegler, B., and Ziegler, A. (2004) *J. Biol. Chem.* **279,** 652–663
57. Waters, M. L. (2002) *Curr. Opin. Chem. Biol.* **6,** 736–741
58. Wedemeyer, W. J., Welker, E., and Scheraga, H. A. (2002) *Biochemistry* **41,** 14637–14644
59. Menssen, R., Orth, P., Ziegler, A., and Saenger, W. (1999) *J. Mol. Biol.* **285,** 645–653
60. Wang, C. R., Castaño, A. R., Peterson, P. A., Slaughter, C., Lindahl, K. F., and Deisenhofer, J. (1995) *Cell* **82,** 655–664
61. Merino, E., Galocha, B., Vázquez, M. N., and López de Castro, J. A. (2008) *Arthritis Rheum.* **58,** 3693–3704
62. Madden, D. R., Gorga, J. C., Strominger, J. L., and Wiley, D. C. (1992) *Cell* **70,** 1035–1048
63. Li, X., Ghandri, N., Piancatelli, D., Adams, S., Chen, D., Robbins, F. M., Wang, E., Monaco, A., Selleri, S., Bouaouina, N., Stroncek, D., Adorno, D., Chouchane, L., and Marincola, F. M. (2007) *J. Transl. Med.* **5,** 22
64. Khan, M. A., Mathieu, A., Sorrentino, R., and Akkoc, N. (2007) *Autoimmun. Rev.* **6,** 183–189
65. Brewerton, D. A., Hart, F. D., Nicholls, A., Caffrey, M., James, D. C., and Sturrock, R. D. (1973) *Lancet* **1,** 904–907
66. Schlosstein, L., Terasaki, P. I., Bluestone, R., and Pearson, C. M. (1973) *N. Engl. J. Med.* **288,** 704–706
67. Yamaguchi, A., Tsuchiya, N., Mitsui, H., Shiota, M., Ogawa, A., Tokunaga, K., Yoshinoya, S., Juji, T., and Ito, K. (1995) *Arthritis Rheum.* **38,** 1672–1677
68. Sobao, Y., Tsuchiya, N., Takiguchi, M., and Tokunaga, K. (1999) *Arthritis Rheum.* **42,** 175–181
69. Falk, K., Rötzschke, O., Takiguchi, M., Gnau, V., Stevanoviæ, S., Jung, G., and Rammensee, H. G. (1995) *Immunogenetics* **41,** 162–164
70. Yagüe, J., Ramos, M., Vázquez, J., Marina, A., Albar, J. P., and López de Castro, J. A. (1999) *Tissue Antigens* **53,** 227–236
71. López-Larrea, C., Mijiyawa, M., González, S., Fernández-Morera, J. L., Blanco-Gelaz, M. A., Martínez-Borra, J., and López-Vázquez, A. (2002) *Arthritis Rheum.* **46,** 2968–2971
72. Díaz-Peña, R., Blanco-Gelaz, M. A., Njobvu, P., López-Vazquez, A.,

Suárez-Alvarez, B., and López-Larrea, C. (2008) *J. Rheumatol.* **35,** 2236–2240
73. Urvater, J. A., Hickman, H., Dzuris, J. L., Prilliman, K., Allen, T. M., Schwartz, K. J., Lorentzen, D., Shufflebotham, C., Collins, E. J., Neiffer, D. L., Raphael, B., Hildebrand, W., Sette, A., and Watkins, D. I. (2001) *J. Immunol.* **166,** 3334–3344
74. Villadangos, J. A., Galocha, B., García, F., Albar, J. P., and López de Castro, J. A. (1995) *Eur. J. Immunol.* **25,** 2370–2377
75. Housset, D., and Malissen, B. (2003) *Trends Immunol.* **24,** 429–437
76. Tynan, F. E., Burrows, S. R., Buckle, A. M., Clements, C. S., Borg, N. A., Miles, J. J., Beddoe, T., Whisstock, J. C., Wilce, M. C., Silins, S. L., Burrows, J. M., Kjer-Nielsen, L., Kostenko, L., Purcell, A. W., McCluskey, J., and Rossjohn, J. (2005) *Nat. Immunol.* **6,** 1114–1122
77. Zamyatnin, A. A. (1972) *Prog. Biophys. Mol. Biol.* **24,** 107–123

3. Sequence-dependent variations in peptide binding mode

3.1 Summary

Comparative proteomic and peptide elution studies point to possible similarities in presentation of the pB27 (RRKSSGGKGGSY) and pCP (RRFKEGGRGGK) peptides by B*2705. The two peptides might thus be involved in the molecular pathogenesis of Chlamydia-induced ReA via molecular mimicry (Ramos et al. 2002, Cragnolini and López de Castro 2008). This prompted us to analyze the complexes of these two peptides with B*2705 using X-ray crystallography and thermodynamic methods to gain an understanding of how the subtle differences between these two peptides that have six corresponding residues in common will influence their binding by B*2705. Therefore, the crystal structures of the B*2705:pB27 and B*2705:pCP complexes were resolved to 1.5 Å resolution each. The structures revealed that both peptides bind B*2705 relatively flexibly, but the pB27 peptide could be localized in three distinct conformations, while the pCP peptide was localized only in a single conformation. To confirm the unprecedented triple conformation of the pB27 peptide, a second crystal structure of the B*2705:pB27 complex was obtained at 1.4 Å resolution from a crystal harvested from a different well of the crystallization tray. However, the conformation of the pB27 peptide was identical in both structures. For a comparative study of the thermodynamic consequences of such conformational plasticity of pB27 in the binding groove of B*2705, the B*2705:pB27 and B*2705:pCP complexes were analyzed by circular dichroism (CD) and differential scanning calorimetry (DSC) which revealed that both complexes are thermodynamically as stable as many other complexes of natural ligands with HLA-B27 subtypes.

These unpublished results show the unusual ability of B*2705 to present pB27 in multiple binding modes, and hint at the potential dynamics of the bound peptide. While evidence for a significant structural overlap (and thus “conventional” molecular mimicry) of pB27 and pCP is lacking, the dynamics of pB27 could potentially make it possible for one of the intermediate conformations of pB27 to mimic pCP.

In the second part of the work, the structural changes induced due to citrullination of pArg5 (i.e., replacement of the imino group with an O, resulting in the change of a single non-hydrogen atom of the guanidinium group) of the pVIPR peptide in B*2705:pVIPR and B*2709:pVIPR complex structures were studied.

3.2 Unpublished results

The unpublished results of an ongoing analysis aimed at investigating the “Exceptional conformational plasticity of a dodecameric self-peptide bound by the HLA-B*2705 antigen” are included.

The investigation has been performed by P. Kumar with the collaboration and guidance of R. Misselwitz, A. Vahedi-Faridi, J.J. Cragnolini, W. Saenger, J.A. López de Castro, A. Ziegler and B. Uchanska-Ziegler.

Unpublished results of an X-ray crystallographic analysis investigating "Exceptional conformational plasticity of a dodecameric self-peptide bound by the HLA-B*2705 antigen"

Laue X-ray diffraction has made it principally possible to gain insight into the dynamics of a protein and its reactivity with ligands (Genick et al. 1997, Schotte et al. 2003, 2004). However, no such information is available for MHC molecules. The existing structural information about peptide presentation by MHC class I molecules obtained through "Bragg" X-ray diffraction suggests that the vast majority of MHC class I molecules bind peptides in single conformations into their peptide binding groove, with the main chain of the peptide and side chains of most of the peptide residues occupying well-defined single conformations (Madden 1995, Ziegler et al. 2009a).

However, there are three structures known so far in which the peptides bound to MHC class I molecules assume more than a single conformation. In the 2.55 Å crystal structure of the rat MHC molecule RT1-A^a in complex with the dodecameric MTF-E peptide, the middle part of the MTF peptide is bound in two drastically different conformations in the two molecules of the asymmetric unit (Speir et al. 2001). In one of these two conformations, the middle part of the peptide participates in extensive crystal contacts, while the other conformation of the peptide forms no such contacts, suggesting that conformational duality of the MTF peptide could be a crystal packing-induced artifact. In the 1.47 Å crystal structure of the B*2705:pVIPR complex in which a single molecule is found per asymmetric unit, the pVIPR peptide is bound in two drastically different conformations in the peptide binding groove of the B*2705 molecule (Hülsmeyer et al. 2004, see also Section 1.6). Similarly, the self-peptide pGR is bound in a dual conformation in the peptide binding groove of the B*2705 molecule in a 1.40 Å crystal structure with a single molecule of the B*2705:pGR complex per asymmetric unit (Rückert et al. 2006). The conformational duality of the pVIPR and the pGR peptides is not likely to be dramatically influenced by crystal packing because there are no distinct crystal contacts formed by the two conformations of the same peptide.

The pB27 peptide (RRKSSGGKGGSY, derived from the cytoplasmic tail residues 309-320 of HLA-B27) is presented as an endogenously processed natural ligand of

three HLA-B27 subtypes, B*2702, B*2704, and B*2705, that are associated with SpA but not by the two subtypes B*2706 and B*2709 that are at best only weakly associated with the disease (Ramos et al. 2002). The presence of the four clustered glycine residues in its sequence and the fact that it is twelve residues long, suggest that pB27 could be flexible even when bound within the groove of the HLA-B27 molecule. Our collaborators in Madrid found, by employing proteomic and peptide elution analyses, that the pCP peptide (RRFKEGGRGGK, from DNA primase of *Chlamydia trachomatis*, residues 211-222), which has a high degree of sequence homology with the pB27 peptide, is naturally processed and presented by the B*2705 molecule (Cragnolini and López de Castro 2008). The high degree of sequence-homology between the pB27 and pCP peptides and their potential flexibility (due to the presence of the four clustered glycine residues and relatively longer lengths than the usual nine residues) triggered the suggestion that molecular mimicry between the two peptides may be involved in pathogenesis of ReA in B*2705-positive individuals. It is noteworthy that the pCP peptide is unlikely to be naturally processed and presented by other SpA-associated subtypes like B*2702, B*2704 and B*2707 due to the presence of the pΩLys residue which is not a suitable anchor for these subtypes (Cragnolini and López de Castro 2008). However, processing and presentation by these SpA-associated subtypes of extended versions of the pCP peptide with a suitable anchor residue at the pΩ position cannot be ruled out.

To gain insights into the possibility of molecular mimicry between the pB27 and pCP peptides in the context of the presentation by the B*2705 molecule, we analyzed the B*2705:pB27 and B*2705:pCP complexes using X-ray crystallography. The X-ray datasets allowed us to model three conformations of the pB27 peptide and a single conformation of the pCP peptide in the peptide binding groove of the B*2705 molecule, and suggest that both peptides are bound in relatively flexible conformations by the B*2705 molecule.

RESULTS

We obtained diffraction datasets from two crystals of the B*2705:pB27 complex at 1.4 and 1.5 Å resolutions and from one crystal of the B*2705:pCP complex at 1.4 Å resolution (Table 3.1). The HC and β_2m of the B*2705 molecule were localized in the crystal unit cells by molecular replacement employing atomic co-ordinates of HC and

β_2m obtained from the structure of the B*2705:m9 molecule (Hülsmeyer et al. 2002) as a search model. Initial electron density maps were interpretable for the entire length of the HC and β_2m, but only the first three residues of the N-terminal part of the peptides and their C-terminal residues (pTyr12 in case of pB27 and pLys11 in case of pCP) could be positioned unambiguously into the electron density maps. The initial models of the B*2705:pB27 and B*2705:pCP molecules were subjected to iterative cycles of restrained maximum likelihood refinement and manual rebuilding. During the process of refinement and model building based on 2Fo-Fc ("omit") and Fo-Fc ("difference") maps, geometric factors and refinement parameters, we were able to position the unassigned residues of the pB27 and pCP peptides in the electron density maps.

Table 3.1. Data collection and refinement statistics

Values in parentheses refer to the highest resolution shell.

Complex	**HLA-B*2705:pB27**			**HLA-B*2705:pCP**
	Crystal 1	Crystal 2		
PDB Code	3kib	-	-	3kil
Data collection				
Space group	$P2_12_12_1$	$P2_12_12_1$		$P2_12_12_1$
Cell Dimensions *a; b; c* [Å] *α, β,γ* [°]	 51.35; 82.48;110.31 90.00; 90.00; 90.00	 51.13; 82.22;109.76 90.00; 90.00; 90.00		 50.93; 82.26; 109.51 90.00; 90.00; 90.00
Resolution range [Å]	50.00 – 1.51 (1.57– 1.51)	50.00-1.44 (1.46-1.44)	50.00-1.55 (1.58-1.55)	50.00 – 1.45 (1.50 – 1.45)
No. of unique reflections	71826 (6,470)	74117 (1788)	63253 (3248)	77821 (7398)
Completeness [%]	98.3 (90.2)	87.7 (42.5)	92.9 (97.5)	94.6 (91.2)
Redundancy	4.1 (2.9)	3.6 (1.7)	4.2 (3.9)	5.4 (4.3)
R_{merge} (%)	5.2 (36.8)	6.8 (72.0)	4.5 (28.9)	6.9 (39.0)
$\langle I \rangle / \langle \sigma(I) \rangle$	22.3 (2.5)	19.0(1.0)	30.9 (4.5)	24.0 (4.1)
Refinement				
Resolution range [Å]	32.16-1.51 (1.55-151)	17.13-1.44 (1.48-1.44)	17.13-1.55 (1.59-1.55)	27.63-1.45 (1.48-1.45)
R_{work} (%)	17.3 (24.0)	17.9 (30.5)	17.8 (21.9)	16.2 (20.9)
R_{free} (%)	20.5 (31.8)	20.7 (33.2)	20.4 (25.7)	18.6 (26.0)
No. of reflections	68132 (4397)	70314 (3449)	59175 (4261)	73857 (5220)
Total no. of non-hydrogen atoms	3905	3858	3789	3898
No. of atoms/average B factor [Å^2] Heavy chain β_2m Peptide Water Glycerol	 2282/16.16 840/16.01 201/8.74 616/26.70 6/17.98	 2271/ 13.08 840/ 15.79 201/12.27 575/ 27.09 6/ 19.44	 2271/14.32 840/15.23 201/7.35 506/19.59 6/14.56	 2302/ 8.23 866/ 10.90 88/ 14.56 639/ 19.07 12/ 11.66
rmsd from ideal geometry bond length [Å] bond angles [°]	 0.030 2.413	 0.008 1.089	 0.004 0.828	 0.011 1.334

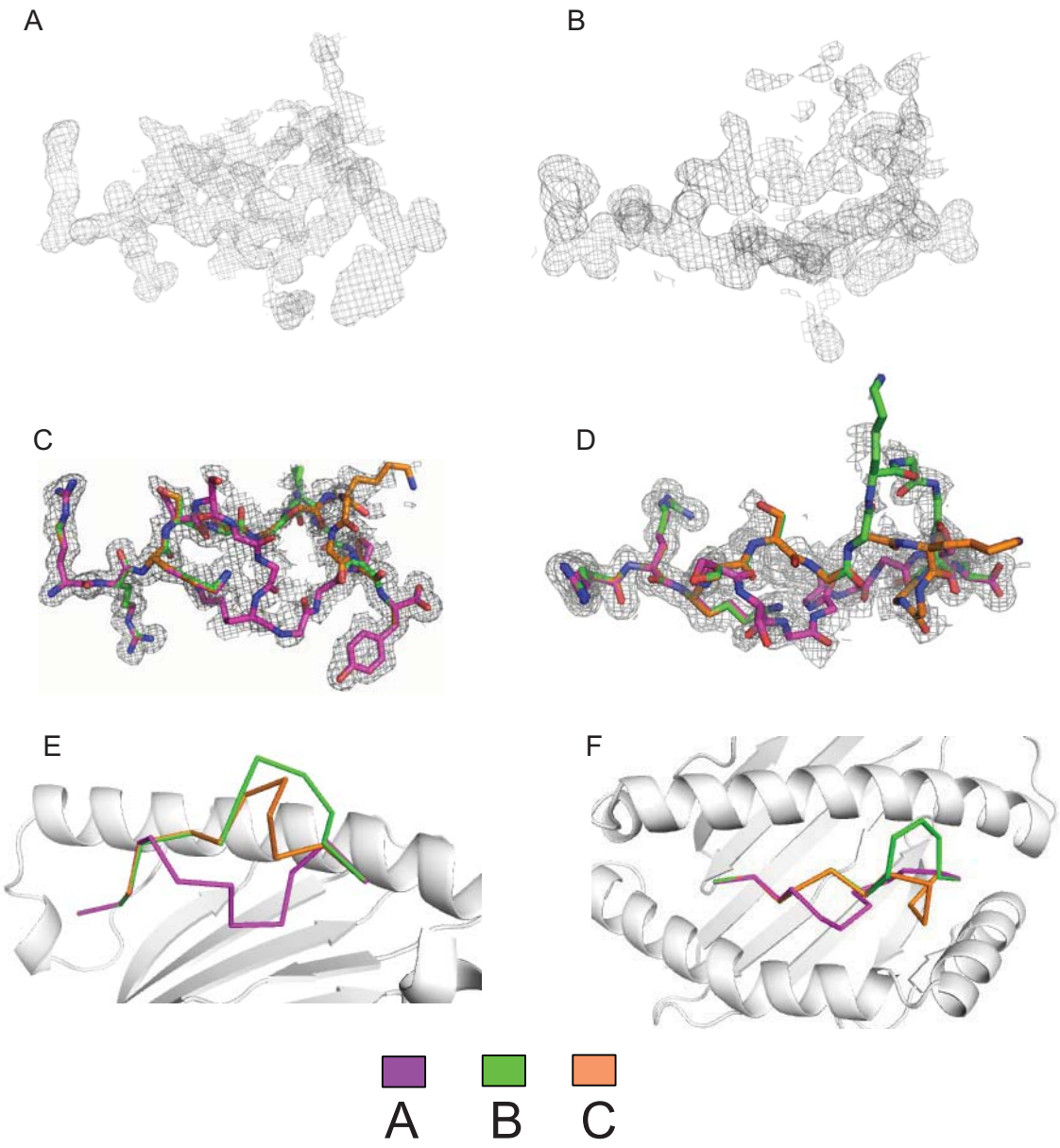

FIGURE 3.1. (A, B) Initial 2Fo-Fc electron density map (0.6 σ contour level) of the pB27 peptide in the binding groove of the B*2705 molecule shown in side (A, from the side of the α2-helix) and top (B, as seen by an approaching TCR) views. This unbiased electron density was calculated from a molecular replacement model that did not include co-ordinates of the peptide. (C, D) Fit of the final refined models of the pB27 peptide into the initial 2Fo-Fc electron density map, shown from the side (C) and top (D). (E, F) Main chains of the three conformations of the pB27 peptide shown from the side (E, α2-helix removed for clarity) and top (F).

In the case of the pB27 peptide, we observed that it is bound in multiple conformations in the peptide binding groove of the B*2705 molecule (Fig. 3.1). We were able to model a “bulged-in” conformation (referred to as conformation A) and two well-defined “bulged-out” conformations (referred to as conformations B and C) (Fig. 3.1C-F). While we initially derived five conformations from the omit map

contoured at 0.6σ, only conformations A, B and C were found to be structurally sensible due to their more acceptable stereochemistry (no cis peptide bonds and D-isomers of peptide residues). Based on the omit and difference electron density maps we were able to conclude that the entire region around conformation A (Fig. 3.2) is occupied by ordered atoms, very likely atoms of the pB27 peptide in various conformations, though identification of all individual conformations that collectively result in the electron density in that region is not possible from these two crystallographic datasets alone. The occupancy of this region (Fig. 3.2) by ordered atoms suggests that the peptide conformation A is merely one of a collection of a large number of conformations that are still ordered enough to appear in electron density maps, but individual conformations are not represented significantly enough in the collection to result in well defined unambiguous electron density for any particular conformation. These observations and the fact that the three modeled conformations fail to account for a significant part of the total electron density in the peptide binding groove of the B*2705 molecule suggest that this part of the pB27 peptide is bound in a highly flexible manner. The three conformations of the pB27 peptide represent only a part of all the conformations assumed by the pB27 peptide in the binding groove of the B*2705 molecule, and among these three, conformations B and C could be considered substantially more stable than conformation A based on structural and geometric indicators such as dihedral angles and residue environments. The kind of meandering of the peptide backbone observed in conformation A (Fig. 3.1C-F) has never been observed before in an MHC-bound peptide.

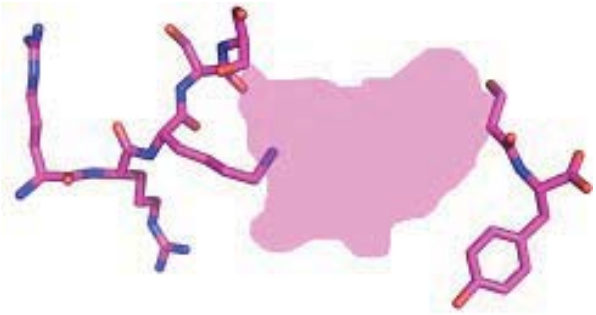

FIGURE 3.2. Segment of the pB27 peptide in conformation A that appears to be flexibly bound in the peptide binding groove of the B*2705 molecule and cannot be clearly modeled. The occupancy of the region colored in purple is most likely due to multiple conformations of pB27 peptide, which collectively result in the electron density observed of this region (see also Fig. 3.1A,B).

The residues of the pB27 peptide are anchored in the A, B and F pockets of the peptide binding groove of the B*2705 molecule via interactions very similar to those observed in previously reported structures of B*2705 complexes (Ziegler et al. 2009a). Despite the conformational ambiguity of the middle part of the peptide, the

HC residues near the middle part of the peptide were able to be modeled in single conformations, suggesting that the conformational multiplicity of the peptide is not associated with similar conformational multiplicity of neighboring HC residues. The enormous variability in peptide conformations and the lack of such conformational variability in the HC residues within the peptide binding groove suggest that the multiple conformations of the pB27 peptide are primarily stabilized by intra-peptide bonds and mostly water-mediated interactions between peptide and HC residues.

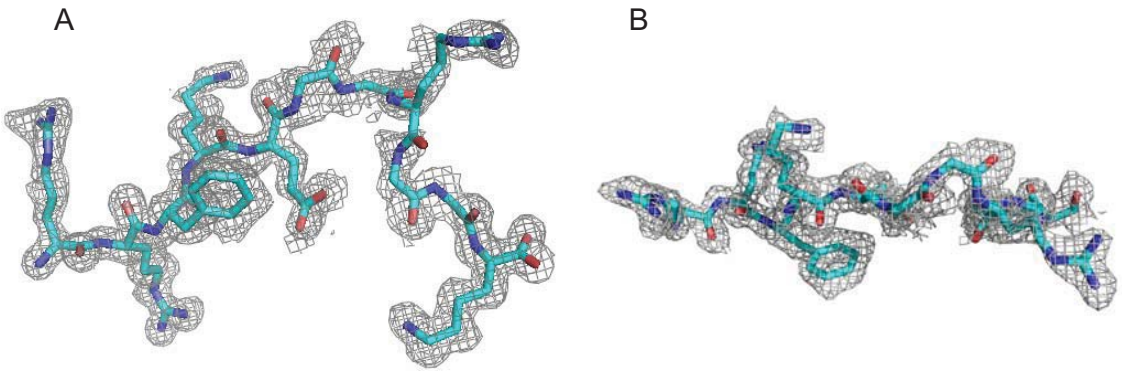

FIGURE 3.3. Side (A) and top (B) views showing the fit of the final model of the pCP peptide in the initial 2Fo-Fc electron density map (0.6 σ contour level) of the B*2705:pCP complex structure.

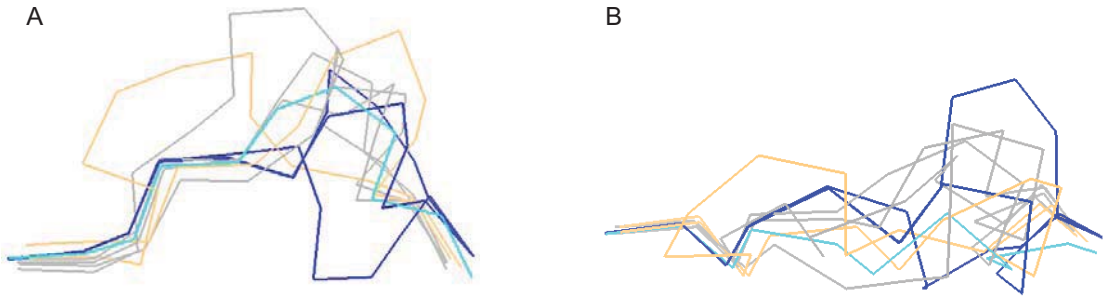

FIGURE 3.4. Binding of long peptides into the MHC class I binding groove. The pB27 (blue), pCP (skyblue) and MTF (yellow) peptides are colored while all other peptides are shown in gray. Only the pB27 peptide (blue) is bound in multiple conformations. Side (A) and top (B) views are shown.

In the case of the B*2705:pCP complex, the electron density maps permit modeling of the pCP peptide only when contoured to 0.6 σ-level, indicating flexibility in conformation of the pCP peptide as well. pCP was modeled in a single, relatively

unambiguous conformation within the peptide binding groove of the B*2705 molecule (Fig. 3.3), which shows that despite its conformational flexibility it is displayed predominantly in a single conformation by the B*2705 molecule. As the pCP peptide has as many glycine residues as the pB27 peptide, it can be concluded that the presence of the four glycine residues in the pB27 peptide alone is not the reason for its presentation in multiple conformations by the B*2705 molecule. A close scrutiny of the structure shows that while interactions of the residues of the middle part of the pCP peptide could also be formed by the corresponding residues of the pB27 peptide if it binds in the same conformation, the interactions of the residue pGlu5 of the pCP peptide (water-mediated hydrogen bonds with Lys70, Thr73, His114, Asp116 and Trp147) are indispensable to its bulged out conformation and the pSer5 residue of the pB27 peptide may not be as effective in bonding with all these residues. Furthermore, the presence of an additional residue in the pB27 peptide in comparison to the pCP peptide makes the main chain of the pB27 peptide ~3 Å longer, potentially affording it additional flexibility. While long peptides except MTF-E and pB27 are never bound in multiple conformations in the binding groove of MHC class I molecules (Fig. 3.4), it is conceivable that the additional residue in the pB27 peptide makes it more flexible than the pCP peptide. We believe that a combination of multiple factors makes the pB27 peptide more flexible than the pCP peptide, which is reflected in the plasticity of its binding mode.

Table 3.2. Thermal denaturation profiles of the B*2705:pB27 and B*2705:pCP complexes measured by DSC and CD spectroscopy

Complex	$T_m(1)$ (°C)	$\Delta H_m(1)$ (kcal/mol)	$T_m(2)$ (°C)	$\Delta H_m(2)$ (kcal/mol)	ΔH_{tot} (kcal/mol)	$T_m(CD)$ (°C)
B*2705:pB27	56.9	117	61.7	154	271	60.1
B*2705:pCP	60.1	119	64.7	163	282	64.3

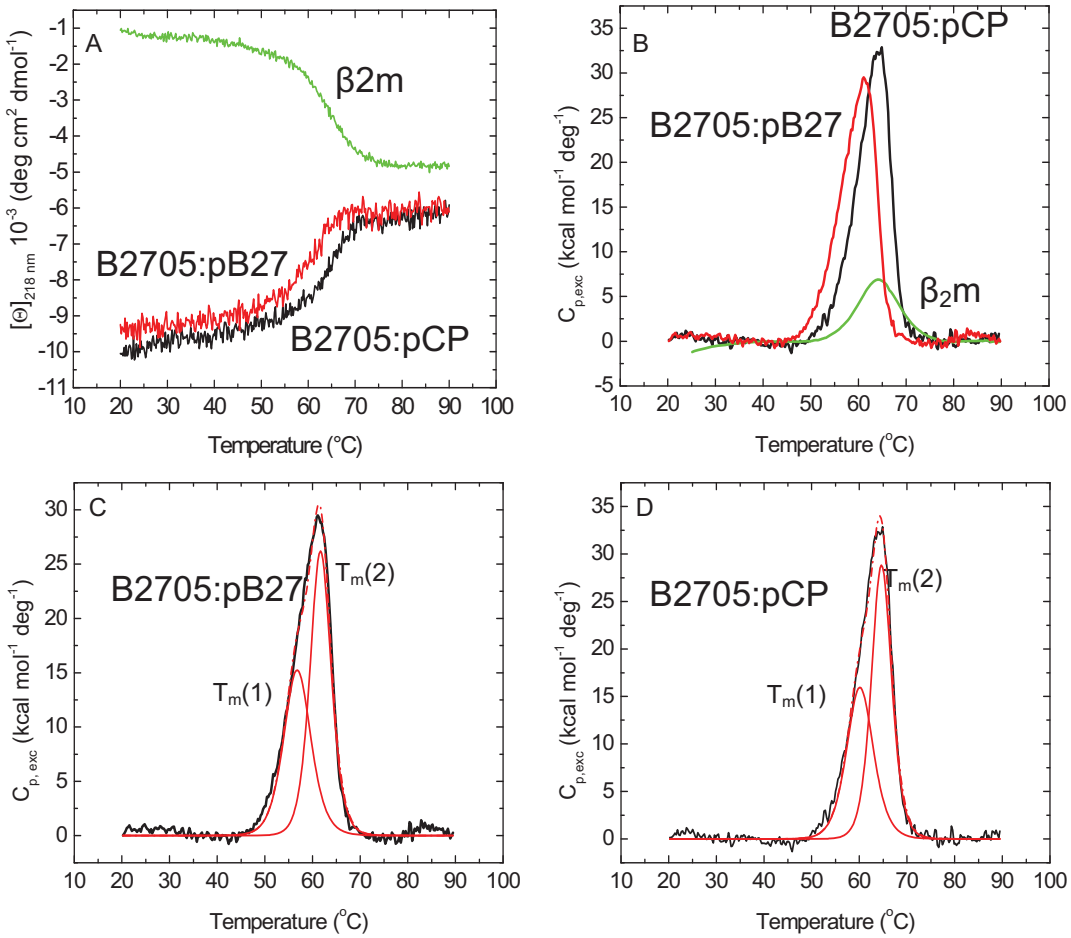

FIGURE 3.5. Thermostability of the B*2705:pB27 and B*2705:pCP complexes. The two complexes are analyzed by circular dichroism (CD) spectroscopy (a) and differential scanning calorimetry (DSC) (b). The thermal melting curves obtained for the two complexes by DSC are deconvoluted into two two-state transitions for both complexes (c, d). The T_m values for both complexes are in the normal range of typical HLA-B27 complexes. The T_m values are about 4°C higher for the B*2705:pCP complex in comparison to the B*2705:pB27 complex (see also Table 3.2).

An analysis of the B*2705:pB27 and B*2705:pCP complexes by circular dichroism (CD) spectroscopy and differential scanning calorimetry (DSC) revealed that the melting temperature values (T_m) of these two complexes are comparable with the T_m values of most HLA-B27 complexes (Fig. 3.5, Table 3.2). The two complexes have very similar thermal denaturation profiles, and both undergo two two-state transitions during thermal denaturation (Fig. 3.5C,D, see also Ziegler et al. 2009a). The T_m values of the B*2705:pCP complex are about 4°C higher than the T_m values of the B*2705:pB27 complex, indicating that the B*2705:pCP complex is slightly more thermostable than the B*2705:pB27 complex. These analyses show that the flexibility

of the pB27 and pCP peptides does not appreciably reduce the thermodynamic stability of their complexes with the B*2705 molecule (Ziegler et al. 2009a).

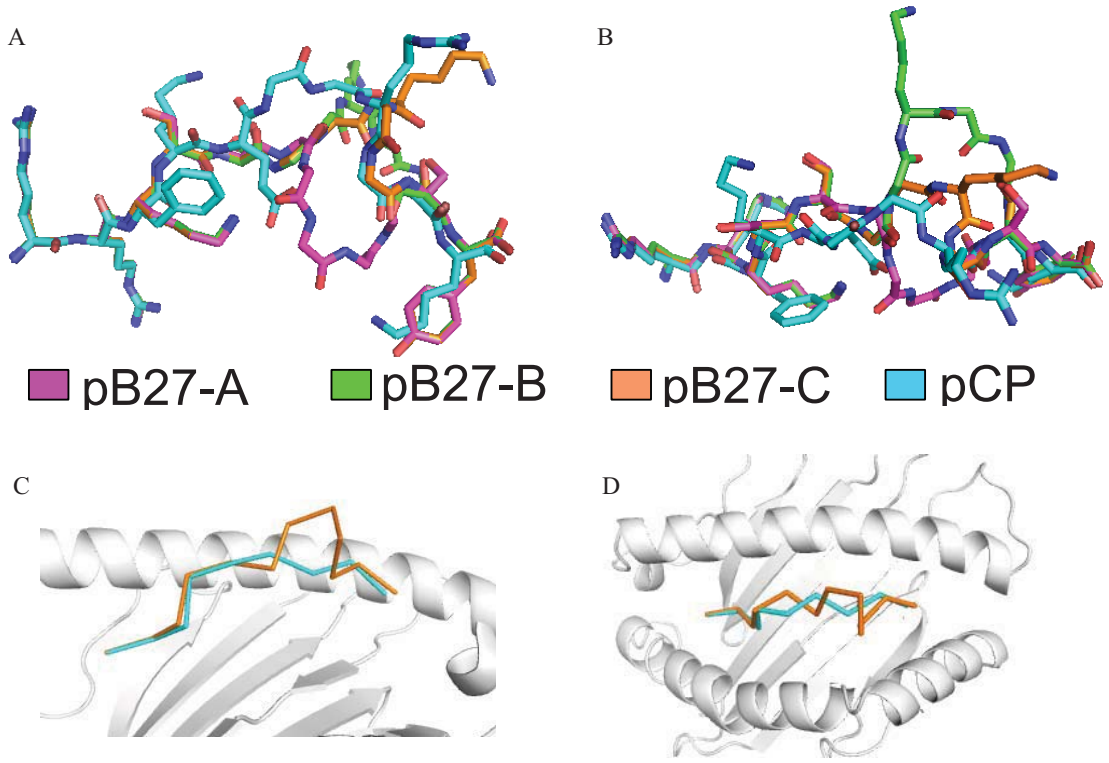

FIGURE. 3.6. Overlay of the pCP and pB27 peptide conformations. Side (A) and top (B) views of the pCP peptide and the three conformations of the pB27 peptide are shown. C (side view, α2-helix removed for clarity) and D (top view) show an overlay of the Cα backbones of the conformation C of the pB27 peptide on the pCP peptide.

An overlay of the conformations of the pB27 and pCP peptides (Fig. 3.6, 7) suggests that no single conformation of the pB27 peptide overlaps significantly with the conformation of the pCP peptide (cf. Ch. 1, Fig. 3.7). Only the conformation C of the pB27 peptide shows marginal overlap with the conformation of the pCP peptide. However, given the conformational multiplicity of the pB27 peptide, the possibility that the bound pB27 peptide dynamically adopts various conformations while bound to the same B*2705 molecule appears plausible. Such a dynamically bound pB27 peptide may likely adopt an intermediate conformation exhibiting a high degree of overlap with the conformation of the pCP peptide, thus opening the possibility of temporal molecular mimicry between these two peptides.

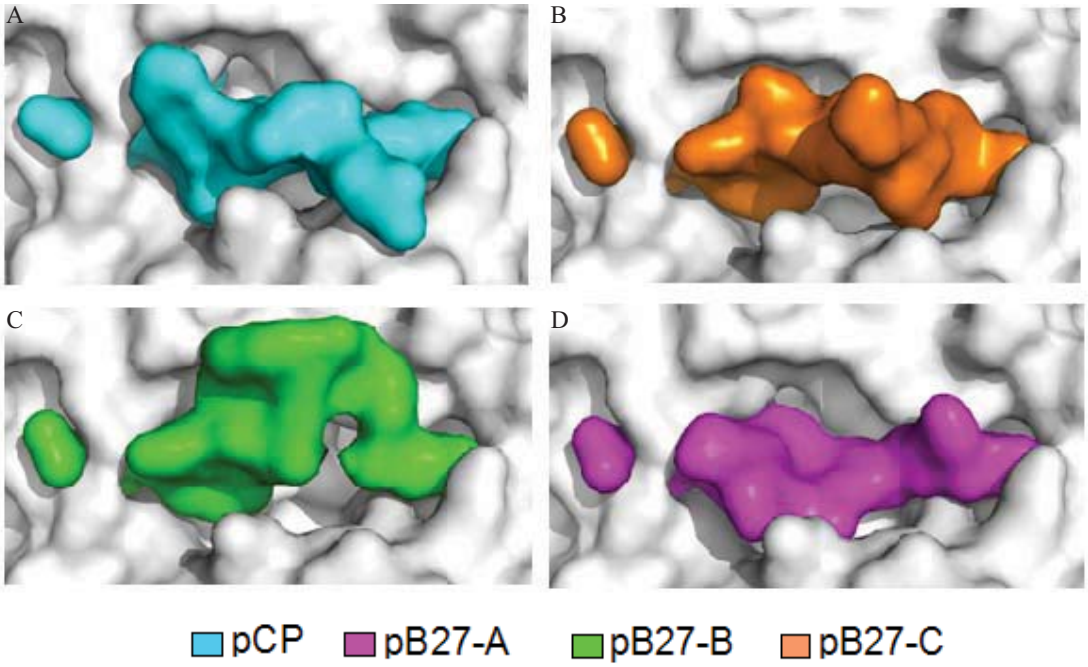

FIGURE 3.7. pCP and pB27 peptides as seen by an approaching TCR. Surface representations of the pCP (A) and pB27 (B, C, D) peptide conformations bound in the peptide binding groove of the B*2705 molecule. The pCP peptide conformation (panel A) bears only marginal similarities with the conformation C of the pB27 peptide (panel B) and has no clear overlap with any of the other two conformations of the pB27 peptide (panels C, D).

The structural multiplicity of the self-peptide pB27 may have implications for T cell selection within the thymus. A part of the autoreactive T cell population with high affinity for any single conformation of the pB27 peptide (bound to the B*2705 molecule) selected during positive thymic selection (Starr et al. 2003) may fail to be eliminated during negative selection (Liu et al. 2006) due to the variability in the conformation of the pB27 peptide in the B*2705:pB27 complex. The pB27 peptide may thus cause survival of autoreactive T cells which may lead to autoimmunity when exposed to potentially arthritogenic peptides that share structural similarity with any of the conformations of the pB27 peptide. Studying immunogenicity of the pB27 and pCP peptide, and cross-reactivity of the CTL generated against these peptides may provide a conclusive understanding of their potential for molecular mimicry in the B*2705 context. That multiple binding modes of self peptides can interfere with proper negative T cell selection has already been proven (Hülsmeyer et al. 2004, Rückert et al. 2006).

3.3 Publications

3.3.1. Beltrami A*, Rossmann M*, Fiorillo MT, Paladini F, Sorrentino R, Saenger W, **Kumar P**, Ziegler A, Uchanska-Ziegler B. (*Equal contribution) Citrullination-dependent differential presentation of a self-peptide by HLA-B27 subtypes. J. Biol. Chem. (**2008**) 283, 27189–27199

Supplemental Material can be found at:
http://www.jbc.org/cgi/content/full/M802818200/DC1

THE JOURNAL OF BIOLOGICAL CHEMISTRY VOL. 283, NO. 40, pp. 27189–27199, October 3, 2008

Citrullination-dependent Differential Presentation of a Self-peptide by HLA-B27 Subtypes*[S]

Received for publication, April 14, 2008, and in revised form, June 19, 2008 Published, JBC Papers in Press, July 23, 2008, DOI 10.1074/jbc.M802818200

Alessandra Beltrami[‡1], Maxim Rossmann[§1], Maria Teresa Fiorillo[¶], Fabiana Paladini[¶], Rosa Sorrentino[¶], Wolfram Saenger[§], Pravin Kumar[‡], Andreas Ziegler[‡2], and Barbara Uchanska-Ziegler[‡]

From the [‡]Institut für Immungenetik, Charité-Universitätsmedizin Berlin, Campus Benjamin Franklin, Freie Universität Berlin, Thielallee 73, 14195 Berlin, Germany, [§]the Institut für Chemie und Biochemie/Kristallographie, Freie Universität Berlin, Takustrasse 6, 14195 Berlin, Germany, and [¶]the Dipartimento di Biología Cellulare e dello Sviluppo, "Sapienza" Università di Roma, Via dei Sardi 70, 00185 Roma, Italy

Inflammatory processes are accompanied by the posttranslational modification of certain arginine residues within proteins to yield citrulline, although it is largely unknown how this modification influences antigen presentation. We employed crystallographic and functional studies to investigate whether the exchange of arginine to citrulline affects the display of a peptide by two human major histocompatibility antigen class I subtypes, HLA-B*2705 and HLA-B*2709. Both differ only in residue 116 within the peptide binding groove despite their differential association with ankylosing spondylitis, an inflammatory rheumatic disorder. The crystal structures described here show that a modified self-peptide, pVIPR-U5 (RRKWURWHL; U = citrulline), is presented by the two HLA-B27 molecules in distinct conformations. These binding modes differ not only drastically from each other but also from the conformations exhibited by the non-citrullinated peptide in a given subtype. The differential reactivity of HLA-B27-restricted cytotoxic T cells with modified or unmodified pVIPR supports the structural findings and shows that the presentation of citrullinated peptides has the potential to influence immune responses.

The citrullination of proteins is a posttranslational modification that influences immune responses and inflammatory reactions (1, 2). It is catalyzed by peptidylarginine deiminases and involves the replacement of the terminal imino group within the side chain of an arginine residue of an extra- or intracellularly expressed protein by an amide group (3), *i.e.* a change from $-(CH_2)_3$-NH-C(NH_2)=NH_2^+ to $-(CH_2)_3$-NH-C(NH_2)=O. The length of the residue side chain and its hydrogen bonding potential are, thus, retained but not its positive charge. Although exceptions have been found (for review, see Ref. 3), citrullinated proteins must usually be regarded as neoantigens as they do not participate in the thymic selection of T cells. Consequently, it has recently been demonstrated that major histocompatibility complex (MHC)[3] class II-restricted T cells are able to distinguish between citrullinated and the respective unmodified peptides presented by MHC antigens (1, 4).

In autoimmune disorders, in which inflammatory lesions are common, citrullination of proteins is apparently a general phenomenon, irrespective of the association of different MHC genes with a given disease (2, 5, 6). Because this protein modification has also consistently been found within synovial tissue from patients with reactive arthritis, an *HLA-B27*-associated disorder (5), fragments derived from citrullinated polypeptides are most likely available for presentation by MHC antigens in patients with ankylosing spondylitis (AS) as well. This is a chronic inflammatory spondyloarthropathy that is even stronger associated with *HLA-B27* than reactive arthritis (7–10). Studies in rats transgenic for *HLA-B27* suggest a direct involvement of the HLA-B27 protein in the pathogenesis of AS (11). Remarkably, the association with AS is *HLA-B27* allele ("subtype")-dependent; for example, the ubiquitous, frequent *HLA-B*2705* subtype (*B*2705* in short) is AS-associated, whereas *HLA-B*2709* (*B*2709* in short) is not (9, 10, 12). Both molecules are heterotrimeric cell surface glycoproteins consisting of a heavy chain (HC), β_2-microglobulin (β_2m), and a peptide that is presented to effector cells (13, 14). The B*2705 protein differs in only a single HC amino acid (Asp-116) from B*2709 (His-116) (12). This residue is located at the floor of the peptide binding groove, contributes to shaping the F pocket, and participates in anchoring the peptide C-terminal side chain. The vast majority of the peptides constituting the B*2705 repertoire can also be found in B*2709 (15, 16) and are presumably displayed similarly, as indicated by comparative crystallographic analyses (17, 18).

* This work was financially supported by Deutsche Forschungsgemeinschaft (SFB 449, B6), VolkswagenStiftung (I/79 983), Berliner Krebsgesellschaft (Ernst von Leyden fellowship to A. B.), Senate of Berlin (NaFöG fellowship to P. K.), Sonnenfeld-Stiftung, Berlin, and Fonds der Chemischen Industrie. The costs of publication of this article were defrayed in part by the payment of page charges. This article must therefore be hereby marked "*advertisement*" in accordance with 18 U.S.C. Section 1734 solely to indicate this fact.

[S] The on-line version of this article (available at http://www.jbc.org) contains supplemental Figs. S1–S5.

The atomic coordinates and structure factors (code 3B6S and 3B3I) have been deposited in the Protein Data Bank, Research Collaboratory for Structural Bioinformatics, Rutgers University, New Brunswick, NJ (http://www.rcsb.org/).

[1] Joint first authors.

[2] To whom correspondence should be addressed. Tel.: 49-30-8445-1817; Fax: 49-30-8445-1820; E-mail: andreas.ziegler@charite.de.

[3] The abbreviations used are: MHC, major histocompatibility complex; HLA, human major histocompatibility antigen; AS, ankylosing spondylitis; β_2m, β_2-microglobulin; B*2705, HLA-B*2705; B*2709, HLA-B*2709; Cir, citrulline; CTL, cytotoxic T lymphocyte; HC, heavy chain; p1,p2, . . . , peptide position 1, 2, . . . ; pVIPR-U5, pVIPR citrullinated at p5; r.m.s.d., root mean square deviation; TCR, T cell receptor.

Some peptides, however, are presented in drastically different conformations by B*2705 and B*2709 (14, 19–21). Particularly striking is the case of a self-peptide (pVIPR, RRKWRRWHL), which is derived from vasoactive intestinal peptide type 1 receptor (residues 400–408). It is bound in a canonical conformation (13), with the middle of the peptide bulging out of the B*2709 subtype binding groove, whereas B*2705 displays pVIPR in a dual binding mode (19). One of the conformations observed in B*2705·pVIPR is identical to that seen in B*2709, whereas a salt bridge between the arginine residue at peptide position 5 (pArg5) and the polymorphic HC residue Asp-116 leads to different HC-peptide contacts in the other conformation. Both conformations are present in approximately equal amounts in the B*2705 peptide binding groove (19).

We employed the subtypes B*2705 and B*2709 and a citrullinated version of pVIPR (pVIPR-U5; RRKWURWHL, U = citrulline) to investigate whether the introduction of a citrulline (pCir5) into a peptide can lead to changes of its binding mode and whether these changes occur in an HLA-B27 subtype-specific manner. The two crystal structures described here show that the pVIPR-U5 binding mode in a given subtype is diametrically opposed to those exhibited by the unmodified pVIPR peptide. Furthermore, the modified peptide is presented in drastically deviating conformations by the two subtypes. Combined with functional studies employing pVIPR-specific cytotoxic T cells, our model study provides the basis to explain how citrullination can affect molecular interactions between MHC molecules and a peptide as well as T cell responses.

EXPERIMENTAL PROCEDURES

Cytotoxicity Assays—Peripheral blood cells were obtained from two B*2705-positive patients with AS. HLA-B27-restricted, pVIPR-specific cytotoxic T lymphocytes (CTLs) were generated and tested for specificity in a standard 4-h cytotoxicity assay as described previously (19). Briefly, ^{51}Cr-labeled T2-B*2705 or T2-B*2709 target cells were either incubated in medium alone (negative control) or in medium containing pVIPR or pVIPR-U5 (70 μM, respectively). The effector/target ratio was 12:1 for the MP2 CTL and 15:1 for the CTL MP9 and MP11 as well as BO45. Spontaneous release of ^{51}Cr-labeled, washed target cells was lower than 15%. During the assay, the medium was devoid of peptide. The results summarize the data obtained from two independent experiments.

Monoclonal Antibodies and Peptide Binding Assays—The monoclonal antibodies ME1 (anti-HLA-B27, B7, B22, B73 HC·β_2m complexes; IgG1 (22)), MARB3 (specific for HC·β_2m-peptide complexes carrying the HLA-Bw4 determinant; IgM (23)), and appropriate negative isotype controls were employed to assess the binding of peptides to cell surface-expressed HLA-B27 subtypes (23). For these tests, the transporter associated with antigen processing 2-negative cell line BM36.1 (24) transfected with B*2705 or B*2709 was employed. The cells were preincubated for 36 h at 26 °C, the last 12 h in serum-free medium, and then incubated for 20 h at 26 °C in the presence of peptide (50 μM). The temperature was then elevated to 37 °C for 4 h followed by a decrease to 4 °C before incubation with appropriate monoclonal reagents and Alexa-labeled goat anti-mouse IgG. Single color analysis by flow cytometry was done on an EPICS-XL instrument (Coulter, Miami, FL) essentially as described (23).

Expression, Purification, and Crystallization of the HLA-B27·pVIPR-U5 Complexes—The high performance liquid chromatography-purified, citrulline-modified peptide (pVIPR-U5) was purchased from Alta Bioscience (Birmingham, UK). B*2705 and B*2709 HC and β_2m were expressed separately in *Escherichia coli* and purified from inclusion bodies following the protocol described previously (17). Inclusion bodies of B*2705 HC or B*2709 HC and β_2m were then dissolved in 50% (w/v) urea and refolded for 2–3 weeks at 4 °C in 400 mM L-arginine-HCl, 2 mM EDTA, 5 mM reduced glutathione, 0.5 mM oxidized glutathione, and 100 mM Tris HCl, pH 7.5, in the presence of the peptide pVIPR-U5 (25). A refolding period of at least 2 weeks has been found essential for efficient formation of heterotrimeric complexes with HLA-B27 HC (17). The complexes were purified by size exclusion chromatography and concentrated in TBS buffer (20 mM Tris-HCl, 150 mM NaCl, 0.01% NaN_3, pH 7.5) to 14.5 mg/ml (B*2705·pVIPR-U5) or 18 mg/ml (B*2709·pVIPR-U5). Crystals of HLA-B27·pVIPR-U5 complexes suitable for x-ray diffraction experiments were obtained using hanging drop vapor diffusion by mixing 1.8 μl of precipitant solution (for B*2705·pVIPR-U5, 24% polyethylene glycol (PEG) 8000, 0.1 M Tris HCl, pH 7.5, and for B*2709·pVIPR-U5, 25% PEG 8000, 0.1 M Tris HCl, pH 8.0) and 1.8 μl of protein solution and equilibrating the droplets with 750 μl of precipitant solution. Streak seeding was used to improve crystal growth. For B*2705 and B*2709, the crystals obtained were square plates with a maximum size of 45 × 45 × 15 μm.

Data Collection, Structure Determination, and Refinement—Crystals of the complexes were cryo-protected by supplementing the precipitant solution with 30% polyethylene glycol 400 (B*2705·pVIPR-U5) and 20% glycerol (B*2709·pVIPR-U5). X-ray data were collected at 100 K on station ID29 at European Synchrotron Radiation Facility, Grenoble using a wavelength of 0.982 Å, processed with DENZO, and scaled with SCALEPACK (26). The structures of B*2705·pVIPR-U5 and B*2709·pVIPR-U5 were determined by molecular replacement using peptide-stripped B*2705·pVIPR (Protein Data Bank (PDB) code 1OGT) and B*2709·pVIPR (PDB code 1OF2) (19) as search models in program MOLREP (27). Restrained maximum-likelihood refinement was performed using program REFMAC5 (28). A topography file for the citrullinated peptide was generated using PRODRG server (29), and the peptide was placed manually into the electron density using COOT (30). Water molecules were included in the initial model with ARP/wARP (31). Further improvement of the structure was achieved by iterative cycles of manual rebuilding with COOT and maximum-likelihood refinement with REFMAC5. Structure validation was performed using programs WHATIF (32) and PROCHECK (33). Angles were calculated with HBPLUS (34) and checked manually with COOT. Data collection and refinement statistics are given in Table 1. The figures were generated using

TABLE 1
Data collection and refinement statistics

	B*2705 · pVIPR-U5	B*2709 · pVIR-U5
Data collection		
Space group	$P2_12_12_1$	$P2_12_12_1$
Unit cell *a*; *b*; *c* (Å)	50.7; 82.8; 110.3	51.3; 82.3; 109.3
α; β; γ (°)	90.00; 90.00; 90.00	90.00; 90.00; 90.00
Resolution (Å)[a]	50.0-1.79 (1.85-1.79)	30.0-1.86 (1.90-1.86)
Unique reflections	39,485 (2,492)	35,295 (2,463)
Completeness (%)[a]	94.72 (82.3)	93.13 (89.9)
Redundancy[a]	4.2 (4.0)	3.1 (2.9)
I/σ[a]	11.7 (2.7)	13.1 (3.5)
R_{sym}[a,b]	0.097 (0.488)	0.071 (0.303)
Refinement		
R_{cryst}[a,c]	0.184 (0.242)	0.189 (0.227)
R_{free}[a,d]	0.224 (0.273)	0.233 (0.291)
Heavy chain, no. of atoms/average B factor (Å^2)	2278/11.8	2285/13.4
β_2m, no. of atoms/average B factor (Å^2)	847/15.8	855/17.9
Peptide, no. of atoms/average B factor (Å^2)	100/15.8	100/17.3
Water, no. of molecules/average B factor (Å^2)	555/26.1	428/28.0
Glycerol, no. of atoms/average B factor (Å^2)	0	36/38.2
Estimated overall coordinate error (Å)[e]	0.14	0.16
r.m.s.d.[f] from ideal geometry, bond length [Å]	0.007	0.007
r.m.s.d.[f] from ideal geometry, bond angles [°]	1.03	1.04
PDB code	3B6S	3B3I

[a] Values in parentheses refer to the highest resolution shell.
[b] $R_{sym} = \Sigma_h\Sigma_i |I_{h,i} - \langle I_h \rangle| / \Sigma_h\Sigma_i I_{h,i}$.
[c] $R_{cryst} = \Sigma_h |F_o - F_c| / \Sigma F_o$ (working set, no σ cut-off applied).
[d] R_{free} is the same as R_{cryst} but calculated on 5 % of the data excluded from refinement.
[e] Estimated overall coordinate error based on R_{free} as calculated by REFMAC 5.1.1999.
[f] r.m.s.d. from target geometries.

PYMOL (35) and LIGPLOT (36). The atomic coordinates and structure amplitudes have been deposited in the Protein Data Bank under accession codes 3B6S (B*2705·pVIPR-U5) and 3B3I (B*2709·pVIPR-U5). The nomenclature used for the citrulline atoms in the PDB files was also employed under "Results" and "Discussion" and Table 2. However, because this nomenclature makes a comparison with the corresponding atoms of arginine residues difficult, the correspondence between the two atom designations is given here (citrulline–arginine): O1-O, C1-C, C2-CA, N2-N, C3-CB, C4-CG, C5-CD, N6-NE, C7-CZ, O7-NH_2, N8-NH1.

RESULTS

*General Features of the B*2705 and B*2709 Subtypes in Complex with pVIPR-U5*—The complexes of the B*2705 and B*2709 subtypes with pVIPR-U5 crystallized isomorphously (same space group and comparable unit cell constants) in the orthorhombic space group $P2_12_12_1$. Both complexes exhibit the typical MHC class I immunoglobulin-like folds (13) and refined to values of R_{cryst} = 18.4% and R_{free} = 22.4% at 1.79 Å and to R_{cryst} = 18.9% and R_{free} = 23.3% at 1.86 Å resolution, respectively (Table 1). Although crystals of these two subtypes with the unmodified pVIPR peptide had been obtained under similar conditions, they crystallized in the different monoclinic $P2_1$ space group (19). Nevertheless, the unit cells are comparable because the axes *a* and *b* are isomorphous, whereas the axis *c* in space group $P2_12_12_1$ is almost twice as long as in $P2_1$ to accommodate four instead of two crystal asymmetric units. A close relation between molecular packing and *C2* symmetries indicates that only marginal changes in crystal packing are required to transform from one space group into the other. Therefore, an in-depth comparison of the structures of B*2705 and B*2709 complexed either with the citrullinated or the unmodified pVIPR peptide is justifiable despite the presence of different space groups in which the complexes crystallized.

The structures of HC and β_2m of both subtypes in complex with pVIPR-U5 are nearly identical, with root mean square deviations (r.m.s.d.) of 0.6 Å. Asp-116 in B*2705 and His-116 in B*2709 are well defined in the respective electron densities, and this was also the case for the peptide (Fig. 1, *A* and *B*, and supplemental Fig. S1). However, pVIPR-U5 is bound in grossly different conformations by the two subtypes. It occurs in B*2705 in a canonical, conventional conformation previously termed "p4α" (Ref. 19; main chain φ (−84.7°) and ψ (−47.5°) torsion angles in an α-helical conformation at p4, and all other φ/ψ torsion angles as in β-strands), with the partially solvent-exposed side chain of pCir5 pointing toward the α2-helix (Fig. 1*C*). In contrast, pVIPR-U5 displays the non-canonical "p6α" binding mode in the B*2709 subtype (main chain φ (−121.7°) and ψ (27.0°) torsion angles in α-helical conformation at p6, and all other φ/ψ torsion angles as in β-strands). As a consequence, the pCir5 side chain is embedded within the binding groove and forms a hydrogen bond with His-116 of the HC (Fig. 1*D*; Table 2). Therefore, the pVIPR-U5 conformation in B*2705 is similar to the canonical binding mode observed for pVIPR in both B*2705 and B*2709 (main chain torsion angles $\varphi = -85.2°$, and $\psi = -32.6°$), whereas the B*2709·pVIPR-U5 structure resembles pVIPR bound to the B*2705 subtype in non-canonical conformation (main chain torsion angles $\varphi = -106.4°$ and $\psi = 34.7°$) (19). The structures of the two subtypes with the citrullinated peptide diverge considerably from p3 to p7 (Fig. 1*E*). However, a comparison of the B factors of the pVIPR-U5 peptide in the two subtypes shows that they are similar, with the exception of pCir5, which exhibits a much higher flexibility in B*2705 than in B*2709, where it is buried within the binding groove (Fig. 1, *F* and *G*).

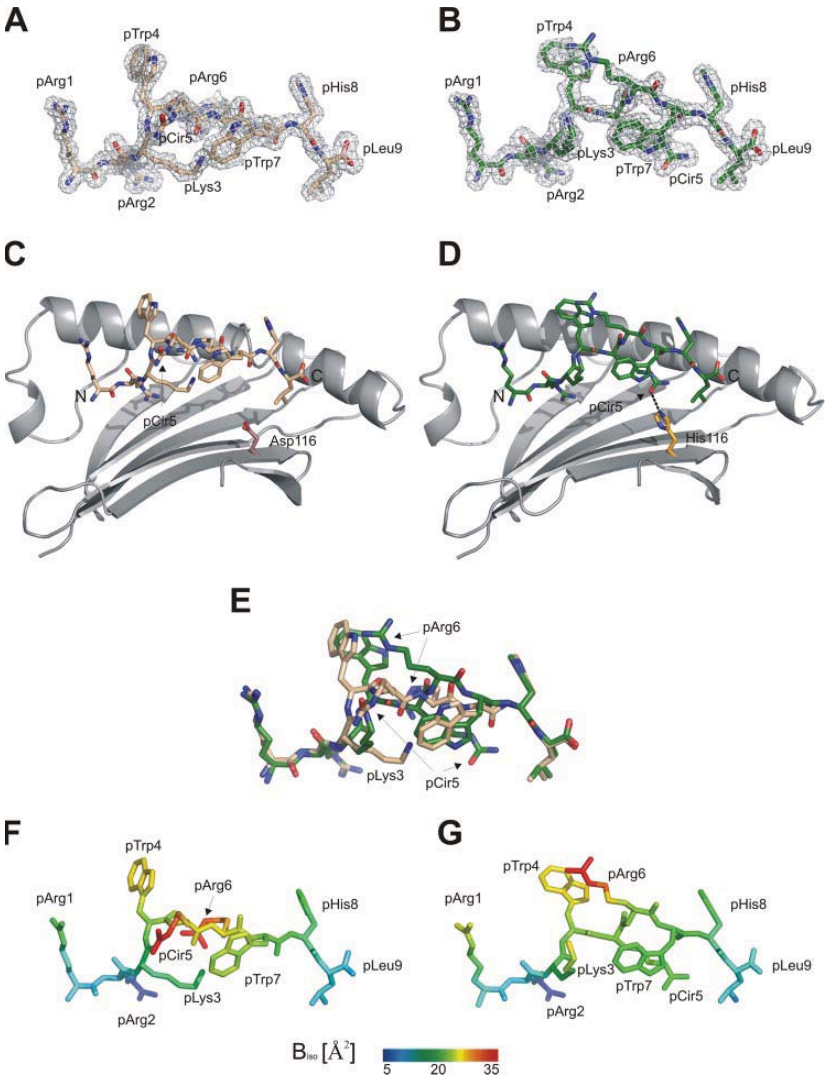

FIGURE 1. **General structure of the pVIPR-U5 peptide bound to B*2705 and B*2709.** *A* and *B*, final $2F_o - F_c$ electron density of pVIPR-U5 conformations in B*2705 (*A*) and B*2709 (*B*), contoured at the 1 σ level. *C* and *D*, conformation of pVIPR-U5 as presented by B*2705 (*C*) and B*2709 (*D*), viewed from the side of the α2-helix (removed) together with a ribbon representation of the floor of the binding groove and the α1-helix. The subtype-specific residue 116 is indicated (Asp-116 and His-116), with the hydrogen bond connecting $pCir5^{O7}$ and $His116^{NE2}$ shown as a *dotted line*. *E*, superimposition of pVIPR-U5 in B*2705 and B*2709, viewed as in *C* and *D*, but with HC removed, showing that the two peptide conformations differ drastically from pLys3 to pTrp7 (colors are as in *C* and *D*). *F* and *G*, pVIPR-U5 bound by B*2705 (*F*) and B*2709 (*G*), color-coded by isotropic B factor.

Despite the different peptide binding modes of pVIPR-U5 in B*2705 and B*2709, the primary anchor pArg2 as well as the secondary anchors pArg1 and pLeu9 are bound nearly identically in the two structures to the pockets B, A, and F, respectively, of the peptide binding groove (supplemental Fig. S1). Virtually identical orientations are also found in the case of the solvent-exposed side chain of pHis8 (supplemental Figs. S2 and S3; Fig. 1, *C–E*). The firm anchoring of pArg2 within the B pocket (37) constitutes an highly conserved feature of all HLA-B27 structures solved so far (Refs. 38, 39; for review, see Ref. 14), whereas the conformations of residues at p1, p8, and p9 resemble those found previously in case of the unmodified pVIPR bound to B*2705 or B*2709 (19).

*Conformation-dependent pVIPR-U5 Interactions in Complexes with B*2705 and B*2709*—As expected from the differential anchoring of the central portion of the two peptides, the Cα backbones and the side chains of the intervening amino acids from p3 to p7 differ drastically in their orientations (Fig. 1*E*). pArg1 and pHis8 as well as pTrp4 are fully solvent-accessible, and pCir5 and pArg6 as well as pTrp7 are partially solvent-accessible in B*2705 (Fig. 1*C*). Furthermore, pCir5 and pArg6 are the most flexible peptide side chains, as indicated by elevated B values (Fig. 1*F*). In the other subtype, however, pCir5 and pTrp7 are buried, and pTrp4 and pArg6 are fully solvent-exposed, whereas pLys3 is partly accessible (Fig. 1*D*). The re-orientation of the peptide in B*2709 leads also to loss of pCir5 flexibility; only pArg6 retains increased B values (Fig. 1*G*).

In B*2705 (supplemental Fig. S2; Table 2), the middle portion of the citrullinated peptide (p3 to p7) forms two very short (2.7 Å) hydrogen bonds with Gln-155 of the HC ($pCir5^{N8} \rightarrow Gln155^{O}$ and $pTrp7^{NE1} \rightarrow Gln155^{OE1}$) and a further, longer (3.1 Å) hydrogen bond ($pLys3^{N} \rightarrow Tyr99^{OH}$). In addition, there are three intrapeptide hydrogen bonds ($pLys3^{O} \rightarrow pArg6^{NH_2}$, $pLys3^{NZ} \rightarrow pCir5^{O1}$, $pTrp4^{O} \rightarrow pArg6^{NH_2}$) and numerous van der Waals contacts (not shown) that stabilize the whole assembly. In contrast, it is the highly characteristic anchoring of the citrullinated residue at p5 in the non-canonical conformation of the peptide in B*2709·pVIPR-U5 (supplemental Fig. S3; Table 2) that distinguishes the binding modes of the peptide in the two HLA-B27 subtypes. Other than in B*2705, pCir5 extends deep into the B*2709 binding groove, with short (2.8–3.0 Å) hydrogen bonds to HC residues His-116 ($pCir5^{O7} \rightarrow His116^{NE2}$), Lys-70 ($pCir5^{O7} \rightarrow Lys70^{NZ}$), and Asp-77 ($pCir5^{N8} \rightarrow Asp77^{OD2}$). This firm anchoring of pCir5 is enforced by an intrapeptide hydrogen bond between the side chain of this residue and pTrp7 ($pCir5^{N6} \rightarrow pTrp7^{O}$) as well as by the favorable angles involving bonds between pCir5 side chain atoms and atoms of the HC or

TABLE 2

Comparison of peptide coordination for pVIPR-U5 and pVIPR bound to the B*2705 and B*2709 subtypes

Only direct polar contacts are included, and water-mediated interactions are omitted. The contacts formed by pArg1, pArg2, pHis8, and pLeu9 are not shown because they are nearly identical in all four complexes (supplemental Figs. S2–S5).

	B*2705:pVIPR-U5				+B*2705:pVIPR-p4α			
Peptide residue	**Atom**	**Contact residue**	**Distance [Å]; D-O-C angle[a]**	**Inter-action**	**Atom**	**Contact residue**	**Distance [Å]; D-O-C angle[a]**	**Inter-action**
pLys3	*buried*				*buried*			
	pLys3^{N}	*Tyr99^{OH}	3.1; 118.9°	[c]H	pLys3^{N}	*Tyr99^{OH}	3.0; 120.0°	H
	pLys3^{O}	pArg6^{NH2}	3.3; 151.0°, [b]	H	pLys3^{O}	pArg6^{NH2}	3.0; 134.2°, [b]	H
	pLys3^{NZ}	pCir5^{O1}	2.8; 146.9°	H	pLys3^{NZ}	pArg5^{O}	2.8; 148.3°	H
pTrp4	*solvent-exposed*				*solvent-exposed*			
	pTrp4^{O}	pArg6^{NH2}	3.4; 115.8°, [b]	H	pTrp4^{O}	pArg6^{NH2}	2.9; 97.8°	H
p5	*partly solvent-exposed* (pCir5)				*solvent-exposed* (pArg5)			
	pCir5^{O1}	pLys3^{NZ}	2.8; 146.9°	H	pArg5^{O}	pLys3^{NZ}	2.8; 148.3°	H
	pCir5^{N8}	¶Gln155^{O}	2.7; 101.7°	H	pArg5^{NH1}	¶Gln155^{OE1}	3.2; 110.7°	H
pArg6	*partly solvent-exposed*				*solvent-exposed*			
	pArg6^{NH2}	pLys3^{O}	3.3; 151.0°, [b]	H	pArg6^{NH2}	pLys3^{O}	3.0; 134.2°, [b]	H
	pArg6^{NH2}	pTrp4^{O}	3.4; 115.8°, [b]	H	pArg6^{NH2}	pTrp4^{O}	2.9; 97.8°	H
					pArg6^{NH1}	§Ile66^{O}	2.7; 130.0°	H
pTrp7	*partly solvent-exposed*				*partly solvent-exposed*			
	pTrp7^{NE1}	¶Gln155^{OE1}	2.7; 106.6°	H				
	B*2705:pVIPR-p6α				**B*2709:pVIPR-U5**			
Peptide residue	**Atom**	**Contact residue**	**Distance [Å]; D-O-C angle[a]**	**Inter-action**	**Atom**	**Contact residue**	**Distance [Å]; D-O-C angle[a]**	**Inter-action**
pLys3	*partly solvent-exposed*				*partly solvent-exposed*			
	pLys 3^{N}	*Tyr99^{OH}	3.0; 118.2°	H	pLys3^{N}	*Tyr99^{OH}	3.0; 119.0°	H
	pLys3^{O}	*Tyr99^{OH}	3.4; 113.7°, [b]	H				
	pLys3^{NZ}	pTrp4^{O}	2.8; 148.6°	H	pLys3^{NZ}	pTrp4^{O}	3.3; 139.8°	H
pTrp4	*solvent-exposed*				*solvent-exposed*			
	pTrp4^{O}	pLys3^{NZ}	2.8; 148.6°	H	pTrp4^{O}	pLys3^{NZ}	3.3; 139.8°	H
p5	*buried* (pArg5)				*buried* (pCir5)			
	pArg5^{NH1}	*Asp116^{OD2}	3.1; 117.6°	[d]SB	pCir5^{N6}	pTrp7^{O}	3.0; 142.6°	H
	pArg5^{NH2}	*Asp116^{OD1}	3.0; 97.3°	SB	pCir5^{O7}	*His116^{NE2}	2.8; 123.5°	H
					pCir5^{O7}	§Lys70^{NZ}	2.9; 115.4°, [b]	H
					pCir5^{N8}	§Asp77^{OD2}	3.0; 133.0°	H
pArg6	*solvent-exposed*				*solvent-exposed*			
pTrp7	*buried*				*buried*			
					pTrp7^{O}	pCir5^{N6}	3.0; 142.6°	H

[+] The binding of B*2709 to pVIPR resembles that of B*2705 to this peptide in p4α conformation (19).
[a] D-O-C angles with D=donor atom (NH or OH): angles calculated with HBPLUS.
[b] D-O-C angles calculated manually with COOT.
[c] H, hydrogen bond.
[d] SB, salt bridge.
* β-sheet floor.
§ α1-helix.
¶ α2-helix.

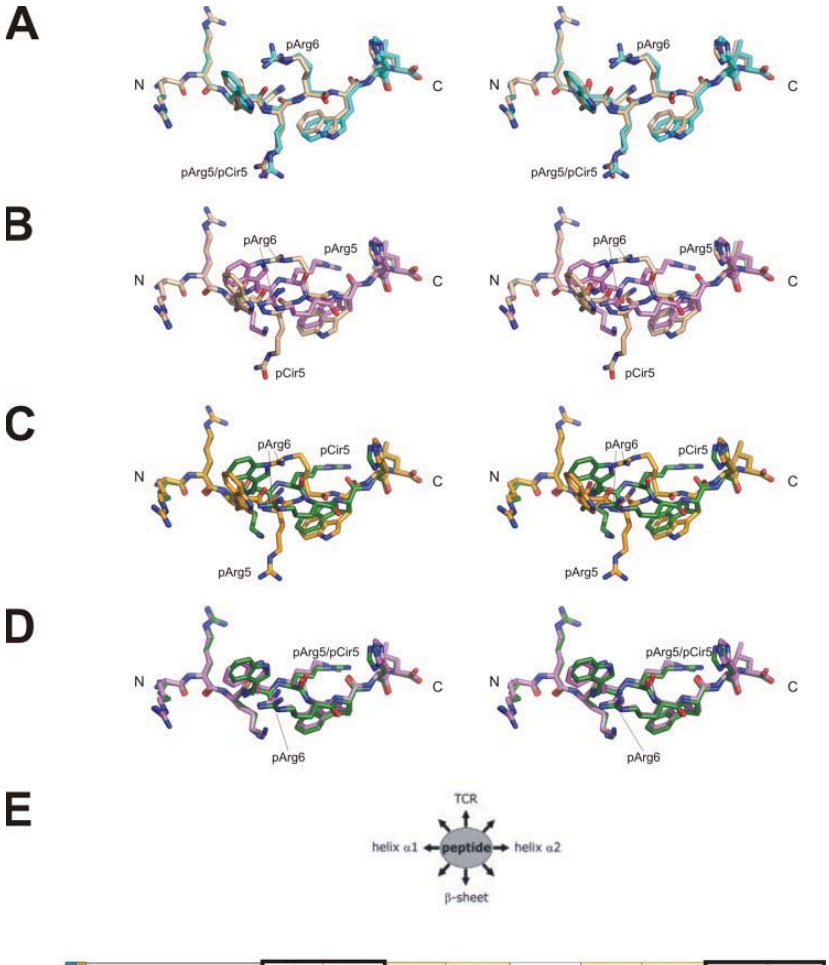

FIGURE 2. **Comparison of pVIPR-U5 and pVIPR as presented by B*2705 and B*2709.** Superimpositions (shown in stereo) as viewed by an approaching TCR; selected amino acids are indicated. *A*, superimposition of pVIPR-U5 (*wheat*) and pVIPR (*cyan*), both in p4α binding mode, as presented by B*2705 molecules. *B*, superimposition of pVIPR-U5 (*wheat*) and pVIPR (*violet*, p6α conformation) in B*2705 molecules. *C*, superimposition of pVIPR-U5 (*green*) and pVIPR (*orange*) complexed to B*2709 molecules. *D*, superimposition of pVIPR-U5 (*green*), as presented by B*2709, and pVIPR (*violet*), as presented by B*2705 in p6α binding mode. *E*, schematic description of side chain orientations when looking from the N to the C termini of pVIPR-p4α (identically presented by B*2705 and B*2709), B*2705·pVIPR-U5-p4α, B*2705·pVIPR-p6α, and B*2709·pVIPR-U5. *Upper panel*, floor of peptide binding groove indicated by "β-sheet," and binding region for TCR (*TCR*). *Lower panel*, the *boxed areas* show residues exhibiting structural identity, whereas the differently *shaded* areas indicate orientation similarity between peptide residues as a consequence of distinct binding modes in B*2705 and B*2709 (directions of *arrows* are as in *upper panel*). The peptide sequences are also given.

the peptide (Table 2). Apart from further intrapeptide and intermolecular interactions involving residues in the middle of the peptide, the non-canonical conformation of pVIPR-U5 also leads to a characteristic stacking of the side chains of pTrp4 and pArg6 (Fig. 1*B*) which we have observed before in the case of the unmodified pVIPR peptide when bound to B*2705 in p6α conformation (19).

The high resolution of the two structures also permitted the unambiguous identification of many water molecules that mediate further interactions both between peptide and HC residues as well as intrapeptide contacts (not shown). However, as found previously in the case of the m9 peptide (17), the polymorphic HC residue 116 is instrumental in the formation of distinct, subtype-specific water networks surrounding Asp/His-116. In particular, those regions within the binding groove are affected where the two peptide conformations differ most, *i.e.* between the D and the F pockets, as described already for the two pVIPR conformations (19).

*Structural Comparison of pVIPR-U5 and pVIPR Complexed with B*2705 and B*2709*—As mentioned above, the four complexes of pVIPR-U5 and pVIPR with B*2705 and B*2709 did not crystallize isomorphously. Nevertheless, the close crystallographic similarity of the structures obtained with the two peptides (Table 1 and Ref. 19) indicates that comparable crystallographic intermolecular interactions associated with crystal packing apply to all of them. Astonishingly, an extensive comparative analysis of these complexes (Figs. 2–4; supplemental Figs. S2–S5; Table 2) reveals that the citrullinated peptide in a given subtype exhibits structural features that are nearly identical to those of the unmodified peptide presented by the other subtype. This similarity is not only observed for the Cα backbones of the two peptides but extends even to details of their side chains.

The structures of B*2705 with the two peptides show at first sight that pVIPR-U5 is bound very similarly to pVIPR in p4α conformation (r.m.s.d. of 0.8 Å for all, and 0.3 Å for the Cα atoms of the peptides) (Fig. 2, *A* and *E*; supplemental Figs. S2 and S4; Table 2). Small deviations are observed only in case of pCir5/pArg5 and pTrp7. However, the structures diverge considerably when B*2705 in complex with pVIPR-U5 and pVIPR in p6α binding mode are compared (r.m.s.d. of 3.6 Å for all, and 1.6 Å for the Cα atoms of the peptides). In this case, the Cα traces as well as the side chains of residues p3 to p7 are clearly distinct between the two structures (Fig. 2, *B* and *E*; supplemen-

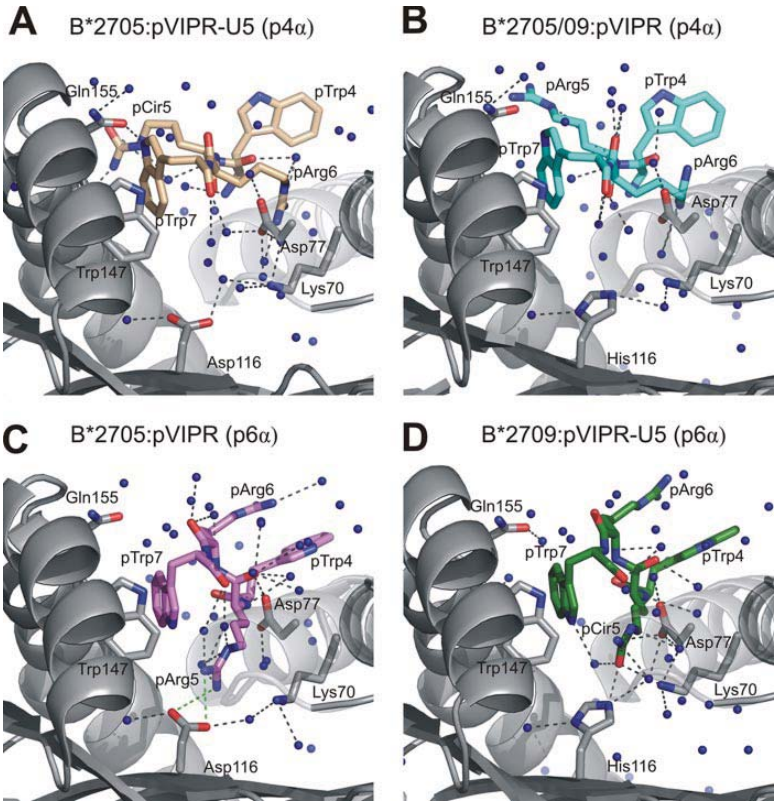

FIGURE 3. **Conformation-dependent peptide contacts with F-pocket residues and water molecules.** The F-pocket architecture and atomic interactions in B*2705·pVIPR-U5 (*A*, *wheat*), B*2705/09·pVIPR-p4α (*B*, *cyan*), B*2705·pVIPR-p6α (*C*, *violet*), and B*2709·pVIPR-U5 (*D*, *green*) with the relevant parts of the peptides are shown. Water molecules are depicted as *blue spheres*, and hydrogen bonds are depicted as *dotted lines*. The view is along the binding groove with the peptide C terminus in *front*, the α1-helix on the *right*, and the α2-helix on the *left*. For clarity, not all hydrogen bonds (see *e.g.* Table 2) are depicted.

tal Figs. S2 and S5; Table 2). Similarly divergent structures are revealed by a comparison of the two peptides in B*2709 (r.m.s.d. of 3.7 Å for all, and 1.5 Å for the Cα atoms of the peptides) (Fig. 2, *C* and *E*; supplemental Figs. S3 and S4; Table 2). In contrast, the structures of pVIPR in p6α conformation (B*2705) and pVIPR-U5 in B*2709 are virtually indistinguishable (r.m.s.d. of 0.8 Å for all, and 0.4 Å for Cα atoms) (Fig. 2, *D* and *E*; supplemental Figs. S3 and S5; Table 2).

The similarity between B*2705·pVIPR-U5/B*2705·pVIPR-p4α and B*2709·pVIPR-U5/B*2705·pVIPR-p6α extends even to details of F pocket architecture (Fig. 3). In the case of the two p4α binding modes, only the orientation of the pCir5/Arg-5 side chains differs appreciably, whereas all other peptide and HC residues retain their locations (Figs. 2*A* and 3, *A* and *B*; Table 2). Even more striking is the conserved architecture around pArg5 and pCir5 in the p6α peptide binding modes. Despite the presence of a bidentate salt bridge to Asp-116 in B*2705·pVIPR-p6α (Fig. 3*C*) as opposed to a hydrogen bond to His-116 in B*2709·pVIPR-U5 (Fig. 3*D*) and some altered intrapeptide contacts, the positions of all peptide and HC side chains are nearly perfectly retained (Fig. 3, *C* and *D*; supplemental Figs. S3 and S5; Table 2). The only slight difference concerns an "upward" movement of the pCir5 side chain (a difference of 1.8 Å between the corresponding pCir5$^{C\gamma}$ and pArg5$^{C\zeta}$ atoms) that is induced by the bulky His-116 side chain in B*2709 (Fig. 3, *C* and *D*).

The two types of peptide conformation also influence the surface properties of the complexes (Fig. 4). Due to the less exposed location of pCir5 in B*2705 in comparison to pArg5 in B*2705 (p4α binding mode) or B*2709 (Fig. 4, *A* and *B*), the exposed peptide surface is smaller in the former complex: 146 Å^2 (B*2705·pVIPR-U5) in contrast to 160 Å^2 in both B*2705·pVIPR-p4α and B*2709·pVIPR, respectively. One consequence of the presence of the positively charged pArg5 in the latter structures is also a pronounced surface charge difference between B*2705·pVIPR-U5 and the two other complexes (Fig. 4, *E* and *F*). In contrast, the "disappearance" of the differently charged residues at peptide position p5 within the peptide binding groove leads to nearly complete congruence of the B*2705·pVIPR-p6α and the B*2709·pVIPR-U5 structures (Fig. 4, *C* and *D*) and identity in surface charge distribution (Fig. 4, *G* and *H*).

Peptide- and Subtype-dependent CTL Recognition—The determination of the structures of the two HLA-B27 subtypes complexed with pVIPR-U5 suggested that pVIPR-specific CTL from a B*2705-positive donor might lose their reactivity when the citrullinated peptide would serve as target, assuming that it is presented also at physiological temperature in the conformation shown by the x-ray structures. We first determined whether pVIPR-U5 could be displayed by B*2705 and B*2709 at the cell surface using a binding assay that employed monoclonal antibodies. One of these (MARB3) is a conformation-sensitive reagent recognizing HLA-B27 molecules only when a peptide is present within the binding groove (23), whereas another (ME1) detects these molecules also in a peptide-devoid state (22). The reactivity of both antibodies with the pVIPR-U5-loaded HLA-B27 subtypes indicates that citrulline-modified pVIPR forms complexes with these molecules that are stable at 37 °C (Fig. 5, *A* and *B*).

We had previously shown that pVIPR-specific CTL can be found in healthy B*2705-positive individuals and are frequently observed in patients with AS, whereas these CTL are only rarely encountered in B*2709-positive individuals (40, 41). Such CTL could readily also be produced in the course of the current studies. As expected, they react with B*2705 and cross-react with the B*2709 subtype presenting the pVIPR peptide. How-

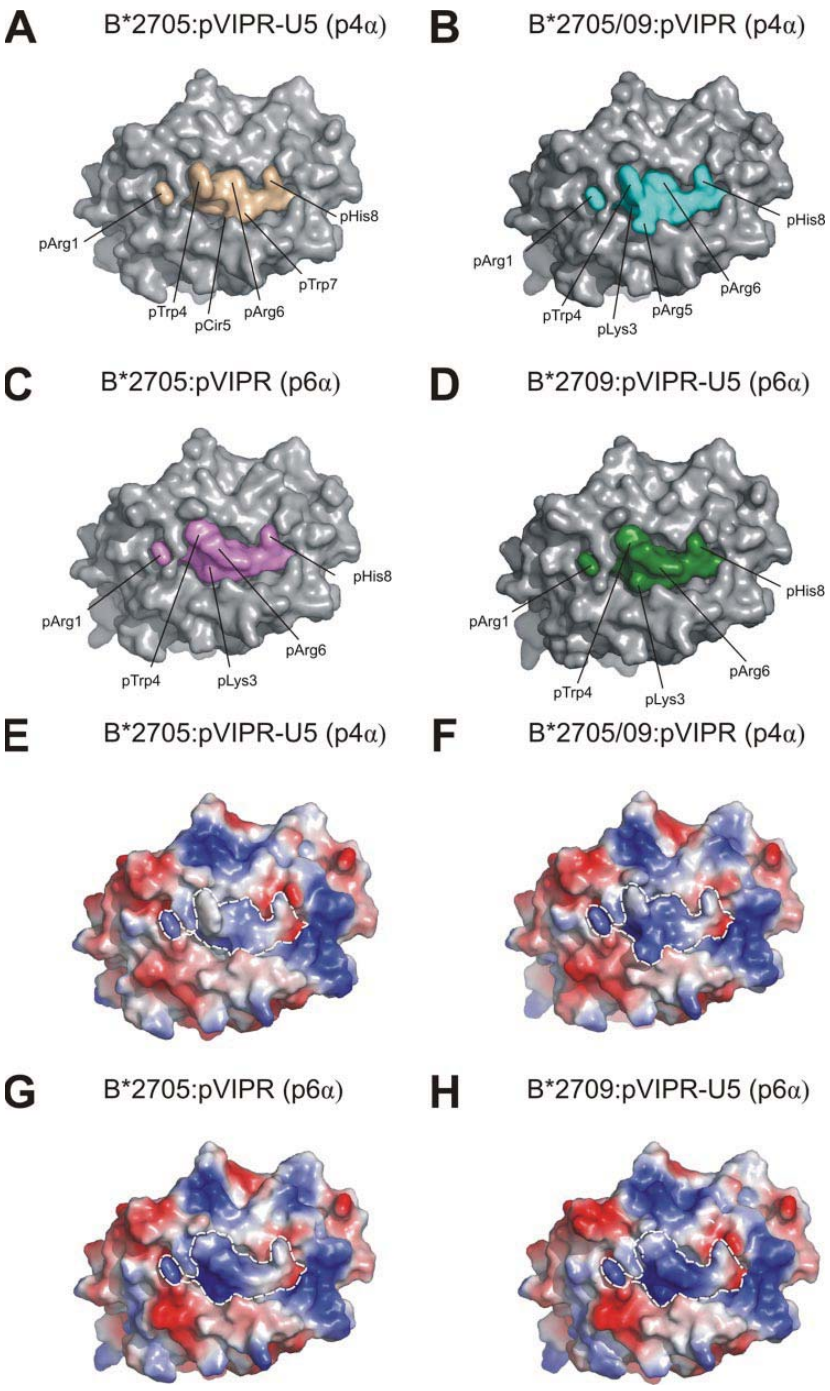

FIGURE 4. **Molecular surfaces of pVIPR-U5 and pVIPR as presented by B*2705 and B*2709.** Molecular surface representations of B*2705 (*A–C* and *E–G*) and B*2709 (*B*, *D*, *F*, and *H*) complexed with pVIPR-U5 or pVIPR, respectively, as viewed by an approaching TCR; color coding is as in Fig. 2. *A–D*, shape similarities and differences; *E–H*, electrostatic surfaces, with *red* indicating a negative charge, and *blue* indicating a positive charge. *Gray* areas are uncharged.

ever, none of the four CTL analyzed reacted with B*2705·pVIPR-U5, and there was only marginal reactivity with B*2709·pVIPR-U5 in case of one CTL (MP11) (Fig. 5*C*).

DISCUSSION

Although the deimination of arginine to yield citrulline had been discovered as early as 1939 (42), the importance of this posttranslational modification has only recently begun to be appreciated (1–6). To a large extent this is due to the finding that early diagnosis of a subset of patients with rheumatoid arthritis is facilitated by determining the presence of autoantibodies directed against cyclic citrullinated peptides (Refs. 43–46; for a recent review, see Ref. 6). T cell studies in combination with considerations based on the structure of MHC class II molecules in complex with unmodified peptides (1, 4) indicate that citrullinated peptides are displayed by these antigens but possibly in conformationally altered forms. Because evidence for an altered presentation of a citrullinated peptide had so far been obtained only indirectly, the present study addresses three issues that are important in the context of inflammatory disorders in general and HLA-B27-associated diseases in particular. (i) How can a citrullinated peptide be bound to and presented by an MHC molecule? (ii) Are the conformations exhibited by a citrullinated peptide and its nonmodified form different? And finally, (iii) do HLA-B27 subtypes that are differentially associated with AS display a given citrullinated peptide in a similar conformation?

X-ray crystallography has been employed here for the first time to analyze the influence of a citrulline within a peptide on its presentation by MHC molecules. We chose to modify the pVIPR peptide because of the highly unusual dual binding mode which it exhibits when bound to the AS-associated B*2705 subtype. Furthermore, the central pArg5 occupies a strategic position (19), making it likely that the exchange of pArg5 by pCir5 had an

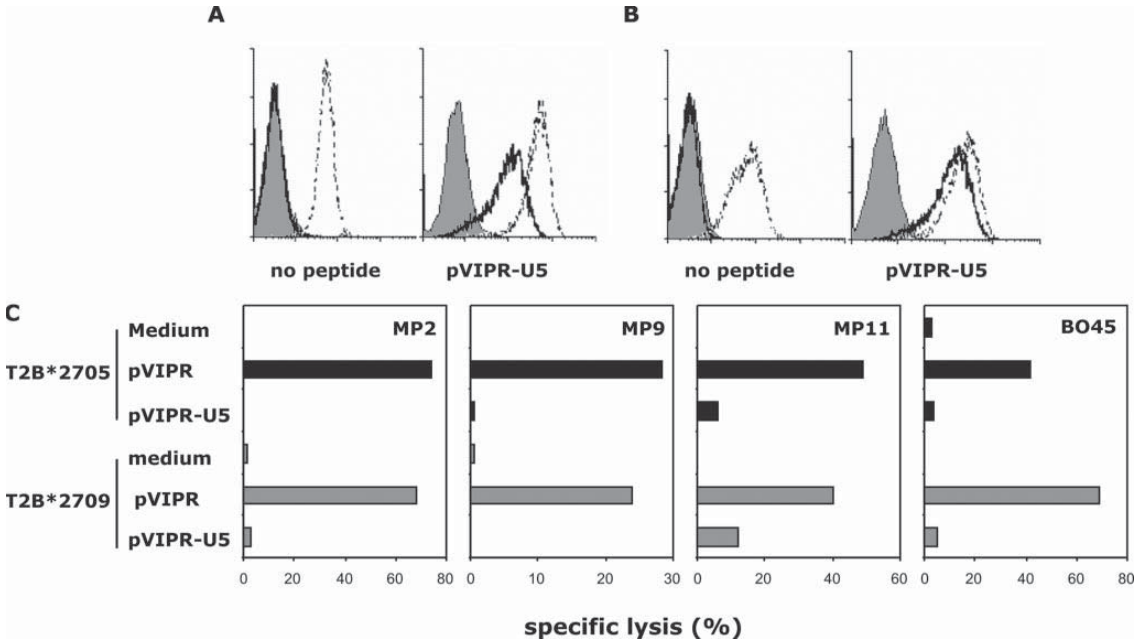

FIGURE 5. **Recognition of pVIPR and pVIPR-U5 by pVIPR-stimulated CTL lines.** *A* and *B*, flow cytometric analysis (*abscissa*, log fluorescence; *ordinate*, cell count) of the reactivity of monoclonal antibodies (*black line*, MARB3; *shaded area*, negative control; *dotted line*, ME1) with the cell lines BM36.1/B*2705 (*A*) and BM36.1/B*2709 (*B*). The HLA-B27 molecules were either devoid of peptide (*left panels*) or loaded with pVIPR-U5 (*right panels*). ME1 reactivity indicates the presence of HLA-B27 antigens, whereas MARB3 reactivity is dependent on the presence of a peptide in the binding groove of these molecules. Untransfected BM36.1 cells (HLA-A1, -Cw4, -B35) were unreactive with all reagents employed (not shown). *C*, standard 4-h ^{51}Cr-release assay in which T2-B*2705 and T2-B*2709 cells incubated in medium alone (as control) or with peptides (70 μM) were used as target cells. CTL lines used as effectors were derived from two B*2705 patients with AS. Spontaneous release of ^{51}Cr-labeled target cells was lower than 15%. Note that the degree of specific lysis differs between the CTL lines.

effect on peptide display, and above all, the frequent presence of cytotoxic T cells against this peptide only in B*2705 individuals suggests a relationship with the development of AS (19, 40, for a review, see Ref. 41). However, it is currently unclear whether vasoactive intestinal peptide type 1 receptor can be modified by citrullination such that pVIPR-U5 could be cleaved from it or whether the proteolysis-derived peptide might itself be subject to citrullination. In this context, it is important to point out that it is principally possible that pVIPR is just an innocent bystander in AS development as unidentified peptides that exhibit structural, but not necessarily sequence similarity with pVIPR might be the pathogenetically relevant targets that are recognized by cross-reactive CTL (20, 21). Therefore, the model character of our study has to be emphasized.

Nevertheless, pVIPR-U5 can be bound by both B*2705 and B*2709 under *in vitro* (Fig. 1) as well as *in vivo* (Fig. 5) conditions, and the loss of the positive charge of pArg5 in pVIPR-U5 is accompanied by loss of the non-canonical (p6α) conformation in B*2705. This is perhaps not surprising since citrullination of pArg5 had removed the positive charge which was considered a prerequisite for attaining this binding mode (19, 20). However, the presence of the citrullinated peptide in a non-canonical conformation in B*2709 was unexpected. Therefore, this peptide is displayed in binding modes that are diametrically opposed to those exhibited by pVIPR (Figs. 1–4; Table 2).

Why is pVIPR-U5 bound to B*2709 in the p6α conformation and to B*2705 in the p4α binding mode? In principle, the amide group of the pCir5 side chain could hydrogen bond to both His-116 and Asp-116 by an ~180° rotation. This would allow interactions either of pCir5^{O7} with His116^{NE2} (in fact found in B*2709) or of pCir5^{N8} with Asp116^{OD1} (not found in B*2705). There are two reasons why the latter scenario could be unfavorable (Fig. 3). First, the distance of the Asp116^{OD1} atom from the Cα-atom corresponds to that of His116^{ND1} and not to that of His116^{NE2}. It would be ~1.3 Å shorter and, therefore, possibly too short to be accommodated by conformational changes of the side chain of pCir5 or the Cα-backbone of the HC. Second, in B*2709·pVIPR-U5, pCir5 side chain atoms are engaged not only in a hydrogen bond to His116^{NE2} but also to Lys70^{NZ} and Asp77^{OD2} of the HC as well as to pTrp7^{O} of the peptide (Table 2). These contacts are both short and well defined because Lys70^{NZ} and Asp77^{OD2} are charged, and there are water-mediated hydrogen bonds to the amide group as well (not shown). If the latter were rotated by ~180° in the B*2705 peptide binding groove, these hydrogen bonds would be replaced by repulsive interactions, because the oxygen of the amide group would now oppose Asp77^{OD2}, and the amino group would be repelled by Lys70^{NZ}. In addition, it appears possible that a short intrapeptide contact (pCir5^{N6} → pTrp7^{O}) would be lost as well, resulting in a further destabilization of pCir5-bound non-canonically to the B*2705 peptide binding groove.

The differential binding modes of pVIPR-U5 to the two HLA-B27 subtypes provide also an explanation for the loss of pVIPR-specific CTL reactivity with B*2705. Although the

canonical binding mode of pVIPR-U5 is similar in structural terms to the conventional conformation observed for pVIPR (Figs. 2–4), the electrostatic surface charges of the two complexes differ substantially in the vicinity of the pArg5/pCir5 exchange (Fig. 4). This property is most likely responsible for the observation that none of the pVIPR-specific CTL exhibited cross-reactivity between the two peptides when displayed by the B*2705 subtype (Fig. 5). Loss of the peptide from the binding groove during the cytotoxicity assay could be excluded because it was possible, using a conformation-sensitive monoclonal antibody, to demonstrate that pVIPR-U5 was stably bound to both subtypes (Fig. 5). Furthermore, the lack of cross-reactivity with B*2709·pVIPR-U5 in the case of the CTL MP2, MP9, and BO45 suggests that these three CTL recognize pVIPR in the canonical conformation because only this binding mode differs from the non-canonical presentation of pVIPR-U5 in B*2709 (Figs. 2 and 4). In contrast, the marginal reactivity observed for MP11 in case of B*2709 (but not B*2705) complexed to pVIPR-U5 could indicate that some T cells within this CTL line recognize the non-canonical conformation of pVIPR in B*2705, as only this binding mode corresponds very closely to pVIPR-U5 bound non-canonically to B*2709.

The unpredictable effect even of seemingly minor changes within a peptide (47–50) or an MHC class I HC (19, 20, 50, 51) on the interaction of an MHC-peptide complex with a TCR has recently been highlighted by extensive structural and dynamic analyses of HLA-A2 in complex with various related peptides derived from a melanoma-associated antigen (52). This study demonstrated that neither cross-reactivity nor selectivity of T cells can reliably be predicted from x-ray structures of HLA-A2-peptide complexes, although the structural differences were much smaller than those reported here. Therefore, our finding that a single, strategically located polymorphic HC residue as well as a single charge difference within a peptide side chain (pArg5 *versus* pCir5) can independently affect the peptide binding mode is in line with the results reported for other MHC-peptide complexes.

It is currently unknown to what extent the citrullination of proteins, let alone that of the pVIPR peptide, influences T cell responses in diseases associated with distinct MHC alleles, as the only two reported cases involve the presentation of citrullinated peptides by selected mouse or human MHC class II antigens (1, 4). Therefore, it would belong into the realm of speculation to ascribe a specific role to citrullinated peptides in the pathogenesis of autoimmune disorders; for example, in the context of molecular mimicry between foreign and self-peptides in AS (14, 20, 21) or other diseases. Whether conformational reorientations of MHC ligands, comparable with those described here, can affect also citrullinated pathogen-derived peptides such as pLMP2 (RRRWRRLTV; from the latent membrane protein 2 of Epstein-Barr virus) remains to be investigated. Like pVIPR, unmodified pLMP2 is presented by the B*2705 and B*2709 subtypes in completely different binding modes (20), and it appears possible that citrullination of pLMP2 would affect its binding modes to HLA-B27 subtypes in ways analogous to those described here for the pVIPR peptide.

Citrullinated peptides have so far not been eluted from HLA-B27 antigens or other MHC molecules, although this may simply be because no attention had been paid to their possible presence. However, preliminary results have shown that HLA-B27-restricted CTL against pVIPR-U5 can be obtained from AS patients,[4] indicating that citrullinated pVIPR can indeed serve as a target in the context of physiological T cell responses. In line with these findings, citrullinated proteins are known to be expressed in synovial tissue of patients with a variety of autoimmune disorders including reactive arthritis, which is, like AS, an HLA-B27-associated disease (5). Furthermore, citrulline-modified polypeptides have been found within the synovia of animals with collagen- and streptococcal cell wall-induced arthritis (53). In addition, an analysis of synovial tissue from a patient with rheumatoid arthritis has demonstrated that 51 (5.2%) of 990 identified synovial proteins exhibited citrullination, and 13 citrullinated autoantigens could unambiguously be assigned by mass spectrometry (54). Apart from fibrinogen, a major citrullinated autoantigen in these patients (55, 56), all other proteins identified in this study (54) were polypeptides for which citrullination had not been described previously. Similarly, a comparative proteomic study (see Ref. 57) with a small number of patients exhibiting three types of rheumatoid disease indicates that citrullination is detectable not only in individuals with rheumatoid arthritis but also in those suffering from AS. There can, thus, be no doubt that a comparative proteomic approach with inflamed tissue from patients with AS and other spondyloarthropathies would lead to novel insights despite the fact that the clinical and pathogenetic parallels between these diseases and rheumatoid arthritis are limited.

In conclusion, the crystallographic and functional comparison of the two HLA-B27 subtypes in complex with pVIPR-U5 and pVIPR that we have carried out reveals three major findings. (i) Both subtypes are able to bind a given citrullinated peptide (pVIPR-U5), but they solve this task differently and present the peptide in drastically distinct conformations; (ii) the corresponding unmodified peptide (pVIPR) is displayed by a given HLA-B27 subtype in a diametrically opposing binding mode; (iii) the structural data provide an explanation for the results obtained with cytotoxic T cells but demonstrate also that citrullinated peptides may influence immune responses in an unpredictable manner.

Acknowledgments—We thank all patients for participation in this study and F. Lucantoni and C. Schnick as well as A. Zank for excellent technical assistance. We are grateful to the beamline staff at the European Synchrotron Radiation Facility, Grenoble and to Drs. B. Loll and R. Misselwitz for criticism of the manuscript.

REFERENCES

1. Ireland, J., Herzog, J., and Unanue, E. R. (2006) *J. Immunol.* **177,** 1421–1425
2. Makrygiannakis, D., af Klint, E., Lundberg, I. E., Löfberg, R., Ulfgren, A. K., Klareskog, L., and Catrina, A. I. (2006) *Ann. Rheum. Dis.* **65,** 1219–1222
3. György, B., Tóth, E., Tarcsa, E., Falus, A., and Buzás, E. I. (2006) *Int. J. Biochem. Cell Biol.* **38,** 1662–1677
4. Hill, J. A., Southwood, S., Sette, A., Jevnikar, A. M., Bell, D. A., and Cairns,

[4] M. T. Fiorillo, R. Sorrentino, and B. Uchanska-Ziegler, unpublished observations.

E. (2003) *J. Immunol.* **171,** 538–541
5. Vossenaar, E. R., Smeets, T. J. M., Kraan, M. C., Raats, J. M., van Venrooij, W. J., and Tak, P. P. (2004) *Arthritis Rheum.* **50,** 3485–3494
6. Klareskog, L., Rönnelid, J., Lundberg, K., Padyukov, L., and Alfredsson, L. (2008) *Annu. Rev. Immunol.* **26,** 651–675
7. Brewerton, D. A., Hart, F. D., Nicholls, A., Caffrey, M., James, D. C., and Sturrock, R. D. (1973) *Lancet* **1,** 904–907
8. Schlosstein, L., Terasaki, P. I., Bluestone, R., and Pearson, C. M. (1973) *N. Engl. J. Med.* **288,** 704–706
9. Khan, M. A., Mathieu, A., Sorrentino, R., and Akkoc, N. (2007) *Autoimmun. Rev.* **6,** 183–189
10. López de Castro, J. A. (2007) *Immunol. Lett.* **108,** 27–33
11. Hammer, R. E., Maika, S. D., Richardson, J. A., Tang, J. P., and Taurog, J. D. (1990) *Cell* **63,** 1099–1112
12. D'Amato, M., Fiorillo, M. T., Carcassi, C., Mathieu, A., Zuccarelli, A., Bitti, P. P., Tosi, R., and Sorrentino, R. (1995) *Eur. J. Immunol.* **25,** 3199–3201
13. Madden, D. R. (1995) *Annu. Rev. Immunol.* **13,** 587–622
14. Ziegler, A., Loll, B., Misselwitz, R., and Uchanska-Ziegler, B. (2008) in *Molecular Mechanisms of Spondyloarthropathies* (López-Larrea, C., ed) Landes Bioscience, Austin, TX, in press
15. Ramos, M., Paradela, A., Vazquez, M., Marina, A., Vazquez, J., and López de Castro, J. A. (2002) *J. Biol. Chem.* **277,** 28749–28756
16. López de Castro, J. A., Alvarez, I., Marcilla, M., Paradela, A., Ramos, M., Sesma, L., and Vázquez, M. (2004) *Tissue Antigens* **63,** 424–445
17. Hülsmeyer, M., Hillig, R. C., Volz, A., Rühl, M., Schröder, W., Saenger, W., Ziegler, A., and Uchanska-Ziegler, B. (2002) *J. Biol. Chem.* **277,** 47844–47853
18. Hülsmeyer, M., Welfle, K., Pöhlmann, T., Misselwitz, R., Alexiev, U., Welfle, H., Saenger, W., Uchanska-Ziegler, B., and Ziegler, A. (2005) *J. Mol. Biol.* **346,** 1367–1379
19. Hülsmeyer, M., Fiorillo, M. T., Bettosini, F., Sorrentino, R., Saenger, W., Ziegler, A., and Uchanska-Ziegler, B. (2004) *J. Exp. Med.* **199,** 271–281
20. Fiorillo, M. T., Rückert, C., Hülsmeyer, M., Sorrentino, R., Saenger, W., Ziegler, A., and Uchanska-Ziegler, B. (2005) *J. Biol. Chem.* **280,** 2962–2971
21. Rückert, C., Fiorillo, M. T., Loll, B., Moretti, R., Biesiadka, J., Saenger, W., Ziegler, A., Sorrentino, R., and Uchanska-Ziegler, B. (2006) *J. Biol. Chem.* **281,** 2306–2316
22. Ellis, S. A., Taylor, C., and McMichael, A. (1982) *Hum. Immunol.* **5,** 49–59
23. Rehm, A., Rohr, A., Seitz, C., Wonigeit, K., Ziegler, A., and Uchanska-Ziegler, B. (2000) *Hum. Immunol.* **61,** 408–418
24. Kelly, A., Powis, S. H., Kerr, L.-A., Mockridge, I., Elliott, T., Bastin, J., Uchanska-Ziegler, B., Ziegler, A., Trowsdale, J., and Townsend, A. (1992) *Nature* **355,** 641–644
25. Garboczi, D. N., Hung, D. T., and Wiley, D. C. (1992) *Proc. Natl. Acad. Sci. U. S. A.* **89,** 3429–3433
26. Otwinowski, Z. (1993) in *Proceedings of the CCP4 Study Weekend: Data Collection and Processing* (Sawyer, L., Isaacs, N., and Bailey, S., eds) pp. 56–62, SERC Daresbury Laboratory, Warrington, UK
27. Collaborative Computational Project 4 (1994) *Acta Crystallogr. Sect. D* **50,** 760–763
28. Murshudov, G. N., Vagin, A. A., and Dodson, E. J. (1997) *Acta Crystallogr. Sect. D* **53,** 240–255
29. Schuttelkopf, A. W., and van Aalten, D. M. (2004) *Acta Crystallogr. Sect. D* **60,** 1355–1363
30. Emsley, P., and Cowtan, K. (2004) *Acta Crystallogr. Sect. D* **60,** 2126–2132
31. Perrakis, A., Harkiolaki, M., Wilson, K. S., and Lamzin, V. S. (2001) *Acta Crystallogr. Sect. D* **57,** 1445–1450
32. Vriend, G. (1990) *J. Mol. Graph.* **8,** 52–56
33. Laskowski, R. A., MacArthur, M. W., Moss, D. S., and Thornton, J. M. (1993) *J. Appl. Crystallogr.* **26,** 283–291
34. McDonald, I. K., and Thornton, J. M. (1994) *J. Mol. Biol.* **238,** 777–793
35. DeLano, W. L. (2002) *PYMOL*, DeLano Scientific, Palo Alto, CA
36. Wallace, A. C., Laskowski, R. A., and Thornton, J. M. (1995) *Protein Eng.* **8,** 127–134
37. Madden, D. R., Gorga, J. C., Strominger, J. L., and Wiley, D. C. (1992) *Cell* **70,** 1035–1048
38. Hillig, R. C., Hülsmeyer, M., Welfle, K., Misselwitz, R., Welfle, H., Saenger, W., Kozerski, C., Volz, A., Uchanska-Ziegler, B., and Ziegler, A. (2004) *J. Biol. Chem.* **279,** 652–663
39. Stewart-Jones, G. B., di Gleria, K. S., McMichael, A. J., Jones, E. Y., and Bowness, P. (2005) *Eur. J. Immunol.* **35,** 341–351
40. Fiorillo, M. T., Maragno, M., Butler, R., Dupuis, M. L., and Sorrentino, R. (2000) *J. Clin. Investig.* **106,** 47–53
41. Fiorillo, M.T., and Sorrentino, R. (2008) in *Molecular Mechanisms of Spondyloarthropathies* (López-Larrea, C., ed) Landes Bioscience, Austin, TX, in press
42. Fearon, W. R. (1939) *Biochem. J.* **33,** 902–907
43. Young, B. J., Mallya, R. K., Leslie, R. D., Clark, C. J., and Hamblin, T. J. (1979) *Br. Med. J.* **2,** 97–99
44. Masson-Bessière, C., Sebbag, M., Girbal-Neuhauser, E., Nogueira, L., Vincent, C., Senshu, T., and Serre, G. (2001) *J. Immunol.* **166,** 4177–4184
45. Vossenaar, E. R., and van Venrooij, W. J. (2004) *Clin. Appl. Immunol. Rev.* **4,** 239–262
46. Bizzaro, N. (2007) *Clin. Chem. Lab. Med.* **45,** 150–157
47. Ding, Y. H., Baker, B. M., Garboczi, D. N., Biddison, W. E., and Wiley, D. C. (1999) *Immunity* **11,** 45–56
48. Sharma, A. K., Kuhns, J. J., Yan, S., Friedline, R. H., Long, B., Tisch, R., and Collins, E. J. (2001) *J. Biol. Chem.* **276,** 21443–21449
49. Kersh, G. J., Miley, M. J., Nelson, C. A., Grakoui, A., Horvath, S., Donermeyer, D. L., Kappler, J., Allen, P. M., and Fremont, D. H. (2001) *J. Immunol.* **166,** 3345–3354
50. Miley, M. J., Messaoudi, I., Metzner, B. M., Wu, Y., Nikolich-Zugich, J., and Fremont, D. H. (2004) *J. Exp. Med.* **200,** 1445–1454
51. Miller, P. J., Pazy, Y., Conti, B., Riddle, D., Appella, E., and Collins, E. J. (2007) *J. Mol. Biol.* **373,** 315–327
52. Borbulevych, O. Y., Insaidoo, F. K., Baxter, T. K., Powell, D. J., Jr., Johnson, L. A., Restifo, N. P., and Baker, B. M. (2007) *J. Mol. Biol.* **372,** 1123–1136
53. Vossenaar, E. R., Nijenhuis, S., Helsen, M. M., van der Heijden, A., Senshu, T., van den Berg, W. B., van Venrooij, W. J., and Joosten, L. A. (2003) *Arthritis Rheum.* **48,** 2489–2500
54. Matsuo, K., Xiang, Y., Nakamura, H., Masuko, K., Yudoh, K., Noyori, K., Nishioka, K., Saito, T., and Kato, T. (2006) *Arthritis Res. Ther.* **8**, R175
55. Nielen, M. M., van der Horst, A. R., van Schaardenburg, D., van der Horst-Bruinsma, I. E., van de Stadt, R. J., Aarden, L., Dijkmans, B. A., and Hamann, D. (2005) *Ann. Rheum. Dis.* **64,** 1199–1204
56. Chapuy-Regaud, S., Nogueira, L., Clavel, C., Sebbag, M., Vincent, C., and Serre, G. (2005) *Clin. Exp. Immunol.* **139,** 542–550
57. Tilleman, K., van Steendam, K., Cantaert, T., de Keyser, F., Elewaut, D., and Deforce, D. (2008) *Rheumatology* **47,** 597–604

SUPPLEMENTAL DATA

Fig. S1 $2F_o$-F_c electron density map (dark blue) of the pVIPR-U5 peptide in the B*2709 subtype, contoured at 1 σ level, before inclusion of the peptide in the refinement. This diagram shows the lack of model bias in peptide modeling in the binding groove (compare Fig. 1B). The HC residue His116 is also depicted, with nitrogen atoms coloured blue (top panel).
The middle and the lower panels show the binding groove of an HLA-B27 molecule with pockets for residues of bound peptides. The binding groove of B*2709 is depicted, in side view, through the transparent α2-helix (middle panel) or displayed as to an approaching TCR (lower panel), with pVIPR-U5 in stick representation. The A pocket accommodates the peptide N-terminus, pArg2 binds within the B pocket, pLys3 interacts with D pocket residues, and amino acids shaping the F pocket bind the side chain of the C-terminal peptide residue. Asp116/His116 at the floor of the binding groove of the B*2705/B*2709 subtypes are part of their F pockets and may interact with pArg5 (pVIPR, B*2705) or, as shown here, with pCir5 (pVIPR-U5, B*2709).

Fig. S2 Simplified lig-plot of contacts (only H bonds are shown, intra-peptide contacts are omitted) within the binding groove of B*2705 with the pVIPR-U5 peptide. Water-mediated contacts are omitted.

Fig. S3 Simplified lig-plot of contacts (only H bonds are shown, intra-peptide contacts are omitted) within the binding groove of B*2709 with the pVIPR-U5 peptide. Water-mediated contacts are omitted.

Fig. S4 Simplified lig-plot of contacts (only H bonds are shown, intra-peptide contacts are omitted) within the binding groove of B*2705 with the pVIPR peptide in p4α binding mode. The contacts observed in B*2709:pVIPR are virtually identical (19). Water-mediated contacts are omitted.

Fig. S5 Simplified lig-plot of contacts (only H bonds are shown, intra-peptide contacts are omitted) within the binding groove of B*2705 with the pVIPR peptide in p6α binding mode. Water-mediated contacts are omitted.

Fig. S1

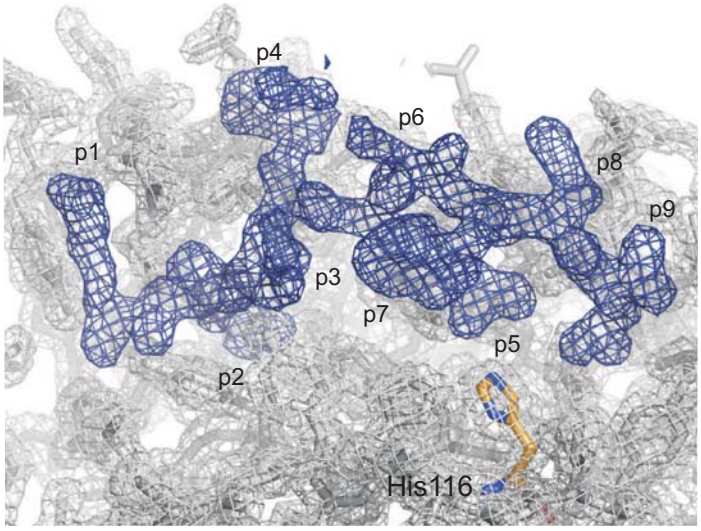

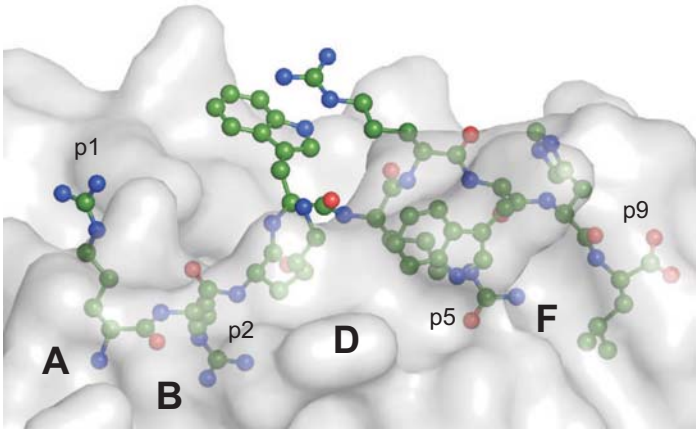

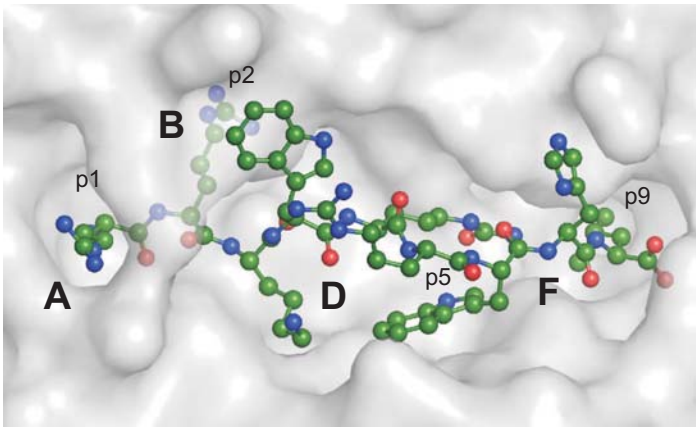

Fig. S2

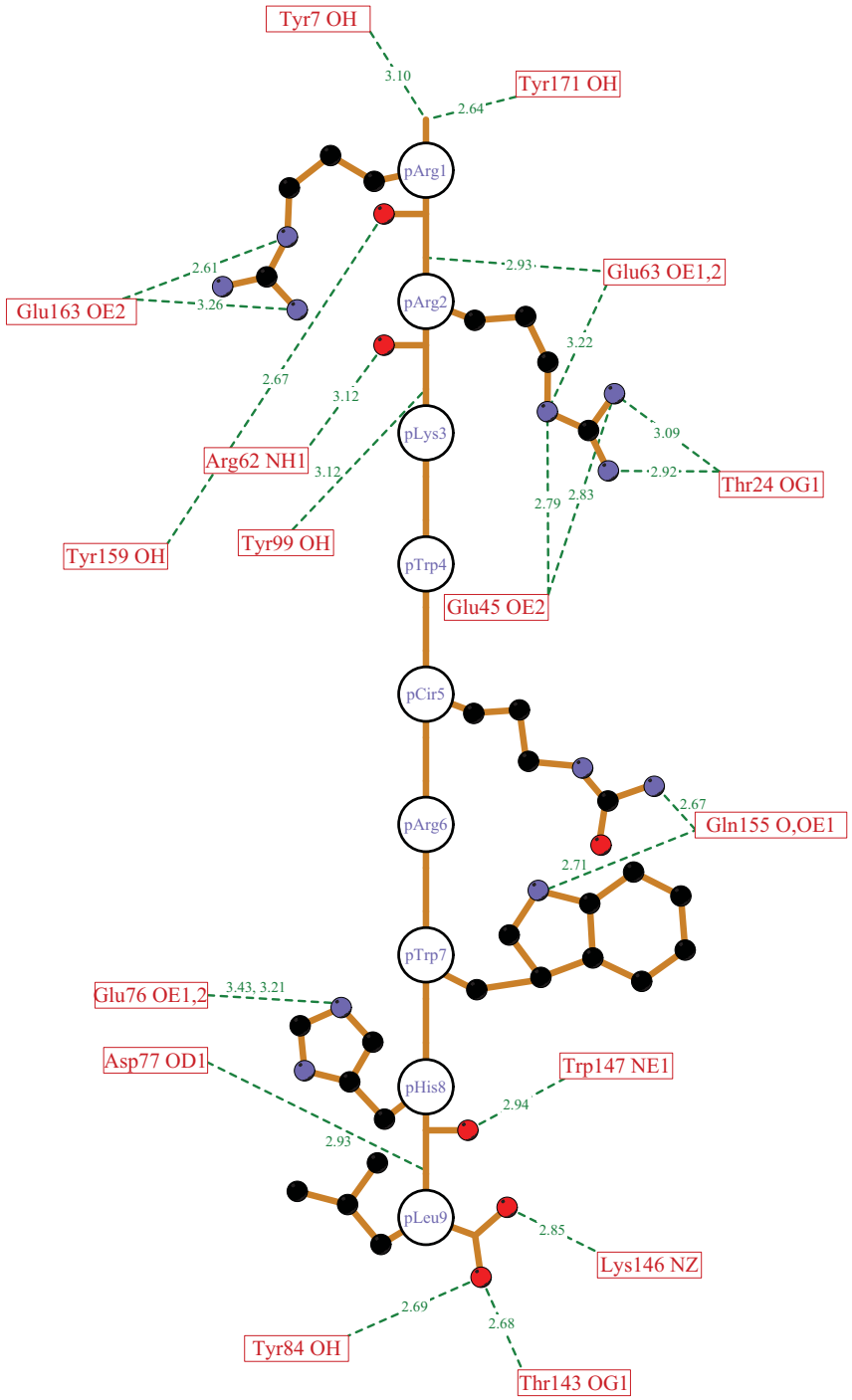
Tyr7 OH
3.10
Tyr171 OH
2.64
pArg1
2.61
Glu163 OE2
3.26
2.93
Glu63 OE1,2
pArg2
3.22
2.67
3.12
pLys3
3.09
Arg62 NH1
3.12
2.92
Thr24 OG1
2.79
2.83
Tyr159 OH
Tyr99 OH
pTrp4
Glu45 OE2
pCir5
2.67
pArg6
Gln155 O,OE1
2.71
pTrp7
Glu76 OE1,2
3.43, 3.21
Asp77 OD1
pHis8
Trp147 NE1
2.94
2.93
pLeu9
2.85
Lys146 NZ
2.69
2.68
Tyr84 OH
Thr143 OG1

Fig. S3

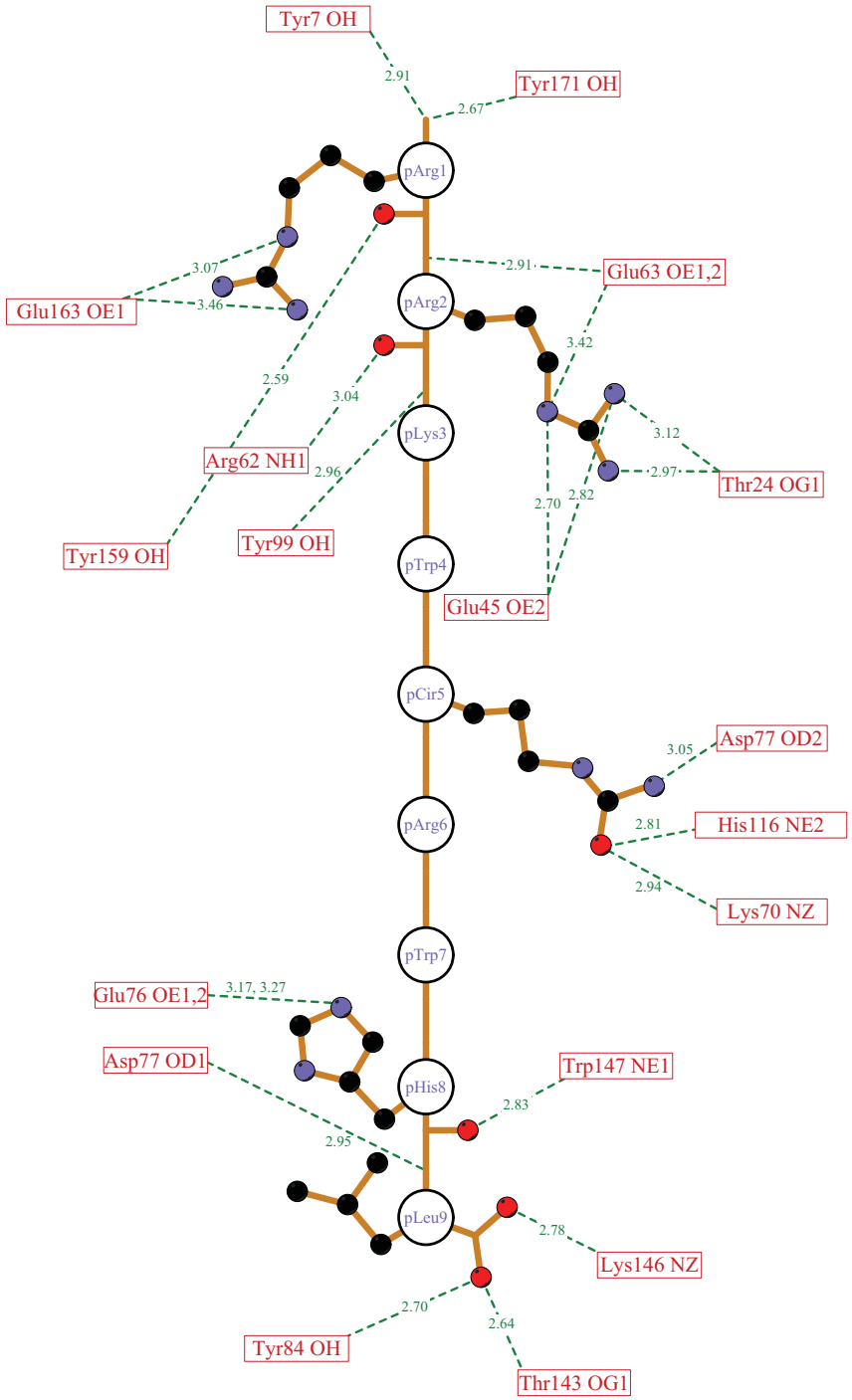
Tyr7 OH
2.91
Tyr171 OH
2.67
pArg1
3.07
Glu163 OE1
3.46
2.91
Glu63 OE1,2
pArg2
3.42
2.59
3.04
pLys3
3.12
Arg62 NH1
2.96
2.97
Thr24 OG1
2.70
2.82
Tyr159 OH
Tyr99 OH
pTrp4
Glu45 OE2
pCir5
3.05
Asp77 OD2
pArg6
2.81
His116 NE2
2.94
Lys70 NZ
pTrp7
Glu76 OE1,2
3.17, 3.27
Asp77 OD1
pHis8
Trp147 NE1
2.83
2.95
pLeu9
2.78
Lys146 NZ
2.70
2.64
Tyr84 OH
Thr143 OG1

Fig. S4

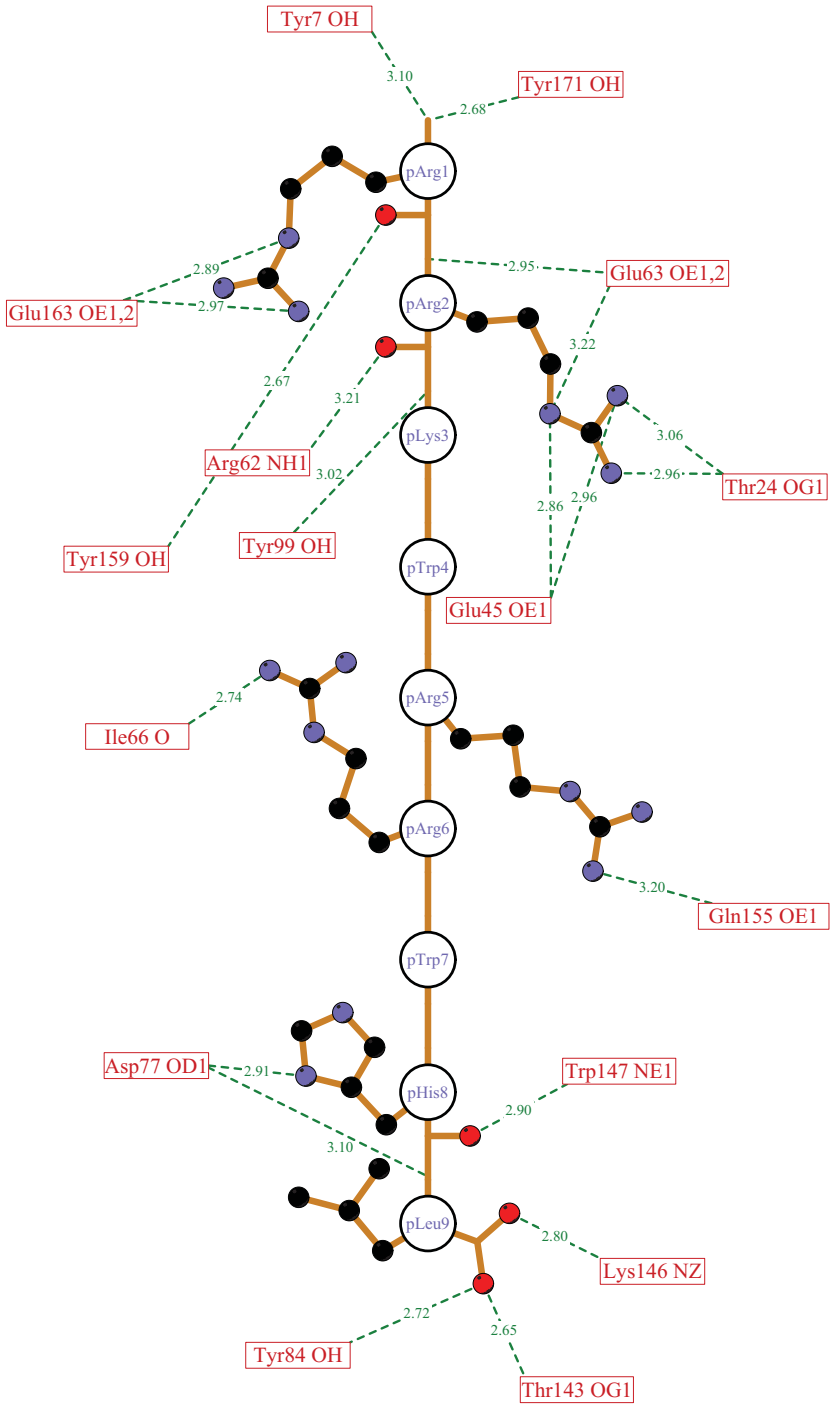
Tyr7 OH
3.10
Tyr171 OH
2.68
pArg1
2.89
Glu163 OE1,2
2.97
2.95
Glu63 OE1,2
pArg2
3.22
2.67
3.21
pLys3
3.06
Arg62 NH1
3.02
2.96
Thr24 OG1
2.86
2.96
Tyr159 OH
Tyr99 OH
pTrp4
Glu45 OE1
pArg5
2.74
Ile66 O
pArg6
3.20
Gln155 OE1
pTrp7
Asp77 OD1
2.91
pHis8
Trp147 NE1
2.90
3.10
pLeu9
2.80
Lys146 NZ
2.72
2.65
Tyr84 OH
Thr143 OG1

Fig. S5

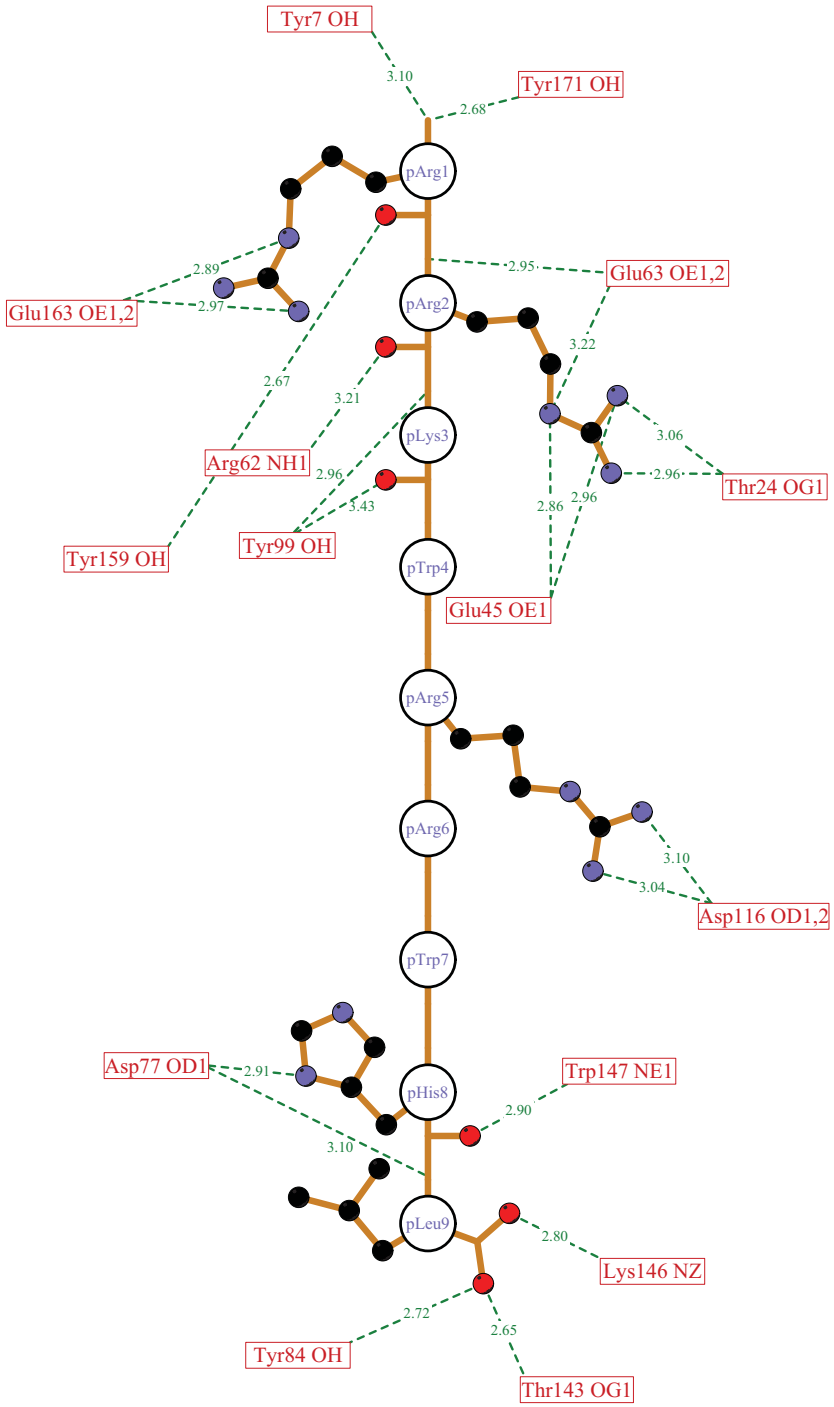
Tyr7 OH
3.10
Tyr171 OH
2.68
pArg1
2.89
Glu163 OE1,2
2.97
2.95
Glu63 OE1,2
pArg2
3.22
2.67
3.21
pLys3
3.06
Arg62 NH1
2.96
2.96
Thr24 OG1
3.43
2.86
2.96
Tyr159 OH
Tyr99 OH
pTrp4
Glu45 OE1
pArg5
pArg6
3.10
3.04
Asp116 OD1,2
pTrp7
Asp77 OD1
2.91
Trp147 NE1
pHis8
2.90
3.10
pLeu9
2.80
Lys146 NZ
2.72
2.65
Tyr84 OH
Thr143 OG1

4. Ligand-induced Changes in MHC Conformation

4.1 Summary

A number of studies have been devoted to analyzing the conformational changes associated with binding of TCR and KIR to pMHC (reviewed in Rudolph et al. 2006 and Boyington and Sun 2002). However, the focus has always been the study of changes and 'induced-fit' in the receptor molecule itself and the subtle conformational changes in pMHC induced by ligand-binding had not yet been studied in any detail. While the structures of a number of pMHC in complex with their TCR or KIR ligands and in free form were available (Rudolph et al. 2002, 2006, Boyington and Sun 2002), the structure of a pMHC-recognizing of an antibody with TCR-like specificity, Fab-Hyb3 (Hülsmeyer et al. 2005, the only such structure available at the time of beginning of the project), was not available in free form. The crystal structure of the pMHC ligand of Fab-Hyb3, HLA-A1:MAGE-A1, was determined in free form, thus paving the way for a comparative analysis of the subtle but systematic conformational alterations induced in pMHC upon binding of TCR, KIR and antibodies with TCR-like specificity (Kumar et al. 2009).

4.2 Publications

4.2.1. Kumar P*, Vahedi-Faridi A*, Saenger W, Ziegler A, Uchanska-Ziegler B. (*Equal contribution) Conformational changes within the HLA-A1:MAGE-A1 complex induced by binding of a recombinant antibody fragment with TCR-like specificity. Prot. Sci. (**2009**) 18, 37– 49

Conformational changes within the HLA-A1:MAGE-A1 complex induced by binding of a recombinant antibody fragment with TCR-like specificity

Pravin Kumar,[1†] Ardeschir Vahedi-Faridi,[2†] Wolfram Saenger,[2] Andreas Ziegler,[1*] and Barbara Uchanska-Ziegler[1]

[1]Institut für Immungenetik, Charité-Universitätsmedizin Berlin, Campus Benjamin Franklin, Freie Universität Berlin, Thielallee 73, Berlin 14195, Germany

[2]Institut für Chemie und Biochemie/Kristallographie, Freie Universität Berlin, Takustrasse 6, Berlin 14195, Germany

Received 30 August 2008; Revised 6 October 2008; Accepted 13 October 2008
DOI: 10.1002/pro.4
Published online 2 December 2008 proteinscience.org

Abstract: Although there is X-ray crystallographic evidence that the interaction between major histocompatibility complex (MHC, in humans HLA) class I molecules and T cell receptors (TCR) or killer cell Ig-like receptors (KIR) may be accompanied by considerable changes in the conformation of selected residues or even entire loops within TCR or KIR, conformational changes between receptor-bound and -unbound MHC class I molecules of comparable magnitude have not been observed so far. We have previously determined the structure of the MHC class I molecule HLA-A1 bound to a melanoma antigen-encoding gene (MAGE)-A1-derived peptide in complex with a recombinant antibody fragment with TCR-like specificity, Fab-Hyb3. Here, we compare the X-ray structure of HLA-A1:MAGE-A1 with that complexed with Fab-Hyb3 to gain insight into structural changes of the MHC molecule that might be induced by the interaction with the antibody fragment. Apart from the expulsion of several water molecules from the interface, Fab-Hyb3 binding results in major rearrangements (up to 5.5 Å) of heavy chain residues Arg65, Gln72, Arg145, and Lys146. Residue 65 is frequently and residues 72 and 146 are occasionally involved in TCR binding-induced conformational changes, as revealed by a comparison with MHC class I structures in TCR-liganded and -unliganded forms. On the other hand, residue 145 is subject to a reorientation following engagement of HLA-Cw4 and KIR2DL1. Therefore, conformational changes within the HLA-A1:MAGE-A1:Fab-Hyb3 complex include MHC residues that are also involved in reorientations in complexes with natural ligands, pointing to their central importance for the peptide-dependent recognition of MHC molecules.

Keywords: HLA-A1; X-ray crystallography; peptide-restricted antibody; T cell receptor; ligand-induced conformational changes

Introduction

Major histocompatibility complex (MHC, in humans HLA) class I molecules are heterotrimeric complexes consisting of a heavy chain (HC), a noncovalently associated light chain, β_2-microglobulin (β_2m), and a peptide. These heterotrimers are also referred to as peptide:MHC complexes (pMHC). Within the endoplasmic reticulum, HC:β_2m complexes specifically bind small fragments of degraded proteins, are then

Grant sponsor: Deutsche Forschungsgemeinschaft; Grant number: SfB 449/B6; Grant sponsor: Senate of Berlin (NaFöG Fellowship).

†Pravin Kumar and Ardeschir Vahedi-Faridi contributed equally to this work.

*Correspondence to: Andreas Ziegler, Institut für Immungenetik, Charité-Universitätsmedizin Berlin, Campus Benjamin Franklin, Freie Universität Berlin, Thielallee 73, 14195 Berlin, Germany. E-mail: andreas.ziegler@charite.de

transported as intact heterotrimers to the surface of antigen presenting cells and subsequently serve as targets for receptors on effector cells such as T or natural killer (NK) cells.[1] Although typical affinities of individual interactions are low, in the micromolar range, the recognition process is highly specific. It permits T cell receptors (TCR) on T cells to distinguish peptides derived from self-antigens and foreign, for example, viral, molecules.[2] In contrast, the binding of killer cell Ig-like receptors (KIR) on NK cells is more promiscuous, because only residues in the vicinity of the peptide C-terminus of a pMHC are involved in the interaction.[3,4] However, the general principles are not yet fully understood that govern recognition or lack of interaction between pMHC and TCR or KIR and determine the biological outcome of an encounter between an effector cell and its target. Particularly puzzling is the occasionally drastic influence of subtle conformational changes of residues within a pMHC complex or a TCR on the response of T cells.[2,5–7]

The polymorphic nature of MHC class I antigens enables them to present a diverse range of peptides, generally varying between 8 and 12 residues in length. These peptides are anchored in the peptide binding groove that is formed by HC residues through specific interactions between side chains of the peptide and residues shaping the peptide-binding pockets of an MHC molecule.[1,8] The specificity of peptide presentation is usually determined by only one or two of such pockets that accommodate primary anchor residues of a peptide,[9] with one or more secondary anchors that fine tune the binding motifs for a given MHC class I antigen.[10] For example, HLA-A*010101 is a human MHC class I allele whose product preferentially binds nonapeptides with the anchor residues Asp or Glu at position 3 and Tyr at position 9. Thr or Ser at position 2 and Leu at position 7 are auxiliary anchor residues.[11–13]

We have previously determined the structure of a recombinant antibody fragment, Fab-Hyb3 (Hyb3 in short), that reacts with HLA-A1 in a peptide-dependent fashion.[14] Within this complex, HLA-A1 is bound to the peptide MAGE-A1 (EADPTGHSY), which is derived from the melanoma antigen-encoding gene (MAGE)-A1 molecule (residues 161–169). To some extent, the binding of the *in vitro* affinity-matured Hyb3 resembles that of a soluble TCR or KIR, but Hyb3 exhibits a ~1000 times higher affinity toward its target than a typical TCR or KIR.[2–4,15] In attempting to understand the basis for this finding, we focus here on changes induced by Hyb3 in the conformation of pMHC residues by comparing the Hyb3-liganded structure (A1:MAGE-A1:Fab-Hyb3, AMF) with that of the newly determined, unliganded HLA-A1:MAGE-A1 complex (AM). The results reveal that four residues, at positions 65, 72, 145, and 146 of the HC, undergo highly significant changes in their side chain orientations because of the interaction with Hyb3. All of these residues are also involved in TCR or KIR binding-induced conformational changes in selected other pMHC.

Results

Structural features of the HLA-A1:MAGE-A1 complex

The HLA-A1 (AM) complex crystallized in space group $P2_12_12_1$ (Table I) with one molecule of the complex in the asymmetric unit. The structure was determined at 1.8 Å resolution and refinement converged at R_{cryst} of 0.194. The electron density map for the structure is of high quality, as shown for the MAGE-A1 peptide [Fig. 1(A)]. Several nonspecific contacts between HLA-A1 complexes stabilize the crystal lattice. However, the bound MAGE-A1 peptide does not participate in these crystal contacts, thereby permitting a detailed comparison with the peptide in the AMF complex. The overall structure of HLA-A1 exhibits the typical HLA class I topography.[1]

The MAGE-A1 peptide was modeled unambiguously into the electron density, revealing relatively inflexible side chain orientations of peptide residues as seen in the qualitative B factor plot [Fig. 1(B)], with the exception of pHis^7. Apart from this residue and residues pPro^4, pThr^5, and pGly^6, which are slightly more flexible in HLA-A1, as well as pGlu^1, which exhibits higher flexibility in the AMF [Fig. 1(C)] than in the AM complex [Fig. 1(B)], the B factor values of peptide residues are very similar in both structures. The MAGE-A1 peptide is buried in the peptide binding groove [Fig. 1(D,E)] and provides only a relatively flat surface for recognition by a TCR or Hyb3. A large number of polar and nonpolar interactions between the MAGE-A1 peptide and HC residues that line the peptide binding groove as well as water-mediated intrapeptide hydrogen bonds stabilize this conformation (not shown). The peptide residues pGlu^1, pAla^2, pAsp^3, pHis^7, and pPhe^9 are accommodated, respectively, in the A, B, D, E, and F pockets of the peptide binding groove [Fig. 1(E)]. The solvent accessibility of the MAGE-A1 peptide residues demonstrates varying degrees of solvent exposure for peptide residues, with pPro^4, pThr^5, pGly^6, and pSer^8 being the most "exposed" residues (solvent accessible surface area (SASA) values per residue: 89.6, 39.7, 43.5, and 52.4 Å^2, respectively) and pAla^2, as well as the anchor residues pAsp^3 and pTyr^9 being the most "occluded" residues (SASA values per residue: 3.9, 10.2, and 7.0 Å^2, respectively).

3D comparison of the AM and the AMF structures

A comparison of HLA-A1 with the liganded complex[14] reveals a number of differences, although the overall structures are very similar. The root mean square (rms) deviation values obtained upon Cα overlay of

Table I. *Crystal Data Collection and Refinement Statistics for the HLA-A1:MAGE-A1 Complex*

Data collection	
Space group	$P2_12_12_1$
Unit cell	
a (Å), *b* (Å), *c* (Å)	51.176, 74.060, 125.940
Resolution (Å)	63.89–1.80 (1.84–1.80)
Unique reflections	41526 (2954)
Redundancy	4.0 (4.2)
Completeness (%)	96.78 (94.75)
I/σ	17.3 (3.82)
R_{sym}[a]	0.071 (0.337)
Refinement	
Resolution (Å)	63.89–1.80 (1.84–1.80)
Reflections	41526 (2954)
R_{cryst}[b]	0.194 (0.280)
R_{free}[c]	0.224 (0.337)
HLA-A1 heavy chain, no. of atoms/average B value (Å^2) (chain A)	2241/16.73
β_2-microglobulin, no. of atoms/average B value (Å^2) (chain B)	853/17.39
MAGE-A1 peptide, no. of atoms/average B value (Å^2) (chain C)	69/19.35
Water, no. of molecules/average B value (Å^2)	587/30.44
Glycerol, no. of molecules/average B value (Å^2)	3/35.53
Estimated overall coordinate error (Å)	0.136
Root mean square deviation from ideal geometry	
Bond length (Å)	0.015
Bond angles (°)	1.451
Ramachandran plot	
Most favored regions (%)	92.8
Additionally allowed regions (%)	6.9
Generously allowed regions (%)	0.3
Disallowed regions (%)	0.0

Values for highest resolution shell are indicated in parentheses.
[a] $R_{sym} = \Sigma_h\Sigma_i|I_{h,i} - \langle I_h\rangle|/\Sigma_h\Sigma_i I_{h,i}$.
[b] $R_{cryst} = \Sigma_h\ |F_o - F_c|/\Sigma F_o$ (working set, no σ cutoff applied).
[c] R_{free} is calculated the same way as R_{cryst}, but for 5% of the data excluded from refinement.

the two complexes are 0.56 Å (for the entire complex), 0.58 Å (only HC), 0.30 Å (only β_2m), and 0.37 Å (only peptide). Independent superposition of individual domains of the HLA-A1 HC shows that the α3 domain exhibits slightly more differences (Cα rms deviation of 0.40 Å) when compared with the α1/α2 domains (Cα rms deviation of 0.38 Å). To observe main chain differences in the peptide binding groove, we overlaid the main chain atoms of the α1- and α2-domains, including all peptide binding groove residues (1–180) of the AMF complex over the corresponding residues of the AM structure (see Fig. 2). This analysis reveals that, for certain locations, particularly in loop regions such as residues 39–42 of the α1-domain and a conspicuous stretch of three residues (149–151) within the N-terminal region of the α2-helix, the positions of the Cα atoms in the two structures differ by more than 1.0 Å. Similar domain-wise analyses of other regions of the structure show Cα shifts larger than 0.5 Å at several positions in the α3 domain and at residues 46–49, 59, and 96–99 in β_2m. The comparison demonstrates also that the α3-domain has most main chain shifts (0.50–1.13 Å) and differences in side chain orientations, although nearly all residues having such differences are part of loop regions.

By clicking on any part of the conventional 2D Figure 3 in the PDF, access to the 3D feature is obtained through the freely available Adobe Reader (Version 9) on any Windows-based computer with a modern graphic card (128+ MB memory) and sufficient RAM (1024+ MB). The "Help" option within the program provides an introduction into the possibilities that are offered. Zoom, rotation in freely chosen directions, or hiding of structural elements (β_2m, HC, peptide, each in one or both of the two structures) permit an interactive access. A better understanding of many structural features is thus provided. In the present case, it is particularly helpful to compare the peptide conformations by zooming in and by rotating the two structures with the HC component hidden (by toggling its visibility off in the model tree) or by comparing the conformation of the HC residues Arg65, Gln72, Arg145, and Lys146, all of which are contacted by Hyb3 (see later).

The preset views permit the reader to follow a "tour" of the molecule resembling a prerendered video file of the structures. However, other than a film, the tour presented here still permits full interaction with the structures at any stage. It begins by depicting the entire HLA-A1 complex from different angles (views 1–3 of the model tree). It then shows a top view of the α1- and α2-domains that form the peptide binding groove with the peptide (view 4) followed by a side view with the peptide, still partially hidden behind the

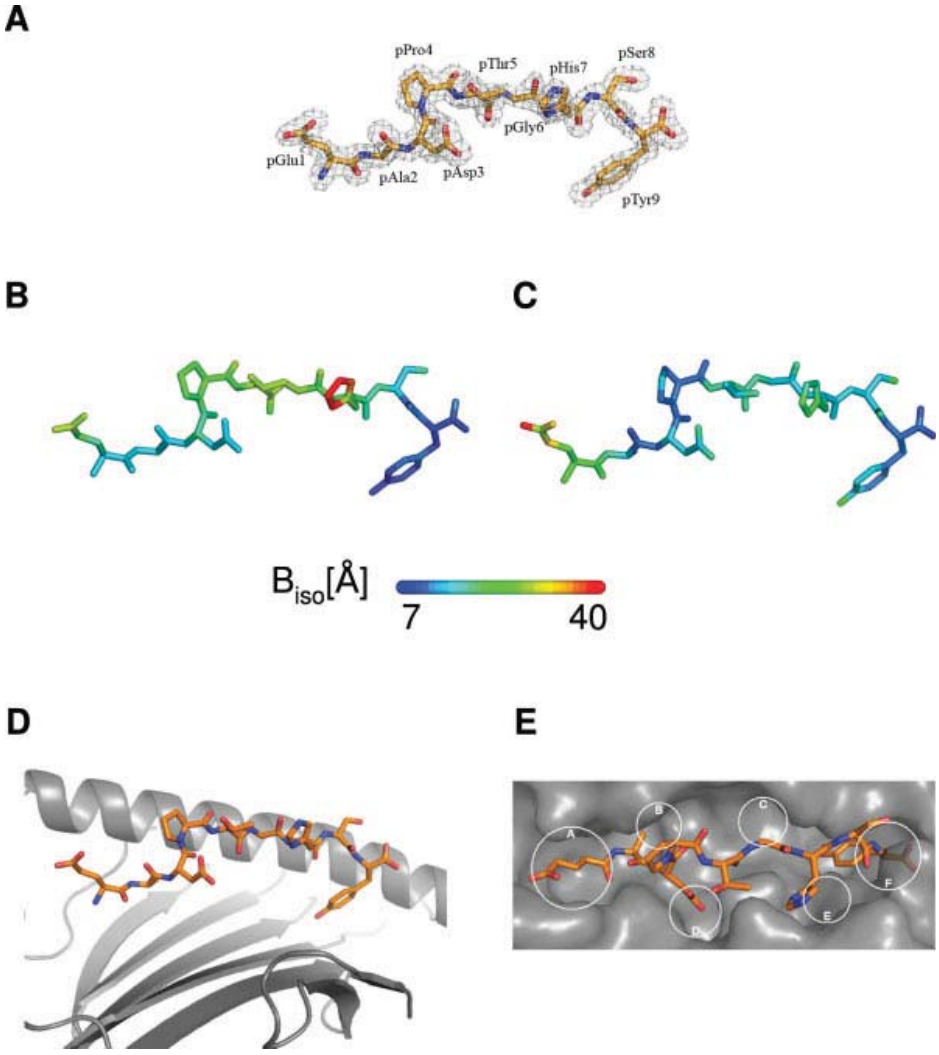

Figure 1. Orientation of the MAGE-A1 peptide in the HLA-A1:MAGE-A1 complex. (**A**) $2F_o - F_c$ electron density contoured to 1.5 σ level around the MAGE-A1 peptide in the HLA-A1 structure. (**B**, **C**) B-factor plot of the MAGE-A1 peptide in the AM (B) and in the AMF complexes (C). Only the imidazole ring of $pHis^7$ is considerably more flexible in the unliganded structure. (**D**, **E**) Orientation of the peptide in the peptide binding groove of HLA-A1 in cartoon (D, α2-helix removed for clarity) and surface representations (E). $pGlu^1$, $pAla^2$, $pAsp^3$, $pHis^7$, and $pPhe^9$ are accommodated, respectively, in the A, B, D, E, and F binding pockets. In all images, the peptide N-terminus is on the left and the C-terminus on the right.

α2-helix (view 5), or freely visible with the α2-helix removed (view 6), and then concentrates on four HC residues that undergo conformational changes upon Hyb3 engagement (views 7, 8). The next series of pictures show initially a view of the entire AMF complex with the six complementarity determining regions (CDR) of Hyb3 (views 9, 10), then zoom into the contact area (view 11), depict the conformations of the four above-mentioned HC residues in liganded as well as unliganded form together with the α1- and α2 domains of the two structures superimposed (views 12, 13), and finally concentrate on the MAGE-A1 peptide that exhibits two slightly distinct conformations when AM and AMF are compared (views 14–16), before the AM complex is shown again (views 17, 18).

Anchoring of MAGE-A1 within the peptide binding groove of AM and AMF

The MAGE-A1 peptide adopts nearly identical conformations in the peptide binding grooves of the Hyb3-liganded and -unliganded structures (Figs. 1 and 3). The middle part of the peptide is buried slightly deeper in the groove in the unliganded form compared with the liganded structure, as C_α shifts of 0.5, 1.1, and 0.6 Å are observed for $pThr^5$, $pGly^6$, and $pHis^7$, respectively (see views 14, 16 of the "tour" provided as part of the interactive 3D representation in Fig. 3). This result is different from that described for the A6 TCR and HLA-A2:Tax,[16] where TCR binding results in pushing the peptide further into the binding groove (2.7 Å for the Cα atom of $pPro^6$; 4.6 Å for Cγ of

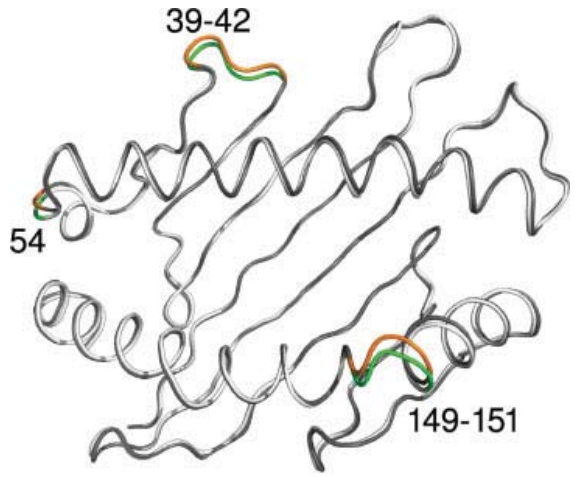

Figure 2. Comparison of HLA-A1 HC in unliganded and liganded forms. A main-chain overlay of the α1- and α2-domains of the HLA-A1 HC in unliganded and Hyb3-liganded forms is shown. Residues with Cα shifts larger than 1 Å are colored in green (Hyb3-liganded) and orange (unliganded). The most remarkable shifts are observed in the region of the peptide binding groove near the C-terminus of the MAGE-A1 peptide (on the right of the image).

pVal^7). A comparison of the solvent accessibility of the peptide residues reveals that pGly^6 and pSer^8 have 18% and 20% higher accessibility, respectively, in HLA-A1, while the values for the other peptide residues are very similar (results not shown).

Two intrapeptide water-bridged hydrogen bonds are present in both structures. The N and O atoms of pAla^2 form a hydrogen bond with a water molecule (WC217 and WX1, respectively), whereas pPro^{4}O and pGly^{6}N contact water molecules at comparable locations in the AM and AMF complexes (not shown). On the other hand, a further water-mediated intrapeptide hydrogen-bond between the same peptide backbone atoms (via WX4) is present only in the Hyb3-liganded structure [compare Fig. 4(A,B)]. It is likely that this feature facilitates the interaction of pPro^4 and pGly^6 with the Trp52A residue of the Hyb3 heavy chain, which is mediated by the same water molecule.[14] However, both structures also exhibit hydrogen bonding features that are not found in the other (see Fig. 4). In the AM complex, pGlu^1 contacts Arg163 indirectly via water WA631, while a comparable water-mediated contact is missing in the liganded complex. In contrast, direct hydrogen bonds linking pGlu^1 with Arg163 or pSer^8 with Trp147 are largely retained in both structures with minor differences in bond lengths. This is exemplified by Arg114 and Arg156: although distinct in detail, the side chains of these residues are coordinated similarly, via a water molecule, to pHis^7 (AM complex) or to pThr^5 and pHis^7 (AMF complex). Finally, pSer^8 is contacted by Trp147 only in the former structure [Fig. 4(A)].

Ligand-induced reorientations of HLA-A1 HC residues

Hyb3 binding is associated with significant side chain orientational perturbations (>2.0 Å) of four HC residues, Arg65, Gln72, Arg145, and Lys146 that show also high buried SASA (BSASA), with Arg65 and Gln72 being the only residues exhibiting values larger than 80 Å^2.[14] In the AM complex, Arg65 of the HC forms water (WA508)-mediated hydrogen bonds with two oxygens (Glu58O and Glu58OE1) and a direct hydrogen bond with Gln62. Furthermore, the side chain of Gln72 is aligned along the α1 helix, contacting Arg75 both directly and indirectly through WA574 in this structure [Fig. 5(A)]. In contrast, in the AMF complex, water molecules are expelled from this area of the interface between the two molecules. Although the diverging resolutions of the two structures do not allow accurate estimates to be made, there are 94 water molecules in the vicinity of the α1- and α2-domains in the AM structure that are not present in the AMF complex (results not shown). As a consequence, Arg65NH1,2 contact Asp30 and Asp31 within CDR-1 of the Hyb3 heavy chain (CDR-H1) through three direct hydrogen bonds, whereas Gln72 interacts with the residues Tyr100C and Phe98 within CDR-H3 [Fig. 5(B)]. Furthermore, the Arg65CZ atom is shifted by 2.73 Å between the two structures, whereas the position of the Gln72CD atom differs by 2.32 Å [Fig. 5(A,B)]. In addition, the contact of Gln72O with Arg75N is shorter in the unliganded structure (3.31 Å as opposed to 3.60 Å).

Further substantial reorientations can be observed for residues that are part of the N-terminal portion of the α2-helix [Fig. 5(C,D)]. In HLA-A1, the side chain nitrogen atoms of Arg145 form a network of water-mediated contacts with Gln141 and Met138 [Fig. 5(C)]. Arg145 engages also in a hydrogen bond with a symmetry-related molecule (not shown). Lys146NZ forms indirect, water-mediated contacts with pTyr^9, pSer^8, and Tyr84 [Fig. 5(C)]. Again, water molecules do not participate any more in the interactions of Arg145 and Lys146 in the AMF complex [Fig. 5(D)]. Arg145 does not engage in any direct or indirect interactions with other HC residues, but instead contacts Arg94 of Hyb3 within CDR-3 of the light chain (CDR-L3) [Fig. 5(D)]. On the other hand, Lys146 forms direct hydrogen bonds with the CDR-L3 residues Ser93 and Asp95A, as well as with the HLA-A1 HC residue Tyr84 and with the C-terminal peptide residue pTyr^9 [Fig. 5(D)]. In addition, Lys146 contacts Asp95A of CDR-L3 also by van der Waals interactions.[14] The position of the Arg145CZ atom differs by 5.54 Å and that of the Lys146NZ atom by 3.60 Å between the AM and AMF complex [Fig. 5(C,D)].

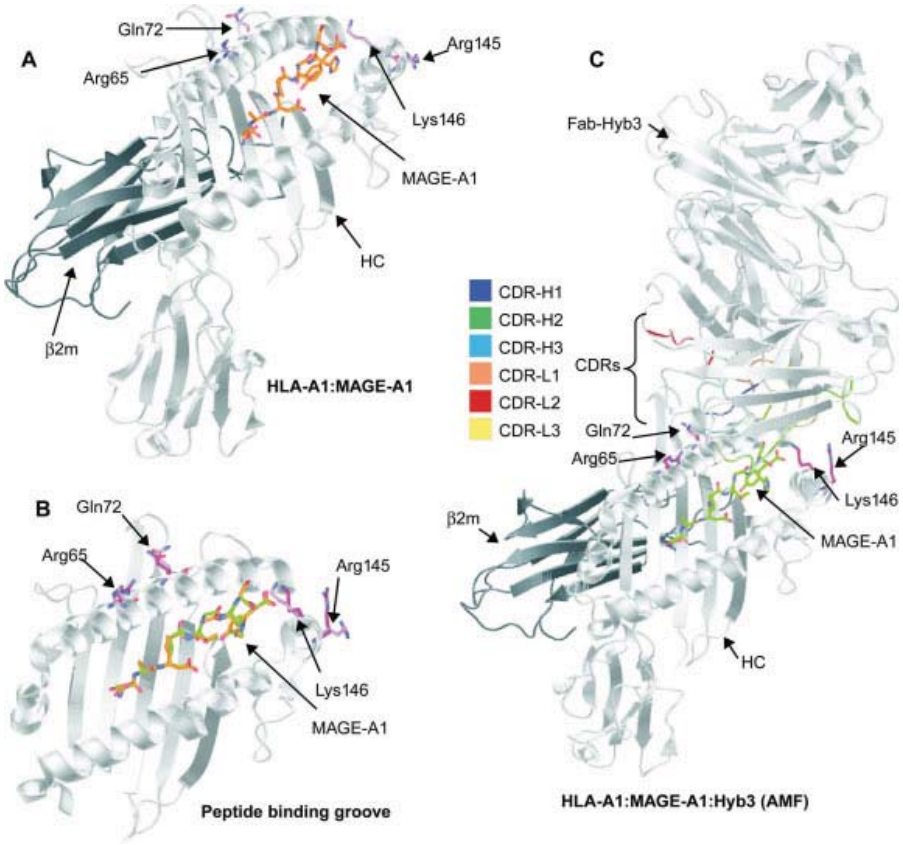

Figure 3. An interactive 3D model depicting conformational changes of HLA-A1:MAGE-A1 in unliganded and liganded forms. The HLA-A1 HC is shown in light gray, β_2m in dark gray, the H-chain and L-chain of Hyb3 also in light gray. The MAGE-A1 peptide is in orange (HLA-A1) and green (AMF), and the complementarity determining regions of Hyb3 are colored blue (CDR-H1), green (CDR-H2), sky-blue (CDR-H3), orange (CDR-L1), red (CDR-L2), and yellow (CDR-L3), respectively. (**A**) View into the binding groove of the HLA-A1 molecule, with the peptide in place. (**B**) Overlay of the peptide binding groove and the MAGE-A1 peptide as displayed in the unliganded and the Hyb3-liganded HLA-A1 molecule. (**C**) The HLA-A1:MAGE-A1:Hyb3 complex seen from the side of the α2-helix of the HLA-A1 molecule. 3D functions are available through a click on any part of the image in the PDF version of the article (the 3D features can be terminated by right-clicking on the 3D display and selecting the "Disable 3D" function from the contextual menu). The model tree icon permits to access individual components of the 3D model. Note that ligHLA-A1 is abbreviated as "AMF" (A1:MAGE-A1:Fab-Hyb3) in the view designations provided as part of the model tree. The displays which the tour presents are briefly designated at the left. Each model can be interactively manipulated using the mouse (rotating, panning and zooming tools can be selected through the toolbar or contextual menu), and readers can access the preset "tour" of the model by clicking on the respective designations (either via the middle section of the model tree when it is displayed, or the drop down menu in the toolbar, or through the contextual menu). By rotating the molecule and by zooming into regions of interest, the understanding of many molecular features is facilitated, in particular the conformational changes of HC residues. Initially, the tour shows views of HLA-A1 from the side, along the binding groove, from the top, and finally depicts the HC residues that undergo conformational changes after being contacted by Hyb3. Thereafter, the Hyb3-liganded complex is considered, and several views are offered that eventually zoom into the contact area between HLA-A1 and Hyb3, demonstrating the conformational changes.

Most of the HC residues that contact the peptide via hydrogen bonds in the AM structure have similar BSASA values also in the AMF complex (not shown). However, there are a number of exceptions: Asn66, Ala69, Thr73, Tyr84, Lys146, and Gln 155 show significant differences in BSASA values due to peptide contacts in the two structures. The BSASA values diverge particularly strongly for Thr73 and Lys146. Each of these two residues contributes ~40 Å^2 of the total HLA-A1 HC surface area that is buried due to peptide binding in HLA-A1, but these values are more than 50% lower in the AMF complex. Gln155, one of the five residues that exhibits >50 Å^2 BSASA in the AM complex, shows a 32.6% reduced BSASA in the AMF structure. Finally, Ala69 and Tyr84, although only small contributors to BSASA (10.2 and 8.3 Å^2, respectively), reveal BSASA values that are about 80% lower in the Hyb3-liganded structure. Overall, the reduction

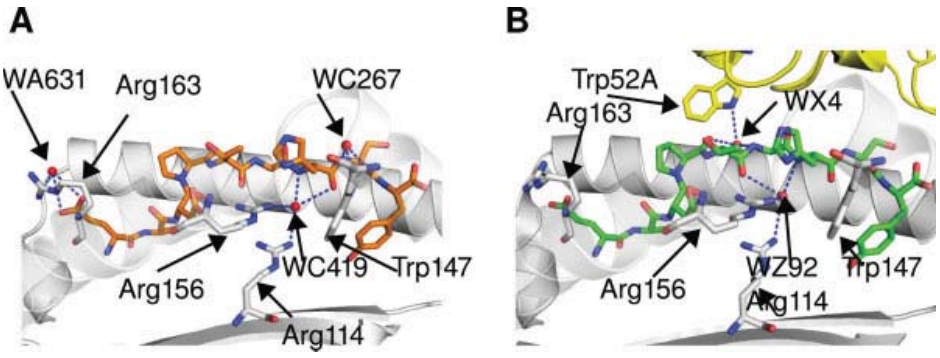

Figure 4. Water-bridged hydrogen bonds involving the MAGE-A1 peptide in unliganded and Hyb3-liganded structures. The HLA-A1 HC is shown in shades of gray in both figures. Ordered water molecules mediating hydrogen bonds are shown in red. Water molecules are labeled with a W succeeded by their chain id in the respective PDB files followed by their number. (**A**) HLA-A1 molecule. The MAGE-A1 peptide is shown in orange and HLA-A1 HC in gray. The pGlu^{1}OE1 and OE2 atoms form a hydrogen bond with Arg163NH2 through WA631, the pHis^{7}N and O atoms contact Arg114NH2 and Arg156NH2 through WC419, and the Trp147NE1 atom forms hydrogen bonds with pSer^{8}N and OG atoms through WC267. (**B**) AMF complex. The MAGE-A1 peptide is shown in green, HLA-A1 HC in white and part of the Hyb3-H chain in yellow. pPro^{4}O and pGly^{6}N interact with Trp52ANE1 of the heavy chain of Hyb3 through WX4, whereas Arg156NH2 and Arg114NH2 contact pThr^{5}O and pHis^{7}N by hydrogen bonds through WA345.

in BSASA between the unliganded and the liganded structures is about 16% when HC residues involved in hydrogen-mediated contacts to the bound peptide are considered.

Discussion

The HLA-A1:MAGE-A1 (AM) complex, whose structure is described here, has been employed as a prime target for melanoma-specific cytotoxic T cells, using studies *in vitro* as well as *in vivo*.[17–19] The expression of this antigen is strictly tumor-associated, because the only cells that are able to display HLA class I or II molecules on their surface together with the MAGE-A1 peptide are malignant cells.[20] It was therefore of considerable interest to acquire not only cellular reagents, but also soluble molecules directed against this highly specific target. We have previously pointed out[21] why recombinant, affinity-matured antibodies mimicking TCR specificity such as Hyb3 are preferable to soluble TCR[22] or conventional monoclonal antibodies (for example, see Refs. 23–31) that interact in a peptide-dependent manner with a pMHC: although a major obstacle to the application of soluble TCR molecules is to increase their affinity (at least 100-fold), necessitating cumbersome *in vitro*-affinity maturation procedures, the major problem with TCR-like monoclonal antibodies is to obtain them at all. Consequently, very few such reagents are currently available, forcing us to employ recombinant antibodies.[14,32]

A number of factors that characterize the binding mode of Hyb3 to its target are likely to contribute to the vastly increased affinity (~1000-fold) when compared with a typical interaction between a pMHC and a natural ligand. This includes strict shape complementarity between the AM complex and Hyb3, associated with burial of large areas of interaction surface together with the exclusion of water molecules that contributes entropically to structural stabilization. Whether the unusual tilt with regard to the main axes of the binding partners (45°) and the diagonal binding mode of Hyb3 (see Fig. 3) play a role as well is unclear, but it is unlikely that a single factor is responsible for the improved affinity of Hyb3 in comparison to that of TCR or KIR.[14] In addition, a Hyb3-induced fit on the structure of HLA-A1 remained to be studied, as the structure of this pMHC in unliganded form was not known before. To shed light on some of these questions, we focus here on conformational changes induced by Hyb3 and natural HLA class I ligands. In comparison to other pMHC structures,[1] the AM complex does not show any unusual features. Possibly, the only conspicuous property is that the structure lacks any particularly remarkable attributes. In the absence of long peptide side chains, the surface which the complex presents to a ligand is rather flat, necessitating strict shape complementarity between the two binding partners and expulsion of water molecules from the interface, as mentioned earlier.

Only four peptide residues are involved in direct interactions with Hyb3, and nearly always peptide main chain atoms are contacted by this ligand.[14] With regard to the HC, five α1-helix residues (65, 69, 72, 73, 80) as well as three α2-helix residues (145, 146, 155) engage in H-bonds with Hyb3, whereas three residues (76, 80, 146) are recognized through van der Waals interactions. A comparison of those residues undergoing pronounced conformational changes (>2.0 Å)

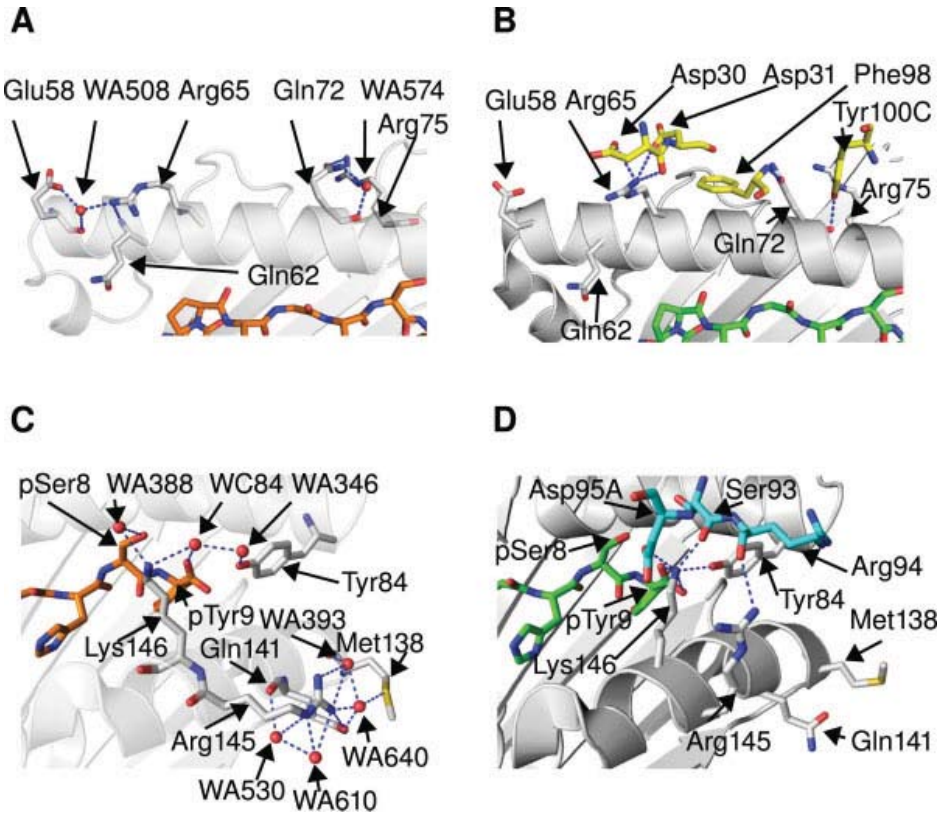

Figure 5. Changes in orientation of HLA-A1 residues directly contacting Hyb3 in Hyb3-liganded structure. Panels A and C show the orientation and interactions of residues Arg65, Gln72, Arg145, and Lys146 (shown in gray) in the unbound HLA-A1:MAGE-A1 complex and in the Hyb3-bound complex, where they form direct hydrogen bonds with Hyb3 (panels B and D). The HLA-A1 HC is shown in gray; the Hyb3-H and-L residues in yellow and sky-blue, respectively, and the MAGE-A1 peptide in orange (unbound complex) or green (Hyb3-bound complex). (**A**) Arg65 forms a hydrogen bond with Gln62 and a water-mediated hydrogen bond with Glu58 in the unliganded structure. Gln72 contacts Arg75 through side chain hydrogen bonds and forms an intraresidue water-mediated hydrogen bond. (**B**) Arg65 hydrogen bonds with Hyb3 CDR-H1 residues Asp30 and Asp31 in the Hyb3-bound complex. In the unliganded and the liganded structures, the Arg65CZ atoms are separated by 2.73 Å. Gln72 is engaged in contacting Tyr100C and Phe98 of Hyb3-CDR-H1. Its CD atom is separated by 2.32 Å in the two structures. (**C**) Arg145 forms a network of water-mediated contacts with Gln141 and Met138 in the unbound complex structure, where it also forms a hydrogen bond with a symmetry-related residue (not shown). Lys146 contacts peptide residues $pTyr^9$ and $pSer^8$. (**D**) Arg145 contacts CDR-L3 residue Arg94 in the Hyb3-liganded structure. Its side chain apex (CZ atom) is separated by 5.54 Å in the two structures. Lys146 contacts the CDR-L3 residues Ser93 and Asp95A, the MAGE-A1 residue $pTyr^9$ and HLA-A1 HC residue Tyr84 through direct hydrogen-bonds. Its NZ apex is separated by 3.60 Å in the two structures.

upon Hyb3 binding (Arg65, Gln72, Arg145, and Lys146; Fig. 5) with comparable reorientations of HC residues in structures of classical pMHC molecules for which information on α1/α2-domain-liganded and unliganded forms is available can thus be performed. Apart from the AMF complex, this comparison includes a recently determined second complex between a pMHC and an antibody, nine complexes of pMHC:TCR and one pMHC:KIR structure (Table II, which provides also the respective references). We have refrained from including the HLA-B*3501:EPLP:ELS4 complex in the comparison because of the atypical flattening of the highly bulged 11-mer EPLP peptide which is induced by the binding of the ELS4 TCR.[49] In 10 of the complexes listed in Table II, peptides in the liganded and unliganded forms overlay with rms deviation values of less than 0.5 Å, indicating that there exist only marginal ligand binding-induced conformational changes for peptide residues. The only elevated rms deviation values (1.01 Å and 0.63 Å) for a bound peptide are noted when the unliganded and the liganded forms of HLA-A2:Tax and $H\text{-}2K^b$:dEV8 are compared (Table II). In the latter case, a reorientation of the side chain of residue pTyr6 appears mainly responsible. A similar overlay of HC residues belonging to the α1- and α2-domains of unliganded and liganded pMHC structures gave a much wider spectrum of rms deviation values (Table II). They varied from 0.38 Å (for AMF) to 0.99 Å (for $H\text{-}2K^b$ with the pBM1 peptide). Although far-reaching effects of conformational

Table II. *Comparison of MHC Class I Structures in Liganded and Unliganded Forms*

MHC molecule	HLA-A1	H-2K^b	HLA-A2	HLA-A2	HLA-B8	HLA-B*3508	H-2K^b	H-2K^b	H-2K^b	H-2K^b	H-2K^{bm3}	HLA-Cw4
Peptide	MAGE-A1	pOV8	p1049	Tax	FLR	LPEP	VSV8	pBM1	dEV8	dEV8	dEV8	C4CON1
Ligand	Fab-Hyb3	25-D1.16	TCR AH1H12.2	TCR A6	TCR LC13	TCR SB27	TCR BM3.3	TCR BM3.3	TCR 2C	TCR 2C	TCR 2C	KIR2DL1
PDB code, pMHC	3BO8[a]	1VAC[33]	1BOG[34]	1HHK[35]	1Mo5[36]	1ZHL[37]	2VAA[39]	1NAN[40]	1LEG[41]	1LEK[41]	1LEK[41]	1QQD[42]
PDB code, pMHC:ligand	1W72[14]	3CVH[43]	1LP9[44]	1AO7[16]	1MI5[45]	2AK4[46]	1KJ2[38]	1NAM[40]	1FO0[47]	2CKB[48]	1MWA[41]	1IMg[4]
pMHC BSASA[b]	990	1134	1193	1021	1135	1609	1482	1058	704	1093	1947	786
Comparisons of pMHC with pMHC:ligand complexes												
HC residues contacting ligand	9	11	9	7	15	5	6	7	9	5	5	8
HC residues shifting >2.0 Å[c]	4	4	1	3	5	4	2	4	1	1	2	2
Peptide residues contacting ligand	3	5	6	5	2	5	3	2	3	3	3	0
Peptide residues shifting >1.0 Å[d]	0	3	0	4	1	2	0	1	0	5	5	0
Comparisons of rms deviation values (in Å) between pMHC and pMHC:ligand complexes												
Peptide	0.37	0.34	0.24	1.01	0.28	0.36	0.14	0.14	0.29	0.63	0.45	0.23
HC[e]	0.38	0.59	0.47	0.54	0.47	0.73	0.52	0.58	0.99	0.73	0.66	0.44
β_2m	0.32	0.88	0.50	0.42	0.38	0.37	0.43	1.36	1.66	0.89	0.75	0.40

[a] This study.
[b] Solvent accessible surface area of pMHC buried due to binding of its ligand.
[c] Ligand-contacting HC residues with side chain apex shift ≥2 Å.
[d] Peptide residues with side chain apex shift ≥1 Å.
[e] Only the α1- and α2-domains of the HC are compared.
In those cases where more than one molecule within the asymmetric unit is present, only the first molecule has been analyzed.

changes or particular residues cannot be excluded (for e.g., see Ref. 50), changes in the α3-domain and β_2m are not considered further here, because Hyb3, TCR, and KIR do not bind to these parts of a pMHC.

A comparison of the solvent-accessible surface areas that are buried upon binding of a ligand (BSASA values, Table II) demonstrates that these values may reach 1947 Å^2, but are often only about 1000 Å^2. Remarkably, both complexes with artificial ligands (AMF and H-2K^b:pOV8:25-D1.16) exhibit typical BSASA values despite their ~1000-fold increased affinity when compared with typical TCR (Table II). Therefore, the BSASA values alone cannot explain the high affinities of antibody molecules that bind pMHC in a TCR-like fashion.

In all nine pMHC:TCR complexes, several HC residues contacting the TCR are affected by changes in side chain orientation. Differences in the orientation of residues 62 (Gln or Arg, 3/9), 65 (Gln or Arg, 5/9), 72 (Gln, 3/9), and 155 (Gln or Arg, 3/9) can most frequently be observed for the TCR-liganded pMHC structures (Table III). For the two published KIR-liganded structures, a comparison is only possible for HLA-Cw4 and KIR2DL1, since a structure of the unliganded HLA-Cw3 is not available. Only two of the HC residues that are contacted by KIR2DL1 undergo conformational changes >2.0 Å: Lys80 and Arg145 (Table III). The degree of reorientation of HC residues that are ligand-contacted is usually ≤4.0 Å (27/30 cases), but may reach 6.66 Å (Arg79, in HLA-B8), 5.54 Å (Arg145, in HLA-A1), or 5.30 Å (Arg65, in HLA-A2) (Table III).

With regard to the HC residues undergoing conformational changes, the results presented here demonstrate that Hyb3 recognizes a conformationally active epitope that could be termed "hybrid," because it is composed of elements which are typically part of footprints on pMHC made by TCR (residues 65 and 72) as well as KIR (residue 145) (Table III).[2–4] Although it is currently still difficult to derive any generalizations from the few available structures with KIR ligands, residue 145 is clearly undergoing conformational reorientations in complexes of Hyb3 and KIR2DL1, the residues 65 and 72 are part of a triangle-shaped group of amino acids that TCR tend to recognize on the surface of pMHC. In case of class I molecules, it incorporates residues 65, 69, 72 (α1-helix), and 155 (α2-helix).[2] A constellation of residues mimicking 65, 69, and 155 has also been found on MHC class II molecules (residues 57 and 61 of the α-chain and 70 of the β-chain). These residues may be key elements of conserved interactions that TCR engage in when contacting MHC class I or class II antigens during positive and negative selection in the thymus (reviewed recently by Marrack *et al.*[51]). Of the conserved HC residues contacted by TCR or Hyb3, one of the KIR molecules contacts the residues 69 and 72.[4]

The results with natural ligands of pMHC lead to the question why a nonnatural ligand, Hyb3, should

Table III. *Comparison of Conformational Changes of Selected HC Residues Between Unliganded and Liganded pMHC*

	Ligand-contacting HC residue with apex shifts ≥2.0 Å (values in Å)											
Liganded pMHC complex	58	62	65	72	79	80	145	146	149	151	154	155
HLA-A1:MAGE-A1:Hyb3			2.7	2.3			5.5	3.6				
H-2K^b:pOV8:25-D1.16		2.6		2.7	2.4			2.0				
HLA-A2:p1049:AHIII12.2			5.3									
HLA-A2:Tax:A6	2.7		2.2									3.1
HLA-B8:FLR:LC13		3.3	3.4	2.2	6.7							3.8
HLA-B*3508:LPEP:SB27			2.0							3.5	3.1	3.5
H-2K^b:pKB1:KB5C20		4.0		3.4								
H-2K^b:VSV8:BM3.3		2.5	3.8					2.3			3.3	
H-2K^b:pBM1:BM3.3								3.2				
H-2K^b:dEV8:2C	3.6			2.9								
H-2K^{bm3}:dEV8:2C			2.4						2.4			
HLA-Cw4:C4CON1:KIR2DL1						3.5	2.7					

rely at least partly also on residues for interaction that are crucial docking points for TCR and KIR. It has been argued that the environments of residues 65, 69, and 155 (class I) as well as those of the corresponding residues of class II antigens permit TCR to interact particularly well with main chain atoms of these amino acids, whereas peptide residues are typically recognized by side chain interactions.[52,53] Predominantly, Hyb3 employs a different strategy to achieve its specificity: of 13 direct H-bonded contacts ≤3.5 Å between HC and Hyb3 residues, only two (with Ala69 and Gln72) are with HC main-chain atoms. Both contacts are very short (2.6 and 2.5 Å, respectively). In contrast, of four such contacts with the MAGE-A1 peptide, only one (with pHis7NE2) is not with a main-chain atom.[14] Very likely, the nonnatural way in which Hyb3 was produced (selection of a low-affinity Fab fragment from a phage display library, phage display-based affinity maturation) releases this reagent from biological constraints that appear to govern the interaction of pMHC with TCR or KIR. For example, it has been proposed that the commonly observed diagonal interaction between pMHC and TCR is influenced by the presence of CD8 molecules within the interaction complex *in vivo*.[44] It is therefore the more remarkable that Hyb3 shares several residues that are often subject to conformational changes upon binding of natural ligands. It could be that the chemical nature of the side chains of residues 65, 72, and 145 (twice Arg, and Gln in case of the HLA-A1 HC) is particularly well suited for an interaction with ligands, irrespective of whether they are natural or artificial.

Although TCR usually assume a diagonal binding mode, there seems, however, a priori no good reason why Hyb3 should not recognize its target from one of the ends of the peptide-binding groove without loss of specificity and affinity. Even a TCR that interacts via such an unorthodox binding mode has recently been described in case of the nonclassical MHC molecule T22 and the γδTCR G8.[54] In conclusion, the recognition of HLA-A1 by Hyb3 resembles in many respects those which have been observed for various pMHC and natural ligands, and this is also the case when conformational reorientations of HC residues due to binding of the different ligands are evaluated. A further understanding of the very high affinity between HLA-A1 and Hyb3 may come from structures of unliganded Hyb3 or HLA-A1 complexed with Fab-G8, the low-affinity ancestor of Hyb3.[32]

Methods

Protein expression, complexation, and purification

The HLA-A1 HC and β_2m were separately expressed in *Escherichia coli* and purified in the form of inclusion bodies. The MAGE-A1 peptide (EADPTGHSY) was purchased from Alta Biosciences, UK. Inclusion bodies of HLA-A1 HC and β_2m were unfolded, mixed with the MAGE-A1 peptide in a refolding buffer (1:2:10 molar ratio), and reconstituted for 7–10 days at 4°C to form the HLA-A1:β_2m:MAGE-A1 complex (AM) as detailed previously.[32,55] The complex was purified by size exclusion chromatography on a Superdex 75HR gel filtration column (Amersham Biosciences) using a pH 7.5 buffer containing 20 m*M* Tris-HCl, 150 m*M* NaCl, and 0.1% NaN_3, concentrated to 15–17 mg/mL and used for crystallization screens.

Crystallization and data collection

The AM complex was crystallized using the PEG-ion screen of Hampton Research, USA in a sitting drop vapor diffusion setup at 18°C, with a reservoir volume of 100 μL and drops made up of 1.1 μL protein and 1.1 μL reservoir solution. A single AM crystal was obtained in a well containing 20% PEG3350 and 0.2 M NaF as reservoir after 18 days. Visible satellite crystals were removed by cutting the crystals into smaller pieces. Following flash-cooling in liquid nitrogen after brief soaking in a cryo-buffer composed of

reservoir and 15% glycerol, X-ray diffraction data was collected at Protein Structure Factory beamline BL-1 of Freie Universität Berlin installed at the BESSY II synchrotron in Berlin. The crystal diffracted to a resolution limit of 1.8 Å, and the collected X-ray data was indexed and integrated using MOSFLM,[56] and then scaled and merged using program SCALA.[57]

Structure determination and analysis

The HLA-A1 molecule was localized in the crystal unit cell by molecular replacement using programs MOLREP[58] and PHASER,[59] with HLA-A1:MAGE-A1:Hyb3 (PDB code 1W72) as search model from which Hyb3, water molecules, and peptide were stripped off. The obtained model was subjected to iterative cycles of restrained-maximum likelihood refinement including isotropic temperature factor adjustment using REFMAC,[60] followed by manual rebuilding using COOT.[61] Water molecules were positioned using CNS.[62] The SASA and BSASA of residues of the structures were calculated with AREAIMOL[63] using a probe radius of 1.4 Å. All superpositions and root mean square (rms) deviation calculations were performed using LSQKAB.[64,67]

The atomic coordinates and structure factors (code 3BO8) have been deposited in the Protein Data Bank (www.pdb.org).

Preparation of 2D and 3D figures

The 2D figures showing structural details were prepared using PyMOL.[65] To view conformational changes and further differences between the two structures (see 3D comparison of the AM and the AMF structures in the results section), we employ here, for the first time in a novel description of the structure of a protein, fully interactive three-dimensional (3D) representations in the electronic version of this article that were created using PyMOL and Adobe Systems' "Acrobat 9 Pro Extended" software. The procedure to create 3D models of a molecular complex has recently been described.[66] Initially, the raw PDB files (3BO8 and 1W72) were opened using PyMOL version 1.0r1. The components to be shown in the final 3D model were selected and each exported separately as VRML2 worlds with appropriate designations (e.g., beta2m.wrl) followed by import into Adobe 3D Reviewer (Adobe Systems, San Jose, CA). The model, complete with all components, was exported as a PDF model with tessellation compression export format. The PDF model was then opened in Adobe Acrobat 9 Pro Extended and an object hierarchy (i.e., model tree) created. Different colors were then assigned to each component followed by saving the complete model as a PDF file.

The three images shown in Figure 3(A–C) as 2D images ("posters") were created from TIFF format desktop screenshots of the desired model views and modified in Corel Draw 11 to show the desired information (i.e., cropped to size, etc) and exported to PDF format as a single file. The previously saved PDF model was opened in Adobe Acrobat 9 Pro Extended and the 2D PDF poster included in the model. After combining the 2D and 3D files, all final viewing settings were fixed, and preset views were selected using the camera tool followed by defining a standard view that would be shown after activation of the 3D mode. Finally, the model was saved as a PDF file. A step-by-step guide to creating PDF-integrated 3D models is available at www.charite.de/immungenetik/model3d.

Acknowledgments

The authors are grateful to Ms. Claudia Alings for help with the crystallization trials and the beamline staff at Bessy II, Berlin for valuable assistance. The authors thank Dr. Jonathan Tyzack (London) for commenting on the 3D model.

References

1. Madden DR (1995) The three-dimensional structure of peptide-MHC complexes. Annu Rev Immunol 13: 587–622.
2. Rudolph MG, Stanfield RL, Wilson IA (2006) How TCRs bind MHCs, peptides, and coreceptors. Annu Rev Immunol 24:419–466.
3. Boyington JC, Motyka SA, Schuck P, Brooks AG, Sun PD (2000) Crystal structure of an NK cell immunoglobulin-like receptor in complex with its class I MHC ligand. Nature 405:537–543.
4. Fan QR, Long EO, Wiley DC (2001) Crystal structure of the human natural killer cell inhibitory receptor KIR2DL1-HLA-Cw4 complex. Nat Immunol 2:452–460.
5. Krogsgaard M, Davis MM (2005) How T cells 'see' antigen. Nat Immunol 6:239–245.
6. Deng L, Mariuzza RA (2007) Recognition of self-peptide-MHC complexes by autoimmune T-cell receptors. Trends Biochem Sci 32:500–508.
7. Godfrey DI, Rossjohn J, McCluskey J (2008) The fidelity, occasional promiscuity, and versatility of T cell receptor recognition. Immunity 28:304–314.
8. Falk K, Rötzschke O, Stevanovic S, Jung G, Rammensee HG (1991) Allele-specific motifs revealed by sequencing of self-peptides eluted from MHC molecules. Nature 351: 290–296.
9. Guo HC, Madden DR, Silver ML, Jardetzky TS, Gorga JC, Strominger JL, Wiley DC (1993) Comparison of the P2 specificity pocket in three human histocompatibility antigens: HLA-A*6801, HLA-A*0201, and HLA-B*2705. Proc Natl Acad Sci USA 90:8053–8057.
10. Rammensee HG, Falk K, Rotzschke O (1993) Peptides naturally presented by MHC class I molecules. Annu Rev Immunol 11:213–244.
11. DiBrino M, Tsuchida T, Turner RV, Parker KC, Coligan JE, Biddison WE (1993) HLA-A1 and HLA-A3 T cell epitopes derived from influenza virus proteins predicted from peptide binding motifs. J Immunol 151:5930–5935.
12. Falk K, Rötzschke O, Takiguchi M, Grahovac B, Gnau V, Stevanovic S, Jung G, Rammensee HG (1994) Peptide motifs of HLA-A1, -A11, -A31, and -A33 molecules. Immunogenetics 40:238–241.
13. Kubo RT, Sette A, Grey HM, Appella E, Sakaguchi K, Zhu NZ, Arnott D, Sherman N, Shabanowitz J, Michel H (1994) Definition of specific peptide motifs for four major HLA-A alleles. J Immunol 152:3913–3924.

14. Hülsmeyer M, Chames P, Hillig RC, Stanfield RL, Held G, Coulie PG, Alings C, Wille G, Saenger W, Uchanska-Ziegler B, Hoogenboom HR, Ziegler A (2005) A major histocompatibility complex-peptide-restricted antibody and T cell receptor molecules recognize their target by distinct binding modes: crystal structure of human leukocyte antigen (HLA)-A1-MAGE-A1 in complex with Fab-Hyb3. J Biol Chem 280:2972–2980.
15. Armstrong KM, Insaidoo FK, Baker BM (2008) Thermodynamics of T-cell receptor-peptide/MHC interactions: progress and opportunities. J Mol Recognit 21:275–287.
16. Garboczi DN, Ghosh P, Utz U, Fan QR, Biddison WE, Wiley DC (1996) Structure of the complex between human T-cell receptor, viral peptide and HLA-A2. Nature 384:134–141.
17. van der Bruggen P, Traversari C, Chomez P, Lurquin C, De Plaen E, Van den Eynde B, Knuth A, Boon T (1991) A gene encoding an antigen recognized by cytolytic T lymphocytes on a human melanoma. Science 254:1643–1647.
18. Chomez P, De Backer O, Bertrand M, De Plaen E, Boon T, Lucas S (2001) An overview of the MAGE gene family with the identification of all human members of the family. Cancer Res 61:5544–5551.
19. Boon T, Coulie PG, Van den Eynde BJ, van der Bruggen P (2006) Human T cell responses against melanoma. Annu Rev Immunol 24:175–208.
20. Renkvist N, Castelli C, Robbins PF, Parmiani G (2001) A listing of human tumor antigens recognized by T cells. Cancer Immunol Immunother 50:3–15.
21. Ziegler A, Coulie PG, Uchanska-Ziegler B (2007) Monoclonal and recombinant antibodies with T cell receptor-like reactivity. Recent Results Cancer Res 176: 229–241.
22. Chlewicki LK, Holler PD, Monti BC, Clutter MR, Kranz DM (2005) High-affinity, peptide-specific T cell receptors can be generated by mutations in CDR1, CDR2 or CDR3. J Mol Biol 346:223–239.
23. Abastado JP, Darche S, Jouin H, Delarbre C, Gachelin G, Kourilsky P (1989) A monoclonal antibody recognizes a subset of the H-2Dd mouse major class I antigens. Res Immunol 140:581–594.
24. Aharoni R, Teitelbaum D, Arnon R, Puri J (1991) Immunomodulation of experimental allergic encephalomyelitis by antibodies to the antigen-Ia complex. Nature 351: 147–150.
25. Murphy DB, Rath S, Pizzo E, Rudensky AY, George A, Larson JK, Janeway CA, Jr (1992) Monoclonal antibody detection of a major self peptide. MHC class II complex. J Immunol 148:3483–3491.
26. Uchanska-Ziegler B, Nössner E, Schenk A, Ziegler A, Schendel DJ (1993) Soluble T cell receptor-like properties of an HLA-B35-specific monoclonal antibody (TÜ165). Eur J Immunol 23:734–738.
27. Wang J, Yu DT, Fukazawa T, Kellner H, Wen J, Cheng XK, Roth G, Williams KM, Raybourne RB (1994) A monoclonal antibody that recognizes HLA-B27 in the context of peptides. J Immunol 152:1197–1205.
28. Eastman S, Deftos M, DeRoos PC, Hsu DH, Teyton L, Braunstein NS, Hackett CJ, Rudensky A (1996) A study of complexes of class II invariant chain peptide: major histocompatibility complex class II molecules using a new complex-specific monoclonal antibody. Eur J Immunol 26:385–393.
29. Dadaglio G, Nelson CA, Deck MB, Petzold SJ, Unanue ER (1997) Characterization and quantitation of peptide-MHC complexes produced from hen egg lysozyme using a monoclonal antibody. Immunity 6:727–738.
30. Porgador A, Yewdell JW, Deng Y, Bennink JR, Germain RN (1997) Localization, quantitation, and in situ detection of specific peptide-MHC class I complexes using a monoclonal antibody. Immunity 6:715–726.
31. Rehm A, Rohr A, Seitz C, Wonigeit K, Ziegler A, Uchanska-Ziegler B (2000) Structurally diverse forms of HLA-B27 molecules are displayed in vivo in a cell type-dependent manner. Hum Immunol 61:408–418.
32. Chames P, Hufton SE, Coulie PG, Uchanska-Ziegler B, Hoogenboom HR (2000) Direct selection of a human antibody fragment directed against the tumor T-cell epitope HLA-A1-MAGE-A1 from a nonimmunized phage-Fab library. Proc Natl Acad Sci USA 97:7969–7974.
33. Fremont DH, Stura EA, Matsumura M, Peterson PA, Wilson IA (1995) Crystal structure of an H-2Kb-ovalbumin peptide complex reveals the interplay of primary and secondary anchor positions in the major histocompatibility complex binding groove. Proc Natl Acad Sci USA 92: 2479–2483.
34. Zhao R, Loftus DJ, Appella E, Collins EJ (1999) Structural evidence of T cell xeno-reactivity in the absence of molecular mimicry. J Exp Med 189:359–370.
35. Madden DR, Garboczi DN, Wiley DC (1993) The antigenic identity of peptide-MHC complexes: a comparison of the conformations of five viral peptides presented by HLA-A2. Cell 75:693–708.
36. Kjer-Nielsen L, Clements CS, Brooks AG, Purcell AW, Fontes MR, McCluskey J, Rossjohn J (2002) The structure of HLA-B8 complexed to an immunodominant viral determinant: peptide-induced conformational changes and a mode of MHC class I dimerization. J Immunol 169:5153–5160.
37. Tynan FE, Borg NA, Miles JJ, Beddoe T, El-Hassen D, Silins SL, van Zuylen WJ, Purcell AW, Kjer-Nielsen L, McCluskey J, Burrows SR, Rossjohn J (2005) High resolution structures of highly bulged viral epitopes bound to the major histocompatibility complex class I. Implications for T-cell receptor engagement and T-cell immunodominance. J Biol Chem 280:23900–23909.
38. Reiser JB, Gregoire C, Darnault C, Mosser T, Guimezanes A, Schmitt-Verhulst AM, Fontecilla-Camps JC, Mazza G, Malissen B, Housset D (2002) A T cell receptor CDR3beta loop undergoes conformational changes of unprecedented magnitude upon binding to a peptide/MHC class I complex. Immunity 16:345–354.
39. Fremont DH, Matsumura M, Stura EA, Peterson PA, Wilson IA (1992) Crystal structures of two viral peptides in complex with murine MHC class I H-2Kb. Science 257: 919–927.
40. Reiser JB, Darnault C, Gregoire C, Mosser T, Mazza G, Kearney A, van der Merwe PA, Fontecilla-Camps JC, Housset D, Malissen B (2003) CDR3 loop flexibility contributes to the degeneracy of TCR recognition. Nat Immunol 4:241–247.
41. Luz JG, Huang M, Garcia KC, Rudolph MG, Apostolopoulos V, Teyton L, Wilson IA (2002) Structural comparison of allogeneic and syngeneic T cell receptor-peptide-major histocompatibility complex complexes: a buried alloreactive mutation subtly alters peptide presentation substantially increasing V(beta) interactions. J Exp Med 195: 1175–1186.
42. Fan QR, Wiley DC (1999) Structure of human histocompatibility leukocyte antigen (HLA)-Cw4, a ligand for the KIR2D natural killer cell inhibitory receptor. J Exp Med 190:113–123.
43. Mareeva T, Martinez-Hackert E, Sykulev Y (2008) How a TCR-like antibody recognizes MHC-bound peptide. J Biol Chem 283:29053–29059.
44. Buslepp J, Wang H, Biddison WE, Appella E, Collins EJ (2003) A correlation between TCR Valpha docking on

MHC and CD8 dependence: implications for T cell selection. Immunity 19:595–606.
45. Kjer-Nielsen L, Clements CS, Purcell AW, Brooks AG, Whisstock JC, Burrows SR, McCluskey J, Rossjohn J (2003) A structural basis for the selection of dominant alphabeta T cell receptors in antiviral immunity. Immunity 18:53–64.
46. Tynan FE, Burrows SR, Buckle AM, Clements CS, Borg NA, Miles JJ, Beddoe T, Whisstock JC, Wilce MC, Silins SL, Burrows JM, Kjer-Nielsen L, Kostenko L, Purcell AW, McCluskey J, Rossjohn J (2005) T cell receptor recognition of a 'super-bulged' major histocompatibility complex class I-bound peptide. Nat Immunol 6:1114–1122.
47. Reiser JB, Darnault C, Guimezanes A, Gregoire C, Mosser T, Schmitt-Verhulst AM, Fontecilla-Camps JC, Malissen B, Housset D, Mazza G (2000) Crystal structure of a T cell receptor bound to an allogeneic MHC molecule. Nat Immunol 1:291–297.
48. Garcia KC, Degano M, Pease LR, Huang M, Peterson PA, Teyton L, Wilson IA (1998) Structural basis of plasticity in T cell receptor recognition of a self peptide-MHC antigen. Science 279:1166–1172.
49. Tynan FE, Reid HH, Kjer-Nielsen L, Miles JJ, Wilce MC, Kostenko L, Borg NA, Williamson NA, Beddoe T, Purcell AW, Burrows SR, McCluskey J, Rossjohn J (2007) A T cell receptor flattens a bulged antigenic peptide presented by a major histocompatibility complex class I molecule. Nat Immunol 8:268–276.
50. Narzi D, Winkler K, Saidowsky J, Misselwitz R, Ziegler A, Bockmann RA, Alexiev U (2008) Molecular determinants of major histocompatibility complex class I complex stability: shaping antigenic features through short and long range electrostatic interactions. J Biol Chem 283: 23093–23103.
51. Marrack P, Rubtsova K, Scott-Browne J, Kappler JW (2008) T cell receptor specificity for major histocompatibility complex proteins. Curr Opin Immunol 20:203–207.
52. Huseby ES, White J, Crawford F, Vass T, Becker D, Pinilla C, Marrack P, Kappler JW (2005) How the T cell repertoire becomes peptide and MHC specific. Cell 122: 247–260.
53. Huseby ES, Kappler JW, Marrack P (2008) Thymic selection stifles TCR reactivity with the main chain structure of MHC and forces interactions with the peptide side chains. Mol Immunol 45:599–606.
54. Adams EJ, Chien YH, Garcia KC (2005) Structure of a gammadelta T cell receptor in complex with the nonclassical MHC T22. Science 308:227–231.
55. Garboczi DN, Hung DT, Wiley DC (1992) HLA-A2-peptide complexes: refolding and crystallization of molecules expressed in *Escherichia coli* and complexed with single antigenic peptides. Proc Natl Acad Sci USA 89:3429–3433.
56. Leslie A. MOSFLM users guide. Cambridge, UK: MRC Laboratory of Molecular Biology; 1995.
57. Kabsch W (1988) Evaluation of single-crystal X-ray diffraction data from a position-sensitive detector. J Appl Crystallogr 21:916–924.
58. Vagin A, Teplyakov A (1997) MOLREP: an automated program for molecular replacement. J Appl Crystallogr 30:1022–1025.
59. McCoy AJ, Grosse-Kunstleve RW, Storoni LC, Read RJ (2005) Likelihood-enhanced fast translation functions. Acta Crystallogr D Biol Crystallogr 61:458–464.
60. Murshudov GN, Vagin AA, Dodson EJ (1997) Refinement of macromolecular structures by the maximum-likelihood method. Acta Crystallogr D Biol Crystallogr 53:240–255.
61. Emsley P, Cowtan K (2004) Coot: model-building tools for molecular graphics. Acta Crystallogr D Biol Crystallogr 60:2126–2132.
62. Brünger AT, Adams PD, Clore GM, DeLano WL, Gros P, Grosse-Kunstleve RW, Jiang JS, Kuszewski J, Nilges M, Pannu NS, Read RJ, Rice LM, Simonson T, Warren GL (1998) Crystallography & NMR system: a new software suite for macromolecular structure determination. Acta Crystallogr D Biol Crystallogr 54:905–921.
63. Lee B, Richards FM (1971) The interpretation of protein structures: estimation of static accessibility. J Mol Biol 55:379–400.
64. Kabsch W, Kabsch H, Eisenberg D (1976) Packing in a new crystalline form of glutamine synthetase from *Escherichia coli*. J Mol Biol 100:283–291.
65. DeLano W. The PyMOL molecular graphics system. San Carlos, CA: DeLano Scientific; 2002.
66. Kumar P, Ziegler A, Ziegler J, Uchanska-Ziegler B, Ziegler A (2008) Grasping molecular structures through publication-integrated 3D models. Trends Biochem Sci 33:408–412.
67. Kabsch W (1976) A solution for the best rotation to relate two sets of vectors. Acta Crystallogr Sect A 32:2.

5. Publication-embedded 3D imagery

5.1 Summary

Publications describing structural biological findings are severely limited in their ability to communicate the entirety of structural information as they communicate 3D information through 2D figures. Graping the structural details described in such publications is especially difficult for readers unfamiliar with structural biology who generally do not have access to molecular visualization programs essential for reading PDB coordinate files independently. These programs also require a “steep learning curve” that the uninitiated has to go through (Hodis and Sussman 2009). The PDB and Proteopedia, a dedicated platform for communicating 3D structural information (Hodis et al. 2008), have made remarkable attempts to fill this knowledge gap by integrating 3D models of each structure deposited in the PDB on their websites that can be viewed using the Jmol viewer, an intuitive, user-friendly interactive web browser applet that has enormously increased access to 3D structural information for nonspecialist readers of scientific publications. However, the inability of Jmol to communicate subtle structural details like the dual conformations of peptides (Hülsmeyer et al. 2004, Rückert et al. 2006) and the more general problem of the necessity to compromise on factors such as ease of use, prerendering, interactivity and availability while choosing a channel for 3D data communication prompted us to look for an alternative method for communicating 3D structural information with least compromise on the said factors. The effort started with an interdisciplinary collaboration with a scientist who had previously engaged in similar endeavors in zoology (Murienne et al. 2008, Ziegler et al. 2008) and culminated in the development of a method to integrate 3D models of macromolecules in PDF format (which is the format of choice for all scientific journals) documents using commercially available softwares. The successful implementation of this procedure would be expected to greatly enhance access of scientists with a limited knowledge of structural biology to molecular structures.

5.2 Publications

5.2.1. Kumar P*, Ziegler A*, Ziegler J, Uchanska-Ziegler B, Ziegler A. (*Equal contribution) Grasping molecular structures through publication-integrated 3D models. Trends Biochem. Sci. (**2008**) 33, 408–412

Note:

This article was featured on the cover page of the September 2008 issue of Trends in Biochemical Sciences and has been the subject of the following two editorials.

1. Dragging (and zooming and rotating) publication of 3D molecular structures into the 21st century Trends Biochem. Sci. (**2008**) 33, 405-407
2. 3D presentation of structural and image data J. Biol. Chem. (**2009**) 284, 21101

Opinion

Cell PRESS

Grasping molecular structures through publication-integrated 3D models

Pravin Kumar[1,*], Alexander Ziegler[2,*], Julian Ziegler[1,3], Barbara Uchanska-Ziegler[1] and Andreas Ziegler[1]

[1] Institut für Immungenetik, Charité–Universitätsmedizin Berlin, Campus Benjamin Franklin, Freie Universität Berlin, Thielallee 73, 14195 Berlin, Germany
[2] Institut für Biologie, Freie Universität Berlin, Königin-Luise-Strasse 1-3, 14195 Berlin, Germany
[3] Current address: Meister-Francke-Strasse 8, 22309 Hamburg, Germany

Although the need for communicating 3D data using simple and intuitive means extends to disciplines as diverse as biology, engineering sciences and the visual arts, none of the currently available molecular-visualization programs depicting potentially highly complex structures are compatible with the portable document format (PDF), the current gold standard of electronic publishing. Therefore, it is highly desirable for authors to be able to provide their readers with a basic 3D display of structures that can be accessed without the need for specialized visualization software. Here, we describe how an interactive 3D model of a molecular complex can be embedded directly into a PDF, thus providing readers with important and educational visual information that would otherwise be more difficult to disseminate.

Benefits of portable document format (PDF)-integrated 3D models

How multidimensional research data are presented in a scientific publication will often be crucial for an in-depth understanding. This is not only the case in structural biology where molecular features have been accessible in print format for many years through static and 'stereo' images [1–5], but is also the case in many other disciplines, such as chemistry, physics or medicine. However, complete access to a 3D model of a molecule that enables direct interaction with all its components, requires not only adequate hardware, but also the skill to operate a molecular-visualization tool appropriately, including the ability to effectively obtain and extract the precise information that is desired. Because these programs are often complicated to handle, there is an urgent need for a simple, effective and interactive representation of 3D structures that would enable both non-specialist and specialist readers of scientific publications to gain access to the most important aspects of the information contained within such structures. This requirement has already been recognized but there is as yet no consensus as to which presentation format is best suited [6,7].

Some examples of attempts to address this issue include internet browser plug-ins, such as Protein Explorer [4] and Jmol [7,8], which provide the possibility of integrating interactive 3D models into scientific and educational webpages, and the iSee platform [6], which offers a unified access system to a variety of components of structural genomics data from genes to complete structures. However, all these technologies require installation of programs or plug-ins by the user before the relevant information can be accessed and, crucially, the information is only accessible when online. The alternative or complementary mechanism is to provide a pre-rendered film of the molecule in a downloadable video format. Although improving the 'viewability' for the reader of the 3D information relative to that of static 2D images, this prevents any direct interaction with the structure, thus limiting its potential educational benefit and restricting the reader to scenes of the molecule dictated by the author. An additional problem for both of these approaches is that the information has to be supplied as a supplement to the original article rather than as a part of it, thus proving an impediment to the reader's access. Significantly, none of these technologies are compatible with the Adobe Systems' PDF, the universally accepted standard of electronic publications. A recent article [9] exemplifies these problems: although a 3D viewer ('FirstGlance in Jmol') with several different viewing options can be activated through a supplementary attachment, all attributes are only available online in a standardized manner through Jmol, precluding any integration into a PDF file, the format by which the article is distributed.

To simplify communication between the author and the reader, the aim must therefore be to depict structural data with the maximum of information about the molecules described but integrated within the electronic publication itself. Here, we show how an interactive, highly informative 3D model that fulfils these requirements can now be assembled and integrated into PDF documents. In addition to the typical 2D representations of static figures, this leads to enhanced, directly accessible 3D information in the content of publications in which structural data are described, thus combining the benefits of all other approaches to the dissemination of 3D structural information into a single, standard format file.

The HLA-B*2705–pVIPR complex

To demonstrate how a 3D model can be created and integrated into a PDF file, we chose the structure [Protein

Corresponding author: Ziegler, A. (andreas.ziegler@charite.de)
* Joint first authors.

0968-0004/$ – see front matter doi:10.1016/j.tibs.2008.06.004 Available online 30 July 2008

Data Bank (PDB) accession code 1ogt] of the human histocompatibility antigen HLA-B*2705 in complex with a peptide (pVIPR; RRKWRRWHL) that is derived from vasoactive intestinal peptide type 1 receptor, residues 400–408. A peculiarity of this molecular complex is the presence of the peptide in two equally occupied binding modes that differ considerably from each other, although all HLA-B*2705 heavy chain (HC) and β_2-microglobulin (β_2m) residues essentially retain the same conformations (there is a Cα root mean square deviation of 0.2 Å between the two complexes) [10].

In a traditional article, the following would be typical of how the structural information is presented to the reader: the heterotrimer consists of HC, β_2m and the self-peptide pVIPR (Figure 1). Although the ends of pVIPR [peptide residues 1 (p1) and p2, and p8 and p9] are bound identically in both conformations, the middle of the peptide (p3 to p7) diverges considerably. This is a consequence of the presence of the HC residue Asp116 (coloured red in Figure 1b–d), which binds to pArg5 by a bidentate salt bridge (yellow in Figure 1b,d) in one of the conformations. In this binding mode (termed non-canonical or p6α; coloured magenta in Figure 1), the main chain φ and ψ torsion angles occur in α-helical conformation only at p6, whereas, in the other, conventional peptide-binding mode (termed p4α; coloured light blue in Figure 1), this is the case only at p4. In both conformations, the other φ/ψ torsion angles, respectively, are as in β-strands. This conformational dimorphism of pVIPR has functional consequences because it is responsible for the inappropriate negative selection of HLA-B*2705–pVIPR-restricted T cells within the thymus [10,11]. In addition, X-ray crystallographic and functional studies show that the non-canonical conformation of pVIPR, but not its canonical counterpart, participates in HLA-B27 subtype-dependent molecular mimicry [10,12–14]. Because of the dual conformation of the peptide, the HLA-B*2705–pVIPR complex is a particularly instructive example to illustrate the advantages offered by PDF-integrated 3D models.

2D and 3D representations of the HLA-B*2705–pVIPR complex

The 2D images shown in Figure 1a,d provide the reader with a general idea of the structure of the HLA-B*2705–pVIPR complex, as would be typical for any other 3D structure presented in an academic paper. A surface representation of the entire molecule is shown in Figure 1a, followed by a view of the binding groove with pVIPR in both binding modes (Figure 1b, semi-transparent surface and cartoon representation). The bidentate salt bridge between HC Asp116 and pArg5 that characterizes the p6α-binding mode is also shown. Finally, Figure 1c,d demonstrate that an omission of HC, β_2m and one of the peptide conformations leads to an unobstructed, simplified view of the remaining pVIPR-binding mode. Representations like these provide the bare minimum of information that must be available for an evaluation of the structure of a molecule. In a conventional

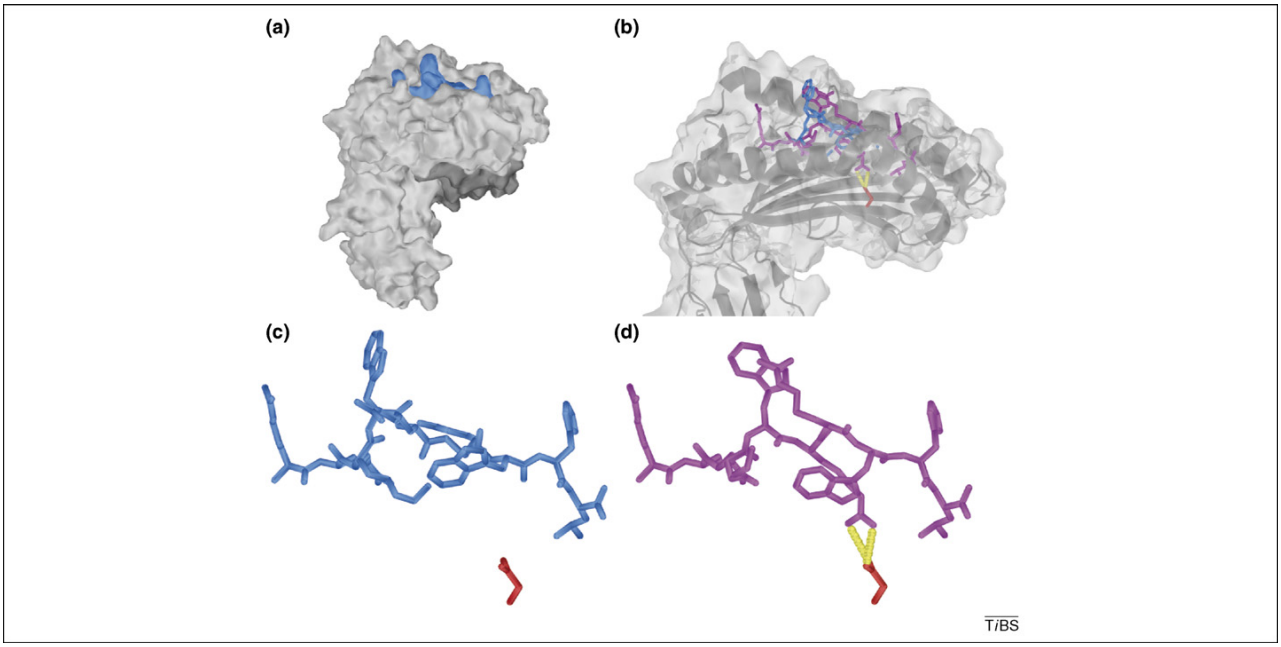

Figure 1. An interactive 3D model of the HLA-B*2705 molecule in complex with the pVIPR peptide. The HLA-B*2705 HC is shown in light grey, β_2m in dark grey and the two conformations of the pVIPR peptide in light blue (p4α) or magenta (p6α). The peptide N terminus is always shown on the left and the C terminus on the right. **(a)** Side view of the molecular surface of the whole molecule (only the p4α conformation of the peptide is shown). **(b)** Differential display of the pVIPR peptide (stick representation) in the canonical (light blue) and non-canonical (magenta) conformations in the HLA-B*2705 binding groove. The anchoring of pVIPR to the floor of the peptide binding groove in the p6α conformation is through a bidentate salt bridge (yellow) between pArg5 and the side chain of Asp116 (red). After removal of HC and β_2m, pVIPR is depicted in p4α **(c)** or p6α **(d)** conformation together with Asp116 and the salt bridge (only d). 3D functions can be activated by clicking on any part of the image in the interactive PDF version of the article (note, to end the 3D view, right-click the 3D display and select 'Disable 3D' from the contextual menu). Components of the 3D model can be accessed using the model tree icon. The model can be manipulated interactively using the mouse (options for selecting rotating, panning and zooming tools are available in the toolbar or contextual menu) and readers can see the preset views by clicking on the respective designations assigned by the authors (through the middle section of the model tree when it is displayed, the drop-down menu in the toolbar or the contextual menu).

publication, Figure 1 would therefore have to be complemented by several additional images providing more structural detail (see, e.g. Ref. [10]).

The alternative and more enlightening approach that we advocate here involves the use of the freely available Adobe Reader (Version 7.1 or later) to access the 3D model of the molecule in an interactive manner – this is achieved by clicking on any part of Figure 1 in the interactive PDF version of this publication (see Supplementary Material online). An introduction into the possibilities that are offered is provided when the 'Help' option within the program is addressed. Already the 'basic' tools, such as zoom, rotation in freely chosen directions or hiding of structural elements (e.g. HC, β_2m or one of the pVIPR conformations) permit an interactive access that facilitates a better understanding of many structural features. In this case, it is particularly helpful to be able to compare the peptide conformations by zooming in and by rotating the two structures with the HC component hidden (by toggling its visibility off in the model tree), both in surface and ball and stick view (which can be alternated easily, also by toggling the view options in the model tree). In this way, it becomes obvious immediately that the Cα backbones and side chains of pVIPR are distinct between the two conformations from p3 to p7, whereas they are virtually identical at the ends of the peptide [10].

With the included preset views, an author-generated 'tour' of the molecule is made available to the reader. This tour provides the reader with the equivalent views that would be typical of a pre-rendered video file of the structures, which is offered normally as supplementary material for download, yet it still enables full interaction with the structures at each stage of the tour. In our case, the tour begins by depicting the entire complex and then shows a 'skeletal' view of all components, zooms into the peptide-binding groove, disentangles the molecular assembly more and more, using various side and top views, and concentrates finally on the two peptide conformations. The HC residue Asp116 and the salt bridge that it forms with pArg5 only in the p6α conformation of pVIPR are also shown. The educational aspect of this tour makes it particularly suited for presentations and teaching without the necessity for online access. Despite these features, the file size of the present publication, including the combined 2D and 3D figure, is not greater than ~3 MB.

Creating an interactive 3D model and integrating it into PDF files

A detailed description of how to build such a model is provided in Box 1. In summary, the HLA-B*2705–pVIPR structure was divided into its individual components. Interactive vector graphics objects of each component were then created using PyMOL, followed by the import of the image objects into the Adobe Acrobat 3D Toolkit and their reassembly. The Toolkit was further used to design the model 'tree' (which is a hierarchy of components of the molecule that enables the reader to set their individual visibility and display style), name sub-structures and select colours for each object. The model was then saved in Adobe Systems' Universal 3D (U3D) file format and the

Box 1. How the PDF-integrated 3D model was created

The 3D model was assembled in a step-by-step manner, which is outlined in Figure I. Initially, the raw PDB file (1ogt) was downloaded from PDB (www.rcsb.org/pdb/home/home.do) and opened using PyMOL version 1.0r1 (http://pymol.sourceforge.net/) in an OpenSUSE 13.2 Linux environment. Here, the components to be shown in the final 3D model were selected (HLA-B*2705 HC, β_2m, HC residue Asp116, the bidentate salt bridge between pArg5 and Asp116 of the HC and the two peptide conformations) and each saved separately in VRML2 format, followed by loading into Adobe Acrobat 3D Toolkit 8.1.0 (Adobe Systems, CA, USA) by drag and drop. Once loaded, the mesh size (i.e. the amount of data representing the surface) of each object was reduced as far as possible by a process of trial and error (down to ~30% of the original size) to keep the final file size to a minimum. The separate objects were then designated (e.g. β_2m), an object hierarchy (i.e. model tree) was created and different colours were assigned to each. The model was saved in the Adobe Universal 3D file format, which was then opened in Adobe Acrobat 3D. The four images shown in Figure 1a–d were created from TIFF-format desktop screenshots of the desired model views and were modified in Adobe Photoshop CS3 to show the desired information (i.e. cropped to size). After combining these TIFF files, a single JPEG-format image file was generated using Adobe Illustrator CS3. Following this operation, the raw U3D file was opened in Adobe Acrobat 3D and the single 2D JPEG image file was combined with it. Then all final viewing settings were defined, such as background colour, standard render mode and lighting. The next step consisted of selecting the preset views using the camera tool and defining a standard view that would be shown after activation of the 3D mode. Finally, the model was saved as a PDF file. An overview of the minimum system requirements needed to create and view 3D PDF models can be obtained through the following websites from Adobe Systems: Adobe Acrobat 3D and Adobe Acrobat 3D Toolkit (www.adobe.com/products/acrobat3d/systemreqs), and Adobe Reader (www.adobe.com/products/reader/productinfo/systemreqs).

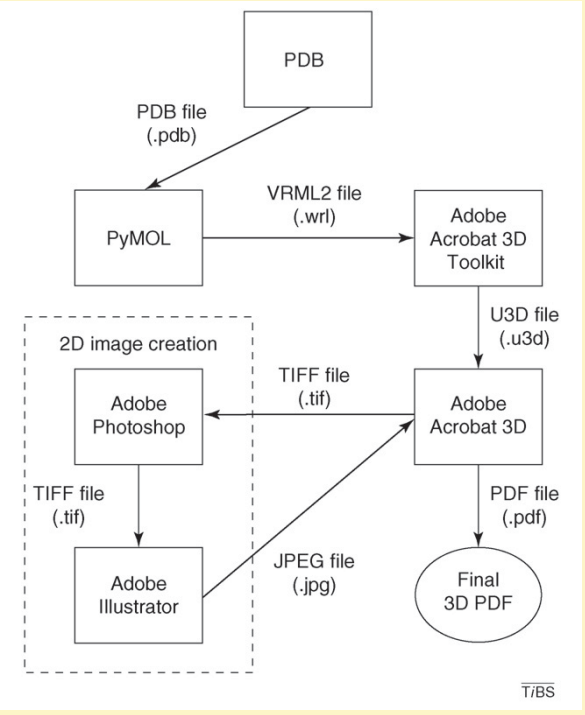

Figure I. Flow diagram depicting the creation process of a PDF-integrated 3D model 'hidden' behind a single 2D image file (Figure 1a–d) of the HLA-B*2705–pVIPR complex. Note: the processes on the left of the flow chart are ones that will hopefully become redundant in the future if the Adobe Acrobat 3D software is ever updated to be able to perform these tasks itself.

U3D file imported directly into a PDF file, using Adobe Acrobat 3D. This program was also used to assign additional features of the model, such as its rendering mode or lighting. The 2D representations in Figure 1a–d were also created during this stage. The last step consisted of preparing and designating the preset views for the reader.

Concluding remarks

It should be noted that the Adobe Acrobat 3D Toolkit enables authors to incorporate many more features into 3D models, such as the labelling of components of the structure, measuring distances, variable lighting options and several additional model-render modes. We have deliberately limited the options that are available in the model presented here to enable the reader to concentrate on the principal features that distinguish the conventional 2D representations of Figure 1a–d from the PDF-integrated 3D models of the molecular structures. These are the 3D-viewing capability, platform-independence, accessibility and, probably of greatest importance, its interactivity that enables the reader to delve into aspects of the structure that would otherwise not be available to them readily. However, it must be pointed out that the program does not yet offer several options available in standard molecular-visualization software (Box 2). These shortcomings of the Adobe Acrobat 3D programs might, in part, be due to their current focus on technical applications rather than the biochemical sciences (i.e. computer-aided design and computer-aided manufacturing). However, other molecular-visualization programs are also not problem-free. For example, when the structure of the HLA-B*2705–pVIPR complex is accessed with 'FirstGlance in Jmol', only the canonical-binding mode of pVIPR can be seen, thereby precluding an understanding of the dual conformation's immunological implications.

Our example demonstrates that the integration of 3D models into electronic publications provides the reader with the ability to visualize complex structures in an interactive, yet intuitive, manner, without having to rely on the often highly sophisticated programs used by structural biologists [1–8]. A wide dissemination of this technology is made possible by the platform independence of programs, such as Adobe Reader. The potential that is thus offered has also not escaped the attention of astrophysicists and zoologists, as two recent reports demonstrate [15,16]. We believe that the incorporation of 3D files into electronic publications will also be of importance in many disciplines of clinical medicine, such as neurology, cardiology and oncology, in which the original data are not accessible through databases, such as PDB.

Several improvements will be needed to establish this procedure as a mainline tool in electronic publishing (Box 2). For example, although a direct export of the PDB file into Adobe Acrobat 3D Toolkit is possible in principle, for the purposes of our article, we had to use a deviation through PyMOL to be able to display the molecule in the commonly used ribbon or surface representations. Therefore, the import options of the relevant PDF-creation programs as well as the export functions of molecular-visualization software need to be scrutinized and improved. Apart from these issues, we have to stress that a considerable responsibility rests with the model-creating author because the diverging interests and program-handling capabilities of the readers must be anticipated.

Box 2. PDF-integrated 3D models: caveats and desirable improvements

Despite the advantages offered by PDF-integrated 3D models, several problems do remain. These belong to three areas: (i) viewing options, (ii) ease of creating the PDF-integrated 3D model and (iii) file-size limitations.

Owing to their design explicitly for structural biology, current molecular visualization programs [1–8] offer far more viewing options than are available for the 3D model shown here. However, many of the features provided might not be essential to convey the most important message about a structure, such as the conformational dimorphism of pVIPR in the HLA-B*2705 subtype. For example, in our case, the omission of the non-canonical pVIPR conformation by 'FirstGlance in Jmol' must be considered a more severe problem than the inability of our PDF-integrated 3D model to display the 'rainbow' viewing option that is offered by the former program for colouring the three chains of the complex. However, the lack of all the display settings available in current specialist software could still be a problem in other cases, so a 'complete' set of viewing options is desirable.

As the flow diagram (Box 1, Figure I) demonstrates, the process of creating a 3D PDF of a molecular structure is presently not as easy as one would hope and a simplification of this procedure would be highly desirable. This could be approached either by developing a U3D to PDF export function in standard molecular visualization programs or by providing the Adobe Acrobat 3D Toolkit with a more advanced import function for raw PDB files (the current import options are unsatisfactory). Clearly, having to use third-party software (here: PyMOL; see also Box 1, Figure I) to obtain the necessary output for the structures is laborious and the current need to perform this step will hopefully become unnecessary in the future.

Finally, it must be stressed that the integration of 3D models into electronic publications results in an extended publication file size, which in some cases might be too large (e.g. if numerous 3D structures need to be included in a single article), especially as many scientific institutions have download limits for individual files of 5–10 MB.

Note added in proof

During the final processing stage of this manuscript, Adobe Systems announced the launch of new Adobe Acrobat and Adobe Reader versions for July 2008 (both in version 9). We have not been able to evaluate the advantages (or disadvantages) offered by these new versions in any depth. However, the links we provide in our article are still valid, the one directing the reader to the Adobe Reader download page, the other link directing the reader to the Adobe Acrobat Version 9 homepage. According to the sales staff at Adobe Systems, the functions of the Adobe Acrobat 3D Toolkit have been incorporated into the new 'Adobe 3D Reviewer' which is sold as part of the new 'Adobe Acrobat Version 9 Pro Extended' package.

Acknowledgements

This work was supported by the VolkswagenStiftung (I/79 983 and a stipend to P.K.) and the Friedrich-Naumann-Stiftung für die Freiheit (fellowship to A.Z.). We thank T. Bartolomaeus (Berlin, Germany) for support and J.A. López de Castro (Madrid, Spain) for his helpful comments on the manuscript.

Supplementary data

Owing to the necessity to provide a standard-format PDF to institutions for their archives, this version of the article cannot currently include the interactive Figure 1. Instead, the fully interactive version of this article is available as Supplementary material in the online version, at doi:10.1016/j.tibs.2008.06.004

References

1 Kraulis, P.J. (1991) MOLSCRIPT: a program to produce both detailed and schematic plots of protein structures. *J. Appl. Crystallogr.* 24, 946–950
2 Merritt, E.A. and Bacon, D.J. (1997) Raster3D: photorealistic molecular graphics. *Methods Enzymol.* 277, 505–524
3 DeLano, W.L. (2002) *The PyMOL Molecular Graphics System.* DeLano Scientific
4 Martz, E. (2002) Protein Explorer: easy yet powerful macromolecular visualization. *Trends Biochem. Sci.* 27, 107–109
5 Fenn, T.D. *et al.* (2003) POVScript+: a program for model and data visualization using persistence of vision ray-tracing. *J. Appl. Crystallogr.* 36, 944–947
6 Abagyan, R. *et al.* (2006) Disseminating structural genomics data to the public: from a data dump to an animated story. *Trends Biochem. Sci.* 31, 76–78
7 Cammer, S. (2007) SChiSM2: creating interactive web page annotations of molecular structure models using Jmol. *Bioinformatics* 23, 383–384
8 Herráez, A. (2006) Biomolecules in the computer: Jmol to the rescue. *Biochem. Educ.* 34, 255–261
9 Röthlisberger, D. *et al.* (2008) Kemp elimination catalysts by computational enzyme design. *Nature* 453, 190–197
10 Hülsmeyer, M. *et al.* (2004) Dual. *HLA-B27 subtype-dependent conformation of a self-peptide. J. Exp. Med.* 199, 271–281
11 Fiorillo, M.T. *et al.* (2000) CD8(+) T-cell autoreactivity to an HLA-B27-restricted self-epitope correlates with ankylosing spondylitis. *J. Clin. Invest.* 106, 47–53
12 Fiorillo, M.T. *et al.* (2005) Allele-dependent similarity between viral and self-peptide presentation by HLA-B27 subtypes. *J. Biol. Chem.* 280, 2962–2971
13 Rückert, C. *et al.* (2006) Conformational dimorphism of self-peptides and molecular mimicry in a disease-associated HLA-B27 subtype. *J. Biol. Chem.* 281, 2306–2316
14 Ziegler, A. *et al.* Implications of structural and thermodynamic studies of HLA-B27 subtypes exhibiting differential association with ankylosing spondylitis. In: *Molecular Mechanisms of Spondyloarthropathies* (López-Larrea, C., ed.), Landes Bioscience (in press)
15 Barnes, D.G. and Fluke, C.J. (2008) Incorporating interactive three-dimensional graphics in astronomy research papers. *N. Astron.* 13, 599–605
16 Ruthensteiner, B. and Hess, M. Embedding 3D models of biological specimens in PDF publications. *Microsc. Res. Tech.* (in press)

Supplementary material 2:

A step-by-step guide to creating PDF-integrated 3D models

This text is a supplement to:

Grasping molecular structures through publication-integrated 3D models

Pravin Kumar[1,*], Alexander Ziegler [2,*], Julian Ziegler[1,3], Barbara Uchanska-Ziegler[1] and Andreas Ziegler[1]

1 Institut für Immungenetik, Charité –Universitätsmedizin Berlin, Campus Benjamin Franklin, Freie Universität Berlin, Thielallee 73, 14195 Berlin, Germany
2 Institut für Biologie, Freie Universität Berlin, Königin-Luise-Strasse 1-3, 14195 Berlin, Germany
3 Current address: Meister-Francke-Strasse 8, 22309 Hamburg, Germany

Trends in Biochemical Sciences, Volume 33, Issue 9, September 2008

http://dx.doi.org/10.1016/j.tibs.2008.06.004

Figure 1:

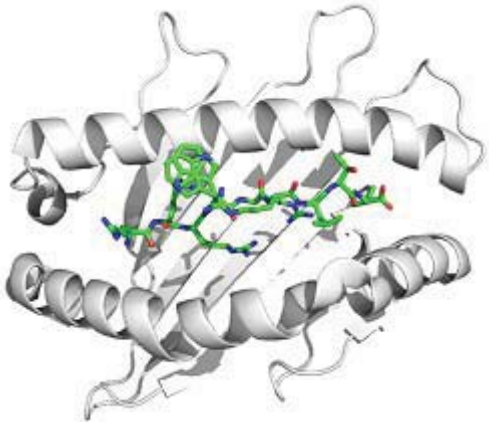

The following is a guide for generating 3D models from a PDB file using a licensed version of PyMOL together with Adobe 3D Reviewer and Adobe Acrobat 9 Pro Extended. It is also available online at http://www.charite.de/immungenetik/model3d.html. The goal of the exercise is to show you how to reproduce the image in Figure 1 as an interactive 3D model in a PDF file, thus teaching you the basics of the process.

PART 1: Model creation using PyMOL

Step 1: The 3D models of the structures in Figure 1 are originally generated using the following script in PyMOL, using the file 1UXS.pdb downloaded from the Protein Data Bank.

Note, if you are unfamiliar with the syntax used in PyMOL, it is possible to use the graphical user-interface (GUI) of the software to manually load the PDB file, configure the display of the molecule and create the image from it.

Script 1:

```
load 1UXS.pdb

bg_color white

hide

select groove, resi 1-180 and chain a

select peptide, resi 1-9 and chain c

show cartoon, groove

color white, groove

show stick, chain c

set_view (\
```

```
    -0.912446856,   -0.163690791,   -0.375027299,\
    -0.052661002,    0.955854416,   -0.289084166,\
     0.405792415,   -0.244024336,   -0.880786359,\
     0.000007013,    0.000006229, -147.386962891,\
     5.790267467,    0.459395200,   11.122777939,\
    96.323867798,  198.451461792,    0.000000000 )
ray
save Fig1.png
```

Step 2: Divide the model into individual components and export their coordinates as VRML2 models. You can use the following PyMOL script.

Script 2:

```
hide everything
show stick, peptide
save peptide.wrl
```

Alternatively you can use the GUI to modify the display settings and use the “Save Image As …VRML2” File menu option (Figure 2).

Figure 2:

5. Publication-embedded 3D imagery

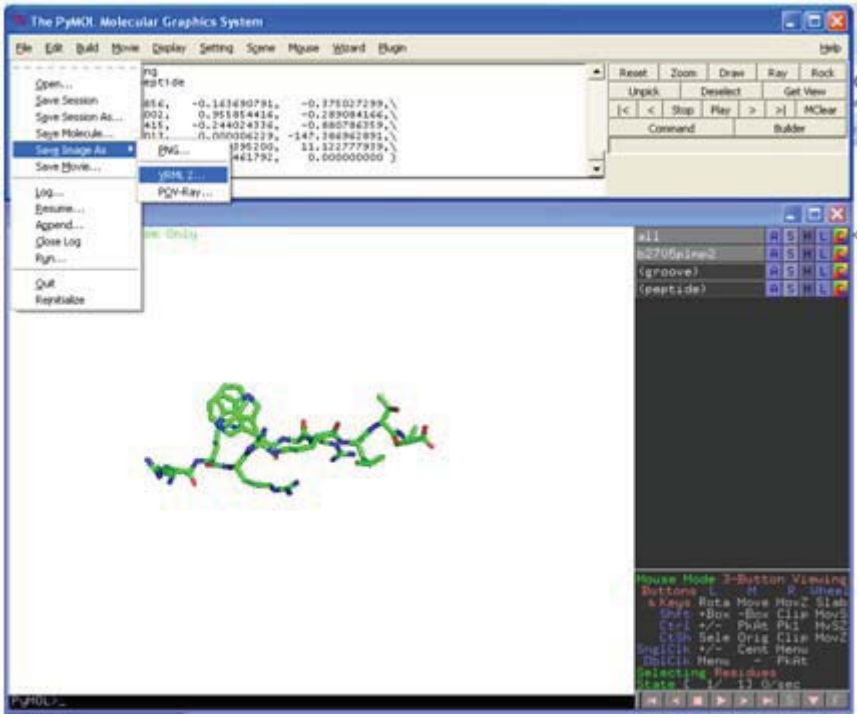

Similarly the second component of the model, the peptide binding groove, can also be exported as a VRML2 model using the following script (or by using the GUI, Figure 3).

Script 3:

```
hide everything

show cartoon, groove

save groove.wrl
```

Figure 3:

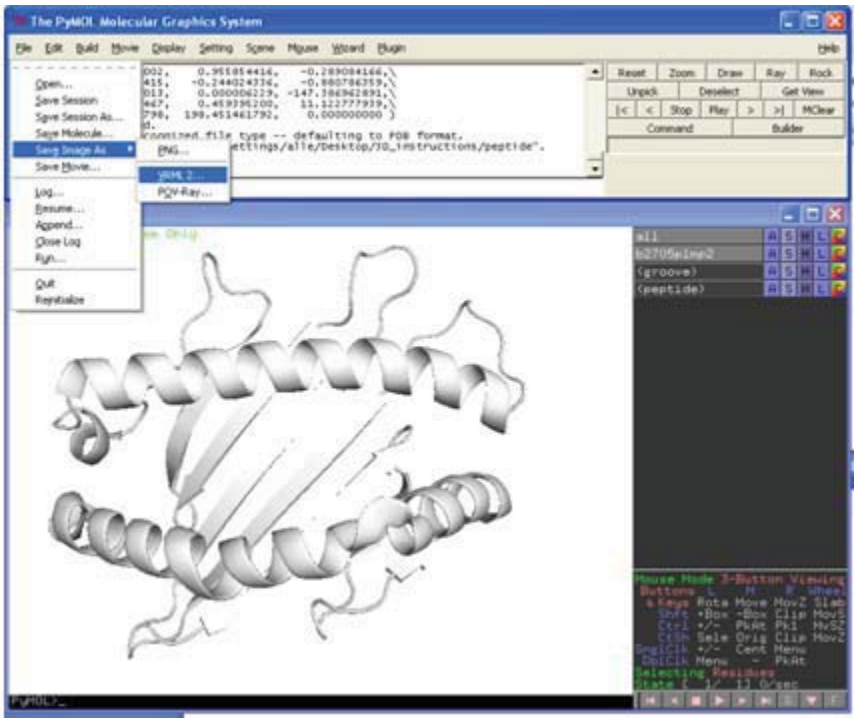

Part II: Figure Creation using Adobe Acrobat 9 Professional Extended

Step 3: Open Adobe 3D Reviewer, which is a part of the Adobe Acrobat 9 Professional Extended software suite. Click the "Open" icon and select ***ALL*** the components of your 3D model (which are all in .wrl format) using the "Ctrl" key, then press "Open" (Figure 4) to import them into Adobe 3D Reviewer.

Figure 4:

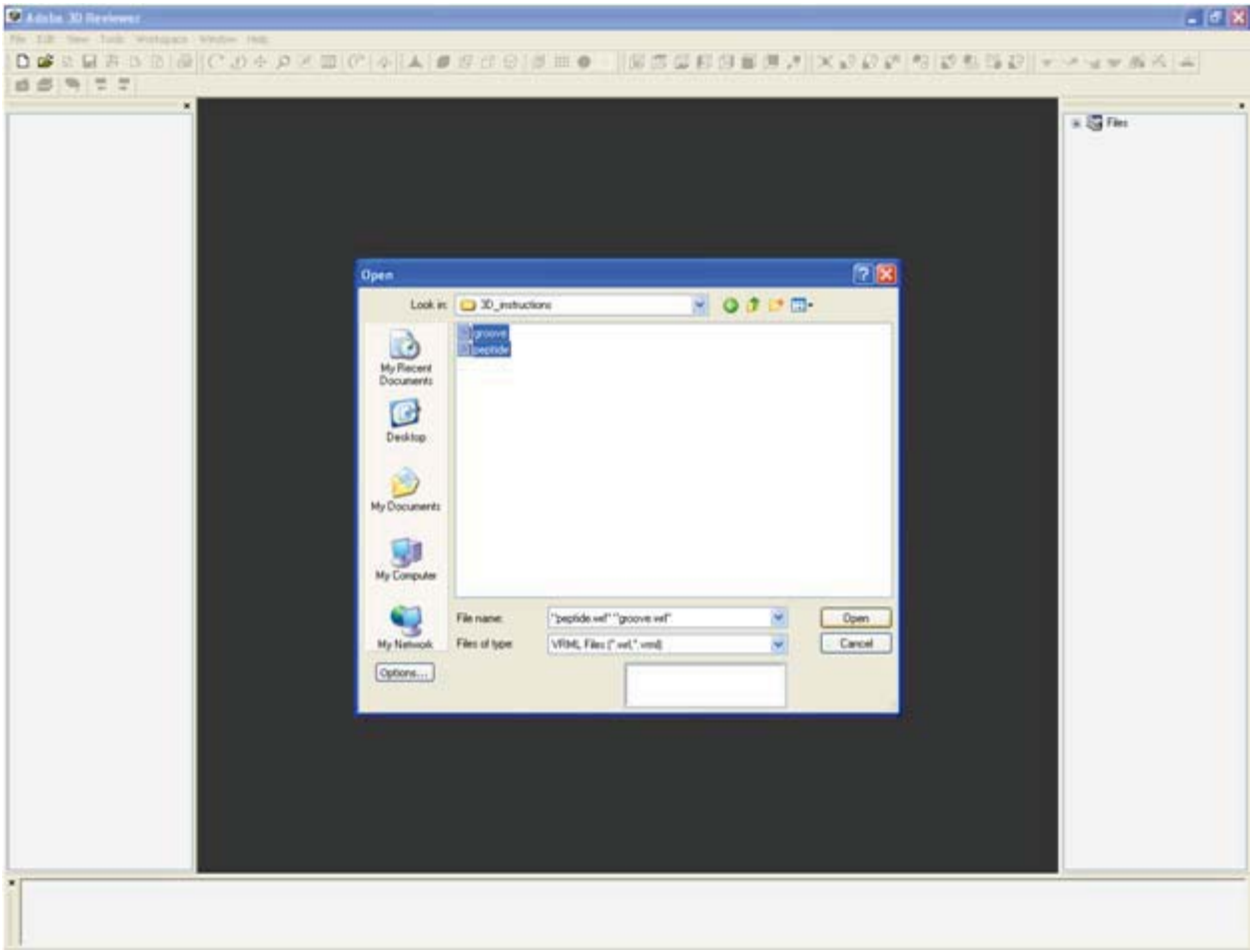

Options to alter the background colour, light settings etc. appear on right clicking on the screen (Figure 5).

Note, we have found that changing the 'Level of Detail' setting does not appear to have any effect for our models or on the final file-size of the PDF – we suggest ignoring this option.

Figure 5:

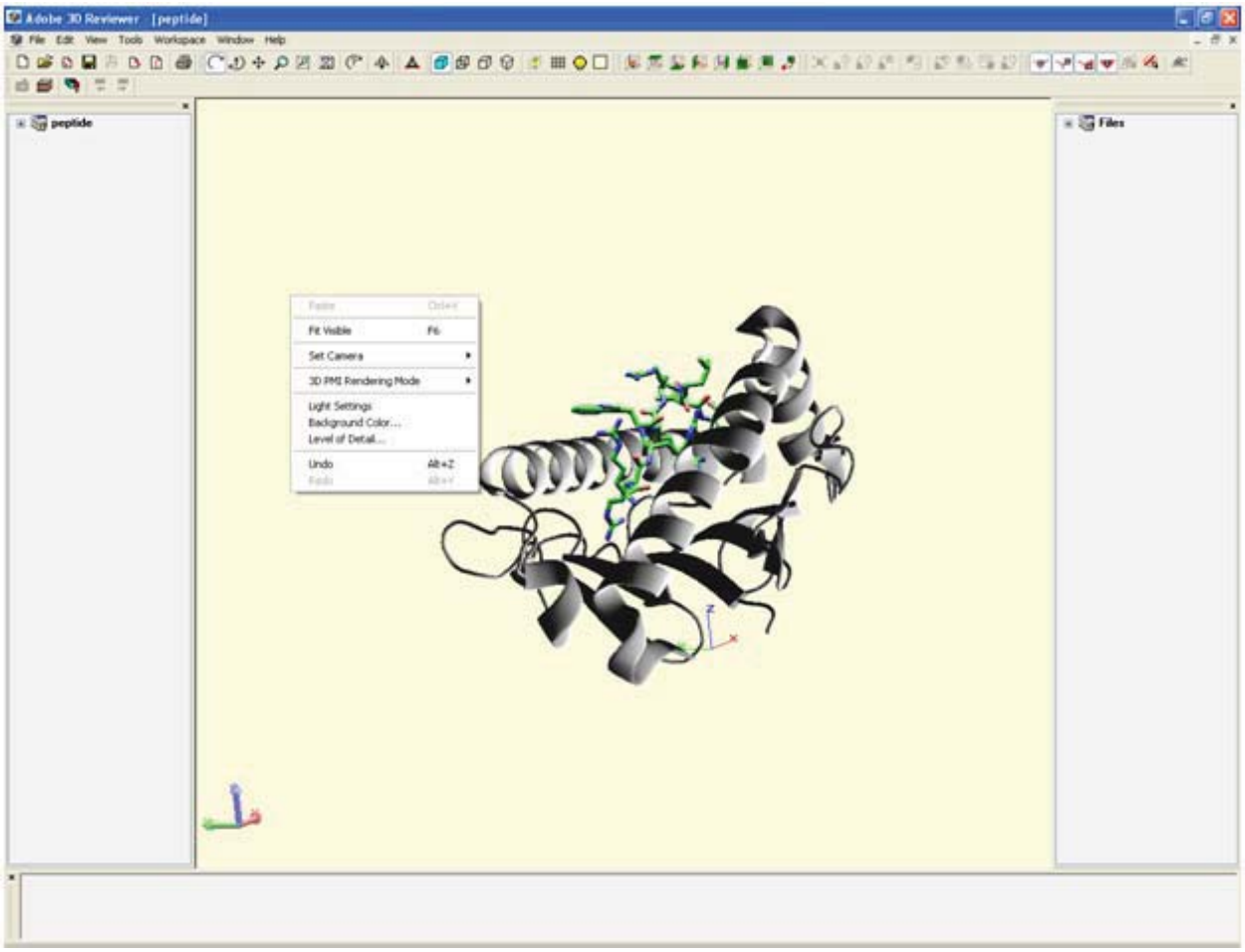

Note: (Not shown here) if you click an object in your model to select it, and then right-click the selection, you will be presented with a contextual menu from which you can select a 'Properties' option. In the dialogue that appears, you can modify the colour of your selected object, which enables you to colour code e.g. different subunits in your final figure.

Export the model as a .u3d file (Figure 6). Note, you must change the export settings by clicking the Options button that appears at the bottom left of the Export dialogue if you wish to create a PDF that is compatible with version 7.1 of Adobe Reader or Acrobat. To do so, choose 'ECMA 1 (7.0 compatible)' for the export format (the default is ECMA 3 which is only compatible with version 8 and higher).

Figure 6:

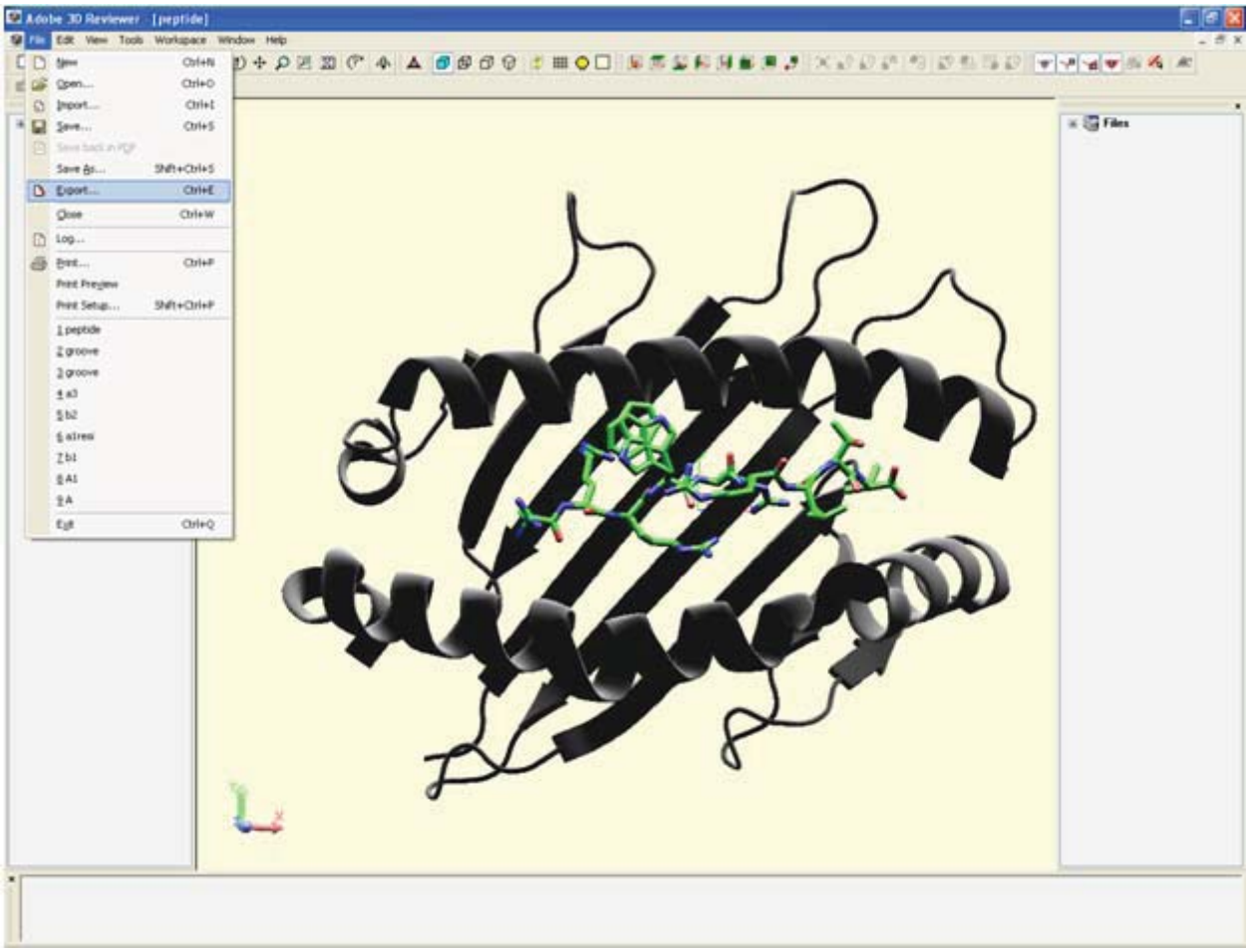

Step 3: Now open Adobe Acrobat 9 Pro Extended. Click the "Open" icon, select the folder in which the Adobe 3D Reviewer file was created, opt to 'Show all files' (the default is PDFs only) and choose the saved .u3d model to be opened (Figure 7). Click OK on the dialogue that is displayed to convert the file.

Note: if compatibility with version 7.1 of Adobe Reader is required, it is important that you do not change any of the conversion settings available in this dialogue from their defaults.

Figure 7:

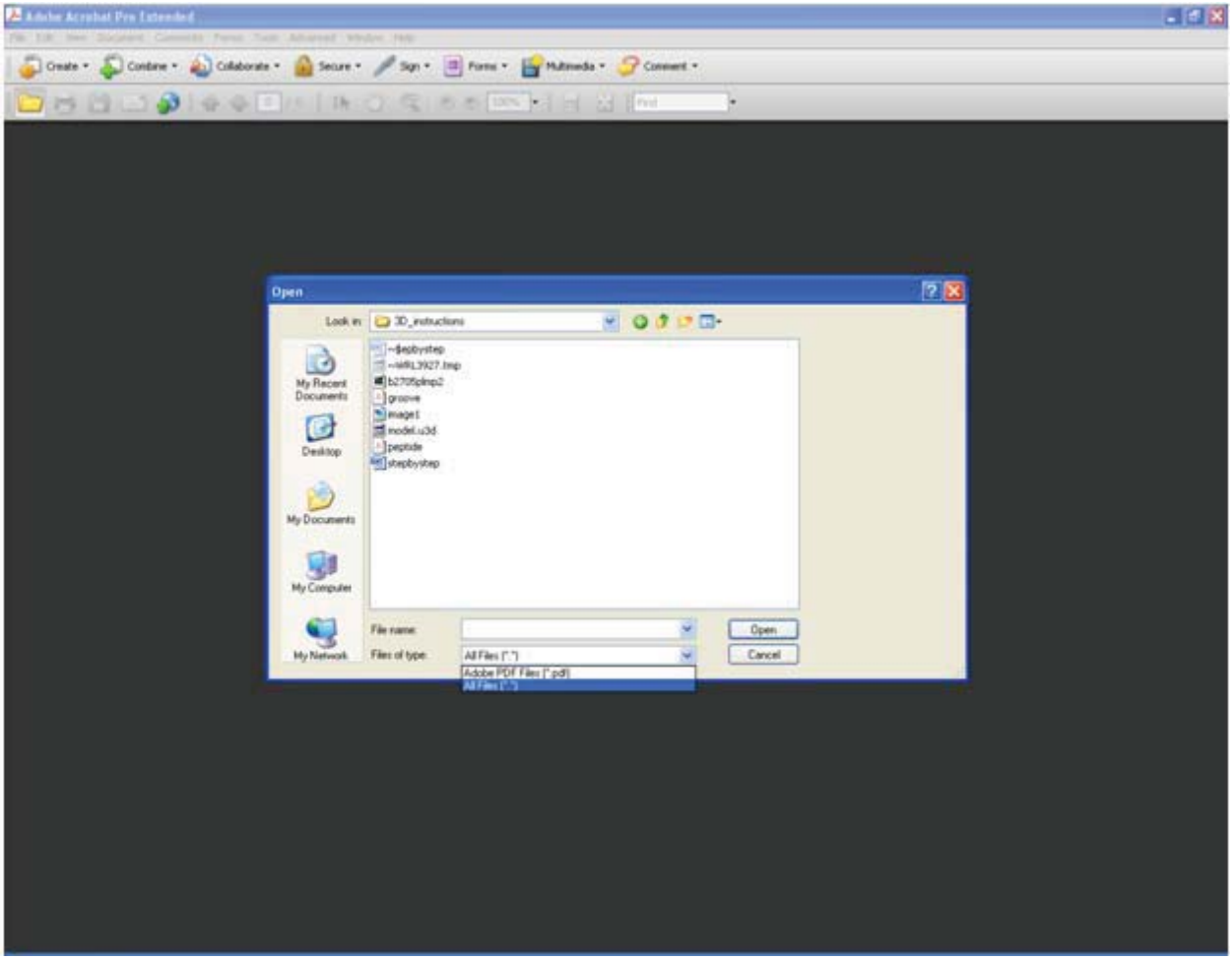

In our example, the opened, converted model looks like this (Figure 8).

Figure 8:

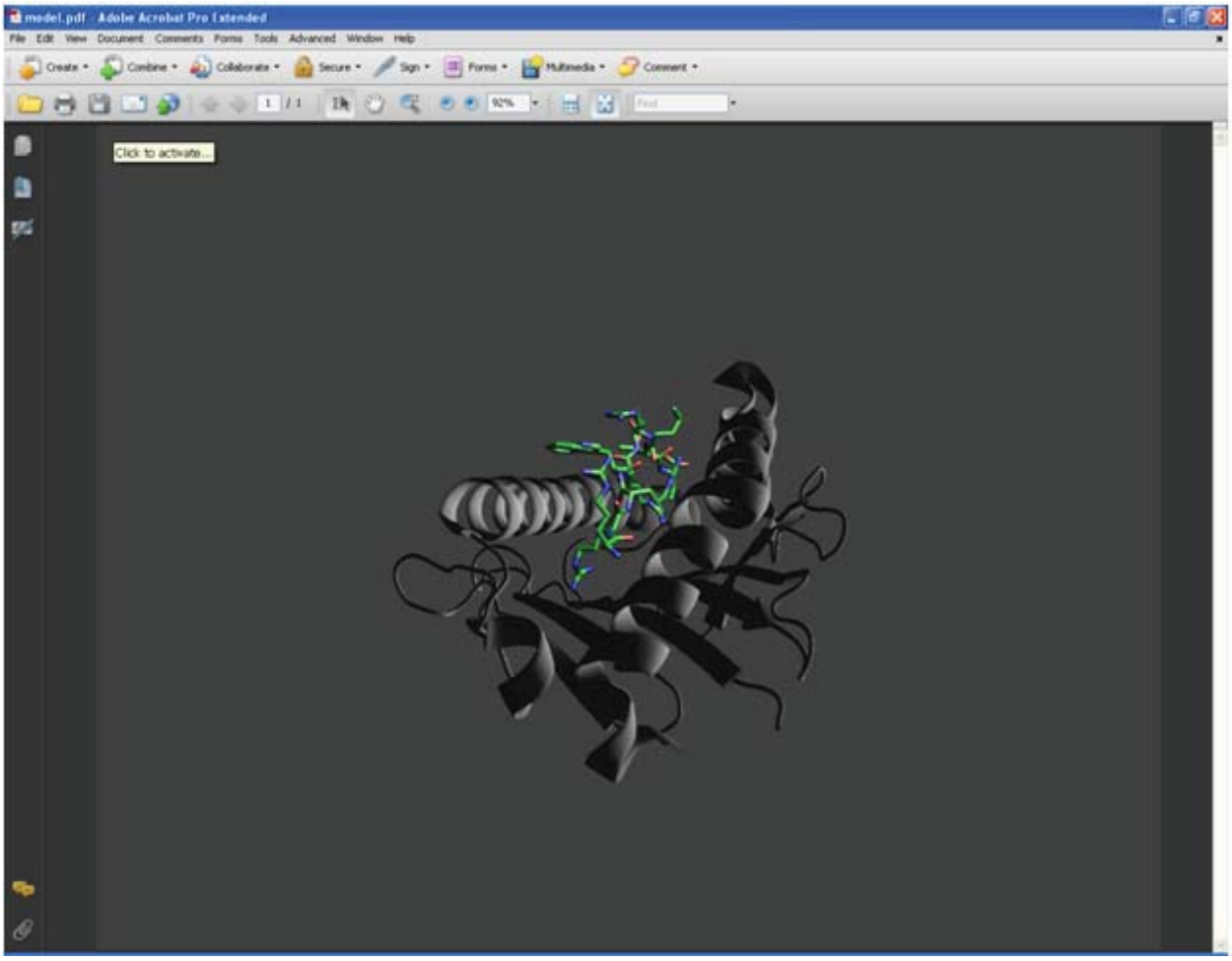

Right click and select “Properties” (Figure 9).

Figure 9:

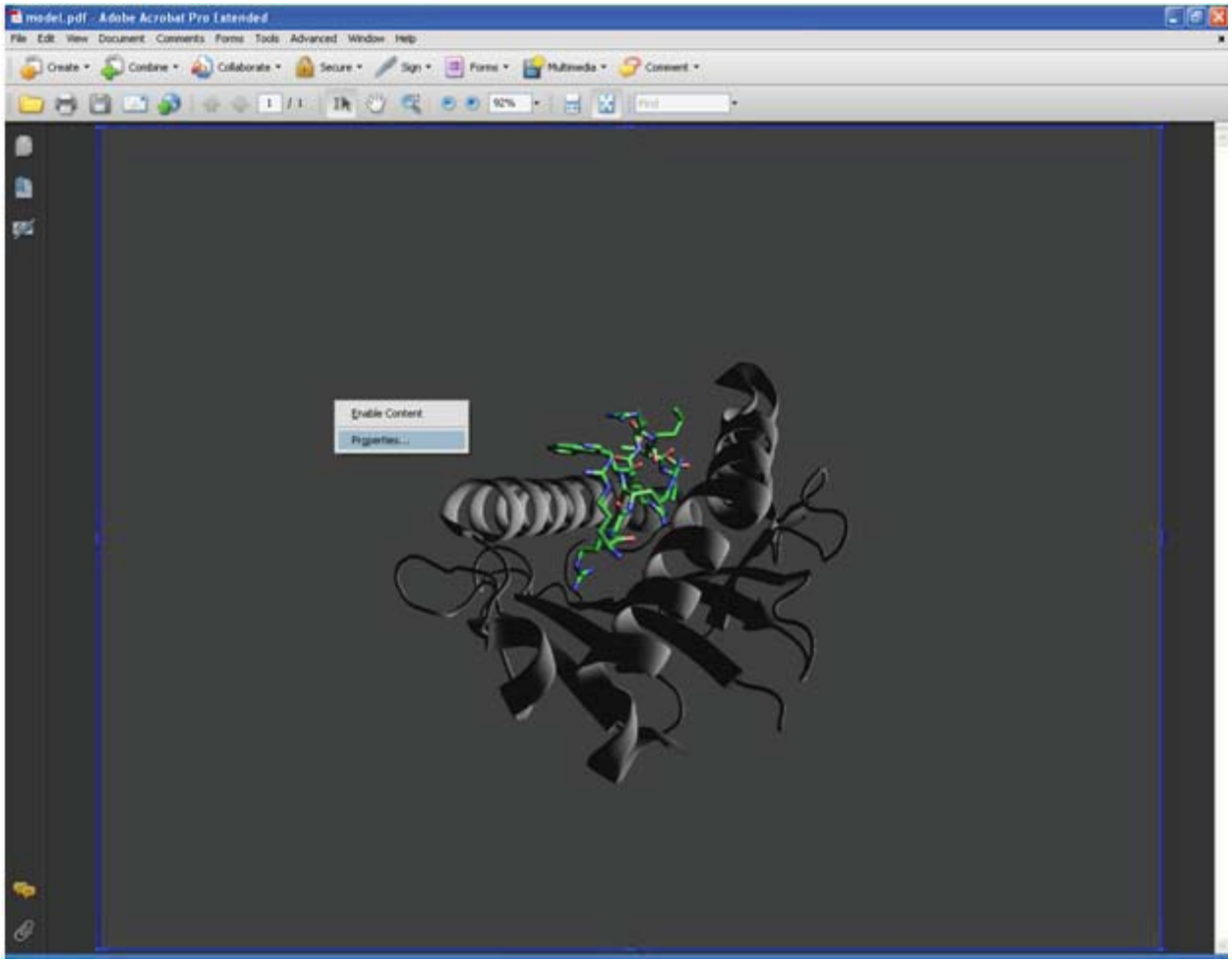

Set the options in the “Launch Settings” tab. If you want to set a specific static 2D image for your interactive model (such as a 2D Figure for an article) click “Create poster from file” (Figure 10), and choose e.g. the Fig1.png that was created in PyMOL earlier. If you skip this step, an image will be created for you from the default view of the 3D model itself.

Figure 10:

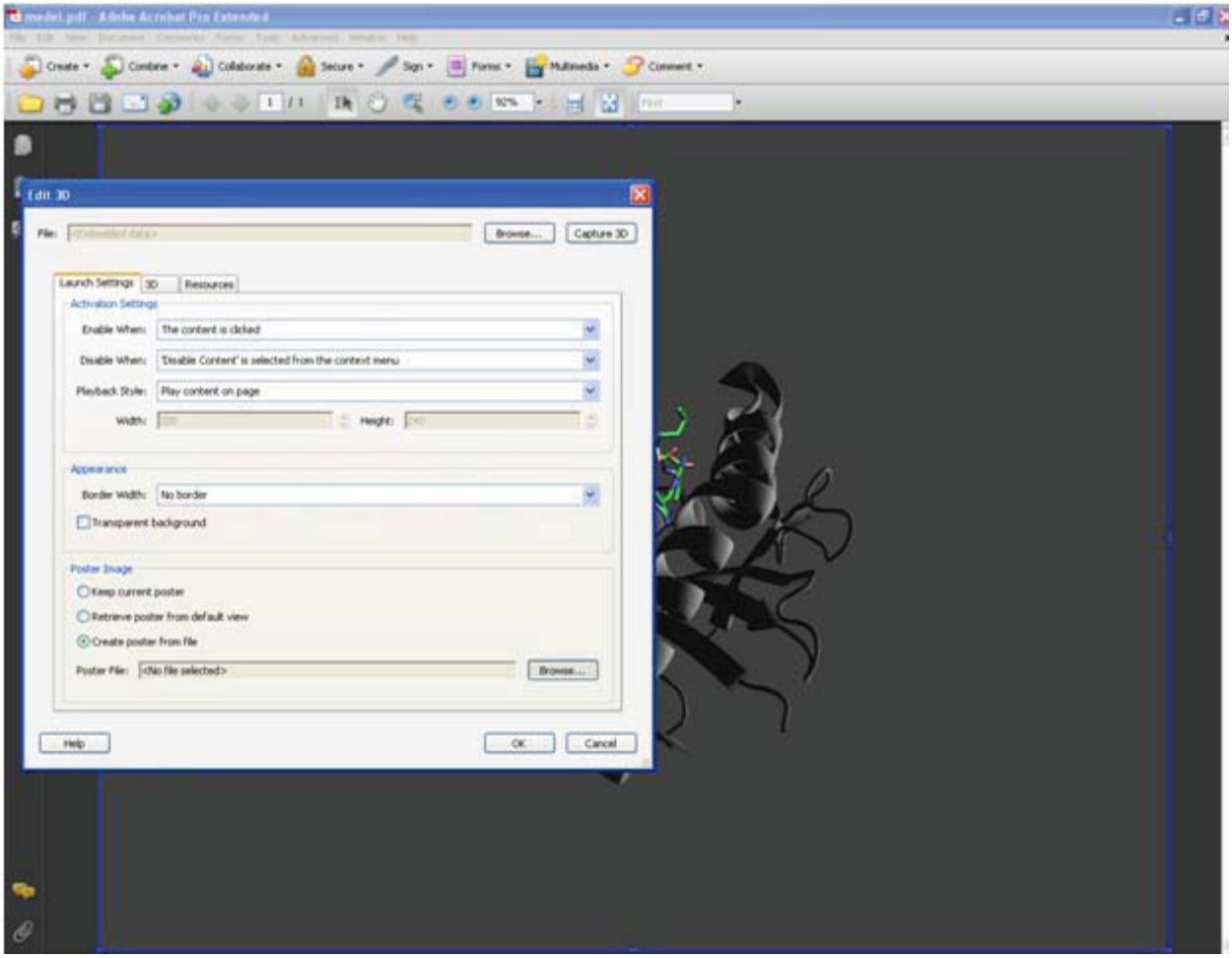

You can change the background color, light settings etc. under the “3D” tab of the same dialogue (Figure 11).

Note: also under this tab are options to have the model tree and toolbar display automatically whenever the interactive 3D model is opened by a reader. At this point it can also be beneficial to opt to ‘Add Default Views’ to your model tree (i.e. views from Top, Left, Right, Bottom, etc.), which will make it easier to perform the stage illustrated in Figure 13 further below.

Figure 11:

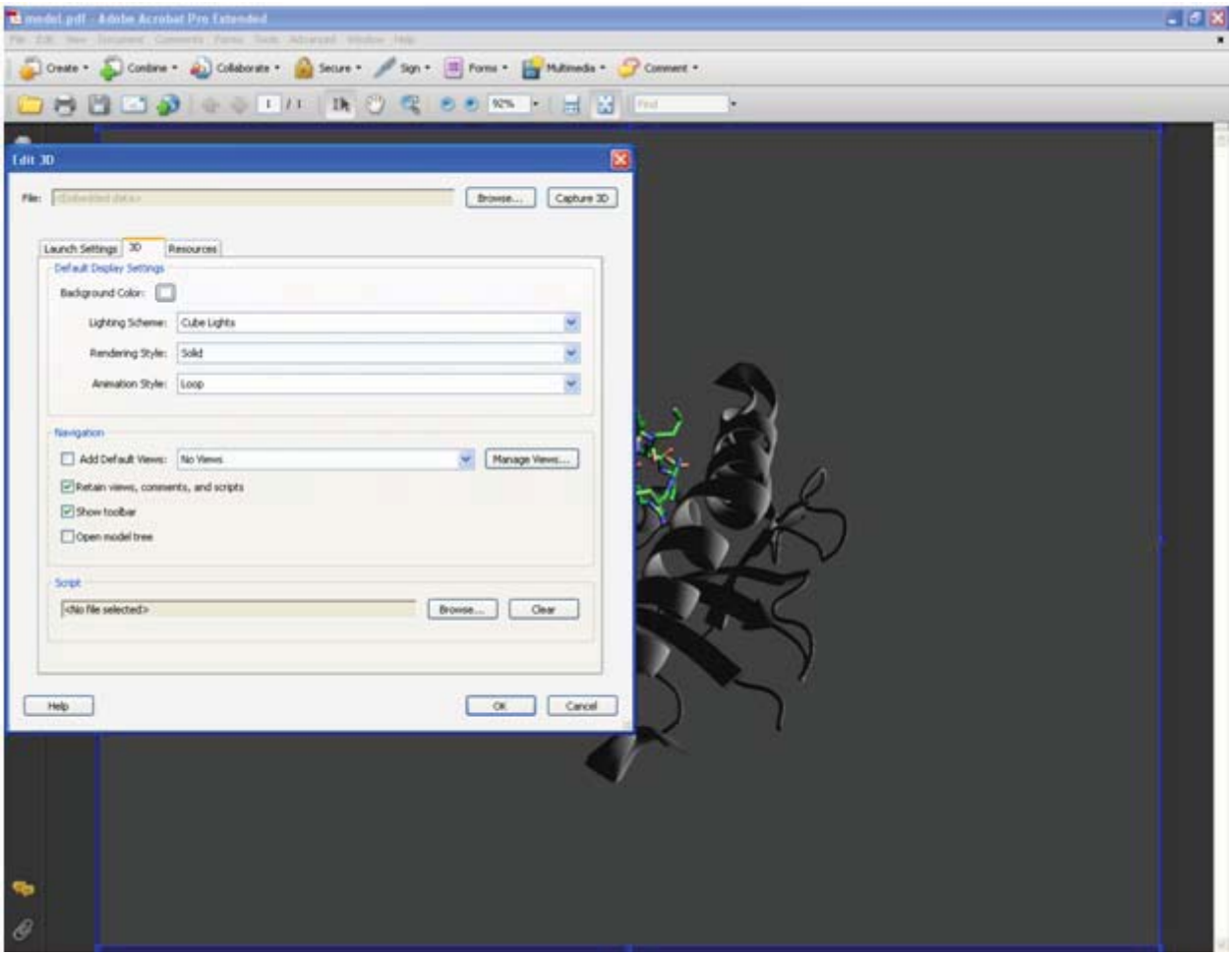

On clicking “OK” you will see the static 2D image you have chosen (Figure 12). Click anywhere on the image to activate the 3D display of the molecule.

Figure 12:

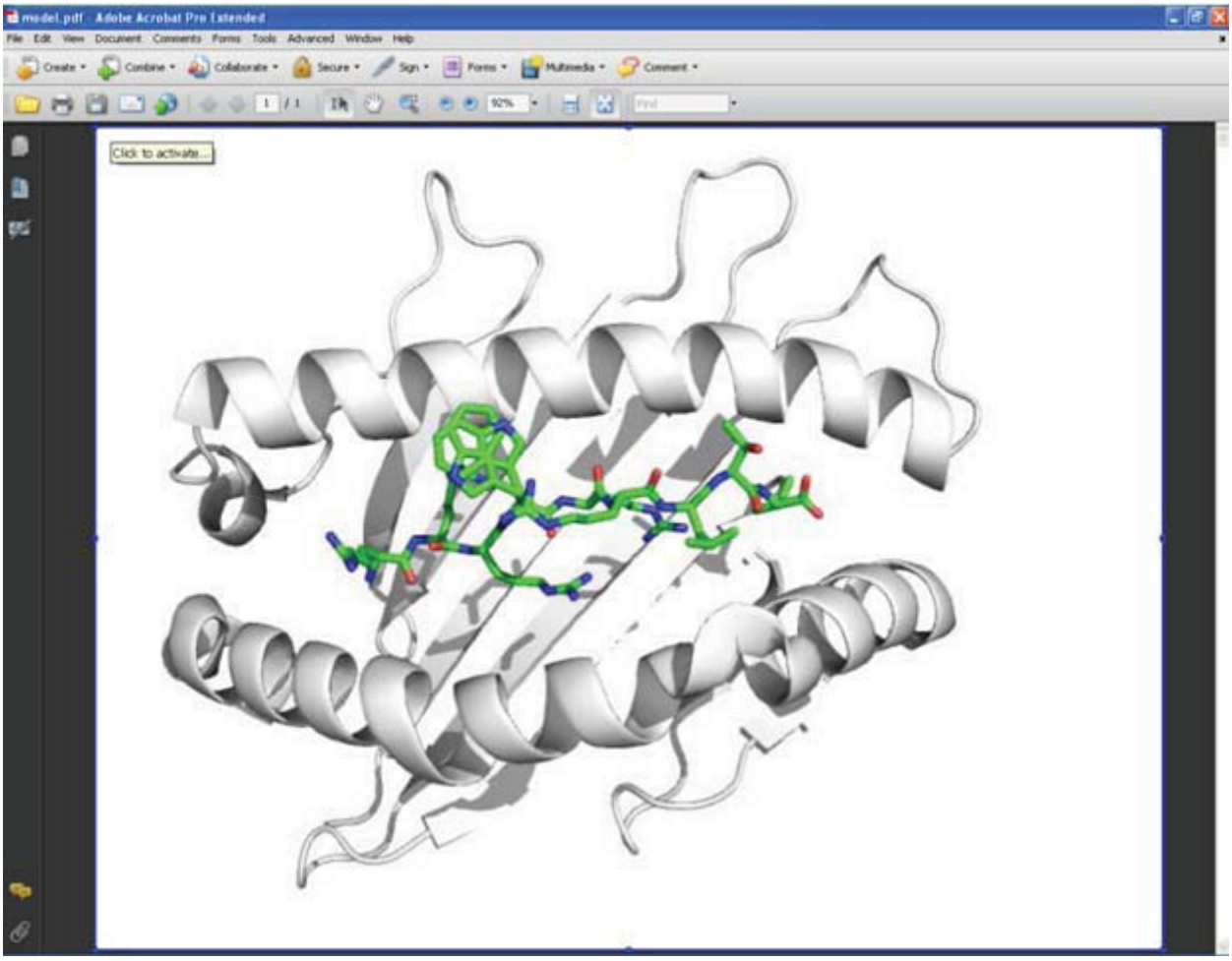

Click on the “Model tree” icon to display the model tree pane (Figure 13). This will permit you to add predetermined views for the reader (if you added the default views above, you can use these as the basis for your own views e.g. by zooming in on them, etc and renaming them).

Figure 13:

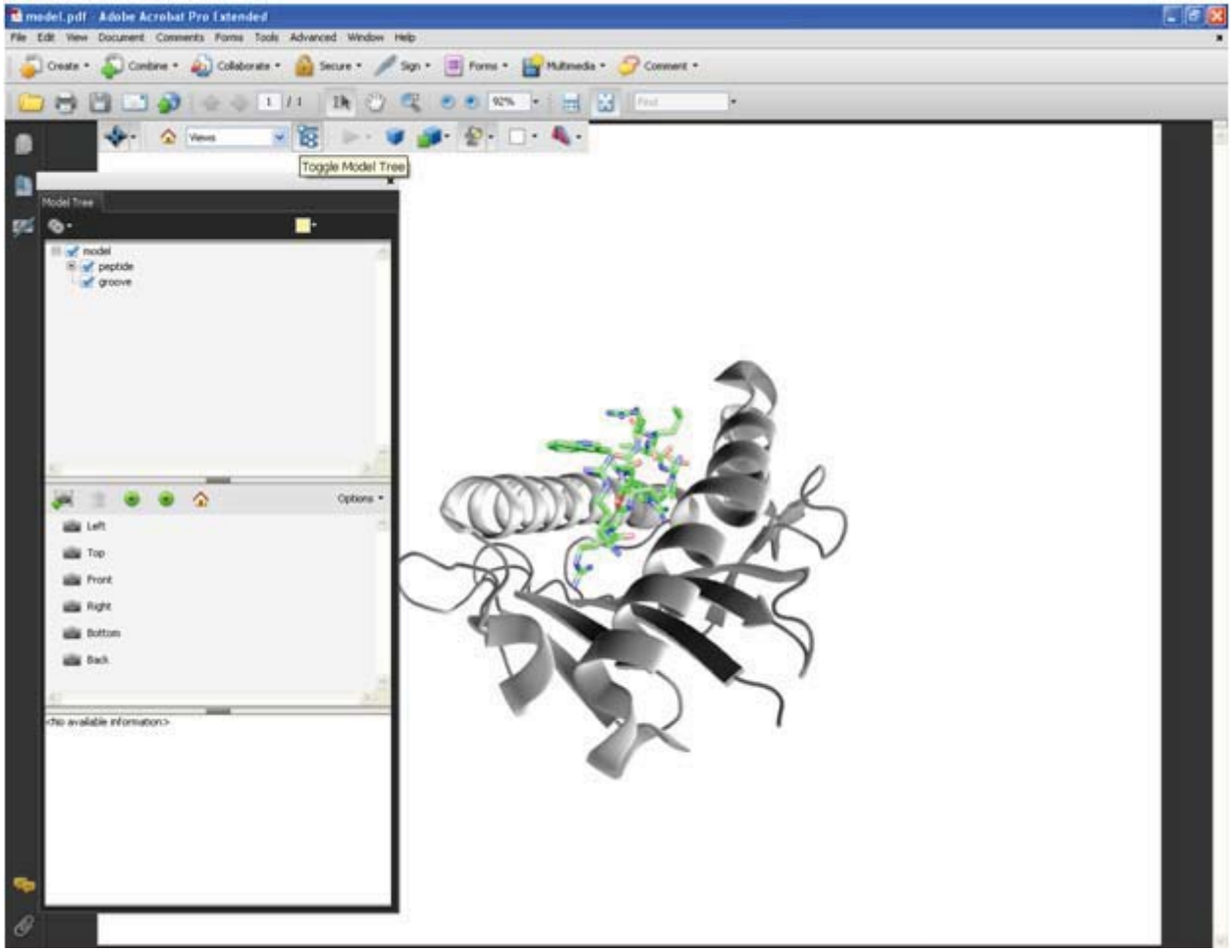

To add further views, after generating a new display for your molecule (by zooming, dragging and rotating with the mouse) click on the “Create View” icon to embed this view in the model tree (Figure 14).

Figure 14:

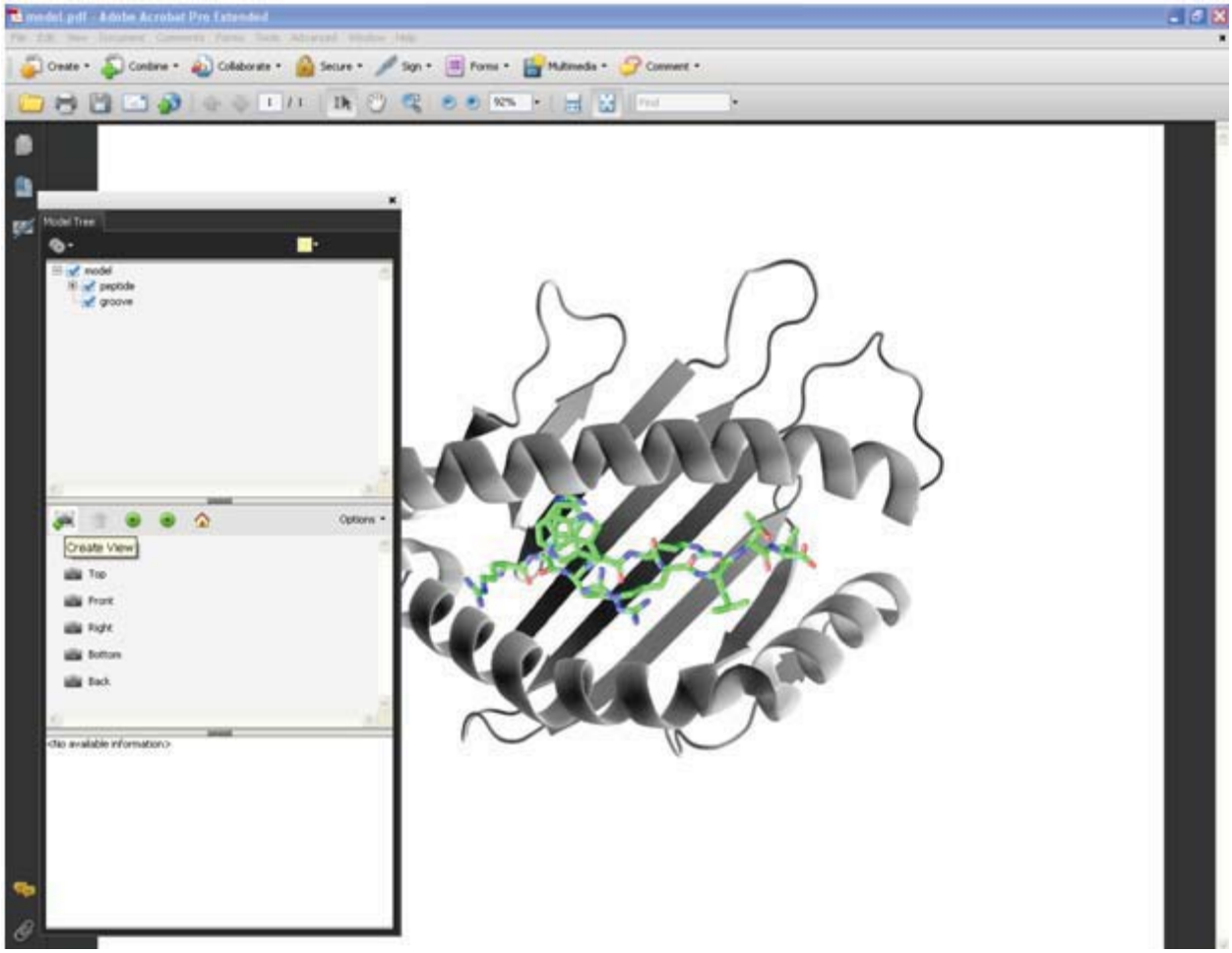

Rename the designation of the new view to your liking by double clicking the “NewView” title (Figures. 15 and 16).

Figure 15:

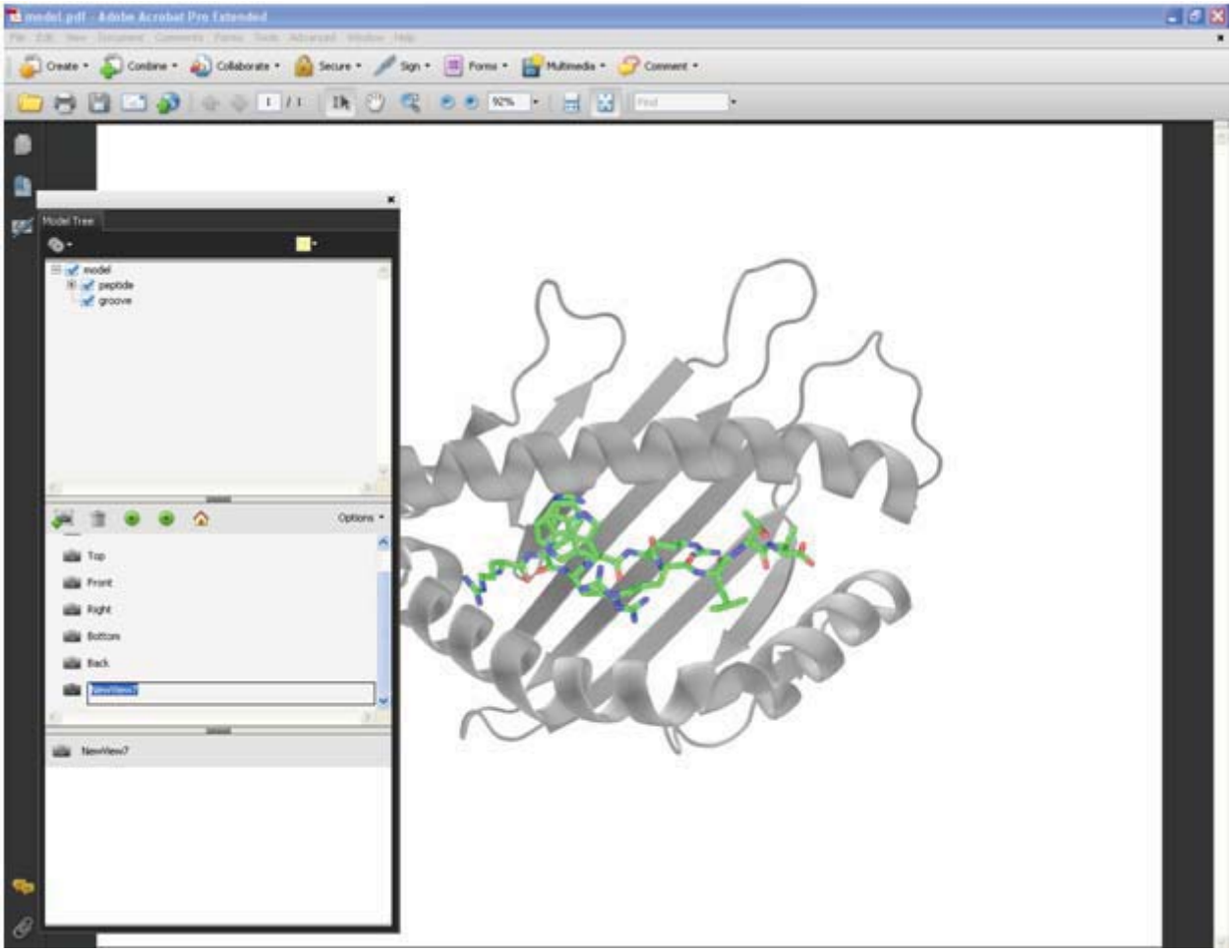

Figure 16:

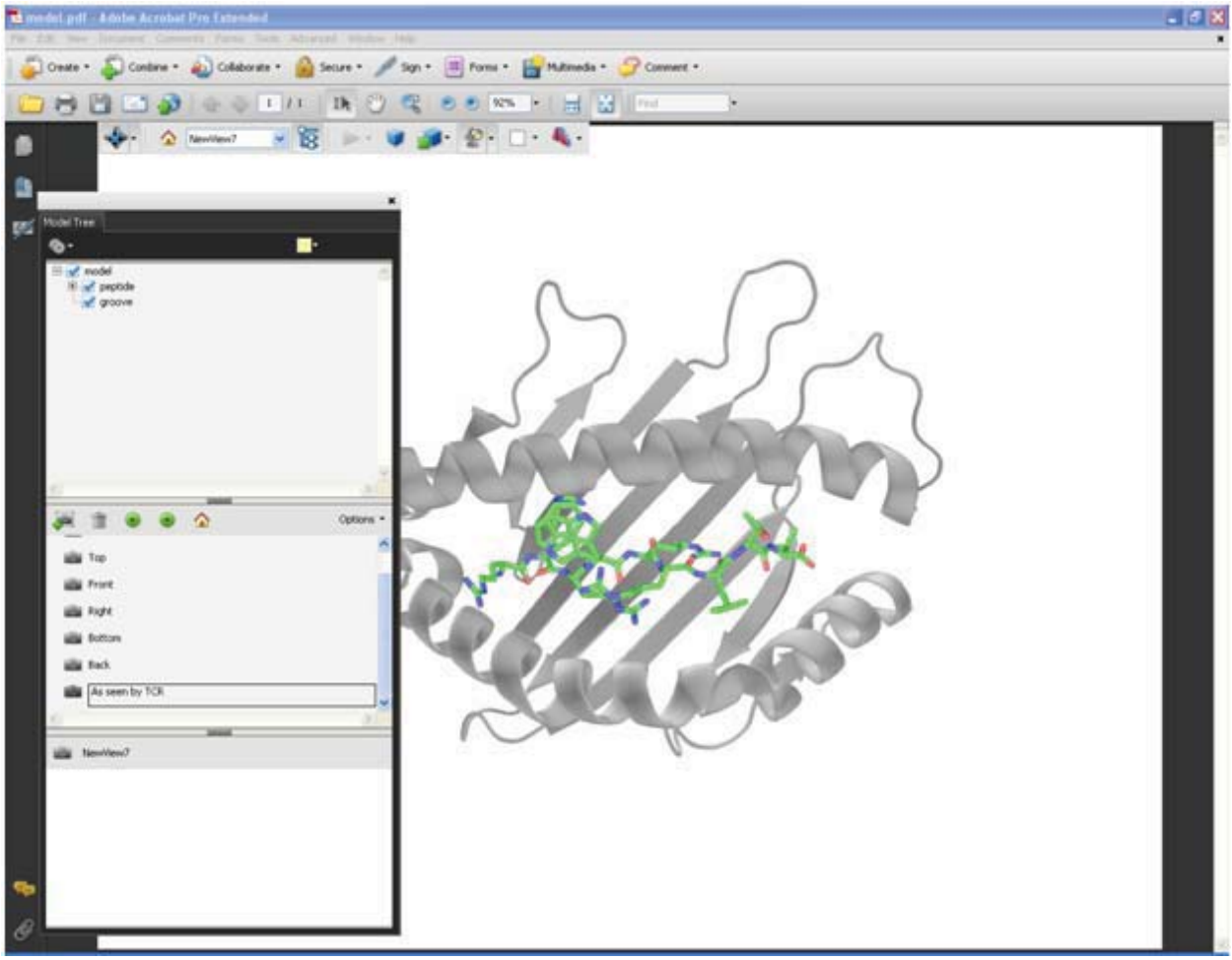
model.pdf - Adobe Acrobat Pro Extended
Create
Combine
Collaborate
Secure
Sign
Forms
Multimedia
Comment
NewView7
Model Tree
model
peptide
groove
Options
Top
Front
Right
Bottom
Back
As seen by TCR
NewView7

From the listing in the model tree, choose a “Default view” that will be seen when the 3D mode is activated by the reader (Figure 17).

Figure 17:

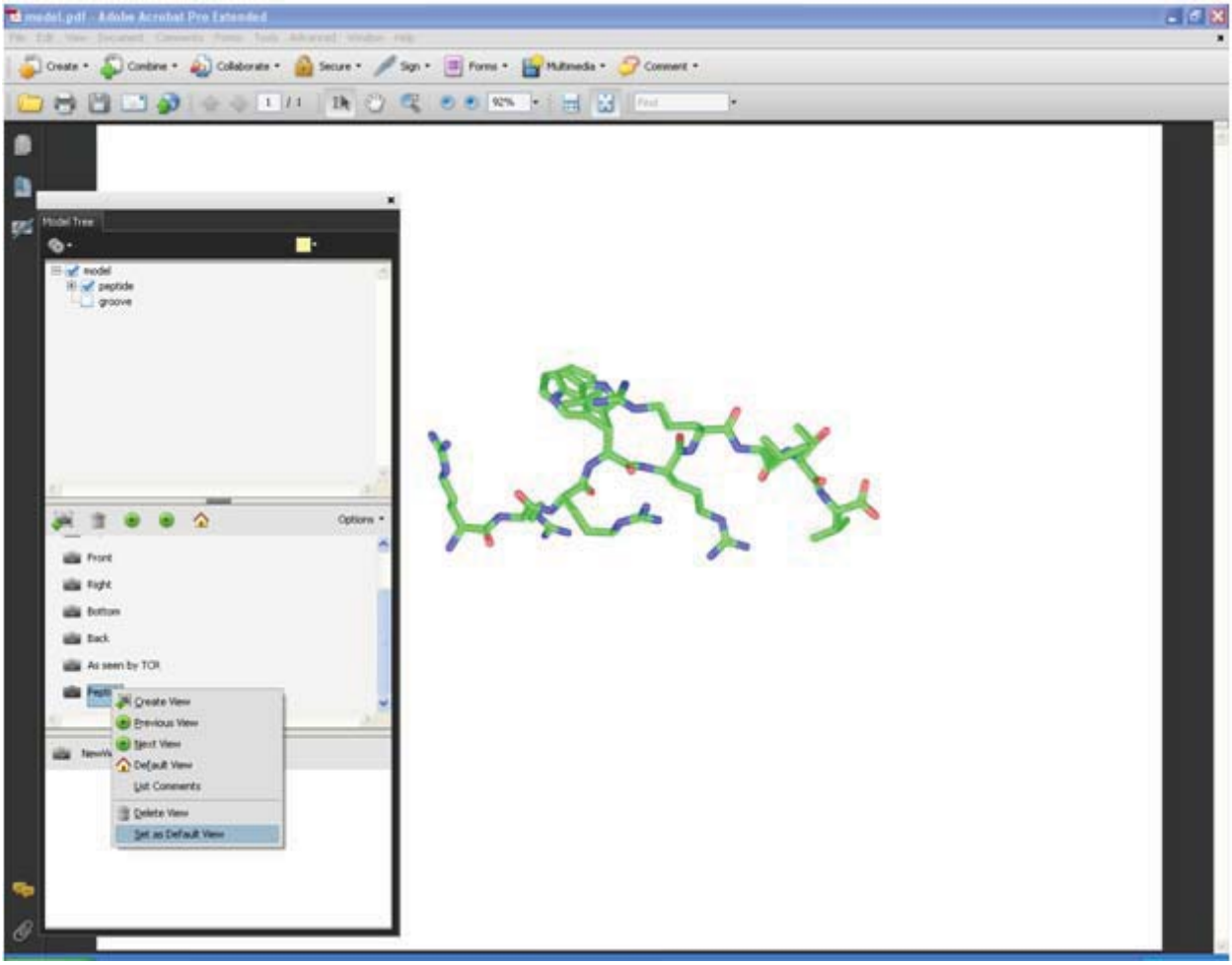

Save the file as a PDF and exit Adobe Acrobat 9 Pro Extended.

Step 4: You will now be able to open the PDF that you have just created in Adobe Reader or Adobe Acrobat 7.1 or higher and view the 3D model.

6. Discussion

This study was undertaken to characterize the effects of MHC polymorphism, peptide sequences and ligand binding that result in conformational variability of pMHC complexes. The comparative analysis of the presentation of pCatA and pLMP2 peptides by B*1402, B*2705 and B*2709 (Kumar et al. 2009a) enabled us to perform a detailed study of the effects of MHC polymorphisms on the binding mode of the presented peptides.

The second part of the work on structural and biophysical analysis of the presentation of the pB27 and pCP peptides by the B*2705 molecule (Kumar et al., unpublished) improved our understanding of how small differences in peptide sequences can lead to drastic differences in their binding mode. The binding of pB27 peptide in three distinct conformations in the binding groove of the B*2705 molecule and the indications of its dynamics indicate that the peptide conformation is dictated by opposing molecular forces within the groove that lead to its ‘molecular frustration’ (Dong et al. 2007). A detailed structural analysis by NMR of the presentation of the pB27 and pCP peptides by the B*2705 molecule may be necessary to identify the molecular factors that are responsible for ‘frustration’ of the pB27 peptide.

The related structural study on the presentation of a citrullinated version of the pVIPR peptide by the B*2705 and B*2709 molecules (Beltrami et al. 2008) helped us appreciate the drastic influence of replacing a single non-hydrogen atom on overall conformation of a peptide.

After studying the effects of HC polymorphism and peptide sequences on the conformational variability of pMHC, the third crucial factor involved in conformational variability of pMHC complexes, ligand binding, was studied by comparing the effects of Fab-Hyb3 binding on the conformation of HLA-A1:MAGE-A1 (Kumar et al. 2009b). A detailed comparison of pMHC structures in free and ligand-bound forms helped us to identify the subtle but, at least to some extent, systematic changes associated with ligand-binding to pMHC.

Finally, a method to embed 3D imagery of molecular structures into PDF documents was developed. It enables the reader to access 3D structural information using the freely available Adobe Reader in a simple and convenient way (Kumar et al. 2008). No extra downloads and installations are necessary to view the 3D contents and the

information would be available to the reader as part of the original article. This finding permits authors to display subtle structural variability such as the dual conformation of a peptide as in the B*2705:pVIPR or the B*2705:pGR structure (Hülsmeyer et al. 2004, Rückert et al. 2006) as part of the article in 3D.

The implications of the studies on conformational variability in MHC class I complexes of B*1402:pCatA, B*1402:pLMP2, B*2705:pCatA, B*2709:pCatA and HLA-A1:MAGE-A1 have been discussed at length in chapters 2-5. I will concentrate here on the importance of conformational dynamics in peptide presentation (which was briefly discussed in the section 3.2 describing the structures of the B*2705:pB27 and B*2705:pCP complexes) and on conserved water molecules in the peptide binding groove of HLA class I molecules.

6.1 Conformational dynamics in antigen presentation by the B*2705 molecule

Both pB27 and pCP peptides are bound in relatively flexible states by the B*2705 (Fig. 3.1, 3.3). The three distinct conformations in which the pB27 peptide is presented and the single conformation in which the pCP peptide is displayed by the B*2705 molecule have no clear overlap (Fig. 3.6, 3.7) to suggest conformational similarity and molecular mimicry of the kind observed between pVIPR and pLMP2 in the context of presentation by the B*2705 molecule (Hülsmeyer et al. 2004, Fiorillo et al. 2005, see also Fig. 1.7). Part of the Cα backbone of the “bulged-out” conformation C of pB27 overlaps with that of the pCP conformation (Fig. 3.6, 3.7). However, the side chain conformations of residues p3 to pΩ-1 are different. The electron density map of the pB27 peptide tacitly suggests dynamic interconversion between the three conformations of pB27, while the single pCP conformation is more clearly and distinctly defined in electron density maps (Fig. 3.1, 3.3). It must, however, be noted that as the conformations of the pB27 and pCP peptides had to be traced from 2Fo-Fc maps contoured at 0.6σ and the electron density maps contoured at higher σ-levels allow only partial localization of the peptide conformations, both the peptides can be expected to be bound in somewhat flexible conformations.

Despite the intrinsic conformational flexibility of the pB27 and pCP peptides, the T_m values obtained by CD and DSC spectroscopy for the thermal denaturation of the B*2705:pB27 and B*2705:pCP complexes are in the range of the values obtained for most other HLA-B27 complexes (Ziegler et al. 2009a) (Fig. 3.5, Table 3.2), indicating

that the two complexes are not destabilized by the flexibility of the bound peptides. The T_m values for the B*2705:pCP complex are 3-4°C higher than those for the B*2705:pB27 complex, suggesting its slightly higher stability.

The conformations of pCP and pB27 do not overlap significantly (Fig. 3.6, 3.7) suggesting a lack of the potential for “conventional” molecular mimicry (Hülsmeyer et al. 2004, Fiorillo et al. 2005) between them. But the dynamics in the conformations of pB27 suggests that some of the intermediate conformations that are not represented in the three conformations modeled from the electron density maps may overlap with the conformation of pCP, thus creating an instantaneous state of antigenic mimicry or “dynamic mimicry”. This dynamic mimicry could result in cross-reactivity of the B*2705-restricted T cells directed against pCP in individuals with a *Chlamydia trachomatis* infection with the B*2705-bound pB27 self-peptide, thereby triggering an autoimmune response which might lead to ReA.

The preliminary evidence of the dynamics of the pB27 conformation provided by the X-ray structures determined in this study requires further analysis by employing additional methods which can provide a more elaborate view of the dynamics and the involved interactions.

Conformational flexibility is an intrinsic feature of proteins that enables their efficiency in molecular interactions essential for their biological function (Dodson and Verma 2006, Teilum et al. 2009). Conformational changes taking place in protein structures during processes such as enzymatic catalysis, protein folding, and protein-ligand interactions are often of large magnitude, and developing an accurate structural model of these processes remains a major challenge (Teilum et al. 2009). While the structure ensembles obtained using nuclear magnetic resonance (NMR) spectroscopy give a more detailed view of the dynamics of the structure, owing to inherent limitations of the method it cannot be employed to study structures of larger proteins with as much ease as X-ray crystallography, although some promising advances have been made in the last years in NMR of large proteins (Fiaux et al. 2002, Tzakos et al. 2006). Not surprisingly, of the 7028 structures deposited in the PDB in the year 2008, about 90% were determined by X-ray crystallography, whereas fewer than 10% were determined by NMR spectroscopy (PDB statistics 2009, www.pdb.org). However, the structural details provided by X-ray crystallography represent a static view of the time- and motion-averaged protein

conformation in the crystal lattice and conformations of short lived intermediate states or low abundance conformations of residue side chains, loops and domains cannot be traced from a single crystal structure as well as is possible using NMR spectroscopy (Yee et al. 2002). Moreover, the physical extent of conformational flexibility cannot be traced from the atomic details described in crystal structure data, although electron density maps and thermal vibration parameters give an indication of the relative mobility of an atom (Levin et al. 2007). Crystallographic temperature factors may include nondynamical contributions such as static disorder and refinement errors and hence cannot be considered a reliable indicator of atomic mobility (Daniel et al. 2003).

An emerging method for studying protein dynamics is molecular dynamics (MD) simulations which permit theoretical calculation of the dynamics of a protein based on its crystal structure (Sherwood et al. 2008). However, the timescale of MD simulations is a crucial factor in determining the amount of the structural details revealed. Conformational changes such as rotation around a covalent bond occur in pico- to nano-second timescales, while conformational changes associated with protein-ligand association/dissociation and protein folding/unfolding may occur in timescales of hours (Teilum et al. 2009). Due to computational limitations, MD simulations rarely extend to the microsecond range and typically cover only nanosecond timescales (e.g. Pöhlmann et al. 2004, Ziegler et al. 2009a). Recent technological advances such as the development of time-resolved X-ray crystallography permits the resolution of the dynamics of the structure of myoglobin over the pico-second to milli-second timescales (Srajer et al. 2001). However, the method is still under development and it would be some time before it can be routinely employed for the analysis of other proteins. Other methods that are being developed to analyze protein dynamics include neutron scattering, small angle X-ray scattering (with ensemble optimization method, Bernadó et al. 2007), Mössbauer spectroscopy and single-molecule Förster resonance energy transfer (FRET) (Daniel et al. 2003, Parak 2003).

Common forms of conformational variability observed in MHC class I molecules include shift of the Cα-atoms located in loop regions in the heavy chain (Kumar et al. 2009b) and in β_2m, shift of the Cα atoms of residues near the N-terminus of the α2-helix (Kumar et al. 2009b), rotation of the α3-domain relative to the α1 and α2

domains (Reiser et al. 2003), rotation of β_2m relative to the α1 and α2 domains (Reiser et al. 2003), partial winding/unwinding of the ends of the α1 and α2 helices which may result in a shift of the entire α3 domain (personal observation), changes in the distance between the axes of the α1 and α2 helices, changes in orientation of side chains of one or more residues of the peptide, and substantial changes in orientation of several peptide residues (Kumar et al. 2009a).

However, the kind of conformational plasticity observed in binding of pB27 to B*2705 has not been seen before for any MHC class I molecule. In the two extreme conformations A and C, the Cα atoms of pLys8 are separated by 11.2 Å. Although it is not possible to conclusively prove the dynamics of different pB27 conformations based on the X-ray data, the structural evidence indicates the possibility of dynamic interconversion among different pB27 conformations. The intermediate conformations may be short-lived, which explains the lack of 'smeared' electron density in the regions intermediate between A, B and C. The details of the dynamics of the pB27 conformations could be studied using MD simulations. An MD simulation study of the B*2709:m9 complex (Pöhlman et al. 2004) revealed that the pΩ residue of the m9 peptide briefly detaches from the F-pocket in a 20ns simulation (see also Ziegler et al. 2009a). Even though the m9 peptide was found to have a suboptimal affinity and architecture for binding to B*2709, the electrostatic interactions that anchor the pΩ side chain of the m9 peptide within the F-pocket appear to be more numerous than the electrostatic interactions responsible for binding of the middle part of the pB27 peptide within the peptide binding groove of B*2705 in the B*2705:pB27 structure. So it may be reasoned that transitions between pB27 peptide conformations may be observed even in nanosecond scale molecular dynamics simulations. On the other hand, it is more than likely that many interactions formed between the pB27 peptide and the B*2705 molecule cannot be deduced from our current model of the complex. Thus, any conclusions drawn about the putative interactions between pB27 and B*2705 need to be carefully evaluated and confirmed by other methods.

6.2 Conserved water molecules in the peptide binding groove of HLA class I molecules

The anchoring of peptides within the binding groove of HLA class I molecules is aided by several water molecules that facilitate crucial interactions between peptide and HC residues and render the structure the necessary flexibility to accommodate

peptides with diverse sequences (Ogata and Wodak 2002, Petrone and Garcia 2004). The flexibility of water networks allows stable binding of a variety of peptides into a given MHC binding groove and may be responsible for the ability of an MHC molecule to adjust its binding surface to accommodate a vast range of peptides

Table 6.1. HLA class I molecules selected for comparison of conserved water molecules

No.	Subtype	Peptide	PDB ID	Resolution (Å)	No. of Water Molecules	Reference
HLA-B27 structures						
1.	B*2709	m9	1k5n	1.0	971	Hülsmeyer et al. 2002
2.	B*2709	pGR	3czf	1.2	741	Loll et al., unpub.
3.	B*2705	pGR	2a83	1.4	712	Rückert et al. 2006
4.	B*2705	pCP	3kil	1.4	625	Kumar et al., unpub.
5.	B*2705	pVIPR	1ogt	1.4	751	Hülsmeyer et al. 2004
6.	B*2705	pB27	3kib*	1.5*	616	Kumar et al., unpub.
7.	B*2705	pLMP2	1uxs	1.5	734	Fiorillo et al. 2005
8.	B*2709	pLMP2	1uxw	1.7	626	Fiorillo et al. 2005
9.	B*2709	pCatA	3bp7	1.8	519	Kumar et al. 2009a
10.	B*2705	pVIPR-U5	3b6s	1.8	555	Beltrami et al. 2008
11.	B*2705	pCatA	3bp4	1.8	515	Kumar et al. 2009a
12.	B*2709	pVIPR-U5	3b3i	1.8	464	Beltrami et al. 2008
13.	B*2705	m9	1jge	2.1	462	Hülsmeyer et al. 2002
14.	B*2709	TIS	1w0w	2.1	451	Hülsmeyer et al. 2005
15.	B*2709	pVIPR	1of2	2.2	360	Hülsmeyer et al. 2004
16.	B*2705	TIS	1w0v	2.2	432	Hülsmeyer et al. 2005
Non-HLA-B27 structures						
17.	B*1402	pCatA	3bxn	1.8	576	Kumar et al. 2009a
18.	B*1402	pLMP2	3bvn	2.5	125 (each complex)	Kumar et al. 2009a
19.	HLA-A1	MAGE-A1	3bo8	1.8	605	Kumar et al. 2009b

* For the purpose of this comparison, the three determined models of the B*2705:pB27 complex are represented by this single model.

(Petrone and Garcia 2004) or a given peptide (e.g. pVIPR) in two clearly distinct conformations (Hülsmeyer et al. 2004).

The analysis of Ogata and Wodak (2002) identified a number of water molecules which are involved in key interactions integral to the MHC-fold and are hence conserved in the majority of MHC class I structures. The three most conserved of these water molecules are postulated to be involved, respectively, in stabilizing the conformation of a twisted β-turn between HC residues 118 and 122, in the anchoring of the peptide N-terminus within the A-pocket of MHC molecules and in determining the position of the N-terminal segment of the α2-helix which also interacts with peptide residues (Ogata and Wodak 2004).

With the objective of understanding the role of water molecules located in the vicinity of the peptides in HLA class I molecules, a comparison of the location of water molecules in 16 high resolution structures of HLA-B27, two structures of B*1402 and one structure of HLA-A1 complexes was performed to identify conserved water molecules (Table 6.1).

6.2.1 Conserved water molecules within the HLA-B27 peptide binding groove

About 110 water molecules appear to be conserved in the 16 HLA-B27 structures included in this study, and over 330 water molecules appear to be conserved in at least 10 of the 16 HLA-B27 structures analyzed. For the purpose of identifying the most crucial water molecules mediating peptide anchoring in the peptide binding groove of HLA-B27, water molecules located within 5Å of peptides in all of the 16 structures were analyzed.

There are 12 water molecules in the vicinity of the bound peptides that are present in at least 10 of the 16 analyzed structures (Table 6.2). Their conservation was determined based on their belonging to a geometrically distinct cluster of water molecules and the retention of interactions mediated by a majority of the members of the water cluster, in cases where water clusters could not be considered to be geometrically isolated enough due to a large spread in the cluster. Maximum spread is defined as the largest Euclidean distance between two members of a water cluster. The Cα-atoms of the α1- and α2-domains of all the 16 structures were overlayed for this comparison.

Table 6.2. Conserved water molecules in the peptide binding groove of HLA-B27 molecules

No.	Coordinates in 1k5n*			No. of structures (out of 16)	Max. spread (Å)	Designation in 1k5n*
	x	y	z			
CW1	12.56	11.51	19.04	16	0.8	A2077
CW2	19.91	12.31	21.02	16	0.5	A2009
CW3	22.31	12.99	19.83	15	1.5	C463
CW4	23.75	14.36	22.12	14	2.1	A2398
CW5	18.51	17.55	14.25	10	1.5	A2409
CW6	20.68	18.58	14.47	14	2.6	C272
CW7	36.11	10.83	22.26	16	0.9	A2056
CW8	37.54	10.76	19.80	13	1.1	A2263
CW9	41.38	14.45	23.11	10	0.4	A2031
CW10	27.24	3.04	23.90	16	1.3	A2179
CW11	38.26	20.20	17.82	16	0.7	A2063
CW12	38.15	21.51	15.38	15	1.1	A2201

*The 1.0 Å resolution structure of the B*2709:m9 complex (1k5n) is the highest resolution HLA class I structure available to date, and was chosen as the standard for all comparisons performed in this chapter due to its high ordered water content (see table 6.1).

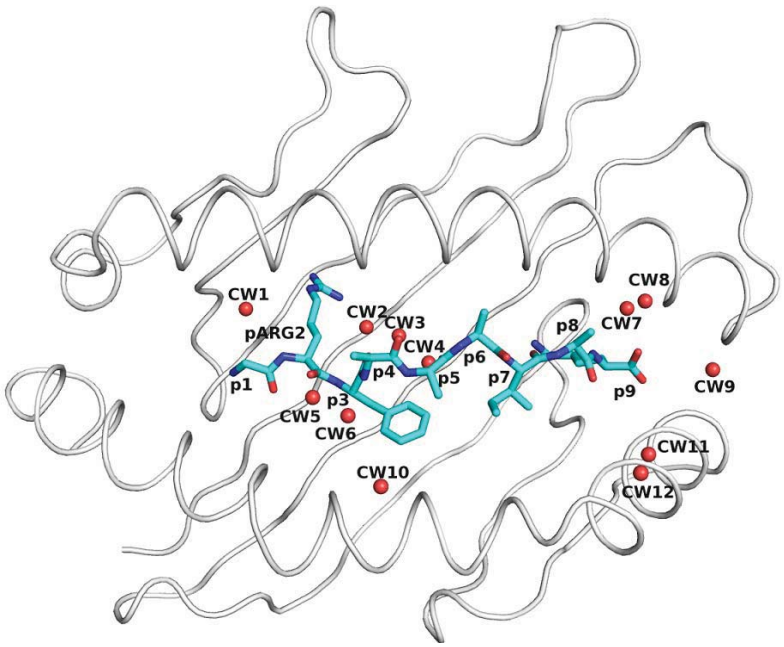

FIGURE 6.1. Conserved water (CW) molecules in the peptide binding groove of HLA-B27 molecules. The location of water molecules in the B*2709:m9 complex is shown. CW1-9 are involved in mediating contacts between peptide and HC, while CW10-12 have less direct roles in peptide anchoring.

Among the twelve conserved water molecules (Fig. 6.1), three (CW10, CW11 and CW12) do not appear to be directly involved in mediating contacts between peptide residues and HC. CW10 serves as an anchor point for hydrogen bonding between Gln155^{O} and the highly variant peptide residues in the middle section of the binding groove. CW11 and CW12 mediate hydrogen bonding between Lys146^{O} and Ala149^{O}. The nine water molecules (CW1-9) that mediate contacts between peptide and HC are located near the N- and C-termini of the peptides, eight of which engage with only main chain atoms of the peptide, while one mediates hydrogen bonding between pArg2, the anchor residue of all HLA-B27-binding peptides, and Tyr99^{OH}.

The conserved water molecules CW1 to CW6 are located near residues 1 to 4 of peptides (Fig. 6.1, 6.2). The water molecule CW1 is involved in anchoring of peptide N-terminal atom p1^{N} by serving as one of the five corners of a pentagonal hydrogen bond network, where it also mediates interaction of Glu63 with the pentagonal hydrogen bond network. It is referred to as water W in section 2.2.2, Fig. 4, and its role has been discussed in detail in that chapter. CW2 mediates hydrogen bonding between the pArg2^{NH1}, His9^{NE2} and Tyr99^{OH} atoms (Fig. 6.2). This is a key interaction for anchoring of peptides, as pArg2 is the primary anchor residue and is found in nearly all ligand peptides of HLA-B27 (Lopez de Castro et al. 2004), and Tyr99 is also found in all HLA-B27 subtypes. Water molecules CW3 and CW4 mediate hydrogen bonding between Glu163 side chain atoms, p2^{O} and p4^{N} atoms, while CW5 and CW6 mediate hydrogen bonding between p3^{O} and Asn97^{OD1} atoms (Fig. 6.2).

On the C-terminal side of the peptide (Fig. 6.3), CW7 mediates interactions among the pΩ-1^{N}, pΩ^{O}, Asp77^{OD1} and Thr80^{OG1} atoms, CW8 bridges hydrogen bonding between Glu76^{OE1} and CW7, and CW9 mediates the interaction between the Tyr84^{OH} and the Lys146^{NZ} atoms, and forms one corner of a pentagonal hydrogen bond network that serves to anchor the C-terminal atoms pΩ^{O} and pΩ^{OXT} of peptides. The water clusters CW3, CW4, CW5, CW6, and CW8 have spreads larger than 1Å, while all others have smaller spreads (Table 6.2). The spreads in the clusters CW3 and CW4 appear to be a consequence of the occasional interaction of the Arg62^{NH2} atom with these two water molecules. The flexibility of the side chains of Arg62 and Glu163 (Hillig et al. 2004) requires rearrangements in the location of the water molecules mediating their interaction with peptides. The spread in the clusters CW5 and CW6 appears to be due to occasional interaction of Lys70^{NZ} and side chain atoms of the

p3 residue with them, while the spread in the CW8 cluster seems to be a consequence of the flexibility in the side chain of Glu76. Furthermore, due to the flexibility of the Lys146 side chain, CW9 is not always necessary to mediate hydrogen bonding between Lys146 NZ and Tyr84^{OH} and is the least conserved of all the conserved water molecules described here, although, when present, it exhibits the lowest degree of deviation (Table 6.2). It has been noted that HLA-B27 subtype-specific differences in water mediated interactions (Fiorillo et al. 2005, Fabian et al. 2009) formed between peptide and HC residues could result in differences in flexibility of the subtypes, thereby altering their biophysical and peptide presentation properties. A tighter network of solvent-mediated interactions have been observed in the B*2709:pLMP2 complex, whereas the hydrophobic section of the pArg5 side chain prevents formation of similar solvent-networks in the B*2705:pLMP2 complex, resulting in a higher flexibility of the peptide (Fiorillo et al. 2004). A detailed analysis may reveal subtype-dependence of water-mediated interaction in HLA-B27 molecules and may help understand differential flexibility of different HLA-B27 subtypes (Fabian et al. 2009).

6.2.2 Comparison of conserved water molecules mediating peptide anchoring in B*1402 and HLA-B27

A comparison of the three structures of B*1402 (two molecules of the B*1402:pLMP2 asymmetric unit, and one molecule of B*1402:pCatA) with the HLA-B27 structures discussed in the previous section, demonstrates that some of the conserved water molecules of HLA-B27 molecules are also present in the B*1402 structures (Fig. 6.2).

As described previously in detail, due to the presence of His171 in B*1402, the hydrogen bond network anchoring the peptide N-terminus is different in B*1402 structures from that in HLA-B27 structures (section 2.2.2, Fig. 4). The conserved water molecule CW1 of HLA-B27 is also present in B*1402 structures (designated as W in Section 2.2.2, Fig. 4), but the differential positioning of peptide N-termini in the B*1402 structures introduces an additional conserved water molecule (designated as W' in Section 2.2.2, Fig. 4) only in the B*1402 structures.

As B*1402 has a Tyr at position 9, the position of CW2 is occupied by the hydroxyl group of Tyr9 (Fig. 6.2B). CW3 is conserved also in B*1402, so that the interactions between pArg2^{NH1}, Tyr99^{OH}, Tyr9^{OH}, p3^{N} and p3^{O} are observed in the B*1402

structures as well. On the other hand, the position of CW4 is occupied by the bulky side chain of Trp97. Furthermore, the presence of Thr at position 163 makes the contact between its shorter side chain with peptide main chain atoms less feasible than in case of HLA-B27, and hence, CW5 and CW6 do not appear to be conserved in B*1402 (Fig. 6.2).

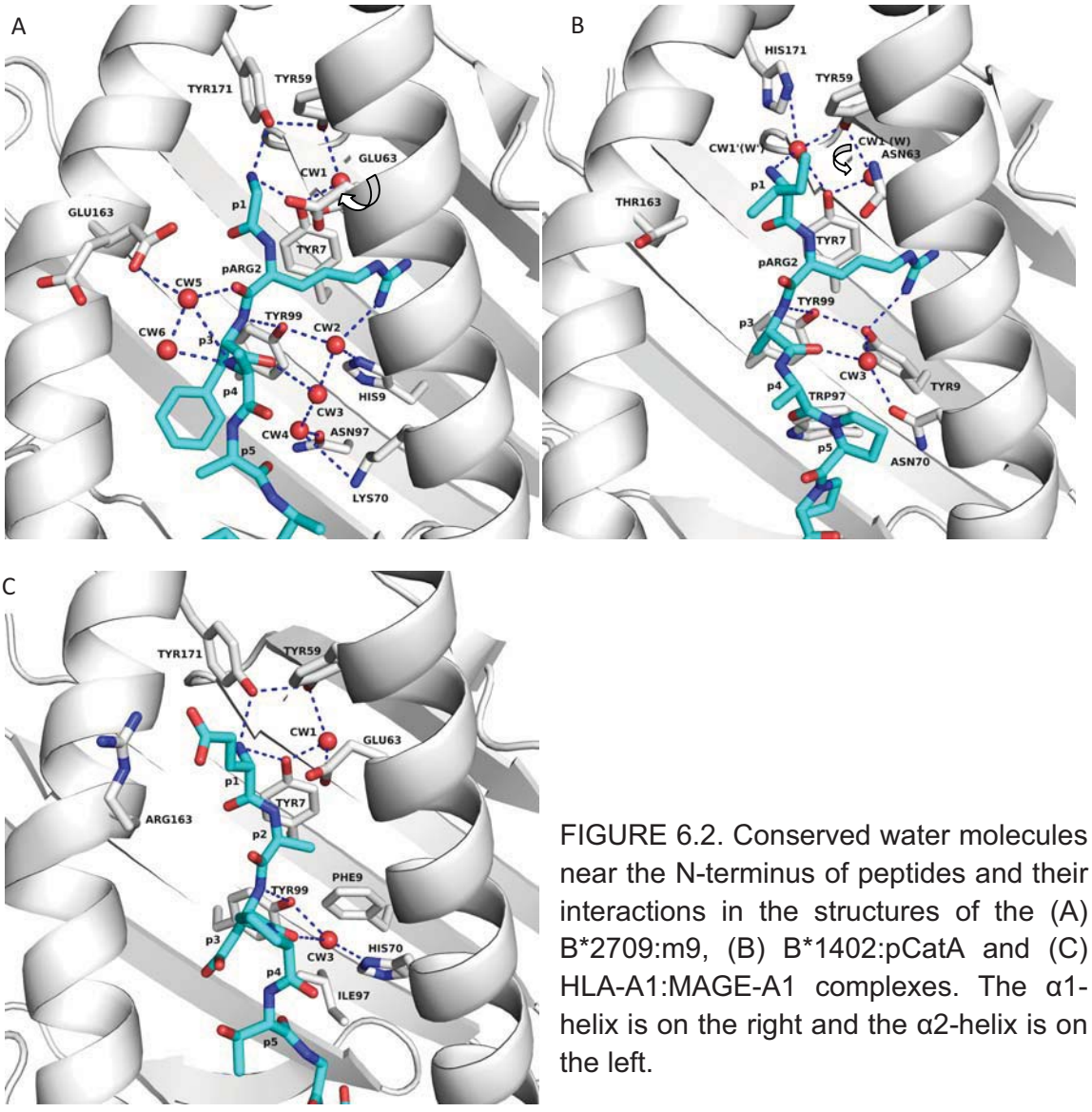

FIGURE 6.2. Conserved water molecules near the N-terminus of peptides and their interactions in the structures of the (A) B*2709:m9, (B) B*1402:pCatA and (C) HLA-A1:MAGE-A1 complexes. The α1-helix is on the right and the α2-helix is on the left.

The anchoring of the C-terminal atoms of peptides in B*1402 (Fig. 6.3B) is very different from that in HLA-B27 structures: neither of the most conserved water molecules near the peptide C-terminus in HLA-B27 (CW7 and CW8) are present in any of the B*1402 structures analyzed. Unlike HLA-B27, the atoms O and OXT of the

C-terminus are anchored primarily through direct hydrogen bonds with Ser77 and Asn80 in B*1402 (Fig. 6.3B). The conserved water molecule CW9 which mediates interaction between Tyr84 and Lys146, is observed in one of the three analyzed structures of B*1402. This is in line with our previous assertion that the presence of this water molecule is peripheral to anchoring of the peptide C-terminal atoms O and OXT, as it appears to be the least conserved of all conserved water molecules of HLA-B27 described in the previous section.

6.2.3 Comparison of conserved water molecules mediating peptide anchoring in HLA-A1 and HLA-B27

A comparison of the HLA-A1:MAGE-A1 structure with the structures of HLA-B27 shows that there are less water molecules mediating peptide anchoring in the binding

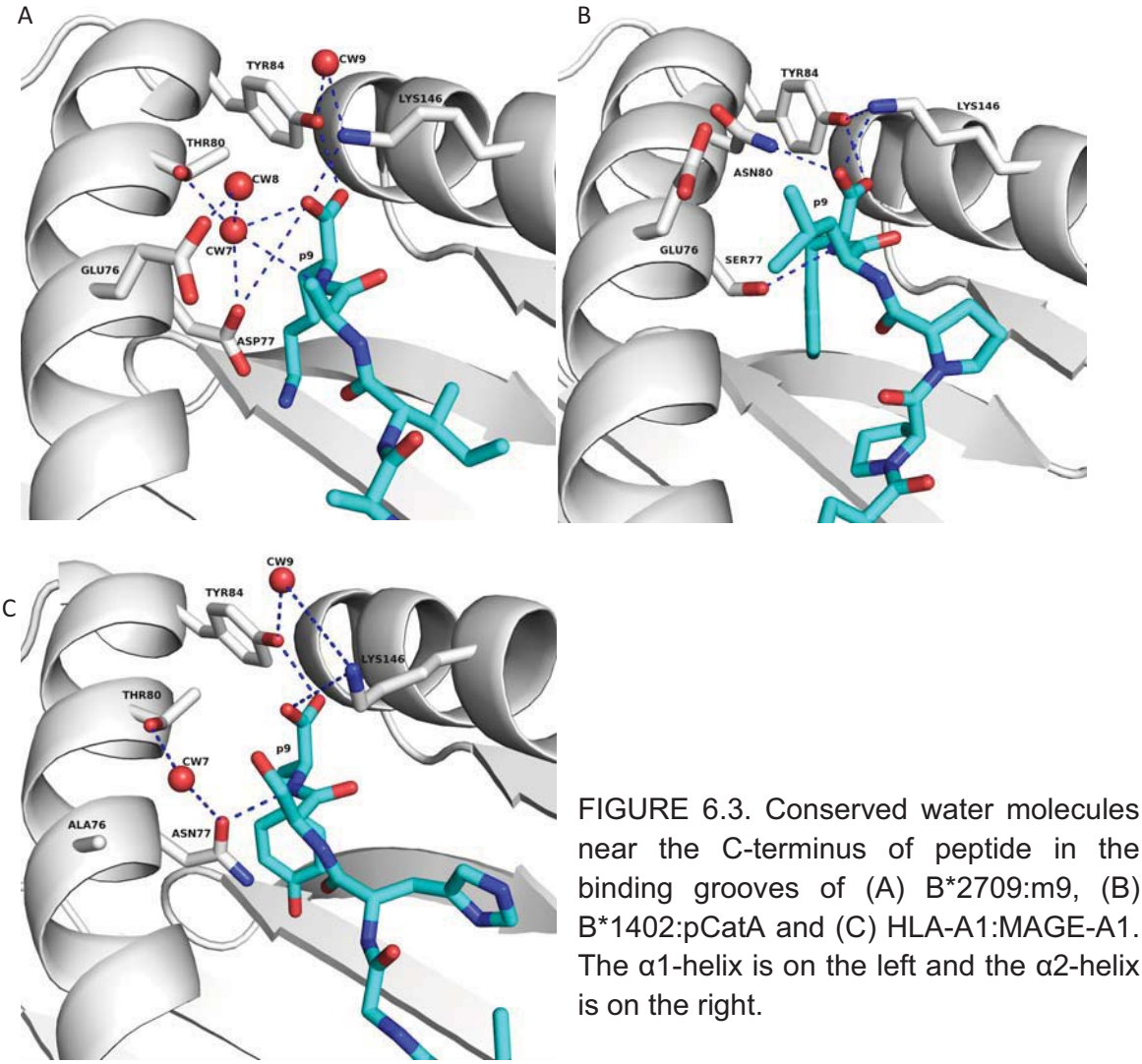

FIGURE 6.3. Conserved water molecules near the C-terminus of peptide in the binding grooves of (A) B*2709:m9, (B) B*1402:pCatA and (C) HLA-A1:MAGE-A1. The α1-helix is on the left and the α2-helix is on the right.

groove of HLA-A1 than HLA-B27. CW1 is also present in HLA-A1 and the N-terminus of the MAGE-A1 peptide is anchored through the pentagonal hydrogen bond network just like in the case of HLA-B27 molecules. As peptide ligands of HLA-A1 do not have pArg2 as an anchor residue, and the apolar residues Phe9 and Ile97 are incapable of forming the kind of water-mediated hydrogen bonds observed in His9 and Asn97 of HLA-B27 molecules, CW2 and CW4 are not observed in the HLA-A1 structure. However, CW3 is present in HLA-A1 and facilitates bonding between $p3^{N}$, $Tyr99^{OH}$, $p3^{O}$ and $His70^{ND1}$ (Fig. 6.3C).

CW5 and CW6 are not observed in HLA-A1, as an Arg is present at position 163 whose longer side chain may enable it to form the hydrogen bonds which Glu163 forms with main chain atoms of the peptide in HLA-B27 structures. However, there seems to be no hydrogen bonding between Arg163 and peptide atoms in the HLA-A1:MAGE-A1 structure. HLA-A1 features polar residues Asn77 and Thr80 but an interaction with the C-terminal O and N atoms of peptide are not observed and the CW7 and CW8 water molecules are not present in the HLA-A1 structure (Fig. 6.3C). However, CW9 is present in the HLA-A1 structure and mediates the same interactions as in many HLA-B27 molecules.

6.2.4 General features of conserved water molecules in HLA-B27, B*1402 and HLA-A1 complexes

For a thorough study of conserved water molecules mediating peptide anchoring in the peptide binding grooves of the HLA-B27, B*1402 and HLA-A1 complexes, a comparison of a large number of structures of all three HLA class I molecules are necessary. General principles regarding the location and role of conserved water molecules in peptide anchoring in these three HLA subtypes cannot be developed at this stage as there are only two structures of the B*1402 molecule and one unliganded structure of the HLA-A1 molecule available. However, it is reasonable to assume that binding of key anchor residues of peptides will be facilitated by conserved water molecules in each of these complexes.

The comparison of the HLA-B27 structures (Table 6.2) reveals that the conserved water molecules participating in the anchoring of atoms closer to the N- and C-termini of peptides have smaller spreads than those facilitating anchoring of atoms located farther from the termini. As the location of residues p1, p2 and pΩ are generally the

same in all MHC class I molecules presenting peptides with at least 9 residues and no Gly at the C-terminal position which would cause protrusion from the F-pocket (Collins et al. 1994), the conserved water molecules that hydrogen bond with the main chain atoms of these three residues should have smaller spreads than conserved water molecules which hydrogen bond with other peptide atoms. The small spread in the location of CW2 in HLA-B27 structures (Table 6.2) and the presence of the hydroxyl group of Tyr9 exactly at the same position in B*1402 structures, indicates its importance for positioning of pArg2 in the B-pocket of HLA-B molecules that have a preference for pArg2 as an anchor residue in a peptide.

The role of the conserved water molecule CW3 in HLA-B27 and B*1402 structures is similar (Fig. 6.2A,B), but in the HLA-A1:MAGE-A1 structure it appears to take a role intermediate between the roles of CW2 and CW3 of HLA-B27 structures in that it directly interacts with both the Tyr99 OH and the p4 N atoms (Fig. 6.2C). The presence of the bulky hydrophobic residue Phe9 in HLA-A1 may have induced this rearrangement. CW4, CW5 and CW6 appear to be much less conserved across the different HLA class I subtypes as substitutions at positions 97, 70, and 163 could make them unnecessary. Even though positions 77 and 80 are occupied by polar residues with similar side chain lengths in all three subtypes, CW7 and CW8 appear to be much less crucial for anchoring of peptide C-termini as is evident from the B*1402 and HLA-A1 structures (Fig. 6.3A-C). Finally, the role of CW9 in anchoring of the peptide C-terminal carboxyl group is to add flexibility to the Lys146 side chain, which shows some variability in different structures and is a common anchor residue of TCR as well as KIR on pMHC (Boyington and Sun 2002, Rudolph et al. 2006, Kumar et al. 2009b, see also chapter 4). Even from this preliminary analysis, it appears that the unique structural features of HLA-B27 enable this molecule to utilize more water molecules to anchor peptide main chain atoms within the binding groove than B*1402 and HLA-A1.

Binding of a free water molecule, which has six translational and rotational degrees of freedom as well as three internal vibrational modes, to a protein involves transformation of the degrees of freedom into nine vibrational modes in the complex and is accompanied by a reduction in entropy (Fischer et al. 2001). In the case of bovine pancreatic trypsin inhibitor, a study revealed that binding of an ordered water molecule resulted in a net increase in vibrational entropy, and hence flexibility, of the

complex (Fischer and Verma 1999, Fischer et al. 2001). Such changes in protein flexibility (and mass distribution or shape) may translate into differences in the spectrum of vibrational frequencies of the molecule which can play a role in signal transduction (Kern and Zuiderweg 2003, Laskowski et al. 2009). As a recent study has shown subtype-specific differences in flexibility of HLA-B27 molecules (Fabian et al. 2009), a study of water-pMHC interactions and their thermodynamic consequences may provide a better understanding of the connection between conformational flexibility of a pMHC and antigen presentation.

6. 4 Concluding remarks

The structural and thermodynamic analyses undertaken in this study contribute to a detailed understanding of conformational variability of MHC class I molecules. The comparative analysis of the structures of B*1402 and HLA-B27 (Kumar et al. 2009a) provide a first view of how two very different HLA-B subtypes present the same peptides. It also provides the first structure of the HLA-B14 molecule, which exhibits a subtype-dependent association with AS similar to HLA-B27. The structural and thermodynamic analyses of the B*2705:pB27 and B*2705:pCP complexes provide a clue to the extent to which peptide malleability can influence peptide conformation, and provide the first example of how an HLA-B27 molecule can present a peptide in three, and possibly even more, drastically distinct conformations. The structures of HLA-B27 molecules complexed with the citrullinated pVIPR peptide (pVIPR-U5) provide an understanding of how a seemingly minor substitution of a single non-hydrogen atom in the peptide can have drastic effects on peptide presentation (Beltrami et al. 2008). The comparative study of structural alterations induced in pMHC as a result of ligand binding (Kumar et al. 2009b) addresses a hitherto largely ignored aspect of ligand binding to pMHC.

The development of the method to embed 3D data in an electronic publication (Kumar et al. 2008) improves the ability of a structural biologist to communicate and disseminate structural information also to individuals from other fields. Finally, the identification of conserved water molecules integral to binding of peptides within the peptide binding groove of the HLA-B27, B*1402 and HLA-A1 antigens points to common, subtype-dependent features of peptide binding by MHC class I molecules.

This study enlarges the existing knowledge of structural variability within MHC class I molecules and attempts to address some of the underlying causes. It may be helpful for future studies addressing alloreactivity, autoimmunity, molecular mimicry and other topics pertaining to antigen presentation by MHC class I molecules. Some of the questions that have arisen during the course of this work may be conclusively answered only after a thorough analysis for the dynamics of MHC class I molecules by employing methods such as NMR or neutron scattering. The unusual conformation of the pB27 peptide in the peptide binding groove of the B*2705 molecule and its potential for “dynamic mimicry” with pCP suggest that studying conformational dynamics in presentation of these two peptides by the B*2705 molecule and investigating their immunogenicity in animal disease-models may be relevant in the context of the ongoing search for *arthritogenic* peptides involved in the pathogenesis of SpA in HLA-B27-positive individuals.

7. References

Ackerman AL, Kyritsis C, Tampé R, Cresswell P. Access of soluble antigens to the endoplasmic reticulum can explain cross-presentation by dendritic cells. Nat Immunol. 2005, 6:107-13.

Adams EJ, Juo ZS, Venook RT, Boulanger MJ, Arase H, Lanier LL, Garcia KC. Structural elucidation of the m157 mouse cytomegalovirus ligand for Ly49 natural killer cell receptors. Proc Natl Acad Sci U S A. 2007, 104:10128-33.

Afzali B, Lechler RI, Hernandez-Fuentes MP. Allorecognition and the alloresponse: clinical implications. Tissue Antigens. 2007, 69:545-56.

Arase H, Mocarski ES, Campbell AE, Hill AB, Lanier LL.Direct recognition of cytomegalovirus by activating and inhibitory NK cell receptors. Science. 2002, 296:1323-6.

Armstrong KM, Piepenbrink KH, Baker BM. Conformational changes and flexibility in T-cell receptor recognition of peptide-MHC complexes. Biochem J. 2008, 415:183-96.

Beck S, Trowsdale J. The human major histocompatability complex: lessons from the DNA sequence. J.Annu Rev Genomics Hum Genet. 2000, 1:117-37

Beltrami A, Rossmann M, Fiorillo MT, Paladini F, Sorrentino R, Saenger W, Kumar P, Ziegler A, Uchanska-Ziegler B. Citrullination-dependent differential presentation of a self-peptide by HLA-B27 subtypes. J Biol Chem. 2008, 283:27189-99.

Benjamin R, Parham P. Guilt by association: HLA-B27 and ankylosing spondylitis. Immunology Today. 1990, 11:137-142.

Bernadó P, Mylonas E, Petoukhov MV, Blackledge M, Svergun DI. Structural characterization of flexible proteins using small-angle X-ray scattering. J Am Chem Soc. 2007, 129:5656-64.

Blachère NE, Darnell RB, Albert ML. Apoptotic cells deliver processed antigen to dendritic cells for cross-presentation. PLoS Biol. 2005, 3:e185.

Bosco N, Kirberg J, Ceredig R, Agenès F. Peripheral T cells in the thymus: have they just lost their way or do they do something? Immunol Cell Biol. 2009, 87:50-7.

Bowness P. HLA B27 in health and disease: a double-edged sword? Rheumatology (Oxford) 2002, 41:857-868.

Boyington JC, Motyka SA, Schuck P, Brooks AG, Sun PD. Crystal structure of an NK cell immunoglobulin-like receptor in complex with its class I MHC ligand. Nature. 2000, 405:537-43.

Boyington JC, Sun PD. A structural perspective on MHC class I recognition by killer cell immunoglobulin-like receptors. Mol Immunol. 2002, 38:1007-21.

Brewerton DA, Caffrey M, Nicholls A, Walters D, Oates JK, James DC. Reiter's disease and HL-A 27. Lancet. 1973a, 302:996-8.

Brewerton DA, Hart FD, Nicholls A, Caffrey M, James DC, Sturrock RD. Ankylosing spondylitis and HL-A 27. Lancet. 1973b, 1:904-7.

Brooks JM, Murray RJ, Thomas WA, Kurilla MG, Rickinson AB. Different HLA-B27 subtypes present the same immunodominant Epstein-Barr virus peptide. J Exp Med. 1993, 178:879-87.

Caillat-Zucman S. Molecular mechanisms of HLA association with autoimmune diseases. Tissue Antigens. 2009, 73:1-8.

Cerwenka A, Lanier LL. Natural killer cells, viruses and cancer. Nat Rev Immunol. 2001, 1:41-9.

Chames P, Hufton SE, Coulie PG, Uchanska-Ziegler B, Hoogenboom HR. Direct selection of a human antibody fragment directed against the tumor T-cell epitope HLA-A1-MAGE-A1 from a nonimmunized phage-Fab library. Proc Natl Acad Sci U S A. 2000, 97:7969-74.

Chang HC, Tan K, Ouyang J, Parisini E, Liu JH, Le Y, Wang X, Reinherz EL, Wang JH. Structural and mutational analyses of a CD8alphabeta heterodimer and comparison with the CD8alphaalpha homodimer. Immunity. 2005, 23:661-71.

Chen Y, Shi Y, Cheng H, An YQ, Gao GF. Structural immunology and crystallography help immunologists see the immune system in action: how T and NK cells touch their ligands. IUBMB Life. 2009, 61:579-90.

Colbert RA, DeLay ML, Layh-Schmitt G, Sowders DP. HLA-B27 misfolding and spondyloarthropathies. Adv Exp Med Biol. 2009, 649:217-34.

Cole DK, Gao GF. CD8: adhesion molecule, co-receptor and immuno-modulator. Cell Mol Immunol. 2004, 1:81-8.

Collins EJ, Garboczi DN, Wiley DC. Three-dimensional structure of a peptide extending from one end of a class I MHC binding site. Nature. 1994, 371:626-9.

Collins EJ, Riddle DS. TCR-MHC docking orientation: natural selection, or thymic selection? Immunol Res. 2008, 41:267-94.

Cragnolini JJ, de Castro JA. Identification of endogenously presented peptides from Chlamydia trachomatis with high homology to human proteins and to a natural self-ligand of HLA-B27. Mol Cell Proteomics. 2008, 7:170-80.

Cresswell P, Ackerman AL, Giodini A, Peaper DR, Wearsch PA. Mechanisms of MHC class I-restricted antigen processing and cross-presentation. Immunol Rev. 2005, 207:145-57.

D'Amato M, Fiorillo MT, Carcassi C, Mathieu A, Zuccarelli A, Bitti PP, Tosi R, Sorrentino R. Relevance of residue 116 of HLA-B27 in determining susceptibility to ankylosing spondylitis. Eur J Immunol. 1995, 25:3199-201.

Daniel RM, Dunn RV, Finney JL, Smith JC. The role of dynamics in enzyme activity. Annu Rev Biophys Biomol Struct. 2003, 32:69-92.

de Vrij J, Uil TG, van den Hengel SK, Cramer SJ, Koppers-Lalic D, Verweij MC, Wiertz EJ, Vellinga J, Willemsen RA, Hoeben RC. Adenovirus targeting to HLA-A1/MAGE-A1-positive tumor cells by fusing a single-chain T-cell receptor with minor capsid protein IX. Gene Ther. 2008, 15:978-89.

DeFranco AL, Locksley RM, Robertson M. The Immune Response in Infectious and Inflammatory Disease 2007 (New Science Press, London, UK) http://www.new-science-press.com/browse/immunity/illustrations/4/

Denkberg G, Reiter Y. Recombinant antibodies with T-cell receptor-like specificity: novel tools to study MHC class I presentation. Autoimmun Rev. 2006, 5:252-7.

DiBrino M, Parker KC, Margulies DH, Shiloach J, Turner RV, Biddison WE, Coligan JE. The HLA-B14 peptide binding site can accommodate peptides with different combinations of anchor residues. J Biol Chem. 1994, 269:32426-34.

Dodson G, Verma CS. Protein flexibility: its role in structure and mechanism revealed by molecular simulations. Cell Mol Life Sci. 2006, 63:207-19.

Dong G, Wearsch PA, Peaper DR, Cresswell P, Reinisch KM. Insights into MHC class I peptide loading from the structure of the tapasin-ERp57 thiol oxidoreductase heterodimer. Immunity. 2009, 30:21-32.

Dong H, Paramonov SE, Aulisa L, Bakota EL, Hartgerink JD. Self-assembly of multidomain peptides: balancing molecular frustration controls conformation and nanostructure. J Am Chem Soc. 2007, 129:12468-72.

Engelhard VH, Altrich-Vanlith M, Ostankovitch M, Zarling AL. Post-translational modifications of naturally processed MHC-binding epitopes. Curr Opin Immunol. 2006, 18:92-7.

Fabian H, Huser H, Loll B, Ziegler A, Naumann D, Uchanska-Ziegler B. HLA-B27 heavy chains distinguished by a micropolymorphism exhibit differential flexibility. Arthritis Rheum. 2009 (In press).

Fan QR, Long EO, Wiley DC.Crystal structure of the human natural killer cell inhibitory receptor KIR2DL1-HLA-Cw4 complex. Nat Immunol. 2001, 2:452-60.

Farag SS, Fehniger TA, Ruggeri L, Velardi A, Caligiuri MA. Natural killer cell receptors: new biology and insights into the graft-versus-leukemia effect. Blood. 2002, 100:1935-47.

Fiaux J, Bertelsen EB, Horwich AL, Wüthrich K. NMR analysis of a 900K GroEL GroES complex. Nature. 2002, 418:207-11.

Fiorillo MT, Maragno M, Butler R, Dupuis ML, Sorrentino R. CD8(+) T-cell autoreactivity to an HLA-B27-restricted self-epitope correlates with ankylosing spondylitis. J Clin Invest. 2000, 106:47-53.

Fiorillo MT, Rückert C, Hülsmeyer M, Sorrentino R, Saenger W, Ziegler A, Uchanska-Ziegler B. Allele-dependent similarity between viral and self-peptide presentation by HLA-B27 subtypes. J Biol Chem. 2005, 280:2962-71.

Fischer S, Verma CS. Binding of buried structural water increases the flexibility of proteins. Proc Natl Acad Sci U S A. 1999, 96:9613-5.

Fischer S, Smith J, Verma C. Dissecting the vibrational entropy change on protein/ligand binding : burial of a water molecule in bovine pancreatic trypsin inhibitor. J. Phys. Chem. B 2001, 105:8050-8055.

Frankild S, de Boer RJ, Lund O, Nielsen M, Kesmir C, 2008 Amino Acid Similarity Accounts for T Cell Cross-Reactivity and for “Holes” in the T Cell Repertoire. PLoS ONE, 3:e1831.

Gao GF, Tormo J, Gerth UC, Wyer JR, McMichael AJ, Stuart DI, Bell JI, Jones EY, Jakobsen BK. Crystal structure of the complex between human CD8alpha(alpha) and HLA-A2. Nature. 1997, 387:630-4.

Garcia KC, Adams EJ. How the T cell receptor sees antigen – a structural view. Cell 2005, 122:333–336.

Gaston H. Mechanisms of Disease: the immunopathogenesis of spondyloarthropathies. Nat Clin Pract Rheumatol. 2006, 2:383-92.

Genick UK, Borgstahl GE, Ng K, Ren Z, Pradervand C, Burke PM, Srajer V, Teng TY, Schildkamp W, McRee DE, Moffat K, Getzoff ED. Structure of a protein photocycle intermediate by millisecond time-resolved crystallography. Science. 1997, 275:1471-5.

Groothuis TA, Neefjes J. The many roads to cross-presentation. J Exp Med. 2005, 202:1313–1318.

Hershko A, Ciechanover A. The ubiquitin system. Annu Rev Biochem. 1998, 67:425-479.

Hillig RC, Hülsmeyer M, Saenger W, Welfle K, Misselwitz R, Welfle H, Kozerski C, Volz A, Uchanska-Ziegler B, Ziegler A. Thermodynamic and structural analysis of peptide- and allele-dependent properties of two HLA-B27 subtypes exhibiting differential disease association. J Biol Chem. 2004, 279:652-63.

Hodis E, Prilusky J, Martz E, Silman I, Moult J, Sussman JL. Proteopedia - a scientific 'wiki' bridging the rift between three-dimensional structure and function of biomacromolecules. Genome Biol. 2008, 9:R121.

Hodis E, Sussman JL. An encyclopedic effort to make 3D structures easier to understand. Trends Biochem Sci. 2009, 34:100-1.

Holler PD, Kranz DM. T cell receptors: affinities, cross-reactivities, and a conformer model. Mol Immunol. 2004, 40:1027-31.

Hülsmeyer M, Hillig RC, Volz A, Rühl M, Schröder W, Saenger W, Ziegler A, Uchanska-Ziegler B. HLA-B27 subtypes differentially associated with disease exhibit subtle structural alterations. J Biol Chem. 2002, 277:47844-53.

Hülsmeyer M, Fiorillo MT, Bettosini F, Sorrentino R, Saenger W, Ziegler A, Uchanska-Ziegler B. Dual, HLA-B27 subtype-dependent conformation of a self-peptide. J Exp Med. 2004, 199:271-81.

Hülsmeyer M, Welfle K, Pöhlmann T, Misselwitz R, Alexiev U, Welfle H, Saenger W, Uchanska-Ziegler B, Ziegler A. Thermodynamic and structural equivalence of two HLA-B27 subtypes complexed with a self-peptide. J Mol Biol. 2005, 346:1367-79.

Hülsmeyer M, Chames P, Hillig RC, Stanfield RL, Held G, Coulie PG, Alings C, Wille G, Saenger W, Uchanska-Ziegler B, Hoogenboom HR, Ziegler A. A major histocompatibility complex-peptide-restricted antibody and t cell receptor molecules recognize their target by distinct binding modes: crystal structure of human leukocyte antigen (HLA)-A1-MAGE-A1 in complex with FAB-HYB3. J Biol Chem. 2005, 280:2972-80.

Janeway CA Jr. How the immune system protects the host from infection. Microbes Infect. 2001, 3:1167-71.

Jensen PE. Mechanisms of antigen presentation. Clin Chem Lab Med. 1999, 37:179-86.

Jones EY. Blueprints for life or death Nat Immunol. 2001, 2:379 – 80.

Josefowicz SZ, Rudensky A.Control of regulatory T cell lineage commitment and maintenance. Immunity. 2009, 30:616-25.

Kern D, Zuiderweg ER. The role of dynamics in allosteric regulation. Curr Opin Struct Biol. 2003, 13:748-57.

Klein J. Natural History of the Major Histocompatability Complex 1986 (John Wiley & Sons, New York, USA)

Koch SD, Uss E, van Lier RA, ten Berge IJ. Alloantigen-induced regulatory CD8+CD103+ T cells. Hum Immunol. 2008, 69:737-44.

Krzewski K, Strominger JL. The killer's kiss: the many functions of NK cell immunological synapses. Curr Opin Cell Biol. 2008, 20:597-605.

Kumar P, Ziegler A, Ziegler J, Uchanska-Ziegler B, Ziegler A. Grasping molecular structures through publication-integrated 3D models. Trends Biochem Sci. 2008, 33:408-12.

Kumar P, Vahedi-Faridi A, Saenger W, Merino E, López de Castro JA, Uchanska-Ziegler B, Ziegler A. Structural Basis for T Cell Alloreactivity among Three HLA-B14 and HLA-B27 Antigens. J Biol Chem. 2009a, 284:29784-97.

Kumar P, Vahedi-Faridi A, Saenger W, Ziegler A, Uchanska-Ziegler B. Conformational changes within the HLA-A1:MAGE-A1 complex induced by binding of a recombinant antibody fragment with TCR-like specificity. Prot Sci. 2009b, 18:37-49.

Lang HL, Jacobsen H, Ikemizu S, Andersson C, Harlos K, Madsen L, Hjorth P, Sondergaard L, Svejgaard A, Wucherpfennig K, Stuart DI, Bell JI, Jones EY, Fugger L. A functional and structural basis for TCR cross-reactivity in multiple sclerosis. Nat Immunol. 2002, 3:940-3.

Lanier LL. NK cell recognition. Annu Rev Immunol. 2005, 23:225-74.

Laskowski RA, Gerick F, Thornton JM. The structural basis of allosteric regulation in proteins. FEBS Lett. 2009, 583:1692-8.

Levin EJ, Kondrashov DA, Wesenberg GE, Phillips GN Jr. Ensemble refinement of protein crystal structures: validation and application. Structure. 2007, 15:1040-52.

Liu YJ. A unified theory of central tolerance in the thymus. Trends Immunol. 2006, 27:215-21.

Lopez de Castro JA, Alvarez I, Marcilla M, Paradela A, Ramos M, Sesma L, Vázquez M. HLA-B27: a registry of constitutive peptide ligands. Tissue Antigens. 2004, 63:424-45.

López de Castro JA. HLA-B27 and the pathogenesis of spondyloarthropathies. Immunol Lett. 2007, 108:27-33.

Madden DR. The three-dimensional structure of peptide-MHC complexes. Annu Rev Immunol. 1995, 13:587-622.

Maenaka K, Maenaka T, Tomiyama H, Takiguchi M, Stuart DI, Jones EY. Nonstandard peptide binding revealed by crystal structures of HLA-B*5101 complexed with HIV immunodominant epitopes. J Immunol. 2000, 165:3260-7.

Maeurer MJ, Storkus WJ, Kirkwood JM, Lotze MT. New treatment options for patients with melanoma: review of melanoma-derived T-cell epitope-based peptide vaccines. Melanoma Res. 1996, 6:11-24.

Marcilla M, Cragnolini JJ, López de Castro JA. Proteasome-independent HLA-B27 ligands arise mainly from small basic proteins. Mol Cell Proteomics. 2007, 6:923-38.

Mareeva T, Martinez-Hackert E, Sykulev Y. How a T cell receptor-like antibody recognizes major histocompatibility complex-bound peptide. J Biol Chem. 2008, 283:29053-9.

May E, Dulphy N, Frauendorf E, Duchmann R, Bowness P, Lopez de Castro JA, Toubert A, Märker-Hermann E. Conserved TCR beta chain usage in reactive arthritis; evidence for selection by a putative HLA-B27-associated autoantigen. Tissue Antigens. 2002, 60:299-308.

Mehra NK, Kaur G. MHC-based vaccination approaches: progress and perspectives. Expert Rev Mol Med. 2003, 5:1-17.

Merino E, Montserrat V, Paradela A, López de Castro JA. Two HLA-B14 subtypes (B*1402 and B*1403) differentially associated with ankylosing spondylitis differ substantially in peptide specificity but have limited peptide and T-cell epitope sharing with HLA-B27. J Biol Chem. 2005, 280:35868-80.

Murienne J, Ziegler A, Ruthensteiner B. A 3D revolution in communicating science. Nature. 2008, 453:450.

Murphy K, Travers P, Walport M. Janeway's Immunobiology 2008 (Garland Science, London, UK)

Natarajan K, Dimasi N, Wang J, Mariuzza RA, Margulies DH. Structure and function of natural killer cell receptors: multiple molecular solutions to self, nonself discrimination. Annu Rev Immunol. 2002, 20:853-85.

Norbury CC, Basta S, Donohue KB, Tscharke DC, Princiotta MF, Berglund P, Gibbs J, Bennink JR, Yewdell JW. CD8+ T cell cross-priming via transfer of proteasome substrates. Science. 2004, 304:1318-21.

Ogata K, Wodak SJ. Conserved water molecules in MHC class-I molecules and their putative structural and functional roles. Protein Eng. 2002, 15:697-705.

Orange JS, Ballas ZK. Natural killer cells in human health and disease. Clin Immunol. 2006, 118:1-10.

Pamer E, Cresswell P. Mechanisms of MHC class I--restricted antigen processing. Annu Rev Immunol. 1998, 16:323-58.

Panda A, Arjona A, Sapey E, Bai F, Fikrig E, Montgomery RR, Lord JM, Shaw AC. Human innate immunosenescence: causes and consequences for immunity in old age. Trends Immunol. 2009, 30:325-33.

Parak FG. Proteins in action: the physics of structural fluctuations and conformational changes. Curr Opin Struct Biol. 2003, 13:552-7.

Peaper DR, Cresswell P. Regulation of MHC class I assembly and peptide binding. Annu Rev Cell Dev Biol. 2008, 24:343-68.

Pecht I, Gakamsky DM. Spatial coordination of CD8 and TCR molecules controls antigen recognition by CD8+ T-cells. FEBS Lett. 2005, 579:3336-41.

Petersen J, Purcell AW, Rossjohn J. Post-translationally modified T cell epitopes: immune recognition and immunotherapy. J Mol Med. 2009, IN PRESS

Petrone PM, Garcia AE. MHC-peptide binding is assisted by bound water molecules. J Mol Biol. 2004, 338:419-35.

Pöhlmann T, Böckmann RA, Grubmüller H, Uchanska-Ziegler B, Ziegler A, Alexiev U. Differential peptide dynamics is linked to major histocompatibility complex polymorphism. J Biol Chem. 2004, 279:28197-201.

Purcell AW, van Driel IR, Gleeson PA. Impact of glycans on T-cell tolerance to glycosylated self-antigens. Immunol Cell Biol. 2008, 86:574-9.

Raghavan M, Del Cid N, Rizvi SM, Peters LR. MHC class I assembly: out and about. Trends Immunol. 2008, 29:436-43.

Ramos M, Alvarez I, Sesma L, Logean A, Rognan D, López de Castro JA. Molecular mimicry of an HLA-B27-derived ligand of arthritis-linked subtypes with chlamydial proteins. J Biol Chem. 2002, 277:37573-81.

Reiser JB, Darnault C, Grégoire C, Mosser T, Mazza G, Kearney A, van der Merwe PA, Fontecilla-Camps JC, Housset D, Malissen B. CDR3 loop flexibility contributes to the degeneracy of TCR recognition. Nat Immunol. 2003, 4:241-7.

Riley JL, June CH, Blazar BR.Human T regulatory cell therapy: take a billion or so and call me in the morning. Immunity. 2009, 30:656-65.

Rudolph MG, Stanfield RL, Wilson IA. How TCRs bind MHCs, peptides, and coreceptors. Annu Rev Immunol. 2006, 24:419-66.

Rückert C, Fiorillo MT, Loll B, Moretti R, Biesiadka J, Saenger W, Ziegler A, Sorrentino R, Uchanska-Ziegler B. Conformational dimorphism of self-peptides and molecular mimicry in a disease-associated HLA-B27 subtype. J Biol Chem. 2006, 281:2306-16.

Schlosstein L, Terasaki PI, Bluestone R, Pearson CM. High association of an HL-A antigen, W27, with ankylosing spondylitis. N Engl J Med. 1973, 288:704-6.

Schotte F, Lim M, Jackson TA, Smirnov AV, Soman J, Olson JS, Phillips GN Jr, Wulff M, Anfinrud PA. Watching a protein as it functions with 150-ps time-resolved x-ray crystallography. Science. 2003, 300:1944-7.

Schotte F, Soman J, Olson JS, Wulff M, Anfinrud PA. Picosecond time-resolved X-ray crystallography: probing protein function in real time. J Struct Biol. 2004, 147:235-46.

Shen L, Rock KL. Cellular protein is the source of cross-priming antigen in vivo. Proc Natl Acad Sci U S A. 2004, 101:3035-40..

Shen L, Rock KL. Priming of T cells by exogenous antigen cross-presented on MHC class I molecules. Curr Opin Immunol. 2006, 18:85–91.

Sherwood P, Brooks BR, Sansom MS. Multiscale methods for macromolecular simulations. Curr Opin Struct Biol. 2008, 18:630-40.

Siala M, Mahfoudh N, Gdoura R, Younes M, Fourati H, Kammoun A, Chour I, Meddeb N, Gaddour L, Hakim F, Baklouti S, Bargaoui N, Sellami S, Hammami A, Makni H. Distribution of HLA-B27 and its alleles in patients with reactive arthritis and with ankylosing spondylitis in Tunisia. Rheumatol Int. 2009, 29:1193-6.

Sieker F, May A, Zacharias M.Predicting affinity and specificity of antigenic peptide binding to major histocompatibility class I molecules. Curr Protein Pept Sci. 2009, 10:286-96.

Smith-Garvin JE, Koretzky GA, Jordan MS. T cell activation. Annu Rev Immunol. 2009, 27:591-619.

Solheim JC. Class I MHC molecules: assembly and antigen presentation. Immunol Rev. 1999, 172:11-9.

Speir JA, Stevens J, Joly E, Butcher GW, Wilson IA. Two different, highly exposed, bulged structures for an unusually long peptide bound to rat MHC class I RT1-Aa. Immunity. 2001, 14:81-92.

Srajer V, Ren Z, Teng TY, Schmidt M, Ursby T, Bourgeois D, Pradervand C, Schildkamp W, Wulff M, Moffat K. Protein conformational relaxation and ligand migration in myoglobin: a nanosecond to millisecond molecular movie from time-resolved Laue X-ray diffraction. Biochemistry. 2001, 40:13802-13815.

Starr TK, Jameson SC, Hogquist KA. Positive and negative selection of T cells. Annu Rev Immunol. 2003, 21:139-76.

Teilum K, Olsen JG, Kragelund BB. Functional aspects of protein flexibility. Cell Mol Life Sci. 2009, 66:2231-47.

Turner MJ, Sowders DP, DeLay ML, Mohapatra R, Bai S, Smith JA, Brandewie JR, Taurog JD, Colbert RA. HLA-B27 misfolding in transgenic rats is associated with activation of the unfolded protein response. J Immunol. 2005, 175:2438-48.

Tzakos AG, Grace CR, Lukavsky PJ, Riek R. NMR techniques for very large proteins and rnas in solution. Annu Rev Biophys Biomol Struct. 2006, 35:319-42.

Vilches C, Parham P. KIR: Diverse, rapidly evolving receptors of innate and adaptive immunity Annu Rev Immunol. 2002, 20:217-51.

Voges D, Zwickl P, Baumeister W. The 26S proteasome: a molecular machine designed for controlled proteolysis. Annu Rev Biochem. 1999, 68:1015-68.

Wang R, Natarajan K, Margulies DH. Structural basis of the CD8 alpha beta/MHC class I interaction: focused recognition orients CD8 beta to a T cell proximal position. J Immunol. 2009, 183:2554-64.

Wilson IA, Bjorkman PJ. Unusual MHC-like molecules: CD1, Fc receptor, the hemochromatosis gene product, and viral homologs. Curr Opin Immunol. 1998, 10:67-73.

Wucherpfennig KW. Presentation of a self-peptide in two distinct conformations by a disease-associated HLA-B27 subtype. J Exp Med. 2004, 199:151-4.

Yee A, Chang X, Pineda-Lucena A, Wu B, Semesi A, Le B, Ramelot T, Lee GM, Bhattacharyya S, Gutierrez P, Denisov A, Lee CH, Cort JR, Kozlov G, Liao J, Finak G, Chen L, Wishart D, Lee W, McIntosh LP, Gehring K, Kennedy MA, Edwards AM,

Arrowsmith CH. An NMR approach to structural proteomics. Proc Natl Acad Sci U S A. 2002, 99:1825-30.

York IA, Rock KL. Antigen processing and presentation by the class I major histocompatibility complex. Annu Rev Immunol. 1996, 14:369-396.

Zawacka A. HLA-B27 subtypes differentially associated to an autoimmune disease: Analysis of peptide display and attempt to define their recognition pattern by the Killer cell Ig-like receptor KIR3DL1. Doctoral Thesis. 2009, Freie Universität Berlin, Germany

Ziegler A, Kentenich H, Uchanska-Ziegler B. Female choice and the MHC. Trends Immunol. 2005, 26:496-502.

Ziegler A, Coulie PG, Uchańska-Ziegler B. Monoclonal and recombinant antibodies with T cell receptor-like reactivity. Recent Results Cancer Res. 2007, 176:229-41.

Ziegler A, Faber C, Mueller S, Bartolomaeus T. Systematic comparison and reconstruction of sea urchin (Echinoidea) internal anatomy: a novel approach using magnetic resonance imaging. BMC Biol. 2008, 6:33.

Ziegler A, Loll B, Misselwitz R, Uchanska-Ziegler B. Implications of structural and thermodynamic studies of HLA-B27 subtypes exhibiting differential association with ankylosing spondylitis. Adv Exp Med Biol. 2009a, 649:177-95.

Ziegler A, Müller CA, Böckmann RA, Uchanska-Ziegler B. Low-affinity peptides and T-cell selection. Trends Immunol. 2009b, 30:53-60.